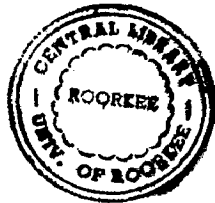


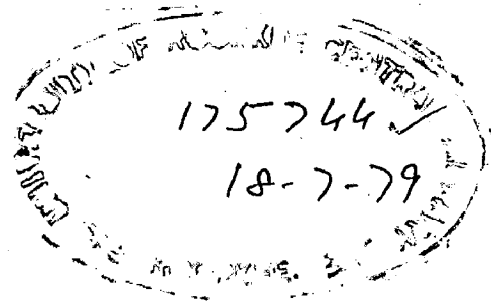
STUDY IN PRODUCTION OF ALLOY POWDERS BY CEMENTATION

A THESIS
submitted in fulfilment
of the requirements for the award of the degree
of
DOCTOR OF PHILOSOPHY
in
METALLURGICAL ENGINEERING



By

R. D. AGRAWAL



2-20-80
8.10.80

DEPARTMENT OF METALLURGICAL ENGINEERING
UNIVERSITY OF ROORKEE
ROORKEE-247672
INDIA
September, 1978

C E R T I F I C A T E

The undersigned hereby certify that the thesis entitled 'STUDY IN PRODUCTION OF ALLOY POWDERS BY CEMENTATION' which is being submitted by Mr.R.D.Agrawal in fulfilment of the requirements for the award of the Degree of DOCTOR OF PHILOSOPHY IN METALLURGICAL ENGINEERING of the University of Roorkee, Roorkee, is a record of the candidate's own work carried out by him under their joint guidance and supervision. The matter embodied in this thesis has not been submitted for the award of any other degree.

It is further certified that Mr.R.D.Agrawal worked for a period of about three and quarter years from May, 1975 to August, 1978 as a part-time research scholar for the preparation of this thesis.

M.L.Kapoor
(M.L.Kapoor)
Professor of Extractive
Metallurgy,
Department of Metallurgical
Engineering,
University of Roorkee,
ROORKEE-247 672.

M.L. Mehta
(M.L.Mehta)
Professor and Head,
Department of Metallurgical
Engineering,
University of Roorkee,
ROORKEE-247 672.

University of Roorkee, Roorkee
Certified that the attached Thesis/
Dissertation has been accepted for the
award of Degree of Doctor of
Philosophy / ~~Master of Engineering~~
Metallurgical Engg. vide notification
No. ~~39~~ 39-55 (Degree) dated... 25. 4. 79
[Signature]
Registrar (Exam.)

18/7/78

A C K N O W L E D G E M E N T S

The undersigned expresses his gratitude and sincere thanks to Dr.M.L.Mehta, Professor and Head of the Department of Metallurgical Engineering, University of Roorkee, Roorkee, for his valuable guidance, active supervision, constructive criticism and help throughout the course of preparation of this thesis and also for providing all the necessary facilities in the Department for carrying out the research work embodied in this thesis.

He also wishes to record his deep sense of gratitude and indebtedness to Dr.M.L.Kapoor, Professor of Extractive Metallurgy, Department of Metallurgical Engineering, University of Roorkee, Roorkee, for the inspiration, guidance, frank constructive criticism, thought-provoking discussions and suggestions he has kindly made available to him during the entire period of scientific investigations and all phases of preparation of the manuscript of this thesis. Without his timely and untiring help, it could not have been possible to present this thesis in its present form.

The author also wishes to record his grateful appreciation of the assistance rendered by Sri V.N.S.Mathur Reader Deptt. of Met.Engg. University of Roorkee for his help in the correction. of the manuscript.

He would also like to record his gratefulness for the assistance rendered by the Laboratory Staff, particularly to Shri Shakti Swaroop Gupta, of the Department of Metallurgical Engineering, during experimentation and for the excellent draftsmanship by Shri M.C.Vaish as also for the flawless typewriting of the manuscript by Shri U.K.Mishra in the preparation of this thesis. He would also like to record his indebtedness for the help rendered directly or indirectly by others in the preparation of this thesis.

Last, but not the least, he wishes to record his affectionate appreciation of the great perseverance shown by his wife and daughters for the entire period spent in preparation of this thesis.



Roorkee:

(Ranchhor Das Agrawal)

Thursday,
the 21st September, 1978.

S Y N O P S I S

Cementation has been used extensively by chemists and metallurgists as an economical process for purification and recovery of metals from dilute solutions. The first application reported in literature dates back to fourth century but scientific investigations on cementation have started only recently. A critical study of published work has indicated that investigations are mostly confined to the kinetics of cementation using disc or cylindrical samples of precipitant metal. No systematic work has been reported on the thermodynamics of the process and even in kinetic studies no uniform picture is available regarding the rate controlling step and the effects of process variables on the kinetics of cementation.

The present work has, therefore, been undertaken to make a systematic study of the thermodynamics and kinetics of cementation and utility of the cement powder product. For this, copper/iron system has been selected because of its considerable industrial importance as an economical and efficient means of copper recovery from dilute solutions. Also, in the present work iron powder has been used in preference to disc or cylindrical samples because it permits a better simulation of the actual industrial practice. The entire work has been

reported in five chapters.

Chapter I deals with the historical developments, literature review and formulation of problem for present investigation.

Chapter II deals with the thermodynamics of cementation and includes the experimental set-up and procedure used for the determination of, (i) the activity coefficient of copper sulphate as a function of concentration of copper sulphate in solution, pH of the solution and concentration of ferrous sulphate in solution, and, (ii) the activity coefficient of ferrous sulphate as a function of its concentration in solution, pH of the solution and concentration of copper sulphate in solution. It also includes the results obtained, their interpretation and applicability of the existing theory. It has been found that, (i) in pure copper sulphate solution the activity coefficient of copper sulphate decreases with increase in its concentration and follows Hückel relationship, (ii) the activity coefficient of copper sulphate and that of ferrous sulphate increases with decrease in pH, (iii) in pure ferrous sulphate solution, the activity coefficient of ferrous sulphate decreases with increase in its concentration and follows Guggenheim relationship, and, (iv) addition of ferrous sulphate to copper sulphate solution decreases its activity coefficient whereas

addition of copper sulphate to ferrous sulphate increases its activity coefficient.

Chapter III deals with the kinetics of cementation and includes the theoretical aspects, experimental set-up and procedure used for studying the kinetics as a function of process variables namely, (i) temperature, (ii) stirring speed, (iii) initial copper ion concentration in solution, (iv) pH of the solution, (v) size of the powder, (vi) solution/powder ratio, and, (vii) atmosphere. Results obtained and their interpretations are also included in this chapter. It has been observed that the overall rate of cementation is controlled by the mass transport in the aqueous solution. To confirm this polarisation studies have also been made, which have testified the above conclusion.

Chapter IV deals with the characteristics of the cement copper powder obtained under different experimental conditions and includes studies of following properties and the explanation of results obtained: (i) particle shape, size and size-distribution, (ii) apparent density, (iii) flow rate, (iv) tap density and friction index, (v) green density and densification parameter, (vi) compression ratio, (vii) sintered density, (viii) green porosity and sintered porosity, (ix) effect of liquid-phase sintering on sintered density

and sintered porosity; and, (x) microstructures of sintered mass. Comparison of these properties with iron powders (for cement powders of low copper content) showed an immense improvement in the green density; densification parameter and sintered density. This leads to the conclusion that these powders form a better substitute for plain iron powders. Powders having high copper content can be used either for the production of those powder metallurgical components which are normally produced with the help of pure copper powders or for extraction of copper through melting.

Chapter V includes summary and conclusions.

Scope for future work is indicated separately.

C. O N T E N T S

	<u>Page</u>
CERTIFICATE	
ACKNOWLEDGEMENT ...	i
SYNOPSIS ...	iii
CONTENTS ...	vii
NOMENCLATURE FOR THERMODYNAMIC STUDIES ...	x
NOMENCLATURE FOR KINETIC STUDIES ...	xii
NOMENCLATURE FOR POWDER CHARACTERISATION STUDIES ...	xvi
LIST OF FIGURES ...	xvii
LIST OF TABLES ...	xxii
CHAPTER I INTRODUCTION ...	1
1.1 General and Historical ...	1
1.2 Literature Survey ...	6
1.3 Formulation of Problem ...	20
CHAPTER II THERMODYNAMICS OF CEMENTATION ...	23
2.1 Introduction ...	23
2.2 Experimental ...	29
2.2.1 Experimental set-up ...	31
2.2.2 Procedure ...	33
2.2.2.1 Preparation of Solutions..	33
2.2.2.2 Experimental ...	35

2.3	Results and Discussion	...	36	
2.3.1	Mean Activity Coefficient of Copper Sulphate in Aqueous Solution	...	36	
2.3.2	Effect of Sulphuric Acid on Activity Coefficient of Copper Sulphate	...	43	
2.3.3	Mean Activity Coefficient of Ferrous Sulphate in Aqueous Solution	...	47	
2.3.4	Effect of Sulphuric Acid on Activity Coefficient of Ferrous Sulphate	..	54	
2.3.5	Effect of Ferrous Sulphate on Activity Coefficient of Copper Sulphate and Vice-versa		59	
2.3.6	Overall Driving-force for Cementation Reaction	...	68	
CHAPTER III KINETICS OF CEMENTATION			...	74
3.1	Introduction	...	74	
3.2	Theoretical	...	74	
3.2.1	Electrode Processes	...	77	
3.2.2	Transport from OHP to the Electrode Surface	...	83	
3.2.3	Transport through Diffuse Double Layer	...	83	
3.2.4	Transport through Boundary Layer	...	87	
3.2.5	Generalised Rate Equation	...	89	
3.3	Experimental	...	93	
3.3.1	Experimental Set-up	...	95	
3.3.2	Procedure	...	97	

3.4	Results and Discussion	...	99
3.4.1	Effect of Temperature	...	114
3.4.2	Effect of Solution Agitation		117
3.4.3	Effect of Initial Copper ion Concentration		121
3.4.4	Effect of Hydrogen ion Concentration (pH)	...	126
3.4.5	Effect of Particle size and Solution/Powder Ratio	..	129
3.4.6	Effect of Atmosphere	...	135
CHAPTER IV	CHARACTERISTICS OF CEMENT COPPER POWDERS	...	140
4.1	General	...	140
4.2	Powder Characteristics	...	141
4.2.1	Particle Shape, Size and Size Distribution	...	141
4.2.2	Apparent Density	...	147
4.2.3	Flow Rate	...	150
4.2.4	Tap Density and Friction Index	..	151
4.3	Process Variables	...	151
4.3.1	Compressibility and Green Density		151
4.3.2	Compression Ratio	...	155
4.3.3	Sintered Density	...	164
4.3.4	Green Porosity and Sintered Porosity	...	164
4.3.5	Liquid Phase Sintering	...	187
CHAPTER V	SUMMARY AND CONCLUSIONS	...	191
	SCOPE FOR FUTURE WORK	...	195
	R E F E R E N C E S	...	196

NOMENCLATURE FOR THERMODYNAMIC STUDIES

α_i	Empirical coefficient of component i in equations for mixed electrolytes
a_i	Activity of the i^{th} component
$a_{A^{n+}}$	Activity of metal ion A^{n+} .
$a_{B^{n+}}$	Activity of metal ion B^{n+}
$[A^{n+}],$ $[B^{n+}]$	Concentrations of metal ions A^{n+} and B^{n+} respectively
A, B and C	Debye Hückel constants
\bar{e}	Electron taking part in reaction
E	Equilibrium electromotive force of cell
E_i^0	Standard electrode potential of component i .
ΔE	Change in electrode potential
F	Faraday constant
f_i	Activity coefficient of component i
$f_{\text{FeSO}_4(0)}$	Activity coefficient of ferrous sulphate in pure ferrous sulphate solution.
$f_{\text{CuSO}_4(0)}$	Activity coefficient of copper sulphate in pure copper sulphate solution.
ΔG	Free energy change in a reaction
Ψ	Parameter defined by equation (2.21)
n and n	Electrode reaction valence for metals A and B respectively.
n_i	Molality of the i^{th} ion

μ	Ionic strength of solution
μ_i	Ionic strength of component i
N_i	Molal concentration of component i
ϕ	Osmotic coefficient defined by equation (2.47).
R	Universal gas constant
T	Temperature in $^{\circ}\text{K}$
x_i	Mole fraction of component i
Z	Electrode reaction valency
Z_+ and Z_-	Valences of cation and anion, respectively.
Z_i	Valency of i^{th} ion

NOMENCLATURE FOR KINETIC STUDIES

α	Transfer coefficient
a	Parameter defined by equation (3.23)
A	Surface area of precipitant
A_c	Cathodic area
A_a	Anodic area
B	Constant, defined in literature
a	Constant, defined in literature
C_i	Concentration of component i
$C_{Cu^{2+}}^0$	Initial concentration of copper ion in solution
$C_{Cu^{2+}}^t$	Concentration of copper ion in solution at time t
$C_{b,i}$	Concentration of component i in the bulk of the aqueous phase
C_D	Concentration of reducible ion at diffuse double layer
C_p	Concentration of reducible ion at diffuse double layer and is equal to C_D
C_c	Concentration of cation at the Outer Helmholtz Plane
C_a	Effective concentration of metal sites capable of reacting in the anodic direction
$\overrightarrow{C}^\ddagger$ and $\overleftarrow{C}^\ddagger$	Concentrations of the activated complex for the anodic and cathodic directions respectively
C_o	Concentration of cation at the Outer Helmholtz Plane and is equal to C_c

$C_{a,i}$	Effective concentration of component i capable of reacting in the anodic direction
δ	Reciprocal of half of the thickness of diffuse double layer
D_i	Diffusion coefficient of component i
d	Particle diameter
E	Potential associated with charge transfer reaction
η	Over-potential defined as $(E - E^0)$
E_m	Mixed potential
F	Faraday constant
$\Delta \bar{G}_0^{\rightarrow}$ and $\Delta \bar{G}_0^{\leftarrow}$	Activation energies for the anodic and cathodic directions respectively, in the absence of potential gradient
\bar{G}^{\rightarrow} and \bar{G}^{\leftarrow}	Activation energies for the anodic and cathodic directions respectively, in the presence of potential gradient
h	Planck constant
I_+ and I_-	Anodic and cathodic current densities respectively
I	Net current density
I_0	Equilibrium exchange current density
$K_{m,i}$	Mean mass transfer coefficient of ion i in solution
k_c	Parameter defined by equation (3.52)
\bar{K}^{\leftarrow} and \bar{K}^{\rightarrow}	Equilibrium constants for equilibrium with the activated complex for cathodic and anodic directions, respectively of a half cell

\overleftarrow{k} and \overrightarrow{k}	Specific rate constants for the cathodic and anodic directions, respectively of a half cell, in the absence of potential field
\overleftarrow{k}	Parameter defined as $\overleftarrow{k} ZF\lambda$
\overrightarrow{k}	Parameter defined as $\overrightarrow{k} ZF\lambda$
k_i and k_i'	Specific rate constants for an ion at the i^{th} minimum to jump forward and backward, respectively, in the absence of a potential
k	Boltzman constant
k	Transmission coefficient
ψ_0	Potential at outer Helmholtz Plane
ψ_x	Potential at distance x from the outer Helmholtz Plane
ϕ	Effective potential difference between outer Helmholtz Plane and electrode, defined as $\phi = E - \psi_0$
λ	Distance between minima on either side of the activated state
L	Thickness of the boundary layer
L'	Characteristic length measure of the size of the system
μ	Viscosity of solution
m	Mass of the iron powder
ν	Kinematic viscosity of solution
Ω	Parameter defined by equation (3.36)
p	Parameter indicating effect of particle size and of solution/powder ratio on cementation kinetics and defined by Eqs. (3.64) and (3.65)

R	Universal gas constant
Re	Reynolds number
ρ	Material density of iron
ρ'	Density of solution
Sh	Sherwood number
Sc	Schmidt number
T	Temperature, $^{\circ}\text{K}$
t_e	Residence time of a Chunk of fluid at the surface of the boundary layer
V	Volume of solution
Z	Charge transfer valency
Z'	Number of electrons required for the total reduction process
Z	Absolute value of ionic charge of an ion
$\left(\frac{d\psi}{dx}\right)_i$	Potential gradient for the i^{th} barrier.

NOMENCLATURE FOR POWDER CHARACTERISATION STUDIES

A	Cross-sectional area of the orifice of the flowmeter funnel
C	Constant
d	Material density of the powder
d_a	Apparent density
K	Constant
R	Surface roughness factor
S_w	Specific surface area
t	Total time of powder flow
W	Total weight of the powder flowing.

LIST OF FIGURES

<u>S.No.</u>	<u>FIG.NO.</u>	<u>PARTICULARS</u>	<u>Page No.</u>
1	2.1	Experimental Set-up for E.M.F. measurements	32
2	2.2	ψ as a Function of Square root of Copper sulphate Concentration	38
3	2.3	Activity Coefficient of Copper Sulphate Versus its Concentration	40
4	2.4	Comparison of Experimental with Theoretical Plots for Activity Coefficient of Copper Sulphate	42
5	2.5	Mean Activity Coefficients of Copper Sulphate and Sulphuric Acid in Mixed Electrolyte Solution	46
6	2.6	Activity Coefficient of Copper Sulphate in Mixed Electrolyte Solution of Copper Sulphate and Sulphuric Acid at various Constant Total Ionic Strengths	48
7	2.7	Empirical Coefficient α Versus Total Ionic Strength in Mixed Electrolyte	49
8	2.8	ψ as a Function of Square root of Ferrous Sulphate Concentration	52
9	2.9	Comparison of Experimental with Theoretical Plots for Activity Coefficient of Ferrous Sulphate	53
10	2.10	Log (Activity Coefficient) Versus Square root of Ionic Strength	55
11	2.11	Mean Activity Coefficients of Ferrous Sulphate and Sulphuric Acid in Mixed Electrolyte Solution	58
12	2.12	Activity Coefficient of Ferrous Sulphate in Mixed Electrolyte Solution of Ferrous Sulphate and Sulphuric Acid at various Constant Total Ionic Strengths	60

<u>S.No.</u>	<u>FIG.NO.</u>	<u>PARTICULARS</u>	<u>PAGE NO.</u>
13	2.13	Mean Activity Coefficients of Copper Sulphate and Ferrous Sulphate in Mixed Electrolyte Solution	62
14	2.14	Activity Coefficient of Copper Sulphate in Mixed Electrolyte Solution of Copper Sulphate and Ferrous Sulphate at various Constant Total Ionic Strengths	64
15	2.15	Activity Coefficient of Ferrous Sulphate in Mixed Electrolyte Solution of Ferrous Sulphate and Copper Sulphate at Different Constant Total Ionic Strengths	69
16	2.16	$(E_{Cu} - E_{Fe})$ Versus $\log (N_{Fe^{2+}}/N_{Cu^{2+}})$ at various Constant Total Molality of Copper Sulphate and Ferrous Sulphate Mixed Electrolyte Solution	71
17	2.17	$(E_{Cu} - E_{Fe})$ Versus $\log (N_{Fe^{2+}}/N_{Cu^{2+}})$ at Various Constant Total Molality of Copper Sulphate, Sulphuric Acid and Ferrous Sulphate Mixed Electrolyte Solution	73
18	3.1	Activation Energy Barrier for Net Cathodic Half Cell	79
19	3.2	Experimental Set-up for Kinetic Studies	96
20	3.3	Experimental Set-up for Polarisation Studies	111
21	3.4	Polarisation Curves for Copper and Iron at 25°C and 1900 rpm	112
22	3.5	Effect of Temperature on Rate of Cementation	115
23	3.6	Arrhenius Plot of Rate Constant of Copper Cementation	116
24	3.7	Effect of Stirring Speed on Rate of Cementation	118

<u>S.No.</u>	<u>FIG.NO.</u>	<u>PARTICULARS</u>	<u>PAGE NO.</u>
25	3.8	Log (Rate constant) Versus Log (rpn) for Copper Cementation	120
26	3.9	Effect of Initial Copper Concentration on Rate of Cementation	122
27	3.10	Rate Constant Versus Log $[C_{Cu^{2+}}]_{initial}$	123
28	3.11	Cation Diffusion Coefficient of Copper as a Function of Concentration at 25°C	125
29	3.12	Effect of pH on Rate of Cementation	127
30	3.13	Effect of pH on Rate Constant of Copper Cementation	128
31	3.14	Effect of pH on Excess Iron Consumption	130
32	3.15	Effect of Size of Iron Powder on Rate of Cementation	131
33	3.16	Log (p) Versus log (d)	133
34	3.17	Effect of Solution/Powder Ratio on Rate of Cementation	134
35	3.18	Log (p) Versus log (m)	136
36	3.19	Effect of Atmosphere on Rate of Cementation	137
37	3.20	Effect of Atmosphere on Excess Iron Consumption	139
38	4.1	Shape of Cement Copper Particles	142
39	4.2	Effect of Iron Powder Particle Size on Size Distribution in Cement Copper Powders Produced	145
40	4.3	Effect of Initial Concentration of Copper on Particle Size Distribution in Cement Copper Powders Produced	146

<u>S.No.</u>	<u>FIG.NO.</u>	<u>PARTICULARS</u>	<u>PAGE NO.</u>
41	4.4	Effect of Iron Powder Particle Size on the Densification Parameter of Cement Copper and Iron Powders	156
42	4.5	Effect of Iron Powder Size on Green Density of Cement Copper and Iron Products	157
43	4.6	Effect of Solution Concentration on Densification Parameter of Cement Copper Powders	158
44	4.7	Effect of Initial Copper Concentration on Green Density of Cement Copper and Iron Products	159
45	4.8	Effect of Iron Powder Size on the Compression Ratio of Cement Copper Powders and Iron Powders	162
46	4.9	Effect of Solution Concentration on Compression Ratio of Cement Copper Powders	163
47	4.10	Comparison of Sintered Density With Green Density for Cement Powder Products	168
48	4.11	Comparison of Sintered Density With Green Density for Cement Copper as well as Iron Products	169
49	4.12	Comparison of Sintered Density With Green Density for Iron Powder Products	170
50	4.13	Effect of Temperature on Sintered Density of Cement Copper Products	171
51	4.14	Effect of Temperature on Sintered Density of Cement Copper and Iron Products	172
52	4.15	Effect of Temperature on Sintered Density of Iron Products	173
53	4.16	Effect of Iron Powder Particle Size on Green Porosity of Cement Copper Products	178

<u>S.NO.</u>	<u>FIG.NO.</u>	<u>PARTICULARS</u>	<u>PAGE NO.</u>
54	4.17	Effect of Iron Powder Particle Size on Sintered Porosity of Cement Copper Products	179
55	4.18	Effect of Solution Concentration on Green Porosity of Cement Copper Products	180
56	4.19	Effect of Solution Concentration on Sintered Porosity of Cement Copper Products	181
57	4.20	Photomicrographs Showing the Effect of Iron Powder Particle Size on Sintered Porosity of Cement Copper Products obtained by Compaction at 2.5 Ton Load and Sintering at 850°C	183
58	4.21	Photomicrographs Showing the Effect of Sintering Temperature on Sintered Porosity of Cement Copper Parts Produced by Compaction at 2.5 Ton Load	184
59	4.22	Photomicrographs Showing the Effect of Compaction Load on Sintered Porosity of Cement Copper Parts Sintered at 850°C	185
60	4.23	Photomicrographs Showing the Effect of Initial Solution Concentration on Sintered Porosity of Cement Copper Products obtained by Compaction at 10 Ton Load and Sintered at 850°C	186
61	4.24	Photomicrographs Showing the Effect of Liquid Phase Sintering on Sintered Porosity of Cement Copper Parts Produced from Two Different Initial Solution Concentrations, Compacted at 2.5 Ton Load and Sintered at 1150°C	190

LIST OF TABLES

<u>S.NO.</u>	<u>TABLE NO.</u>	<u>PARTICULARS</u>	<u>PAGE NO.</u>
1	2.1	Standard Half-cell Potentials at 25°C	27
2	2.2	Calculated Equilibrium Constants in Cementation Reactions at 25°C	28
3	2.3	E.M.F. data on the Cell Cu CuSO ₄ KCl(Sat.) Hg ₂ Cl ₂ (s) Hg at 25°C	37
4	2.4	E.M.F. data on Cell Cu CuSO ₄ , H ₂ SO ₄ KCl(Sat.) Hg ₂ Cl ₂ (s) Hg at 25°C	44
5	2.5	E.M.F. data on Cell Fe FeSO ₄ KCl(Sat.) Hg ₂ Cl ₂ (s) Hg at 25°C	50
6	2.6	E.M.F. data on the Cell Fe FeSO ₄ , H ₂ SO ₄ KCl(Sat.) Hg ₂ Cl ₂ (s) Hg at 25°C	57
7	2.7	E.M.F. data on the Cell Cu CuSO ₄ , FeSO ₄ KCl(Sat.) Hg ₂ Cl ₂ (s) Hg at 25°C	61
8	3.1	Results of Temperature Parameter Study	100
9	3.2	Results of Stirring parameter Study	101
10	3.3	Results of Initial Copper Ion Concentration study.	102
11	3.4	Results of pH Parameter Study	103
12	3.5	Results of Particle size Parameter Study	104
13	3.6	Results of Solution/Powder Ratio Study	105

<u>S.NO.</u>	<u>TABLE NO.</u>	<u>PARTICULARS</u>	<u>PAGE NO.</u>
14	3.7	Results of Atmosphere Parameter Study	106
15	4.1	Effect of the Size of the Iron Powder on Particle Size and Size Distribution of the Cement Copper Powder Produced	143
16	4.2	Effect of the Initial Copper Concentration in Solution on Particle Size and size Distribution of the Cement Copper Powder Produced	144
17	4.3	Effect of the Particle Size of the Iron Powder on Flow Rate, Apparent Density, Tap Density and Friction Index	148
18	4.4	Effect of the Initial Copper Concentration in Solution on flow Rate, Apparant Density, Tap Density and Friction Index	149
19	4.5	Weight, Diameter and Height of the various Green Compacts	152
20	4.6	Effect of the Size of the Iron Powder on Green Density, Densification parameter and compression Ratio of the Cement Copper Powder Produced and the Iron Powder	153
21	4.7	Effect of the Initial Concentration of Copper in Solution on Green Density, Densification Parameter and Compression Ratio of the Cement Copper Powder Produced and the Values of these Properties for the Iron Powder Used as Precipitant	154
22	4.8	Composition and Density of Cement Copper Powders	160

<u>S.NO.</u>	<u>TABLE NO.</u>	<u>PARTICULARS</u>	<u>PAGE NO.</u>
23	4.9	Weight diameter and height of the various Sintered Products	165
24	4.10	Effect of the Size of Iron Powder on Sintered Density of the Cement Copper Product and Iron Product	166
25	4.11	Effect of Initial Copper Concentration in Solution on Sintered Density of the Cement Copper Product and Sintered Density of the Iron Product	167
26	4.12	Effect of the Size of the Iron Powder on Green Porosity of the Cement Copper Product and the Iron Product	174
27	4.13	Effect of the Size of the Iron Powder on Sintered Porosity of the Cement Copper Product and the Iron Product	175
28	4.14	Effect of the Initial Copper Concentration in Solution on Green Porosity of the Cement Copper Product and of the Iron Product	176
29	4.15	Effect of Initial Copper in Solution on Sintered Porosity of the Cement Copper Product and of the iron Product	177
30	4.16	Results of Liquid Phase Sintering of Cement Copper Compact Produced at 2.5 Ton load and Sintered at 1150°C	188

C H A P T E R - I

INTRODUCTION

1.1 General and Historical

Metals commonly occur in nature in oxidised forms as oxides, sulphides, halides, carbonates, silicates etc. The reduction of these compounds to metallic state is done with the help of technically and economically feasible reagents. The actual extraction process employed and flowsheet used for any particular case depends upon several economic and technical factors, viz., the source of metal i.e. ore, concentrate or metallurgical waste, the physical and chemical properties of the metal to be extracted, relative stabilities of different compounds present in the ore and formed during processing, desirable tonnage and purity of the product. These extraction processes can be classified into pyro-, electro- and hydro-metallurgical. The pyrometallurgical processes, in which various process operations are performed at high temperatures leading to faster reaction rates, have the advantage of delivering the product on a large scale and at high productivity. These processes are, therefore, used extensively for the extraction and refining of most of the metals. However, they suffer from the limitations of most stringent requirements of the quality of ores, concentrates, fuels, refractory materials and fluxes. In some cases the metal to be produced may form alloys/

compounds with other elements during the process and may thus render these processes impractical for the production of these metals. The electrometallurgical processes have the advantage of unlimited reducing power. These processes can employ either aqueous or fused-salt baths—the choice depending primarily upon the reactivity of the metal, availability of suitable electrolyte and electrode materials. The major limitation for the application of these processes is the availability of cheap and plentiful supply of electricity. The other drawbacks of these processes include high capital cost, low current efficiencies, polarisation effects at low concentration of metal values in solution, co-deposition of impurities and occasionally undesirable characteristics of cathode deposits. Hydrometallurgical processes make use of chemical reactions predominantly in aqueous phase at room or moderate temperatures for the winning of metal. Because of the ever-increasing demand for high-purity metals coupled with non-availability of high-grade ores the adoption of hydrometallurgical processes, especially for the extraction of metals from metallurgical wastes, low-grade ore deposits or old dumps and refractory silicate ores has been steadily rising in recent years. Developments in leaching such as pressure-leaching, use of new solvents and pre-treatment techniques for direct leaching of native metals, sulphides, arsenides,

tellurides and other refractory ores coupled with advances in purification of leach liquors by conventional chemical methods, solvent extraction and ion-exchange processes had a considerable impact on the applicability of this field of metal extraction. Out of the four conventional methods of recovery of metal from purified leach liquors, viz., electrowinning from aqueous or fused-salt baths, gaseous reduction by hydrogen, chemical precipitation of metal compounds and cementation, the last method has additional advantage of its suitability for recovery of value from very dilute solutions. In cementation a more electro-positive metal ion in solution, when brought into contact with a less electropositive metal, is displaced from the solution and cemented on the latter metal. Because of its importance in the recovery of metal values from metallurgical wastes and low-grade ores, considerable work is being done to understand the fundamentals of cementation which is applicable not only for recovery of metallic values from leach liquors of any concentration but also has been extensively used for purification of leach liquors prior to recovery by other methods. The present work is taken up with a view to understand the mechanism and kinetics of this process and to broaden the field of application of the product obtained.

The word cementation has been derived from Cementation (Spanish meaning precipitation) and refers to a

metal displacement or metal contact reduction reaction which has been known and used from ancient times.

Mellor¹ refers to the Writings of Zosimus in fourth-century about reduction of copper from salts solution by iron. Basil Valentine² in his book *Currus Triumphalis Antimonii* refers to copper cementation. Several ancient European chemists regarded cementation as an example of the transmutation of metals. Paracelsus the Great² cites use of iron for preparing venus (copper) by the 'Rustics of Hungary' in his 'Book Concerning the Tincture of the Philosophers'. Agricola³ in his book 'De Natura Fossiliun' refers to a peculiar water drawn from a shaft near Schmolnity in Hungary that erodes iron and turns it into copper. The Chinese of Sung Dynasty⁴ used cementation method for the production of copper from copper sulphate. By 1585 A.D., metal trees formed by adding mercury to silver or gold solutions were known⁵. The copper was reported to be produced commercially as early as the sixteenth century³ in Rio Tinto in Spain from mine waters by precipitation on iron and yearly production in 1833 was 140 tons⁶. By the middle of nineteenth century, cement-copper was produced commercially in Ireland, England, Germany and Hungary^{3,7}. By 1875 cement copper produced in Hungary amounted to 200 tons per year. In the United States, copper cementation was carried out on water pumped from the Butte Mines, Montana in 1888

and yearly production in 1910 was 2279 tons^{3,8}. The earlier studies on cementation are reported to be carried out by Boyle⁵ and later extended by Stahl⁵ to arrive at the 'affinity' series which can be identified with the electro-chemical series of modern chemistry. First quantitative studies were carried out a century later by Bergman⁹ who determined the weights of metal displaced in various reactions. The first rate study of a cementation reaction was made by Gladstone and Tribe¹⁰ in 1871 who investigated the reaction between copper metal and silver nitrate. With the help of studies in several cementation reactions, by about 1900, many scientific conclusions were drawn, namely, (i) not all the reactions predicted by the electrochemical series take place, for example, nickel does not displace either copper or silver from solutions, (ii) co-deposition is a common phenomenon, for example, copper precipitated from solution by iron or zinc is contaminated with these metals, (iii) the reaction rate depends on the anion, for example, the displacement of copper by aluminium is much more rapid in the presence of chloride ions than sulphate ions. However, most of the articles published until about 1960 dealt with plant practices only^{7,8,11-20} and only a few reports²¹⁻²³ on the investigations of the variables studied under crude laboratory experimentation were published.

1.2 Literature Survey

In recent years several workers²⁴⁻⁵³ have studied the cementation process due to its importance which was discussed under section 1.1, with a view to understand physico-chemical principles of the process. Handorf²⁴ studied the cementation of lead and silver from brine solutions by metallic iron and found that (i) the cementation reaction in case of lead was chemically controlled whereas for silver it was diffusion controlled, (ii) the cementation rate was sensitive to changes in temperature and concentration of chloride ions and was strongly affected by the presence of foreign ions. Van Hahn and Ingraham²⁵ concluded from their works on kinetics of palladium cementation on electropolished copper that (i) the cemented deposit was porous at low concentration whereas it was dense and adherent at higher concentration of perchloric acid in aqueous solution, (ii) at lower concentrations and in initial stages of high concentration the rate was found to be interfacial or aqueous phase transport controlled whereas it was found to be solid phase transport controlled in the final stages at higher concentration. Their investigation on cementation of silver on copper²⁶ revealed that (i) the rate of reaction in acidic solution was fast and the resulting deposit was loosely adherent and porous and (ii) the rate of reaction in cyanide solution was slow and the

deposits were dense and adherent. They also investigated the cementation of silver on zinc²⁷ in perchloric acid and in alkaline cyanide solutions and arrived at similar conclusions.

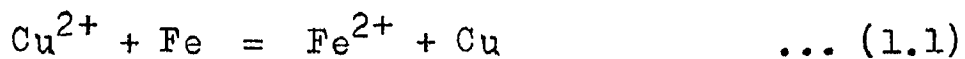
An exhaustive study on cementation of copper on rotating iron discs by Nadkarni et al.²⁸ and Nadkarni and Wadsworth²⁹ revealed the following:

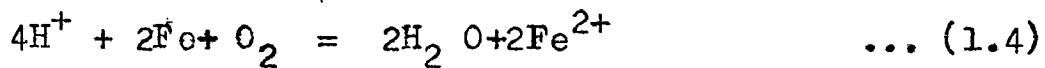
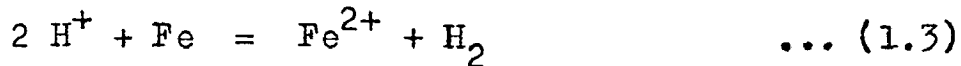
- i) Copper cementation was first order reaction with its rate only slightly dependent upon initial copper concentration and pH,
- ii) at low speeds of rotation the rate was directly proportional to square-root of rpm whereas at high stirring speeds the kinetics became independent of the speed,
- iii) the precipitated copper adhered to the iron as a spongy layer at low speeds, peeled off in the form of bright strip at medium speeds, as a fine powder at high speeds and at very high stirring speeds, particularly with high-purity iron, the precipitated copper approached colloidal size,
- iv) the precipitated copper adhered more strongly to the iron as the impurity content of the iron increased,
- v) oxygen in solution caused excess iron consumption,

vi) under hydrogen atmosphere, excess iron consumption was less than under nitrogen.

Miller and Wadsworth³⁰ examined the kinetics of copper cementation on metallic nickel pellets. They arrived at the conclusions that (i) cementation was a first order reaction rate process, (ii) when the nickel was sufficiently agitated to keep it suspended and in translational motion in the reaction solution, the rate of reaction became independent of further increase in stirring speed, (iii) the rate of cementation decreased slightly with increasing copper ion and acid concentration, (iv) nickel consumption increased with increasing acid concentration, (v) the overall rate of reaction appeared to be diffusion controlled at higher temperatures and interfacial reaction controlled at lower temperatures.

Rickard and Fuerstenau³¹ carried out an electrochemical investigation of copper cementation by iron. They studied the anodic polarisation curves for iron dissolution and cathodic polarisation curves for copper deposition and ferric ions and hydrogen ions reduction. From the results they predicted the relative rates of the reactions:





They reported the following:

- i) the first two reactions were first order with respect to the reacting ions and the rate controlling step was diffusion of ions to the cathodic surface,
- ii) the specific rate constant for first reaction was approximately twice as large as that for second reaction,
- iii) the rate of reaction (1.3) in an oxygen-free solution increased with decrease in pH,
- iv) in solution containing oxygen, the rate of hydrogen reduction was controlled by diffusion of oxygen and was proportional to the square root of the partial pressure of oxygen dissolved in solution.

Ingraham and Kerby³² investigated the kinetics of cadmium cementation on both cylindrical and circular faces of a rotating zinc disc in buffered sulphate solutions and found that (i) the rate was more rapid on the cylindrical face than on the circular face, (ii) at higher temperatures and at pH values above 6.4 the rate of deposition increased due to an increase in the cathodic area of the deposit, (iii) the rate may also be increased by decreasing the thickness of the diffusion layer by rapid stirring,

(iv) the presence of small amounts of copper, cadmium, lead, iron or aluminium in the zinc did not affect the cementation rate, but when small amounts of copper, cobalt and arsenic were present in the solution, cadmium deposition rate decreased shortly after it started, (v) small amounts of copper in solution became cemented with the cadmium to form a coarse deposit of Cd_3Cu .

MacKinnon and Ingraham³³ studied the kinetics of copper cementation on pure aluminium disc in acidic sulphate solution and concluded that (i) at low initial copper ion concentration there were two rate controlling processes - ionic diffusion control at temperatures above $40^{\circ}C$ and surface reaction control at temperatures below $40^{\circ}C$, whereas at higher initial copper ion concentrations the rate was interfacial reaction controlled, (ii) cementation rate increased with decrease in pH. Their studies on copper cementation on aluminium canning sheet³⁴ revealed that rate of copper cementation per unit area was from 1.4 to about 1.9 times greater on canning sheet than on pure aluminium. Further, they studied the kinetics of silver cementation on aluminium canning sheet in alkaline argento-cyanide solution³⁵ and compared the results with those obtained previously for silver cementation on copper²⁶ and zinc²⁷ and arrived at the conclusion that (i) the cementation of silver on aluminium was a diffusion controlled process, (ii) in silver/aluminium

system the rate constant increased with increasing silver ion concentration whereas in silver/zinc system the rate constant was almost independent of silver ion concentration, (iii) the silver formed in silver/aluminium system was a powdery deposit whereas in silver/zinc system it was a smooth, adherent deposit, (iv) when the leach solution contained impurities such as gold, copper, selenium, and alkaline sulphide, thio-sulphates and thiocyanate, the rate constant, in general, decreased. MacKinnon et al's³⁶ work on the kinetics of copper cementation on nickel disc showed that at low temperatures the process was interfacial reaction controlled whereas at high temperatures it was diffusion controlled, and that the rate of cementation increased with decreasing pH of the solution.

Strickland and Lawson^{37,38} studied the cementation of copper on zinc from dilute aqueous solutions using a rotating disc geometry and found that (i) copper concentrations of the order of 10 ppm leads to the formation of a porous, adherent deposit on the zinc surface which has a significant influence on the reaction rate, (ii) when the specific mass (mass/surface area) of the deposit was less than about 0.35 mg/cm^2 , the surface may be considered as smooth and the rate was described by simple convective counter-diffusion of

zinc and copper ions through a laminar diffusion boundary layer to the deposit-solution interface, (iii) in the presence of additional deposit, the diffusional mass transport was increased by increased surface roughness, (iv) the rate constant was dependent on the degree of agitation and varied linearly with the square root of the stirring speed. They further studied³⁹ the kinetics of cementation of cadmium with zinc, lead with zinc, and silver with zinc, copper and cadmium, all from dilute solutions and found similar results.

Biswas and Reid⁴⁰⁻⁴³ examined the kinetic and practical aspects of the extraction of copper by cementation on iron and inferred that (i) the rate of cementation increased with increasing speed but there was a limiting stirring speed above which the cementation rate remained constant, (ii) the specific rate of cementation decreased significantly with increasing initial copper concentration and became very low at high initial copper concentrations due to the dense crust of copper deposit, (iii) the reaction rate decreased with increasing pH upto a pH of about 2.5, after which the reaction rate increased as the pH increased to 4.5, (iv) the presence of even a small amount of sodium sulphate in the feed solution significantly increased the cementation rate, (v) reaction rate increased significantly with temperature and the higher temperature allowed the use of a

higher initial copper concentration before the formation of dense crust of copper, (vi) at higher temperatures the copper powder formed acquired reducing properties which resulted in an iron consumption less than the theoretical value for cementation. Miller and Beckstead⁴⁴ studied the surface deposit effects in the kinetics of copper cementation by iron and found that the cementation reaction was controlled by boundary layer diffusion processes at all temperatures and concentrations, and that the rate constant increased with increase in initial copper concentration upto 200 ppm and then decreased with further increase in concentration. Fisher and Groves^{45,46} investigated the kinetics of cementation of copper on iron and reported that (i) the rate of cementation was significantly enhanced by the increased cathodic areas provided by the porous copper deposit or the presence of a fluidised bed of copper particles contacting the iron precipitant, (ii) the rate of cementation decreased as ionic strength increased, (iii) characteristics of the deposit changed from smooth, adherent deposit below 22°C to porous slightly adherent deposit above 22°C, (iv) the iron consumption increased as pH decreased, (v) the presence of oxygen in the system caused a decrease in the reaction rate but the presence of hydrogen atmosphere in the system had no effect on the process.

Lee et al⁴⁷ worked on the cementation of cadmium on zinc and found that (i) the rate of cementation was controlled by diffusion of cadmium ions to the surface, (ii) the change in the initial cadmium ion concentration showed 'two-step' behaviour on rate constant which reached a maximum at about 50 ppm initial cadmium concentration and thereafter decreased as concentration increased, (iii) as the initial concentration of zinc sulphate in solution increased, the cadmium cementation rate decreased. Their work⁴⁸ under oxygen-containing atmosphere revealed that rate controlling mechanism changed from mass transfer under a nitrogen atmosphere to a mixed or chemical control as the quantity of oxygen dissolved in the solution increased and that the deposit morphology under different oxygen concentrations changed remarkably and influenced the deposition rate significantly. Sareyed-Din and Lawson⁴⁹ studied the kinetics of precipitation of nickel on to iron disc and found that under inert atmosphere conditions the cementation rate was controlled by both diffusion and surface reaction processes and that the presence of oxygen in the atmosphere above the reacting system increased the nickel deposition rate drastically. Their studies⁵⁰ of cementation on to particulates in two different systems: Copper/zinc and nickel/iron revealed that (i) both reactions were mass-transport

controlled, (ii) the specific reaction rate increased with increasing agitation until full particle suspension was reached, (iii) for fully suspended particles the rate constant increased with increasing particle size.

Palmer et al⁵¹ examined the kinetics of aqueous arsenic (III) reduction to amorphous arsenic with cadmium metal and reported that with arsenic concentrations greater than 0.2 gm per litre, the reduction of arsenyl ion on the cadmium surface was rate controlling whereas, at lower concentrations, reaction rate was mass-transfer controlled. Power and Ritchie⁵² worked on the mercury (II)/copper system and found that the reaction rate was first order in mercury (II) ions, the first order rate constant being proportional to the square root of the rotation speed and concluded that the reaction was diffusion controlled. Lee et al⁵³ investigated the effect of precipitant surface roughness on cementation kinetics for cadmium/zinc, copper/zinc and copper/cadmium systems and arrived at empirical mass-transfer correlations.

Most of the studies reported in literature are confined to the investigations on the kinetics of cementation and the type of the deposit using disc or cylindrical samples of precipitant. No systematic work has been reported on the thermodynamics of the process. Even in

kinetic studies the literature show that no uniform picture is available regarding the rate controlling step in the overall reaction. Some of the authors^{24,35,37,38,44,47,50,52} have asserted that mass transport in the aqueous phase controls the overall rate of reaction whereas the others^{24,25,48} have assumed the interfacial reaction to be the rate controlling one. A third group of investigators^{25,30,33,36,49,51} have come to the conclusion that the overall reaction has different rate controlling steps at different stages including mixed control as one of the rate controlling phases. No work has been reported which clearly elucidates the conditions under which a particular step or steps control the overall reaction rate.]

Though in most of the cases the variables studied for kinetic investigations are the same namely, rate of stirring, initial concentrations of the solution, temperature, pH, atmosphere, the resulting effects reported of these variables differ vastly from one author to other. In case of the effect of speed of stirring some investigators^{28-30,40,41} have reported that the rate constant becomes independent of rpm at high stirring rates, some⁵⁴ could not find any region where the rate is independent of stirring speed, while others^{25,33} concluded that rate constant is independent of stirring speed under certain sets of conditions of temperature and

concentration and varies with speed under some other sets of conditions. A group of these investigators^{28-30,37,38,51,52} found that rate constant is proportional to the square root of rpm while others^{32,33} reported a linear variation of rate constant with speed and also the constant of proportionality varied from author to author. Contradictory conclusions^{28,29,55} are reported regarding the effect of stirring speed on the amount of metal dissolved in excess of the stoichiometric amount required for cementation.

Various effects of initial concentration of solution on rate constants are reported. It is reported to be independent of initial concentration of metal ion by some investigators^{24,27,51,55}, increase with increasing initial concentration by some other workers³³⁻³⁵ and decrease with increasing initial concentration by still some other investigators^{29,30,34,40-43,45,46,49}. In contrast to the above conclusions some of the authors^{44,47,48} have inferred two step behaviour in which case rate constant increases with increasing initial concentration to certain concentration and then it decreases with further increase in concentration. Most of them have reported a change in rate controlling step with change in concentration while Miller and Beckstead⁴⁴ asserted that process is diffusion controlled at all concentrations. In most of the investigations the effect of surface

deposit has been disregarded^{27,28,40,56}. Even the group which studied the effect of surface deposit on rate of cementation mentioned conflicting results - either rate enhancement^{26,27,31,34,35,37-39,44-48} or rate retardation^{25-27,36}.

As far as the effect of pH is concerned, the rate constant is reported to either play only a minor role^{28,29,45} in cementation, or increase with decrease in pH upto certain pH and then remain constant with further decrease in pH^{30,33,36}, or remain constant over a certain range of pH but decrease below and increase above that range⁴⁶, or decrease markedly with increase in pH²⁵ or remain constant below a certain pH value but increase above that pH³² or else decrease with decrease in pH⁵⁷ or even decrease with increase in pH upto certain pH value and then rise with increase in pH⁴⁰. Different reasons have been given for such varying effects of pH.

Referring to the effect of temperature, Miller and Beckstead⁴⁴ are of the view that the reaction is diffusion controlled over all ranges of temperatures while others^{25,30,33,36,58} are of the opinion that reaction is diffusion controlled at high temperature and interfacial reaction controlled at lower temperature. The temperature at which this change in mechanism occurs also varies from one worker to the other. Also there is

discrepancy in the value of the activation energy reported by various investigators. Rising temperature is reported to have little effect on total metal dissolution by Schlitt and Richards⁵⁵ and to increase it by Nadkarni and Wadsworth²⁹.

Use of hydrogen atmosphere is reported to reduce the total iron consumption in copper/iron system by some workers²⁹ and to have no effect by other investigators⁴⁶. Rate constant is reported to be independent of atmosphere by some workers⁵¹, while some authors⁴⁶ reported a decrease in reaction rate in oxygen atmosphere and some⁴⁹ noticed that rate constant is a linear function of oxygen partial pressure. Some investigators^{47,48} have reported a change in the reaction mechanism from diffusion control in nitrogen to surface reaction control in oxygen atmosphere. Some workers^{29,44} reported negligible effect of back reaction while others^{47,48} reported a changing effect of back reaction on rate constant depending on the type of atmosphere used. Other authors did not study the back reaction.

Effect of foreign ions on cementation process has been studied only by few workers^{26,32,34,35,40,45} and conflicting results have been obtained with regard to the effects of certain ions on rate constant. For example, Schlitt and Richards⁵⁵ reported that magnesium

ion decreases the rate constant while MacKinnon and Ingraham³⁴ contradicted it.

The above discussion shows that the overall process of cementation is not clearly understood in a number of important aspects namely thermodynamics, mechanism of the process and the effects of process variables on the kinetics. This requires a unified systematic study of this process in all its aspects. It is with this as one of the aims that the present work is taken up.

1.3 Formulation of Problem

With the help of electro-chemical series a number of cementation systems can be selected for study. In the present investigation copper/iron system has been selected because of its considerable industrial importance as an economical and efficient means of copper recovery from dilute solutions. In the present work iron powder has been used in preference to disc or cylindrical samples as the product can find a direct application in powder metallurgical industries. Use of powder precipitant permits a better simulation of the actual situation as in industrial practice scrap iron is used which has also a large surface area.

As discussed in the previous section 1.2, it was

felt necessary in the present investigation to study the thermodynamics and kinetics of cementation, the utility of the cement product and industrial feasibility of the process.

In the thermodynamic part, a systematic study of the thermodynamics of the aqueous phase is to be made on the following lines:

- i) Theoretical thermodynamic analysis of the cementation, and,
- ii) Experimental determination of thermodynamic parameters which will include the following:
 - a) activity coefficient of copper sulphate as a function of its concentration, pH of solution and concentration of ferrous sulphate in solution,
 - b) activity coefficient of ferrous sulphate as a function of its concentration and pH of solution, and,
 - c) applicability of the results of the existing theories to the results obtained in (a) and (b).

The kinetic aspects are studied under the following headings:

- i) The mechanism of cementation,
- ii) Development of a rate expression for the overall rate of cementation,
- iii) Dimensional analysis
- iv) Experimental determination of the effects of the following process variables on the rate constant:
 - a) speed of stirring,
 - b) pH of the solution,
 - c) initial concentration of the solution,
 - d) temperature,
 - e) size of the powder, and,
 - f) solution/powder ratio.

In the product utility part, the following characteristics of the cement product are to be studied:

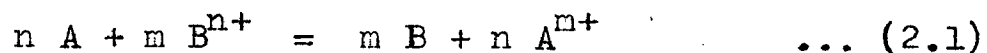
- i) Particle size distribution,
- ii) Flow rate,
- iii) Apparent density,
- iv) Friction index,
- v) Chemical composition,
- vi) Green density and densification parameter,
- vii) Compression ratio,
- viii) Sintered density,
- ix) Sintered porosity, and,
- x) Microstructure of the sintered mass.

C H A P T E R - II

THERMODYNAMICS OF CEMENTATION

2.1 Introduction

The basic cementation reaction between the cation B^{n+} present in an aqueous solution or melt and a metal A is given by an equation:



Essentially, the system is a set of short-circuited electrolytic microcells and the electrochemical nature of such a reaction can be seen more clearly if equation (2.1) is separated into oxidation and reduction half-reactions. At the anodic site on the surface of the metal A, oxidation is taking place:



At the cathodic site, the cation of the second metal is being reduced:



The free energy change, ΔG , of the reaction (2.1) is related to the change in electrode potential, ΔE , by the expression:

$$\Delta G = -n.m.F \Delta E \quad \dots (2.4)$$

where F is the Faraday's constant and m is the number of electrons taking part in the reaction. Single electrode potentials E_A of the half-cell reaction (2.2) and E_B of the reverse of the half-cell reaction (2.3) are defined by the usual electro-chemical nomenclature by,

$$E_A = E_A^{\circ} - \frac{RT}{mF} \ln \left[\frac{a_{A^{m+}}}{a_A} \right] \quad \dots (2.5)$$

and

$$E_B = E_B^{\circ} - \frac{RT}{nF} \ln \left[\frac{a_{B^{n+}}}{a_B} \right] \quad \dots (2.6)$$

Assuming that there is no solid solution formation between A and B, so that $a_A = a_B = 1$, the relations (2.5) and (2.6) can be simplified as:

$$E_A = E_A^{\circ} - \frac{RT}{mF} \ln a_{A^{m+}} \quad \dots (2.7)$$

and

$$E_B = E_B^{\circ} - \frac{RT}{nF} \ln a_{B^{n+}} \quad \dots (2.8)$$

Clearly, the condition for cementation reaction to occur is that the electrode potential E_A must exceed the electrode potential E_B , i.e.,

$$E_A > E_B \quad \dots (2.9)$$

or

$$E_A^{\circ} - \frac{RT}{mF} \ln a_{A^{m+}} > E_B^{\circ} - \frac{RT}{nF} \ln a_{B^{n+}} \quad \dots (2.10)$$

or

$$(E_A^{\circ} - E_B^{\circ}) > \frac{RT}{F} \ln \frac{[a_{A^{m+}}]^{1/m}}{[a_{B^{n+}}]^{1/n}}$$

or

$$\frac{[a_{A^{m+}}]^{1/m}}{[a_{B^{n+}}]^{1/n}} < \exp\left[\frac{F}{RT}(E_A^{\circ} - E_B^{\circ})\right] \quad \dots (2.11)$$

By definition

$$a_{A^{m+}} = f_{A^{m+}} \cdot [A^{m+}] \quad \dots (2.12)$$

and

$$a_{B^{n+}} = f_{B^{n+}} \cdot [B^{n+}] \quad \dots (2.13)$$

where $f_{A^{m+}}$ and $f_{B^{n+}}$ are the activity coefficients of the ion A^{m+} and B^{n+} respectively and $[A^{m+}]$ and $[B^{n+}]$ are the analytical concentrations of the ions A^{m+} and B^{n+} respectively. Therefore, relation (2.11) can be rewritten as:

$$\frac{[A^{m+}]^{1/m}}{[B^{n+}]^{1/n}} < \frac{f_{B^{n+}}^{1/n}}{[f_{A^{m+}}]^{1/m}} \exp\left[\frac{F}{RT}(E_A^{\circ} - E_B^{\circ})\right] \quad \dots (2.14)$$

From the relationship (2.14), it is clear that, for a clear understanding of the thermodynamics of cementation, a knowledge of the variation of the activity coefficients with concentration of the ions in solution is most essential. For dilute solutions activity coefficient can be taken to be equal to 1, so that

$$f_{B^{n+}} = f_{A^{m+}} = 1 \quad \dots (2.15)$$

The relation (2.14) can, therefore, be expressed as

$$\frac{[A^{m+}]^{1/m}}{[B^{n+}]^{1/n}} < \exp \left[\frac{F}{RT} (E_A^{\circ} - E_B^{\circ}) \right] \quad \dots (2.16)$$

from the above relation, it is clear that as the driving potential ($E_A - E_B$) increases, the concentration of metal ion B^{n+} in solution decreases. The cementation reaction will proceed until the driving potential ($E_A - E_B$) approaches zero, the condition at which the metals and ions have approached equilibrium.

The condition for equilibrium is given by

$$\frac{[A^{m+}]^{1/m}}{[B^{n+}]^{1/n}} = \exp \left[\frac{F}{RT} (E_A^{\circ} - E_B^{\circ}) \right] \quad \dots (2.17)$$

or

$$\ln \frac{[A^{m+}]^n}{[B^{n+}]^m} = \frac{nmF}{RT} (E_A^{\circ} - E_B^{\circ}) \quad \dots (2.18)$$

where, $[A^{m+}]^n / [B^{n+}]^m =$ equilibrium constant, K , for the cementation reaction. Therefore,

$$K = \exp \left[\frac{nmF}{RT} (E_A^{\circ} - E_B^{\circ}) \right] \quad \dots (2.19)$$

Calculated values of the equilibrium constant, K , for different cementation systems, using relation (2.19) and data from Table 2.1 are given in Table 2.2. These values show that invariably in all the cementation

TABLE-2.1 : Standard Half-cell Potentials at 25°C *

Half cell	E° Volts	Half cell	E°, Volts
$\text{Al} = \text{Al}^{3+} + 3\bar{e}$	+ 1.660	$\text{H}_2 = 2\text{H}^+ + 2\bar{e}$	0.000
$\text{Zn} = \text{Zn}^{2+} + 2\bar{e}$	+ 0.763	$\text{Bi} = \text{Bi}^{3+} + 3\bar{e}$	-0.320
$\text{Fe} = \text{Fe}^{2+} + 2\bar{e}$	+ 0.440	$\text{Cu} = \text{Cu}^{2+} + 2\bar{e}$	-0.337
$\text{Cd} = \text{Cd}^{2+} + 2\bar{e}$	+ 0.403	$\text{Co} = \text{Co}^{3+} + 3\bar{e}$	-0.400
$\text{In} = \text{In}^{3+} + 3\bar{e}$	+ 0.342	$\text{Cu} = \text{Cu}^+ + \bar{e}$	-0.521
$\text{Co} = \text{Co}^{2+} + 2\bar{e}$	+ 0.277	$\text{Ag} = \text{Ag}^+ + \bar{e}$	-0.799
$\text{Ni} = \text{Ni}^{2+} + 2\bar{e}$	+ 0.250	$\text{Hg} = \text{Hg}^{2+} + 2\bar{e}$	-0.800
$\text{Pb} = \text{Pb}^{2+} + 2\bar{e}$	+ 0.126	$\text{Pd} = \text{Pd}^{2+} + 2\bar{e}$	-0.987
$\text{Fe} = \text{Fe}^{2+} + 2\bar{e}$	+ 0.036		

* Abstracted from reference 59.

TABLE-2.2: Calculated Equilibrium Constants in cementation Reactions at 25°C

Cementation Reaction	Equilibrium constant, K
$3 \text{ Ag}^+ + \text{Al} = 3 \text{ Ag} + \text{Al}^{3+}$	$10^{125.18}$
$2 \text{ Ag}^+ + \text{Cu} = 2 \text{ Ag} + \text{Cu}^{2+}$	$10^{15.68}$
$2 \text{ Ag}^+ + \text{Fe} = 2 \text{ Ag} + \text{Fe}^{2+}$	$10^{42.05}$
$2 \text{ Ag}^+ + \text{Zn} = 2 \text{ Ag} + \text{Zn}^{2+}$	$10^{53.01}$
$2 \text{ Bi}^{3+} + 3\text{Fe} = 2 \text{ Bi} + 3\text{Fe}^{2+}$	$10^{77.38}$
$\text{Cd}^{2+} + \text{Zn} = \text{Cd} + \text{Zn}^{2+}$	$10^{12.21}$
$3 \text{ Cu}^{2+} + 2\text{Al} = 3 \text{ Cu} + 2\text{Al}^{3+}$	$10^{203.33}$
$\text{Cu}^{2+} + \text{Cd} = \text{Cu} + \text{Cd}^{2+}$	$10^{25.11}$
$\text{Cu}^{2+} + \text{Fe} = \text{Cu} + \text{Fe}^{2+}$	$10^{26.37}$
$3 \text{ Cu}^{2+} + 2\text{In} = 3 \text{ Cu} + 2\text{In}^{3+}$	$10^{69.13}$
$\text{Cu}^{2+} + \text{Ni} = \text{Cu} + \text{Ni}^{2+}$	$10^{19.92}$
$\text{Cu}^{2+} + \text{Zn} = \text{Cu} + \text{Zn}^{2+}$	$10^{37.33}$
$\text{Hg}^{2+} + \text{Cu} = \text{Hg} + \text{Cu}^{2+}$	$10^{15.71}$
$\text{Ni}^{2+} + \text{Fe} = \text{Ni} + \text{Fe}^{2+}$	$10^6.44$
$\text{Pb}^{2+} + \text{Fe} = \text{Pb} + \text{Fe}^{2+}$	$10^{-0.65}$
$\text{Pb}^{2+} + \text{Zn} = \text{Pb} + \text{Zn}^{2+}$	$10^{21.62}$
$\text{Pd}^{2+} + \text{Cu} = \text{Pd} + \text{Cu}^{2+}$	$10^{22.06}$

couples used in practice the value from the aqueous phase can be completely removed. The literature review as given in section 1.2, has clearly indicated that the thermodynamic properties of the aqueous phase considerably affects the course of the process. Therefore, their study, though not very important from the point of view of the equilibrium extent of recovery of valuables, is of considerable importance for understanding as well as formulating the kinetics of the reactions involved. Hence, the following sections of this chapter relate to the study of the thermodynamics of aqueous phase containing the salts which are generally present during cementation of copper on iron.

2.2 Experimental

Purified copper-leach-solution which is commonly used in practice for cementation contains copper sulphate and sometimes sulphuric acid at different concentrations. Therefore, the first step to thermodynamic studies is to investigate the variation of the activity coefficient of copper sulphate with its concentration and that of sulphuric acid. During cementation in an inert atmosphere iron passes into solution as ferrous ion, so a study of the effect of ferrous sulphate on the activity coefficient of copper sulphate at various concentrations would also be required. Thus, thermodynamic investigations

for the cementation of copper included the following studies:

- a) Effect of concentration of copper sulphate on its mean activity coefficient.
- b) Effect of concentration of ferrous sulphate on its mean activity coefficient.
- c) Effect of ferrous sulphate on the mean activity coefficient of copper sulphate and vice versa, and,
- d) Effect of sulphuric acid on the mean activity coefficient of copper sulphate as well as ferrous sulphate.

Methods used for the determination of activity coefficient can be classified into two categories; namely, (a) those based on measurement of activity of solvent, and, (b) those based on measurement of activity of solute. The first category which includes vapour pressure, depression of freezing point and elevation of boiling point measurements is not accurate enough for the ionic solutions. Therefore, in the present investigation, E.M.F. method which falls under the second category has been preferred. The E.M.F. cells used for potential measurement can be classified into (a) cells with liquid junctions, and, (b) cells without liquid junctions. In the present case a cell with liquid junction was used.

2.2.1 Experimental set-up:

E.M.F. measurements can be made using a chemical cell which consists of the reversible working electrode, a non-polarisable reference electrode, a salt bridge and the electrolyte. The determination of electrode potentials involves, in principle, the combination of the given electrode with the standard reference electrode and measurement of potential difference between them with a suitable potential measuring device. The chemical cell used in the present work is shown in Fig.2.1. It consisted of a beaker and a round bottom corning glass flask of one litre capacity, fitted with three standard taper joints of corning glass for passing purified nitrogen gas and introducing working electrode, test solution and solution bridge. The working electrode was the pure metal electrode in contact with its own ions. Saturated calomel electrode was selected as standard non-polarisable reference electrode due to its constant and reproducible potential and ease of preparation and use. The electrolytic contact of calomel electrode with the working electrode was achieved through a solution bridge, the orifice of which was the Luggin capillary. The liquid junction potential was minimised by filling-in the same electrolyte at the same concentration to both sides of the cell and into the solution bridge. As the simple E.M.F. measuring devices such as voltmeters often draw

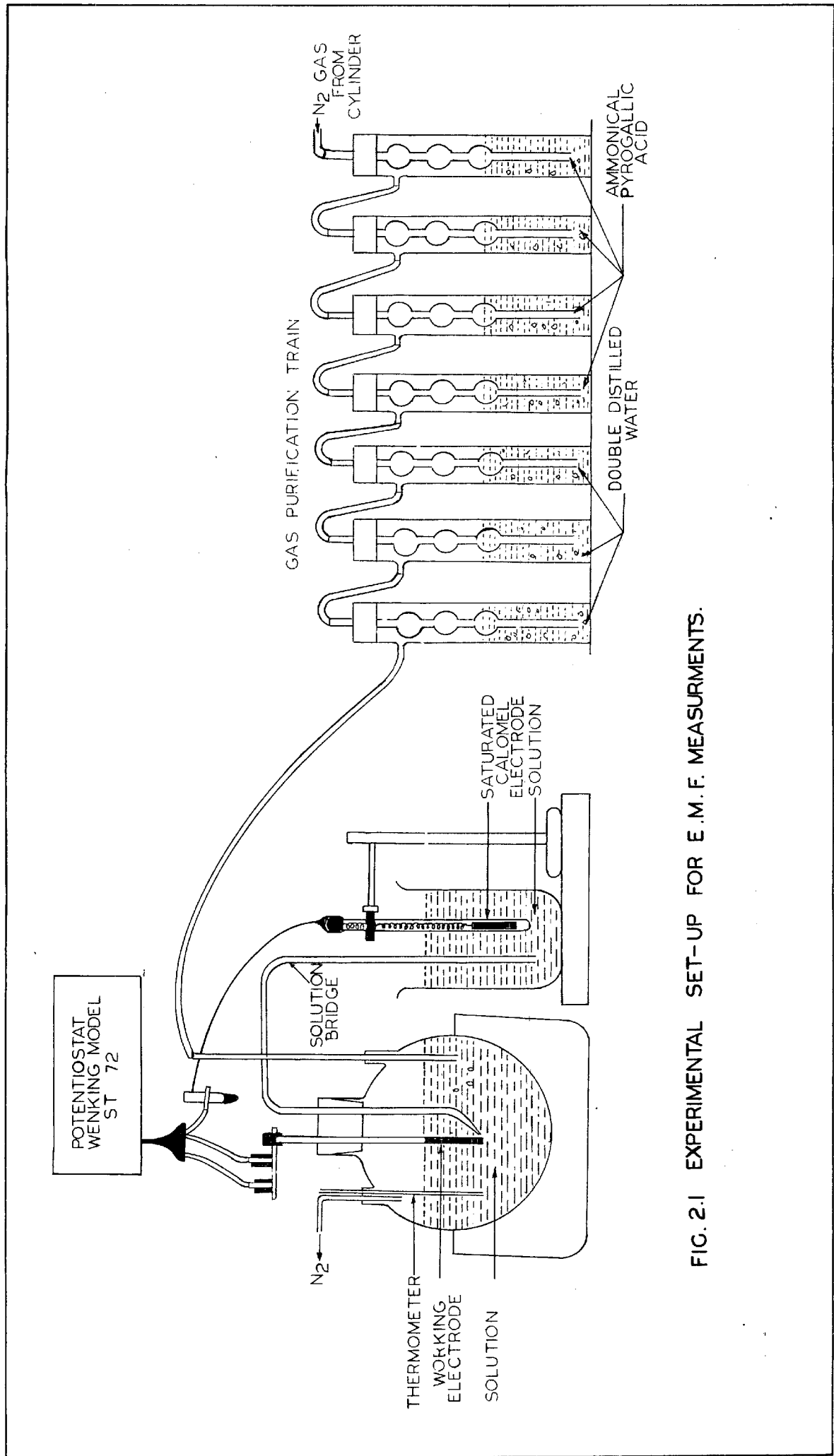


FIG. 2.1 EXPERIMENTAL SET-UP FOR E.M.F. MEASUREMENTS.

a substantial amount of current and, therefore, affect and change the quantity being measured, a standard potentiostat Wenking model ST 72 was used in its potential measurement mode. Pure iron working electrode was fabricated from pure iron powder of electrolytic grade. For this, iron powder was compacted at high pressure and sintered under purified hydrogen gas atmosphere at 1100°C for 3 hours, cooled in hydrogen gas and then rolled and re-reduced and annealed under purified hydrogen gas at 1100°C for 3 hours. Copper electrode was fabricated from the pure electrical conductor grade copper. Nitrogen gas was purified by passing it through three columns of ammonical pyrogallic acid solutions and two columns of double-distilled water and was purged to deaerate the test solution before potential measurements and to maintain a neutral atmosphere over the solution during potential measurements. During the whole process the temperature of the cell was recorded and was controlled at 25°C .

2.2.2 Procedure

2.2.2.1 Preparation of solutions

For the determination of activity coefficient of copper sulphate as a function of its concentration, the solutions of copper sulphate were prepared from analytical reagent grade, B.D.H. make copper sulphate.

For the determination of activity coefficient of ferrous sulphate as a function of its concentration, initially the solution of ferrous sulphate was obtained by dissolving analytical reagent grade, B.D.H. make ferrous sulphate in distilled water. Since the crystals of ferrous sulphate were partially oxidised to ferric state, purified hydrogen gas was passed through the solution for a long time. However, even after 36 hours, the ferrous iron could not exceed 91%. Therefore, the solutions of ferrous sulphate were prepared by using the following method. Pure iron powder of electrolytic grade was added to the deaerated copper sulphate solutions of different initial concentrations and cementation reaction was carried out at high stirring speed under purified nitrogen atmosphere. The amount of iron powder added to each solution was much in excess over the theoretical amount required for complete cementation of all copper present in solution. When the copper was cemented out the solutions were analysed for copper, ferrous and ferric iron. The solutions in which copper and ferric iron could not be detected were diluted to the required ferrous sulphate concentrations. Using these, copper sulphate-ferrous sulphate solutions of different molalities were also prepared.

For the determination of activity coefficient of copper sulphate in copper sulphate-sulphuric acid mixtures

and that of ferrous sulphate in ferrous sulphate-sulphuric acid mixtures, analytical reagent grade, B.D.H. make, sulphuric acid was used for the preparation of the required solutions.

2.2.2.2 Experimental:

The working electrode was polished on emery paper, washed with distilled water, dried, held in benzene vapour for five minutes to remove grease and finally rinsed again with distilled water and dried before use. Electrode was cleaned in a similar way before each experiment. In the calomel reference electrode, freshly prepared saturated solution of potassium chloride obtained from analytic reagent grade, B.D.H. make potassium chloride, was filled up. The test solution was filled in the flask and de-aerated before passing purified nitrogen gas for 40 minutes before potential measurements. The solution bridge was prepared by sucking this solution into the bridge and the beaker. Working and reference electrodes were connected to the terminals of the potentiostat. The potential readings were noted with time and once it attained a constant value this was recorded as the equilibrium E.M.F. of the cell. Nitrogen flow was stopped while measuring the potential.

2.3 Results and Discussions

2.3.1 Mean Activity Coefficient of Copper sulphate in Aqueous solution:

E.M.F. studies on solutions of different concentrations of copper sulphate were conducted at 25°C. Concentrations studied and the corresponding E.M.F. values are given in Table 2.3. In order to calculate the mean activity coefficient of copper sulphate with the help of Nernst equation which is stated below, one requires the knowledge of standard electrode potential E° :

$$E = E^{\circ} + \frac{RT}{ZF} \ln N_{\text{CuSO}_4} + \frac{RT}{ZF} \ln f_{\text{CuSO}_4} \quad \dots (2.20)$$

where, E = Equilibrium potential of the cell

E° = Standard potential of the cell

N_{CuSO_4} = Molal concentration of copper sulphate in the solution

and,

f_{CuSO_4} = Mean activity coefficient of copper sulphate in solution.

To determine E° , a function ψ defined by the following expression is plotted against square root of copper sulphate molality in dilute solution range as shown in Fig. 2.2

$$\psi = E - \frac{RT}{ZF} \ln N_{\text{CuSO}_4} \quad \dots (2.21)$$

TABLE-2.3: E.M.F. data on the cell $\text{Cu}|\text{CuSO}_4||\text{KCl}(\text{Sat.})\text{Hg}_2\text{Cl}_2(\text{S})|\text{Hg}$ at 25°C

S.N.	N_{CuSO_4} (mole/1000 gm)	E.M.F. (mV)	$\text{Log } f_{\text{CuSO}_4}$
1	0.001	8.0	-0.1525
2	0.002	16.0	-0.1824
3	0.005	25.0	-0.2752
4	0.010	31.0	-0.3728
5	0.020	36.0	-0.5044
6	0.035	40.0	-0.6118
7	0.050	43.0	-0.6651
8	0.100	46.0	-0.8644
9	0.200	52.0	-0.9621
10	0.500	57.0	-1.1905
11	1.000	62.0	-1.3220

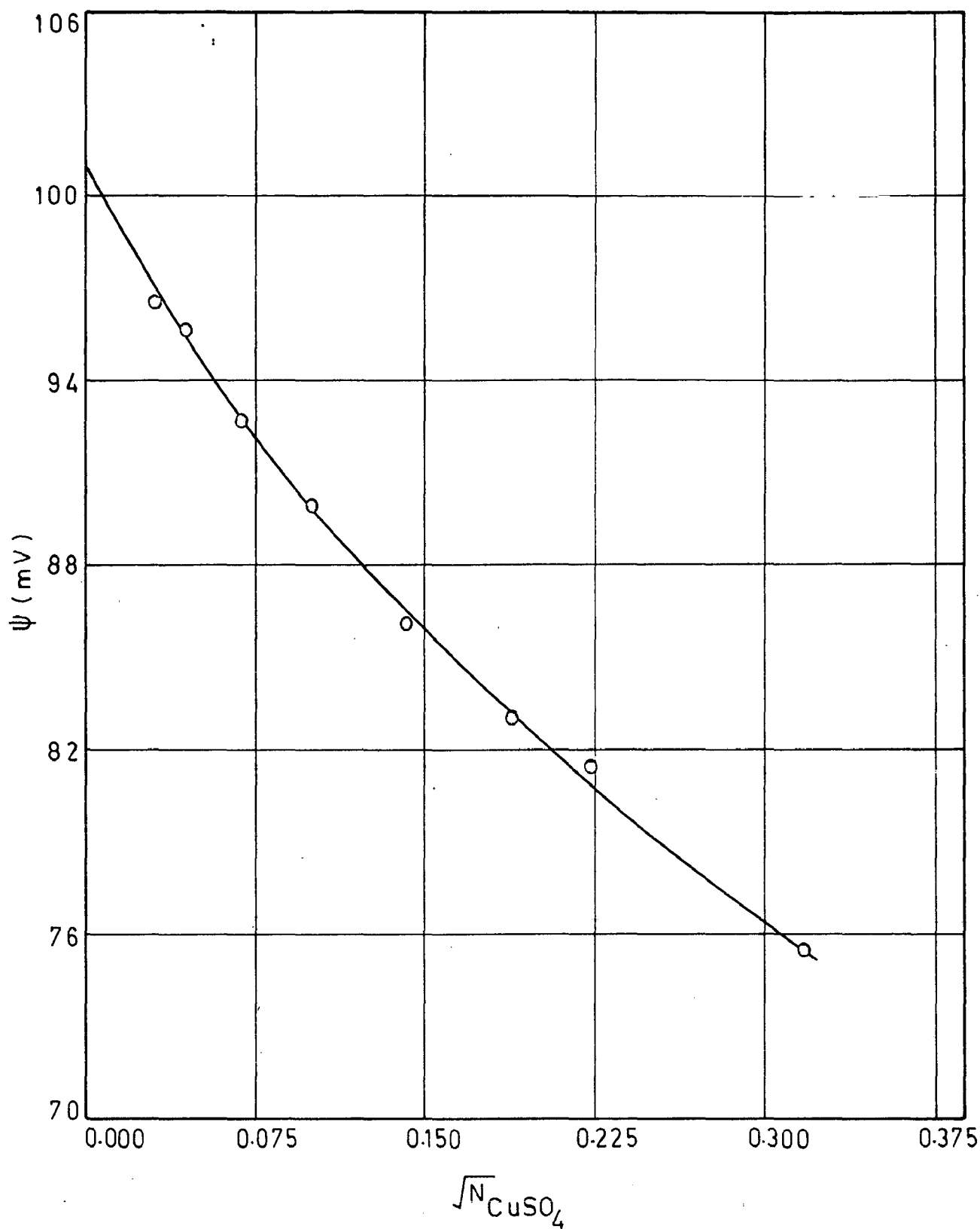


FIG.2.2- ψ AS A FUNCTION OF SQUARE ROOT OF COPPER SULPHATE CONCENTRATION.

From this Figure, a value of $E^{\circ} = 101.0 \text{ mV}$ is obtained. This value corresponds well with the reported literature values^{59,60,61} showing thereby the correct functioning of the cell.

With the help of this E° value and equation(2.20), mean activity coefficient of copper sulphate is calculated as function of its concentration and is plotted in Fig.2.3. Also plotted in this Figure, are the results of other workers⁶²⁻⁶⁴. This Figure shows that agreement between the results of the present study and of other workers is very good. This also serves as an index for the correct functioning of the cell.

Fig. 2.3 shows that, with increase in the concentration of copper sulphate in solution, the activity coefficient goes on decreasing. This fact is in qualitative agreement with the Debye Hückel theory. In order to describe the behaviour of the aqueous solutions quantitatively, a number of relationships have been suggested.

These are as follows:

i) Debye Hückel theory relationship⁶⁵

$$\log f = - \frac{A |z_+ z_-| \sqrt{\mu}}{1 + a B \sqrt{\mu}} \quad \dots (2.22)$$

ii) Limiting Debye-Hückel law⁶⁵

$$\log f = - A |z_+ z_-| \sqrt{\mu} \quad \dots (2.23)$$

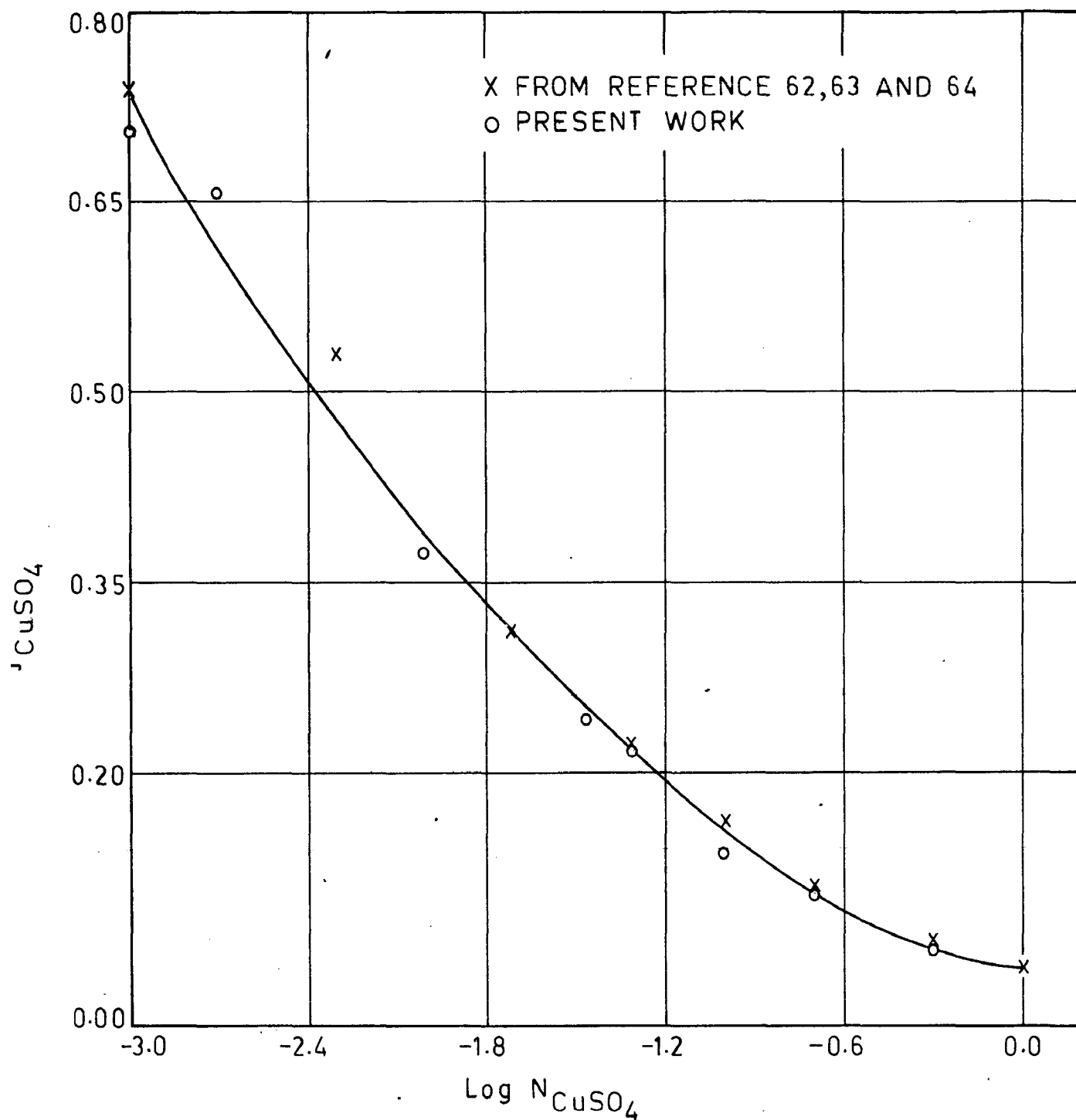


FIG. 23 ACTIVITY COEFFICIENT OF COPPER SULPHATE VS. ITS CONCENTRATION.

iii) Güntelberg relationship⁶⁶

$$\log f = - \frac{A |Z_+ Z_-| \sqrt{\mu}}{1 + \sqrt{\mu}} \dots (2.24)$$

iv) Hückel equation⁶⁷

$$\log f = - \frac{A |Z_+ Z_-| \sqrt{\mu}}{1 + a B \sqrt{\mu}} + C \cdot \mu \dots (2.25)$$

v) Guggenheim relationship⁶⁸

$$\log f = - \frac{A |Z_+ Z_-| \sqrt{\mu}}{1 + \sqrt{\mu}} + C \cdot \mu \dots (2.26)$$

In the above expressions, Z_+ and Z_- are the valencies of the cation and anion species respectively, A , B and C are constants depending upon the properties of the ions, and μ represents the ionic strength of the solution and is defined by the expression

$$\mu = \frac{1}{2} \sum_i m_i Z_i^2 \dots (2.27)$$

where m_i is the molality of i^{th} ion and Z_i is its valency. In order to test the applicability of the above relationships, best-fit curves for suitable values of A , B and C are drawn in Fig. 2.4 for each of these relationships. As all these above relationships can be transformed into a polynomial in $\sqrt{\mu}$ by taking series expansion of the necessary terms, it is thought proper to analyse the present data in terms of polynomials of

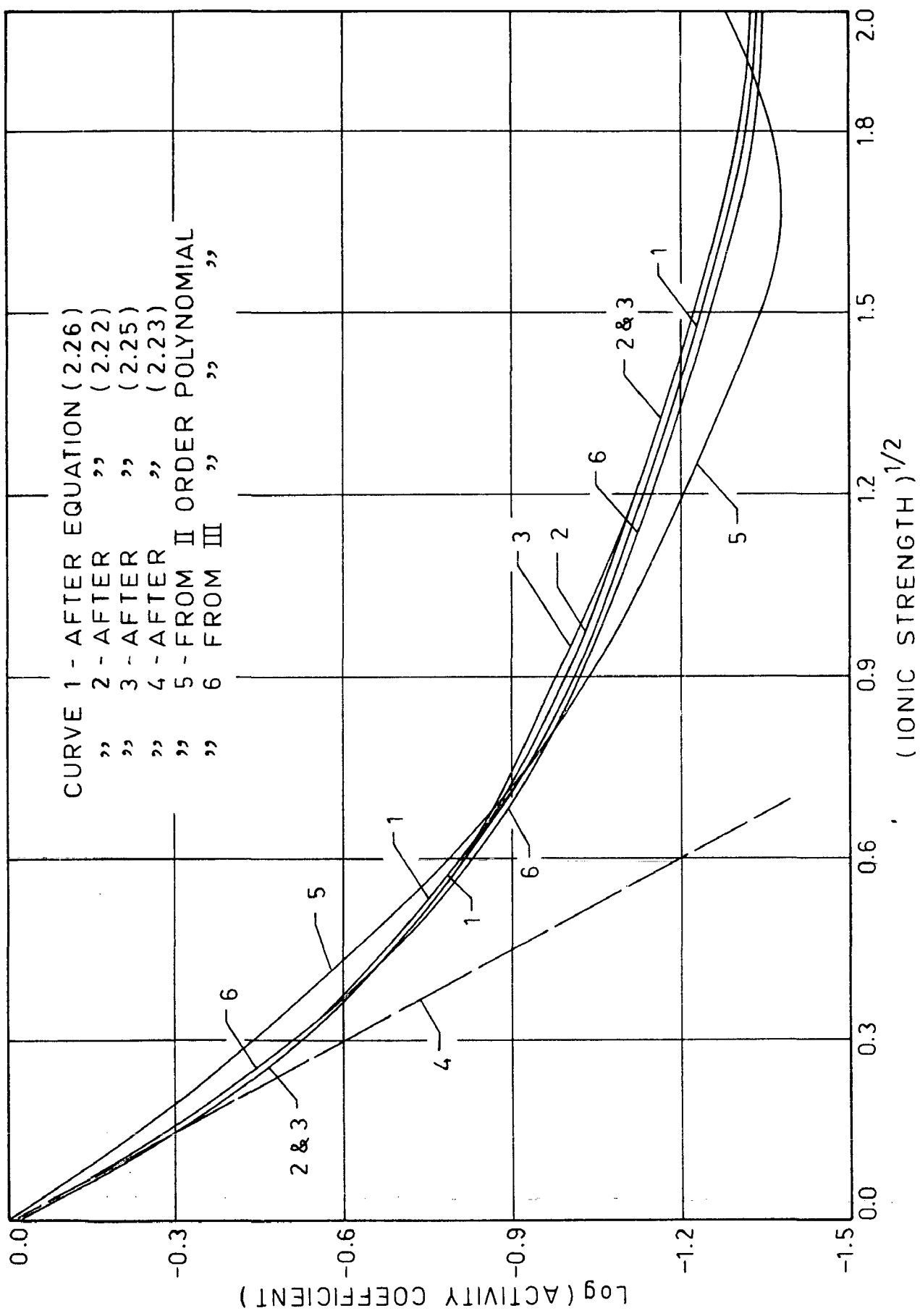


FIG.2.4 COMPARISON OF EXPERIMENTAL WITH THEORETICAL PLOTS FOR ACTIVITY COEFFICIENT OF COPPER SULPHATE.

various degrees. These plots are also drawn in Fig. 2.4, which shows that among all the plots, the experimental data can be most suitably represented by either the following forms of the Hückel relationship

$$\log f = - \frac{2.4048 \sqrt{\mu}}{1 + 1.32 \sqrt{\mu}} - 0.004\mu \quad \dots (2.28)$$

or by the following form of the polynomial of third degree

$$\log f = - 2.0954 \sqrt{\mu} + 1.3872 (\sqrt{\mu})^2 - 0.3389 (\sqrt{\mu})^3 \quad \dots (2.29)$$

Constants found with best fit analysis are in agreement with the literature values^{60,65}. As a concluding remark one can state that the agreement between the present data and the literature values testifies that present set-up can be used for studying the thermodynamic properties of aqueous copper sulphate solutions.

2.3.2 Effect of Sulphuric acid on Activity coefficient of Copper sulphate:

E.M.F. measurements on mixed electrolyte solutions of copper sulphate and sulphuric acid of varying concentrations were conducted at 25°C. Concentrations studied and the corresponding E.M.F. values are given in Table 2.4. To calculate the mean activity coefficient of copper sulphate, Nernst equation (2.20) has been used. To get a clear concept regarding the effect of sulphuric

TABLE-2.4: E.M.F. data on Cell $\text{Cu} | \text{CuSO}_4, \text{H}_2\text{SO}_4 || \text{KCl}(\text{Sat.}) | \text{Hg}_2\text{Cl}_2(\text{s}) | \text{Hg}$ at 25°C

S. No.	N_{CuSO_4} (mole/1000gn)	E.M.F. (V) at Various Concentrations of Sulphuric Acid (mole/1000gn)				
		0.0050	0.0200	0.0500	0.0800	0.1000
1.	0.0200	0.0350	0.0340	0.0320	-	-
2.	0.0400	0.0410	0.0390	0.0380	-	-
3.	0.0600	0.0440	0.0430	0.0420	-	0.0410
4.	0.0800	0.0460	0.0450	0.0440	0.0440	0.0430
5.	0.1000	0.0470	0.0460	0.0460	0.0450	0.0440
6.	0.1200	0.0480	0.0480	0.0470	0.0460	0.0460
7.	0.1400	0.0490	0.0490	0.0480	0.0480	0.0470
8.	0.1600	0.0500	0.0490	0.0490	0.0480	0.0480
9.	0.1800	0.0510	0.0500	0.0500	0.0490	0.0490
10.	0.2000	0.0520	0.0520	0.0510	0.0510	0.0500
11.	0.2200	0.0530	0.0520	0.0520	0.0510	0.0510

acid on the activity coefficient of copper sulphate, a plot of activity coefficient versus square-root of total molality is shown in Fig. 2.5. The top curve in this represents the activity coefficient of sulphuric acid in aqueous solution at 25°C in the absence of any other solute. The lowest curve in this Figure represents the activity coefficient of copper sulphate as a single electrolyte in aqueous solution at 25°C. The third, fourth and fifth curves from the top represent variation in activity coefficient of copper sulphate in solutions of varying total concentrations but fixed mole fractions of copper sulphate: $x_{\text{CuSO}_4} = 0.25$, $x_{\text{CuSO}_4} = 0.5$ and $x_{\text{CuSO}_4} = 0.75$ respectively. The shape of the curves for the mixed electrolyte is similar to that for copper sulphate itself but these curves are somewhat raised. Thus activity coefficient of copper sulphate is increased by the substitution of sulphuric acid for copper sulphate in the solution and as the proportion of sulphuric acid is increased, the activity coefficient of copper sulphate increases. The second curve from the top in the Fig. 2.5 represents the activity coefficient of copper sulphate for the limiting case of zero concentration of copper sulphate in a solution of sulphuric acid.

In order to quantitatively express the effect of sulphuric acid on the activity coefficient of copper sulphate \log of the activity coefficient of copper

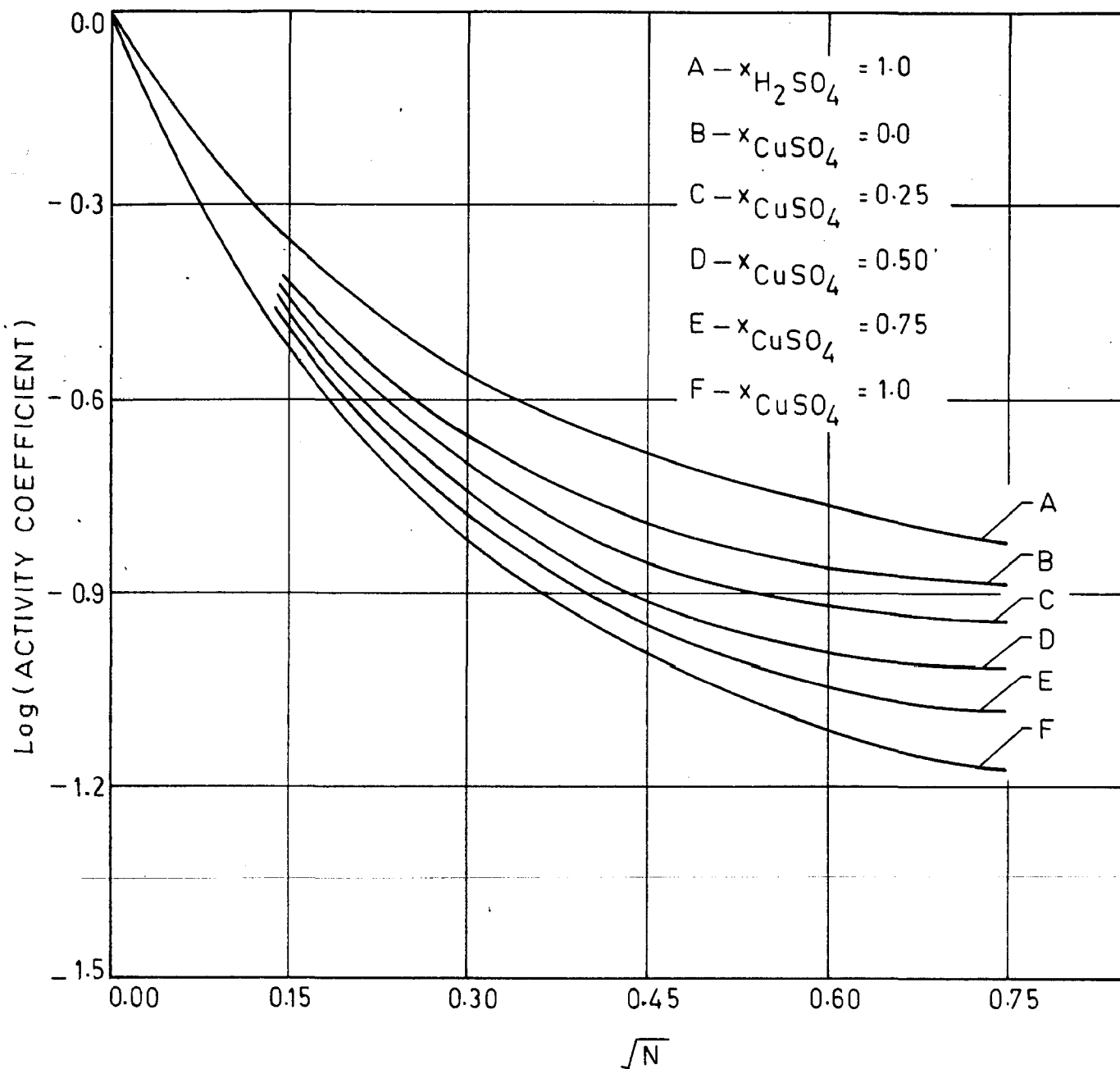


FIG.2.5 MEAN ACTIVITY COEFFICIENTS OF COPPER SULPHATE AND SULPHURIC ACID IN MIXED ELECTROLYTE SOLUTION.

sulphate is plotted against the mole fraction of copper sulphate keeping the total ionic strength of the solution to be constant. Fig. 2.6 shows that these plots are linear in nature as is the case for silver sulphate in magnesium, cadmium, lithium, aluminium and zinc sulphate solutions⁶⁹. Thus one can express the activity coefficient of copper sulphate by the following linear relationship:

$$\log f_{\text{CuSO}_4} = \log f_{\text{CuSO}_4(0)} - \alpha_{\text{CuSO}_4} (1-x_{\text{CuSO}_4}) \dots (2.30)$$

where $f_{\text{CuSO}_4(0)}$ stands for the activity coefficient of copper sulphate in a solution containing copper sulphate only and α is an empirical coefficient. From this Figure, α_{CuSO_4} for various total ionic strengths of the solution is calculated and is plotted against ionic strength in Fig. 2.7. The coefficient α is found to vary with total ionic strength, having a higher value at lower ionic strength and nearly constant value at higher ionic strength.

2.3.3 Mean Activity Coefficient of Ferrous sulphate in Aqueous solution:

E.M.F. measurements on solutions of ferrous sulphate of varying concentrations were made at 25°C. Concentrations studied and the corresponding E.M.F. values are given in Table 2.5. In order to calculate the activity coefficient of ferrous sulphate with the help of Nernst equation, standard electrode potential E° was

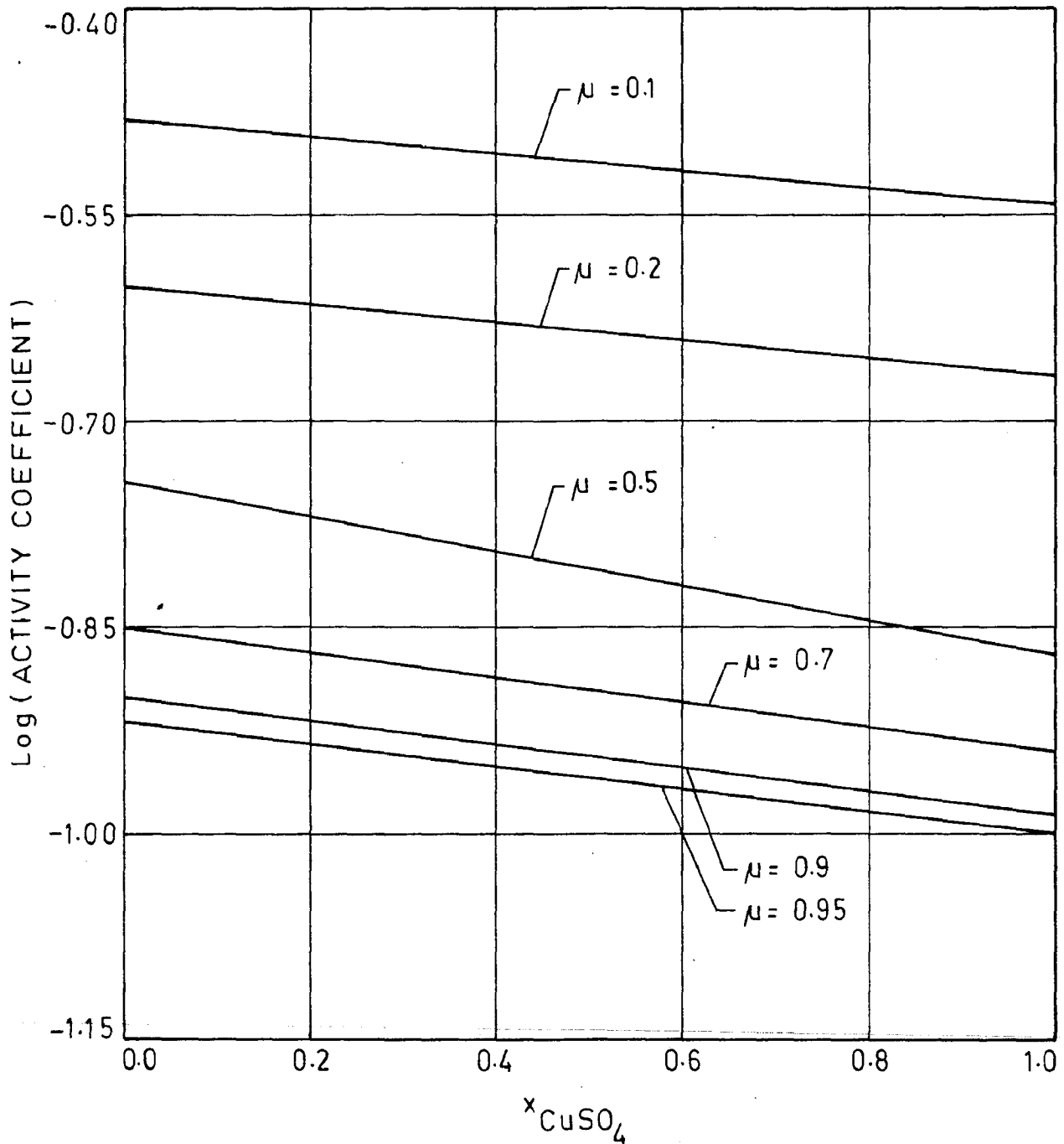


FIG.2.6 ACTIVITY COEFFICIENT OF COPPER SULPHATE IN MIXED ELECTROLYTE SOLUTION OF COPPER SULPHATE AND SULPHURIC ACID AT VARIOUS CONSTANT TOTAL IONIC STRENGTHS.

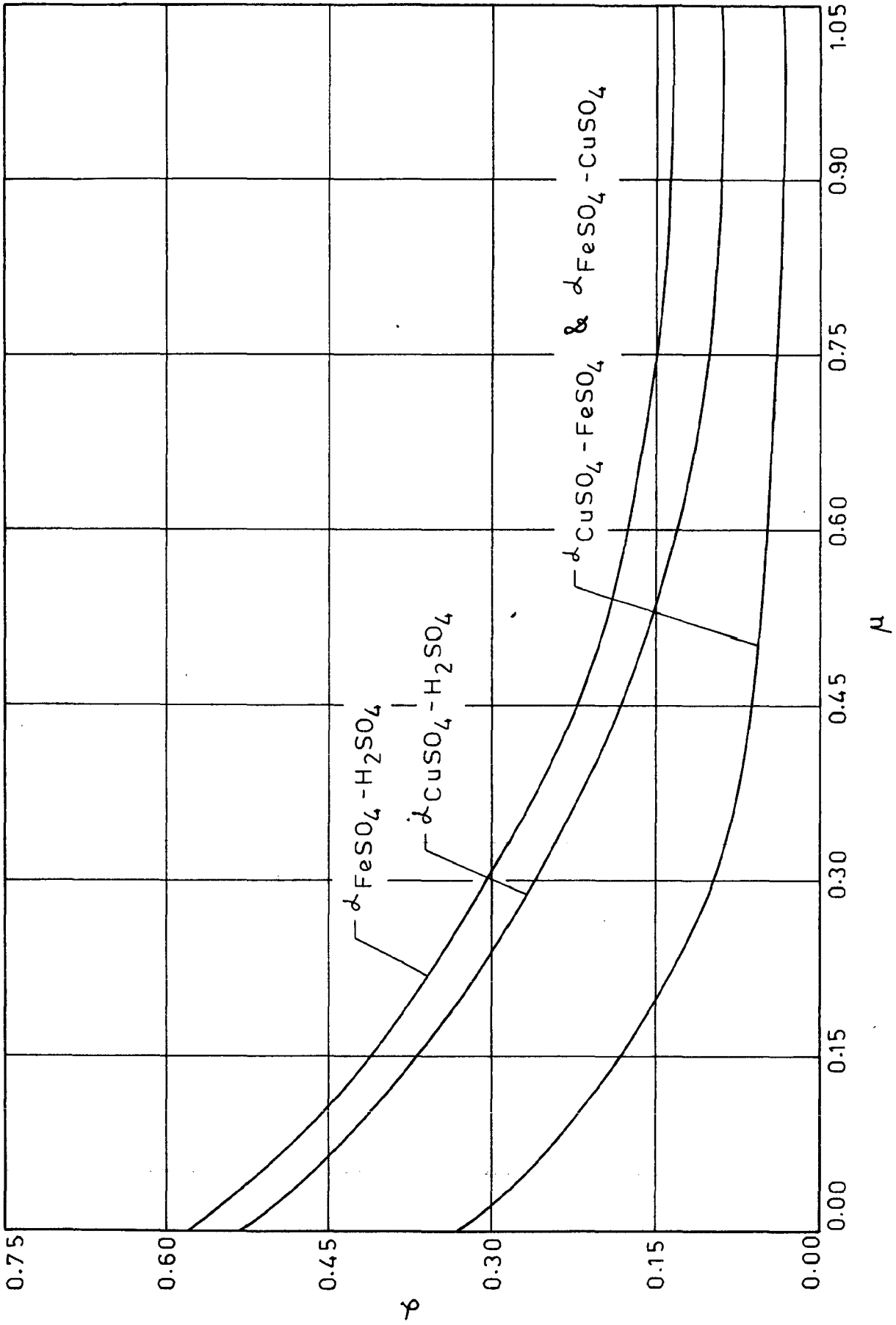
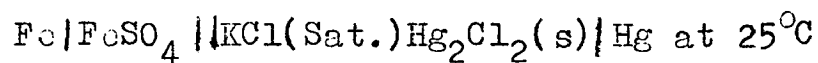
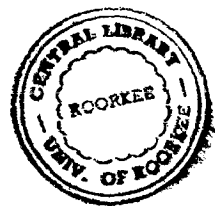


FIG.2.7 EMPIRICAL COEFFICIENT α VS. TOTAL IONIC STRENGTH IN MIXED ELECTROLYTE.

TABLE-2.5 : E.M.F. data on Cell



S. No.	N_{FeSO_4} (mole/1000gm)	E.M.F. (mV)	Log f_{FeSO_4}
1.	0.001	- 779	- 0.1525
2.	0.002	- 772	- 0.2163
3.	0.005	- 763	- 0.3091
4.	0.010	- 757	- 0.4067
5.	0.020	- 752	- 0.5383
6.	0.050	- 746	- 0.7328
7.	0.100	- 742	- 0.8983
8.	0.200	- 737	- 1.0299



175744

CENTRAL LIBRARY UNIVERSITY OF ROORKEE
ROORKEE

obtained by plotting the function ψ against square-root of ferrous sulphate molality in dilute solution range as shown in Fig. 2.8. From this Figure, a value of $E^{\circ} = -686$ mV is obtained. This value is well in agreement with the reported literature values⁵⁹⁻⁶¹ showing thereby the correct functioning of the cell.

With the help of this E° value and the Nernst equation, mean activity coefficient of ferrous sulphate is calculated as a function of its concentration and is plotted in Fig. 2.9. For a quantitative description of the behaviour of this aqueous solution, the relationships (2.22) to (2.26) have been used and the best-fit curves for each of these relationships are also drawn in Fig. 2.9 using suitable values of constants A, B and C. The present data have also been analysed in terms of polynomials of various degrees. These plots are also shown in Fig. 2.9 which shows that among all the plots the experimental data can be most suitably represented by either the following form of the Guggenheim relationship:

$$\log f = - \frac{2.5114 \sqrt{\mu}}{1 + \sqrt{\mu}} + 0.1938\mu \quad \dots (2.31)$$

or by the following form of the polynomial of third order:

$$\log f = -2.4170 \sqrt{\mu} + 1.9893 (\sqrt{\mu})^2 - 0.6425(\sqrt{\mu})^3 \quad \dots (2.32)$$

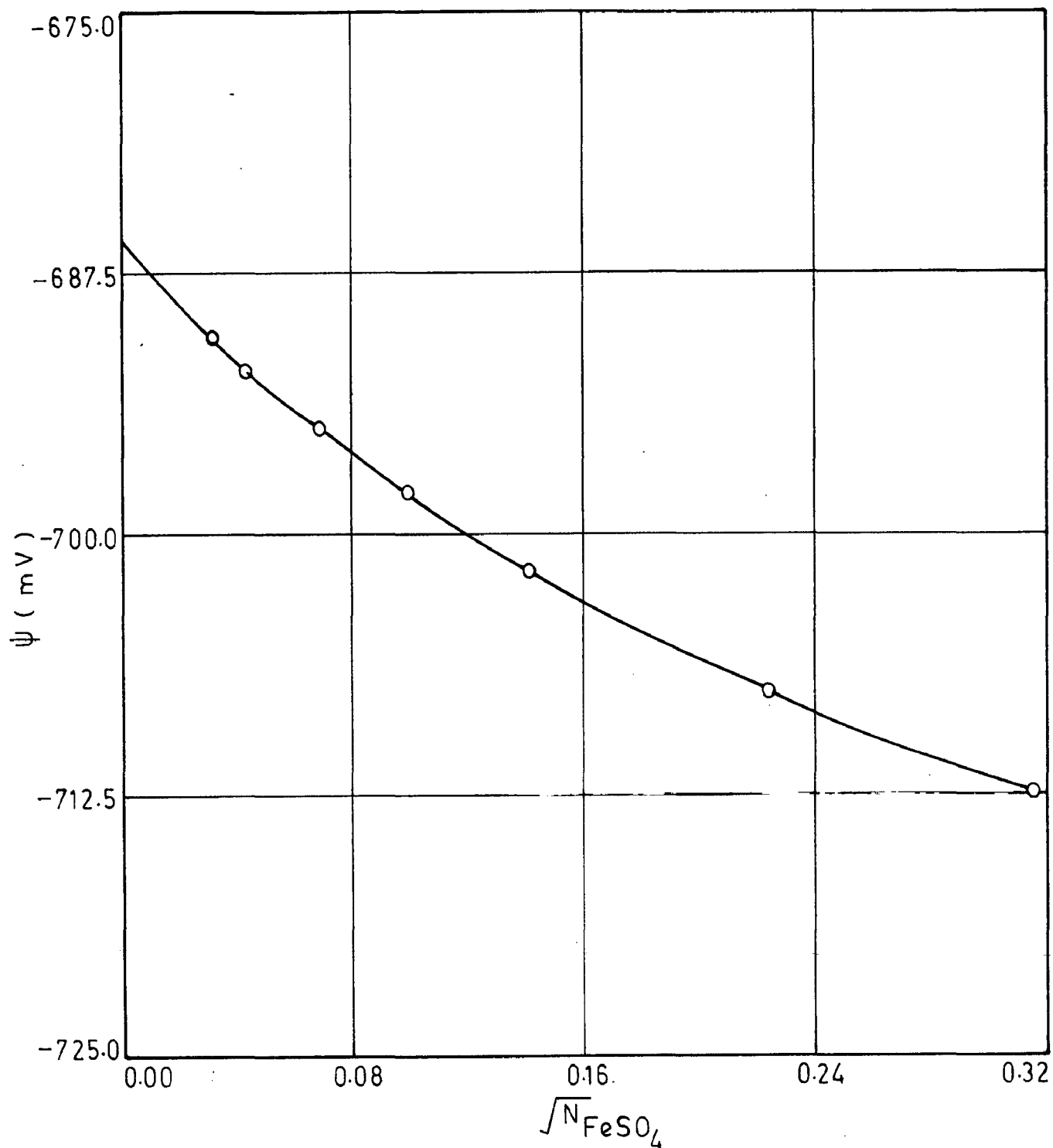


FIG.2.8- ψ AS A FUNCTION OF SQUARE ROOT OF FERROUS SULPHATE CONCENTRATION.

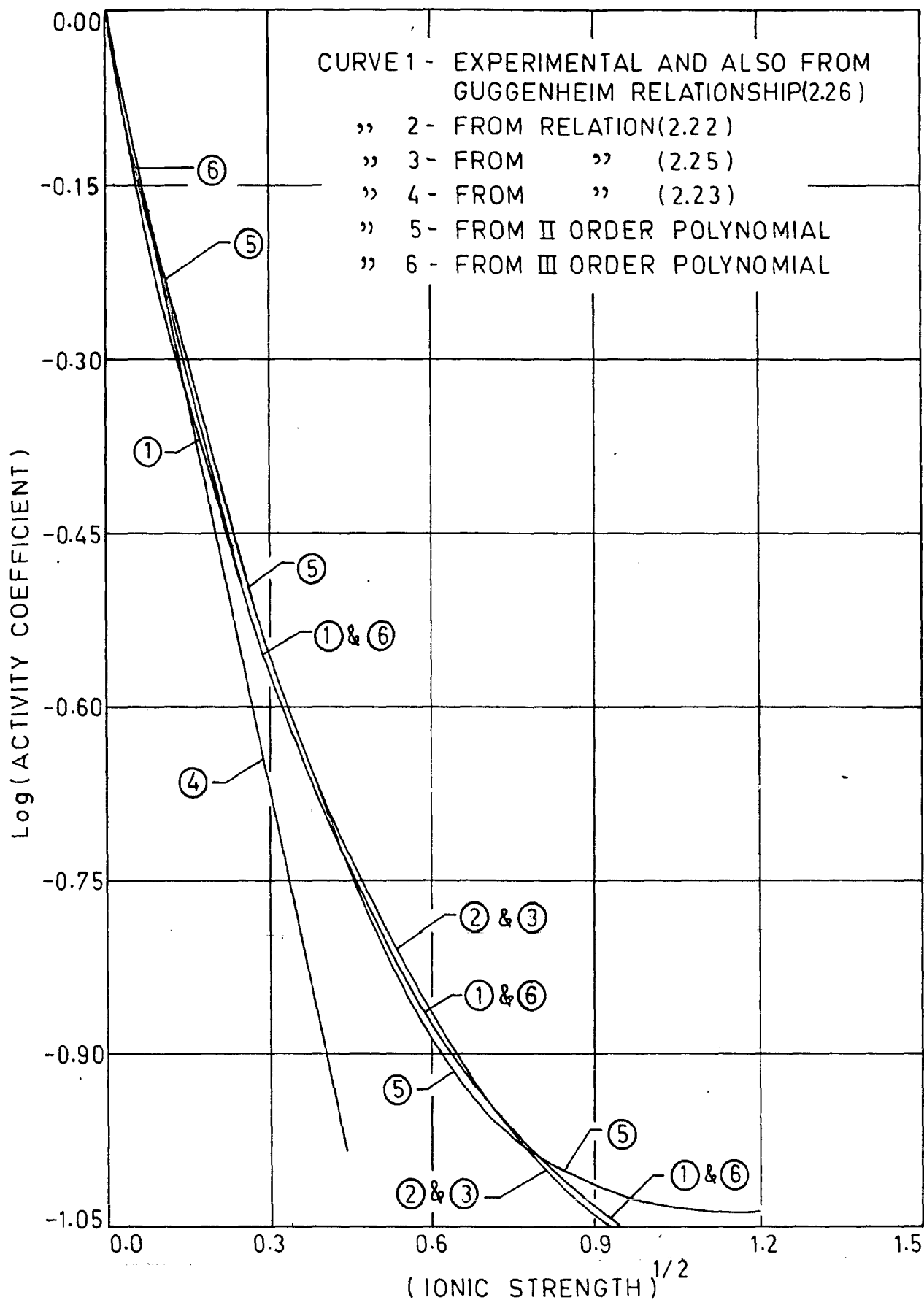


FIG. 2.9 COMPARISON OF EXPERIMENTAL WITH THEORETICAL PLOTS FOR ACTIVITY COEFFICIENT OF FERROUS SULPHATE.

This system has not yet been studied merely because of difficulty in making this solution which is capable of getting quickly oxidised under atmospheric conditions. The method presently employed suggests a method of experimental study of such solution and has provided the data on this as yet unknown important solution.

From Debye-Hückel theory it is seen that the activity coefficient of an ionic solute is a function of its ionic radius. Ionic radius of iron (Fe^{2+}) is nearly equal to that of zinc (Zn^{2+}) and is greater than that of copper (Cu^{2+}). In order to compare activity coefficient of copper sulphate with that of ferrous sulphate, activity coefficient of various sulphates is plotted against the square-root of ionic strength in Fig. 2.10. It is seen from this Figure that copper sulphate and zinc sulphate show very similar behaviour as predicted by Debye-Hückel theory. From the present data, constants A and C are found to be 0.6278 and 0.1938 respectively for ferrous sulphate solution at 25°C .

2.3.4 Effect of Sulphuric acid on Activity coefficient of Ferrous sulphate:

E.M.F. studies on mixed electrolyte solutions of ferrous sulphate and sulphuric acid of varying concentrations were conducted at 25°C . Concentrations studied

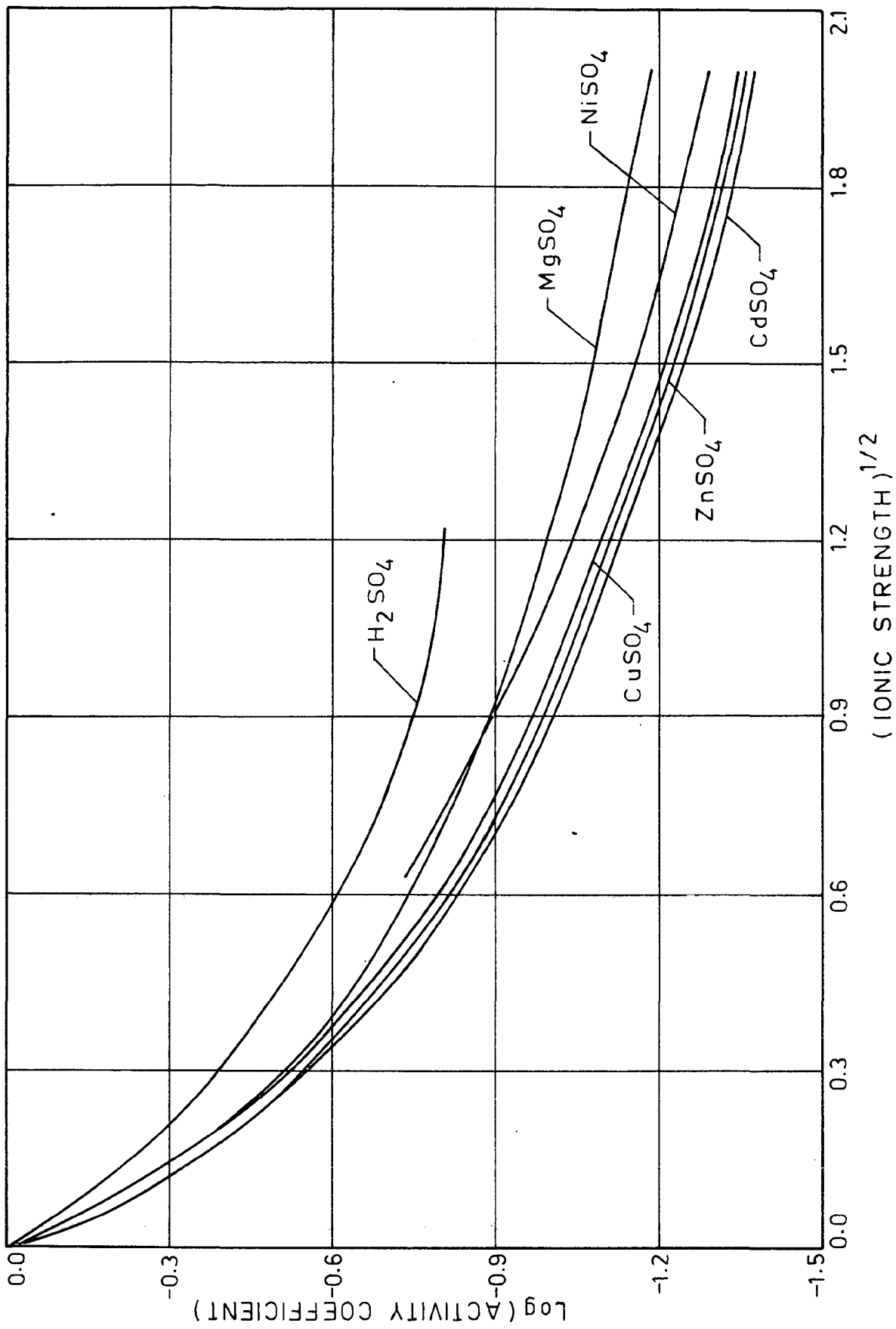
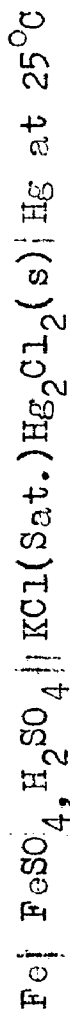


FIG.2.10 Log (ACTIVITY COEFFICIENT) VS. SQUARE ROOT OF IONIC STRENGTH.

and E.M.F. values are given in Table 2.6. Mean activity coefficient of ferrous sulphate is calculated with the help of Nernst equation and a plot of activity coefficient versus square-root of total molality is shown in Fig. 2.11. The top curve in Fig. 2.11 represents the activity coefficient of sulphuric acid in aqueous solution at 25°C in the absence of ferrous sulphate and the lowest curve in this Figure stands for the activity coefficient of ferrous sulphate as the only electrolyte in aqueous solution at 25°C. The third, fourth and fifth curves from the top represent variation in activity coefficient of ferrous sulphate in solutions of different total concentrations but fixed mole fractions of ferrous sulphate, viz., $x_{\text{FeSO}_4} = 0.25$, $x_{\text{FeSO}_4} = 0.50$ and $x_{\text{FeSO}_4} = 0.75$ respectively. It is seen from this Figure that the activity coefficient of ferrous sulphate is increased by the substitution of sulphuric acid for the ferrous sulphate in the solution and as the proportion of sulphuric acid is increased, the activity coefficient of ferrous sulphate increases. The second curve from the top in the Fig. 2.11 represents the activity coefficient of ferrous sulphate for the limiting case of zero concentration of ferrous sulphate in a solution of sulphuric acid.

Linear nature of the plots of the log of the activity coefficient of ferrous sulphate versus its mole fraction for the constant total ionic strength of

TABLE-2.6: E.M.F. data on the Cell



S. No.	N_{FeSO_4} (mole/1000gn)	E.M.F. (V) at Various Concentration of Sulphuric Acid (mole/1000 gn)	0.0050	0.0200	0.0500	0.0800	0.1000
1.	0.0200	-0.751	-0.753	-0.756	-	-	-
2.	0.0400	-0.746	-0.747	-0.749	-	-	-
3.	0.0600	-0.744	-0.744	-0.746	-	-	-0.748
4.	0.0800	-0.741	-0.743	-0.743	-0.745	-0.745	-0.745
5.	0.1000	-0.740	-0.741	-0.742	-0.743	-0.743	-0.743
6.	0.1200	-0.740	-0.740	-0.741	-0.741	-0.741	-0.742
7.	0.1400	-0.738	-0.739	-0.739	-0.740	-0.740	-0.740
8.	0.1600	-0.738	-0.738	-0.739	-0.739	-0.739	-0.740
9.	0.1800	-0.737	-0.737	-0.738	-0.738	-0.738	-0.738
10.	0.2000	-0.736	-0.737	-0.737	-0.737	-0.737	-0.738
11.	0.2200	-0.736	-0.736	-0.736	-0.736	-0.737	-0.737
12.	0.2400	-0.735	-0.735	-0.736	-0.736	-0.736	-
13.	0.2600	-0.734	-0.735	-	-	-	-
14.	0.2800	-0.734	-	-	-	-	-

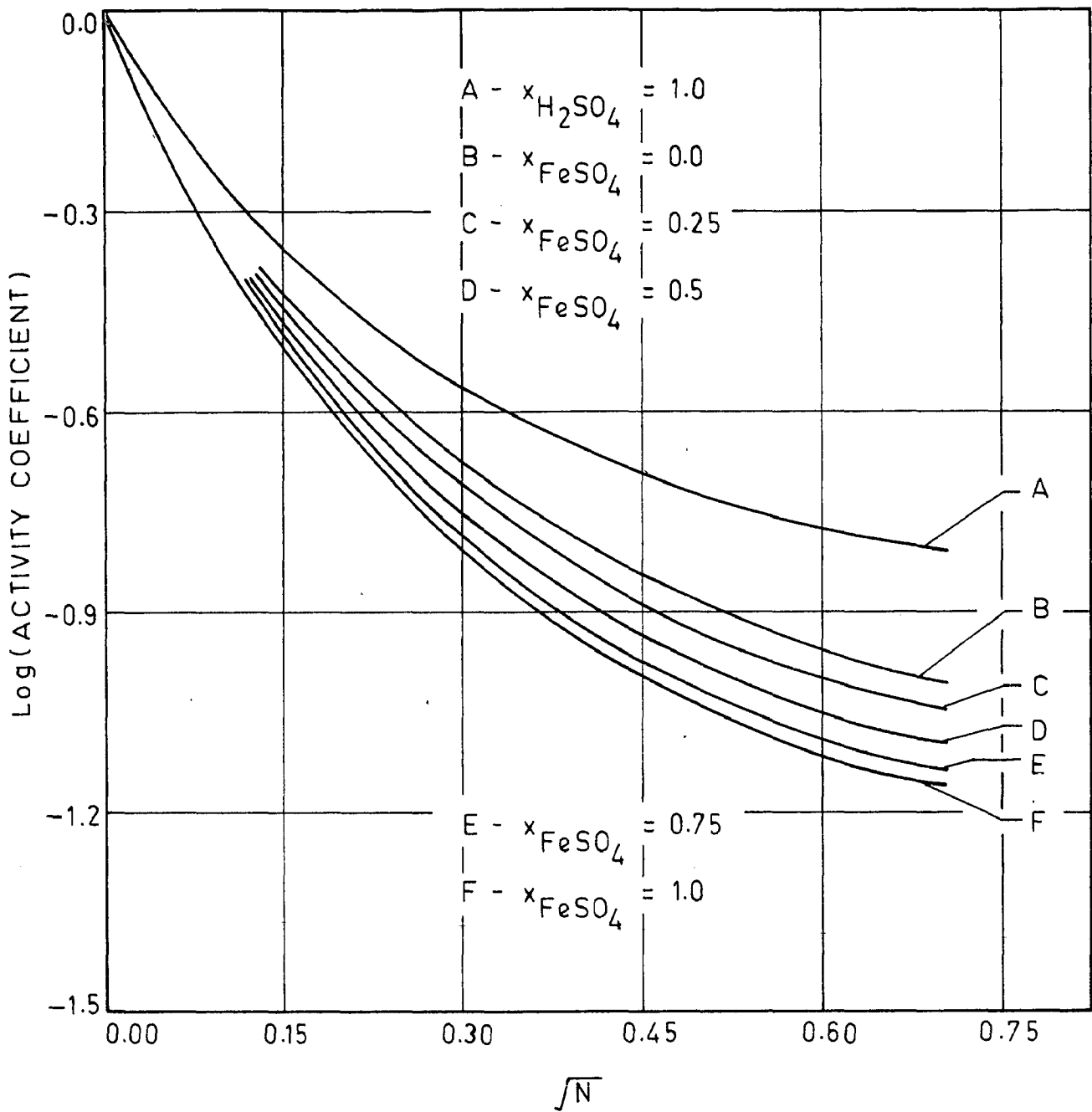


FIG.2.11 MEAN ACTIVITY COEFFICIENTS OF FERROUS SULPHATE AND SULPHURIC ACID IN MIXED ELECTROLYTE SOLUTION.

the solution, as shown in Fig. 2.12, leads to the conclusion that one can express the activity coefficient of ferrous sulphate by the linear relationship:

$$\log f_{\text{FeSO}_4} = \log f_{\text{FeSO}_4(0)} - \alpha_{\text{FeSO}_4} \cdot (1 - x_{\text{FeSO}_4}) \dots (2.33)$$

From this Figure, α_{FeSO_4} for various total ionic strengths of the solution is calculated and is plotted against total ionic strength in Fig. 2.7. The function α is found to vary with ionic strength, having a higher value at lower ionic strength and nearly constant value at higher ionic strength.

2.3.5 Effect of Ferrous sulphate on Activity coefficient of Copper sulphate and vice versa:

E.M.F. studies on mixed electrolyte solutions of copper sulphate and ferrous sulphate of different concentrations were conducted at 25°C. Concentrations studied and E.M.F. measured are given in Table 2.7. To calculate mean activity coefficient of copper sulphate, Nernst equation has been used. A plot of activity coefficient versus square-root of total molality is shown in Fig. 2.13. Also plotted in this Figure are the top curve which stands for the activity coefficient of copper sulphate in aqueous solution at 25°C in the absence of ferrous sulphate and the lowest curve which stands for the

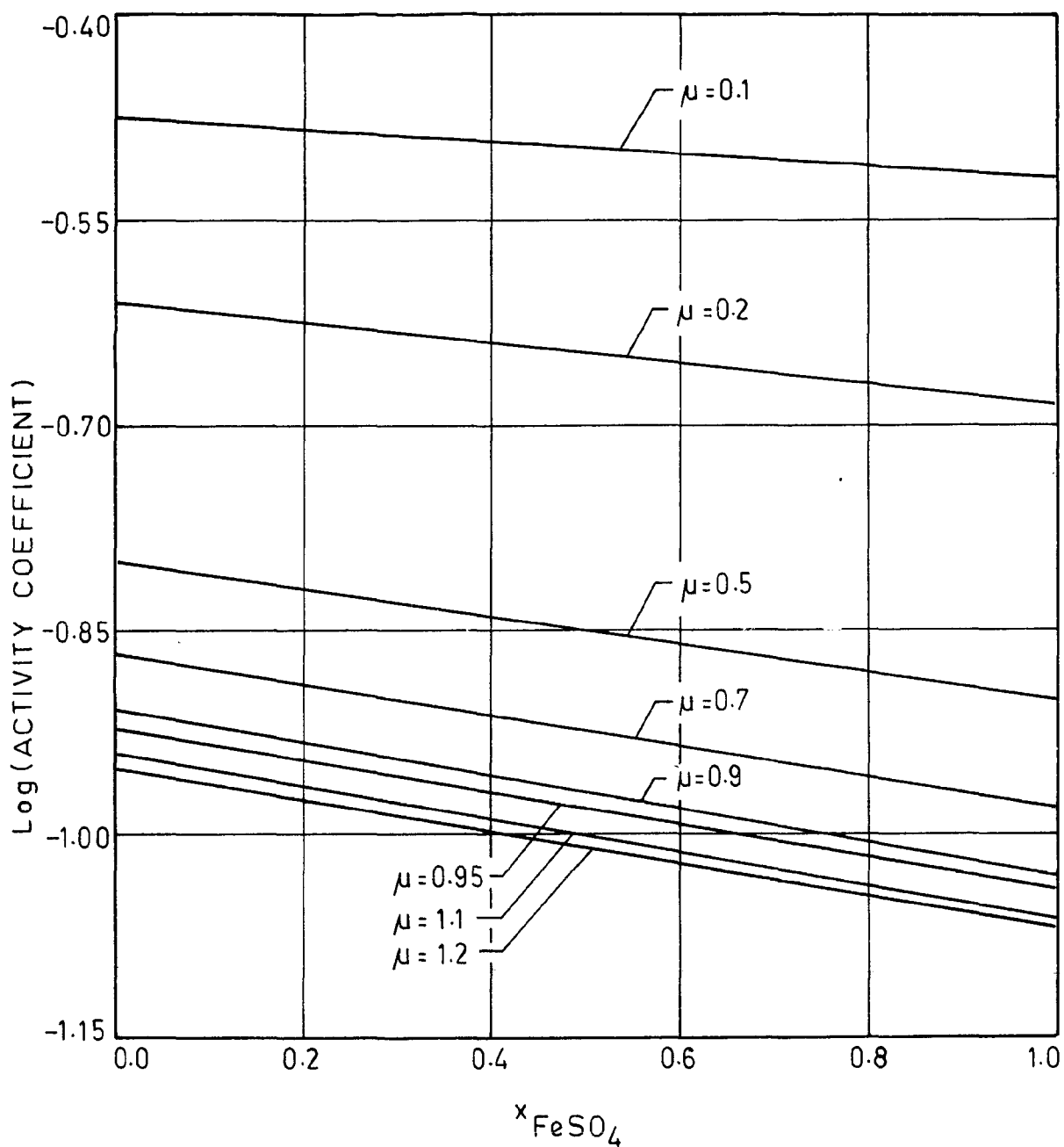
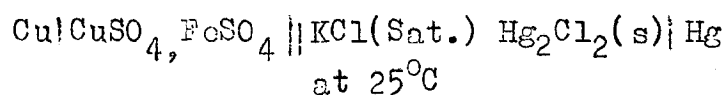


FIG.2.12 ACTIVITY COEFFICIENT OF FERROUS SULPHATE IN MIXED ELECTROLYTE SOLUTION OF FERROUS SULPHATE AND SULPHURIC ACID AT VARIOUS CONSTANT TOTAL IONIC STRENGTHS.

TABLE-2.7: E.M.F. data on the Cell



S. No.	N_{FeSO_4} (mole/1000gn)	N_{CuSO_4} (mole/1000gn)	E.M.F. (V)
1.	0.0005	0.0240	0.0370
2.		0.0520	0.0440
3.		0.0740	0.0450
4.		0.0930	0.0470
5.		0.1120	0.0480
6.		0.1330	0.0490
7.		0.1520	0.0520
8.		0.1740	0.0510
9.		0.2130	0.0520
10.	0.0100	0.0230	0.0350
11.		0.0410	0.0400
12.		0.0830	0.0460
13.		0.1230	0.0480
14.		0.1510	0.0490
15.		0.1830	0.0510
16.		0.2040	0.0520
17.		0.2110	0.0520
18.	0.0250	0.0260	0.0350
19.		0.0430	0.0390
20.		0.0720	0.0430
21.		0.0910	0.0450
22.		0.1120	0.0470
23.		0.1430	0.0480
24.		0.1740	0.0500
25.		0.1930	0.0510
26.		0.2040	0.0510

S. No.	N_{FeSO_4} (mole/1000gm)	N_{CuSO_4} (mole/1000gm)	E.M.F. (V)
27.	0.0500	0.0760	0.0420
28.		0.0930	0.0440
29.		0.1230	0.0460
30.		0.1440	0.0480
31.		0.1640	0.0490
32.		0.1830	0.0500
33.		0.1980	0.0510
34.	0.0750	0.0530	0.0370
35.		0.0720	0.0410
36.		0.0840	0.0420
37.		0.1030	0.0440
38.		0.1340	0.0460
39.		0.1520	0.0470
40.		0.1770	0.0490
41.		0.1940	0.0490
42.	0.1000	0.0270	0.0290
43.		0.0430	0.0340
44.		0.0740	0.0390
45.		0.0910	0.0420
46.		0.1050	0.0430
47.		0.1360	0.0460
48.		0.1580	0.0470
49.		0.1710	0.0480
50.		0.1980	0.0490

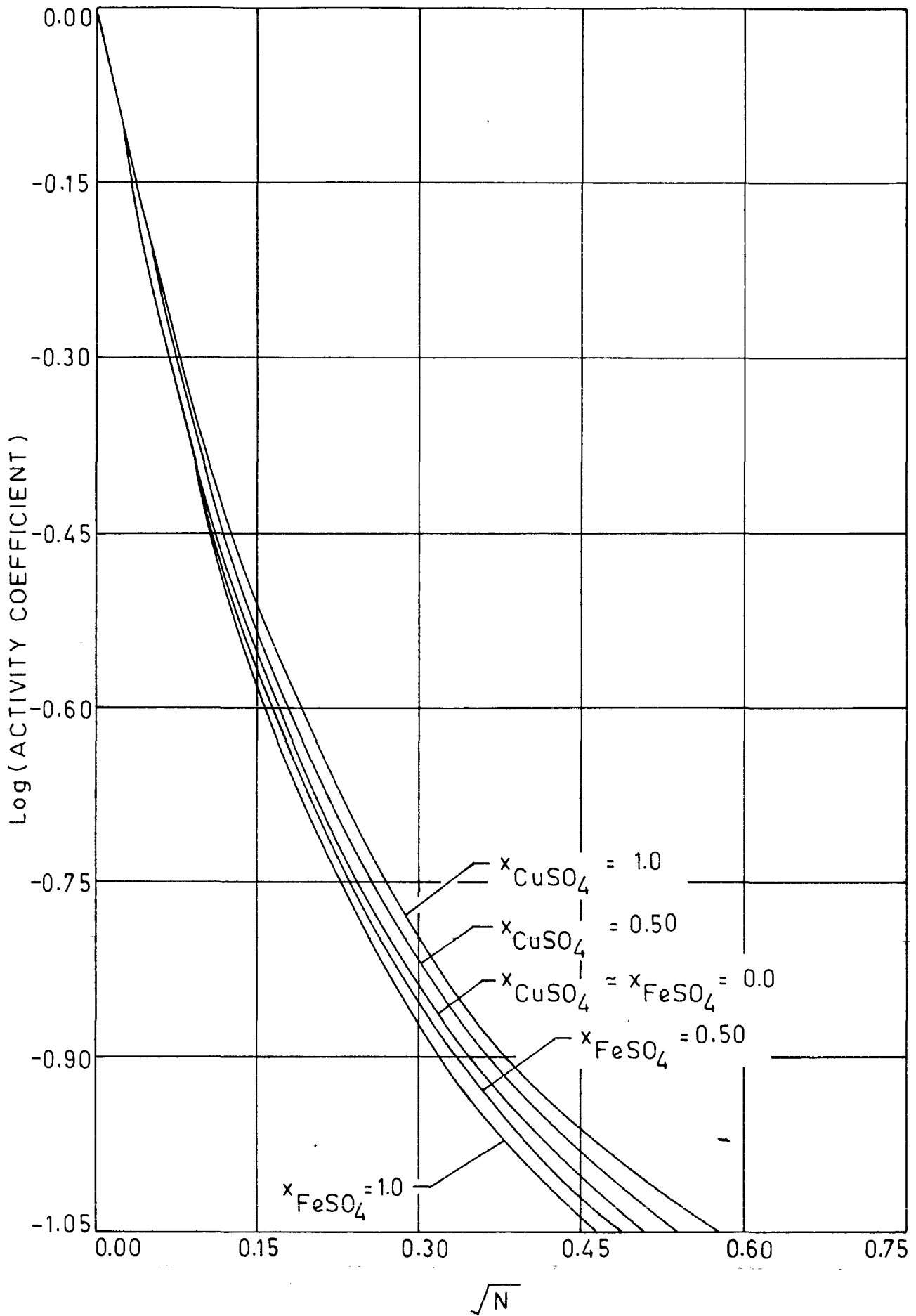


FIG.2.13 MEAN ACTIVITY COEFFICIENTS OF COPPER SULPHATE AND FERROUS SULPHATE IN MIXED ELECTROLYTE SOLUTION.

activity coefficient of ferrous sulphate as the only electrolyte in aqueous solution at 25°C. The second curve from the top represents the activity coefficient of copper sulphate for the limiting case of zero concentration of copper sulphate in a solution of ferrous sulphate. The third curve from the top shows the variation of the activity coefficient of copper sulphate in solution of 0.5 mole fraction of copper sulphate as the total concentration is changed. It is seen from the Figure that the activity coefficient of copper sulphate is lowered by the substitution of ferrous sulphate for the copper sulphate in solution.

To express quantitatively the effect of ferrous sulphate on the activity coefficient of copper sulphate log of the activity coefficient of copper sulphate is plotted against its mole fraction keeping the total ionic strength of the solution constant. Fig. 2.14 shows that these plots are linear in nature which leads to the conclusion that the activity coefficient of copper sulphate can be expressed by the following linear relationship:

$$\log f_{\text{CuSO}_4} = \log f_{\text{CuSO}_4}(0) - \alpha_{\text{CuSO}_4} \cdot (1 - x_{\text{CuSO}_4}) \dots (2.34)$$

From this Figure, function α_{CuSO_4} for various total ionic strengths is calculated and is plotted against

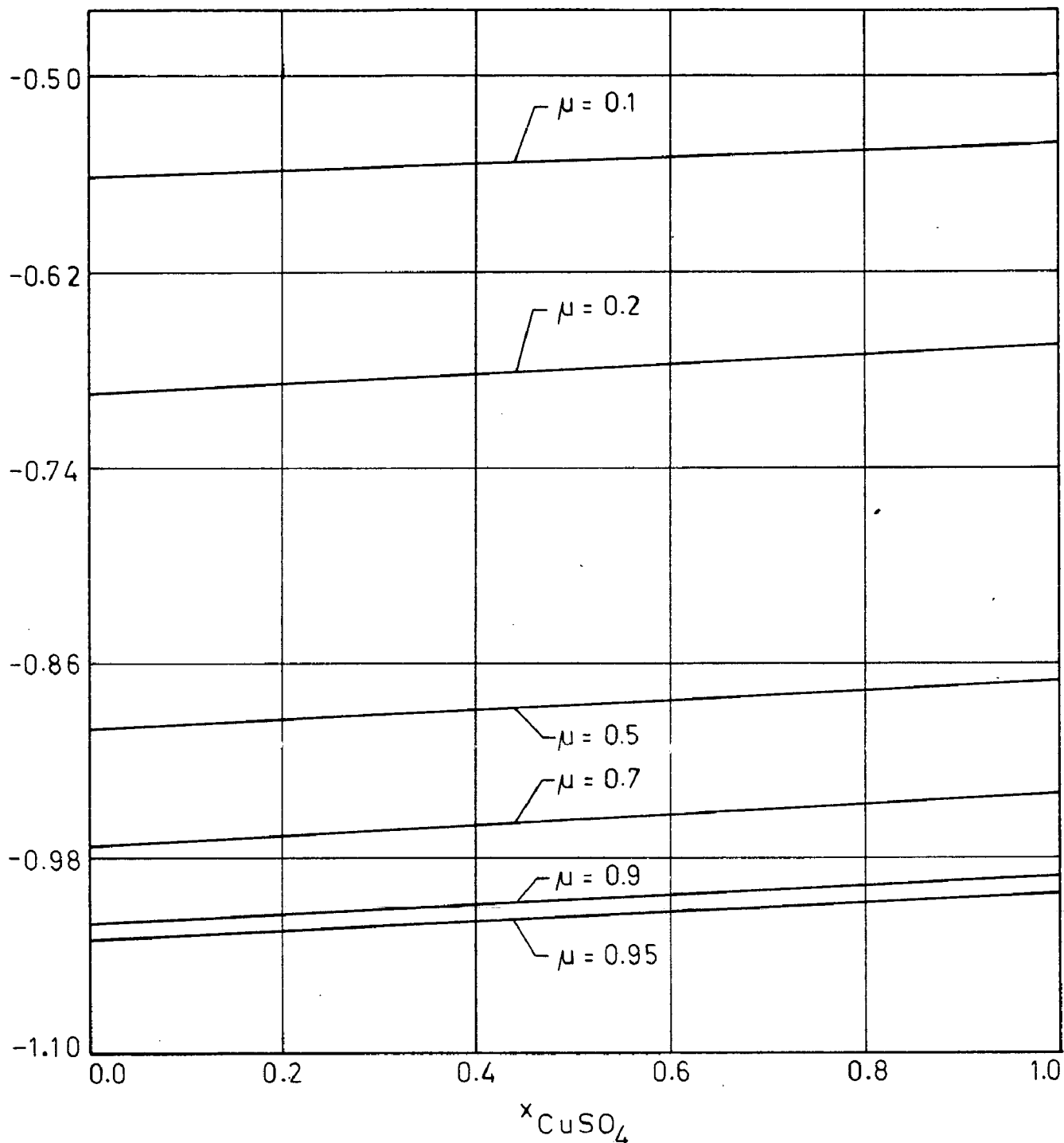


FIG.2.14 ACTIVITY-COEFFICIENT OF COPPER SULPHATE IN MIXED ELECTROLYTE SOLUTION OF COPPER SULPHATE AND FERROUS SULPHATE AT VARIOUS CONSTANT TOTAL IONIC STRENGTHS.

ionic strength in Fig. 2.7. The function is found to vary with ionic strength having a higher value at lower ionic strength and nearly constant value at higher ionic strength.

The effect of copper sulphate on the activity coefficient of ferrous sulphate cannot be studied by E.M.F. measurements since copper would be displaced from the solution by the iron electrode and cemented on it. Therefore, for evaluation of its effect, Gibbs-Duhem equation has been used which in the present case can be written in the following form:

$$x_{\text{CuSO}_4} \cdot d \ln a_{\text{CuSO}_4} + x_{\text{FeSO}_4} \cdot d \ln a_{\text{FeSO}_4} + x_{\text{Water}} \cdot d \ln a_{\text{Water}} = 0 \quad \dots (2.35)$$

where x_{CuSO_4} , x_{FeSO_4} , x_{Water} and a_{CuSO_4} , a_{FeSO_4} , a_{Water} are the mole fractions and activities of electrolytes copper sulphate, ferrous sulphate and water respectively. Since the variation of $\log f_{\text{CuSO}_4}$ in a mixture may be represented by the equation

$$\log f_{\text{CuSO}_4} = \log f_{\text{CuSO}_4(0)} - \alpha_{\text{CuSO}_4} \cdot \mu_{\text{FeSO}_4} \quad \dots (2.36)$$

and assuming that activity coefficient of ferrous sulphate can be written in the form

$$\log f_{\text{FeSO}_4} = \log f_{\text{FeSO}_4(0)} - \alpha_{\text{FeSO}_4} \cdot \mu_{\text{CuSO}_4} \quad \dots (2.37)$$

and

$$\mu_{\text{CuSO}_4} + \mu_{\text{FeSO}_4} = \mu = \text{constant} \quad \dots (2.38)$$

Gibbs-Duhem equation thus can be written in the form:

$$\begin{aligned} \frac{\mu_{\text{CuSO}_4}}{2} \cdot d \ln f_{\text{CuSO}_4} + \frac{\mu_{\text{FeSO}_4}}{2} \cdot d \ln f_{\text{FeSO}_4} + \frac{d\mu_{\text{CuSO}_4}}{2} \\ + \frac{d\mu_{\text{FeSO}_4}}{2} = - 55.51 \, d \ln a_{\text{water}} \end{aligned} \quad \dots (2.39)$$

Introducing the variables $0 \leq x \leq 1$ so that

$$\mu_{\text{CuSO}_4} = x \cdot \mu \quad \dots (2.40)$$

$$\mu_{\text{FeSO}_4} = (1-x) \cdot \mu \quad \dots (2.41)$$

$$d \log f_{\text{CuSO}_4} = - \alpha_{\text{CuSO}_4} \cdot d\mu_{\text{FeSO}_4} = \alpha_{\text{CuSO}_4} \cdot \mu dx \quad \dots (2.42)$$

$$d \log f_{\text{FeSO}_4} = - \alpha_{\text{FeSO}_4} \cdot d\mu_{\text{CuSO}_4} = - \alpha_{\text{FeSO}_4} \cdot \mu dx \quad \dots (2.43)$$

$$d \mu_{\text{CuSO}_4} = - d \mu_{\text{FeSO}_4} \quad \dots (2.44)$$

equation (2.39) becomes

$$\begin{aligned} \left(\frac{\alpha_{\text{CuSO}_4}}{2} + \frac{\alpha_{\text{FeSO}_4}}{2} \right) x \, dx - \frac{\alpha_{\text{FeSO}_4}}{2} \, dx \\ = - \frac{55.5}{2.3 \mu^2} \, d \ln a_{\text{water}} \end{aligned} \quad \dots (2.45)$$

upon suitable rearrangement. Expressing the activity coefficient of water in terms of Osmotic coefficient ϕ in the above relation and integrating the resultant relation over entire range of x , that is, between limits $\alpha = 0$ to $x = 1$, gives the relation:

$$\alpha_{\text{CuSO}_4} - \alpha_{\text{FeSO}_4} = \frac{2}{2.3\mu} (\phi_{\text{CuSO}_4} - \phi_{\text{FeSO}_4}) \quad \dots (2.46)$$

Since ϕ is not known it can be expressed in terms of activity coefficient by the relation

$$\phi = 1 + \frac{1}{\mu} \int_1^f \mu \, d \ln f \quad \dots (2.47)$$

Substitution of the relation (2.47) in equation (2.46) gives the final relation

$$\alpha_{\text{FeSO}_4} = \alpha_{\text{CuSO}_4} - \frac{2}{2.3\mu} \left[\int_1^{f_{\text{CuSO}_4}} \mu \, d \ln f_{\text{CuSO}_4} - \int_1^{f_{\text{FeSO}_4}} \mu \, d \ln f_{\text{FeSO}_4} \right] \quad \dots (2.48)$$

As other functions of this relation are known, α_{FeSO_4} can be calculated by graphical integration of this relation. The calculated values of α_{FeSO_4} are plotted against total ionic strength in Fig. 2.7. The function α_{FeSO_4} is found to vary with ionic strength, having a higher value at lower ionic strength and nearly constant

value at higher ionic strength. From this Figure $\log f_{\text{FeSO}_4}$ is plotted against the mole fraction of ferrous sulphate using total ionic strength as parameter in Fig. 2.15. From this Figure, the limiting value of activity coefficient of ferrous sulphate as well as the activity coefficient of ferrous sulphate for $x_{\text{FeSO}_4} = 0.5$ are calculated as function of total molality of solution and are plotted in Fig. 2.13. The Fig. 2.13 shows that the substitution of copper sulphate for ferrous sulphate in solution increases the activity coefficient of ferrous sulphate. It is also observed that the limiting value of the activity coefficient of ferrous sulphate is the same as that of copper sulphate.

With the reported data and effect of one electrolyte on the activity coefficient of other in the mixed electrolyte solution discussed in previous sections, one can find out the combined effect of sulphuric acid and ferrous sulphate on the activity coefficient of copper sulphate and that of sulphuric acid and copper sulphate on the activity coefficient of ferrous sulphate, since the variation of the activity coefficient of an electrolyte with its mole fraction at constant total ionic strength is linear in nature in all cases.

2.3.6 Overall Driving-force for Cementation Reaction:

In actual cementation system the driving force for

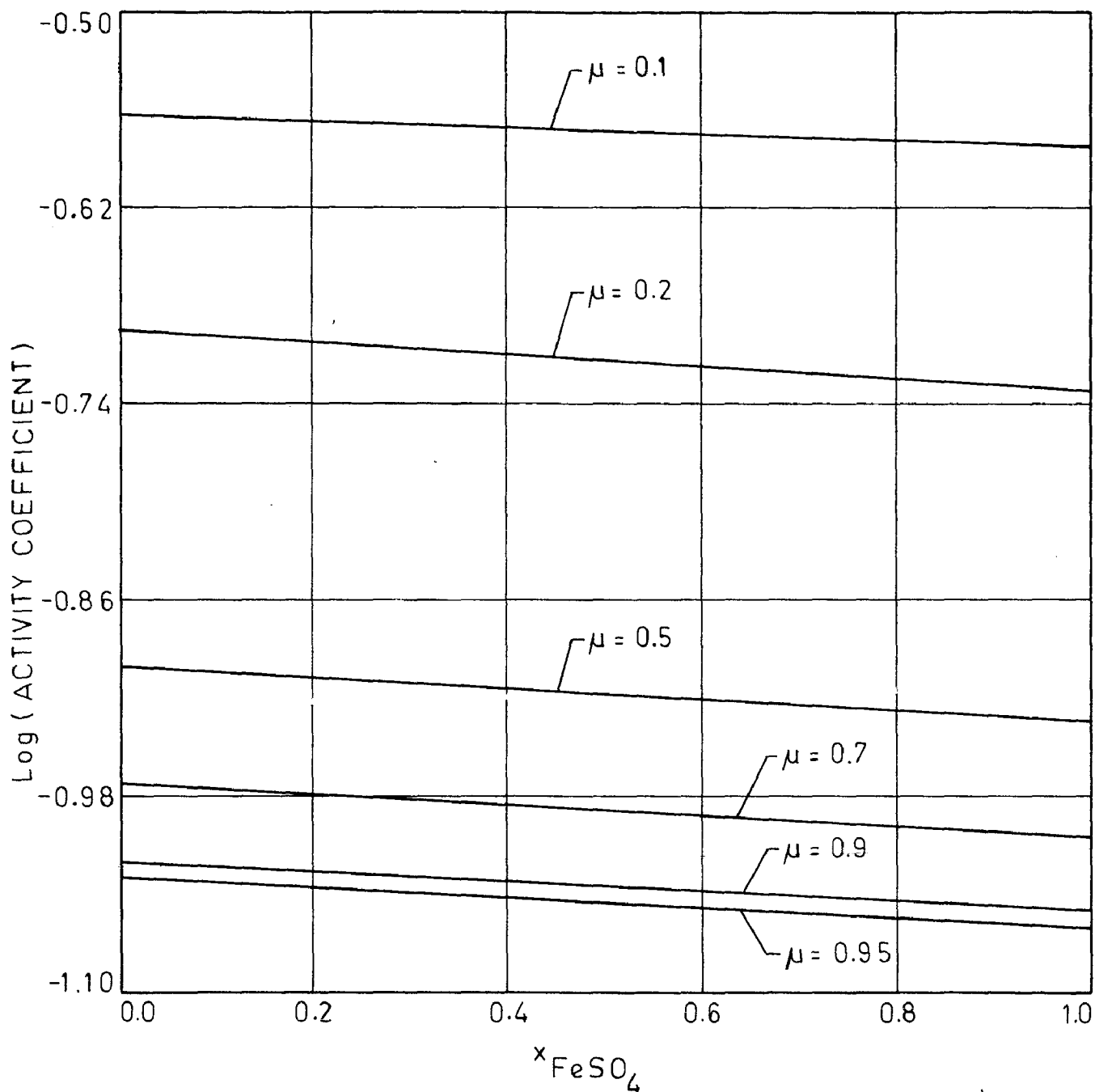


FIG.2.15 ACTIVITY COEFFICIENT OF FERROUS SULPHATE IN MIXED ELECTROLYTE SOLUTION OF FERROUS SULPHATE AND COPPER SULPHATE AT DIFFERENT CONSTANT TOTAL IONIC STRENGTHS.

cementation can be calculated in terms of $(E_{\text{Cu}} - E_{\text{Fe}})$ with the help of Nernst equation. A plot of $(E_{\text{Cu}} - E_{\text{Fe}})$ against $\log \frac{N_{\text{Fe}^{2+}}}{N_{\text{Cu}^{2+}}}$ is shown in Fig. 2.16 for constant total molality. It is seen from this Figure that, (i) the driving force for cementation decreases linearly with increasing replacement of Cu^{2+} by Fe^{2+} from solution, (ii) driving force is higher for higher total molality of the solution at higher $N_{\text{Fe}^{2+}}/N_{\text{Cu}^{2+}}$ ratio but it is lower for higher total molality of the solution at lower $N_{\text{Fe}^{2+}}/N_{\text{Cu}^{2+}}$ ratio, this change in behaviour being due to change in activity coefficient with concentration.

When cementation is carried out in presence of sulphuric acid, the effect of sulphuric acid on the driving force can be evaluated using the equations:

$$\log f_{\text{CuSO}_4} = \log f_{\text{CuSO}_4(0)} + \left[\alpha_{\text{FeSO}_4 - \text{CuSO}_4} \cdot \frac{N_{\text{FeSO}_4}}{(N_{\text{CuSO}_4} + N_{\text{FeSO}_4})} + \alpha_{\text{CuSO}_4 - \text{H}_2\text{SO}_4} \cdot \frac{N_{\text{H}_2\text{SO}_4}}{(N_{\text{H}_2\text{SO}_4} + N_{\text{CuSO}_4})} \right] \cdot \mu \dots (2.49)$$

$$\log f_{\text{FeSO}_4} = \log f_{\text{FeSO}_4(0)} + \left[\alpha_{\text{CuSO}_4 - \text{FeSO}_4} \cdot \frac{N_{\text{CuSO}_4}}{(N_{\text{CuSO}_4} + N_{\text{FeSO}_4})} + \alpha_{\text{FeSO}_4 - \text{H}_2\text{SO}_4} \cdot \frac{N_{\text{H}_2\text{SO}_4}}{(N_{\text{H}_2\text{SO}_4} + N_{\text{FeSO}_4})} \right] \cdot \mu \dots (2.50)$$

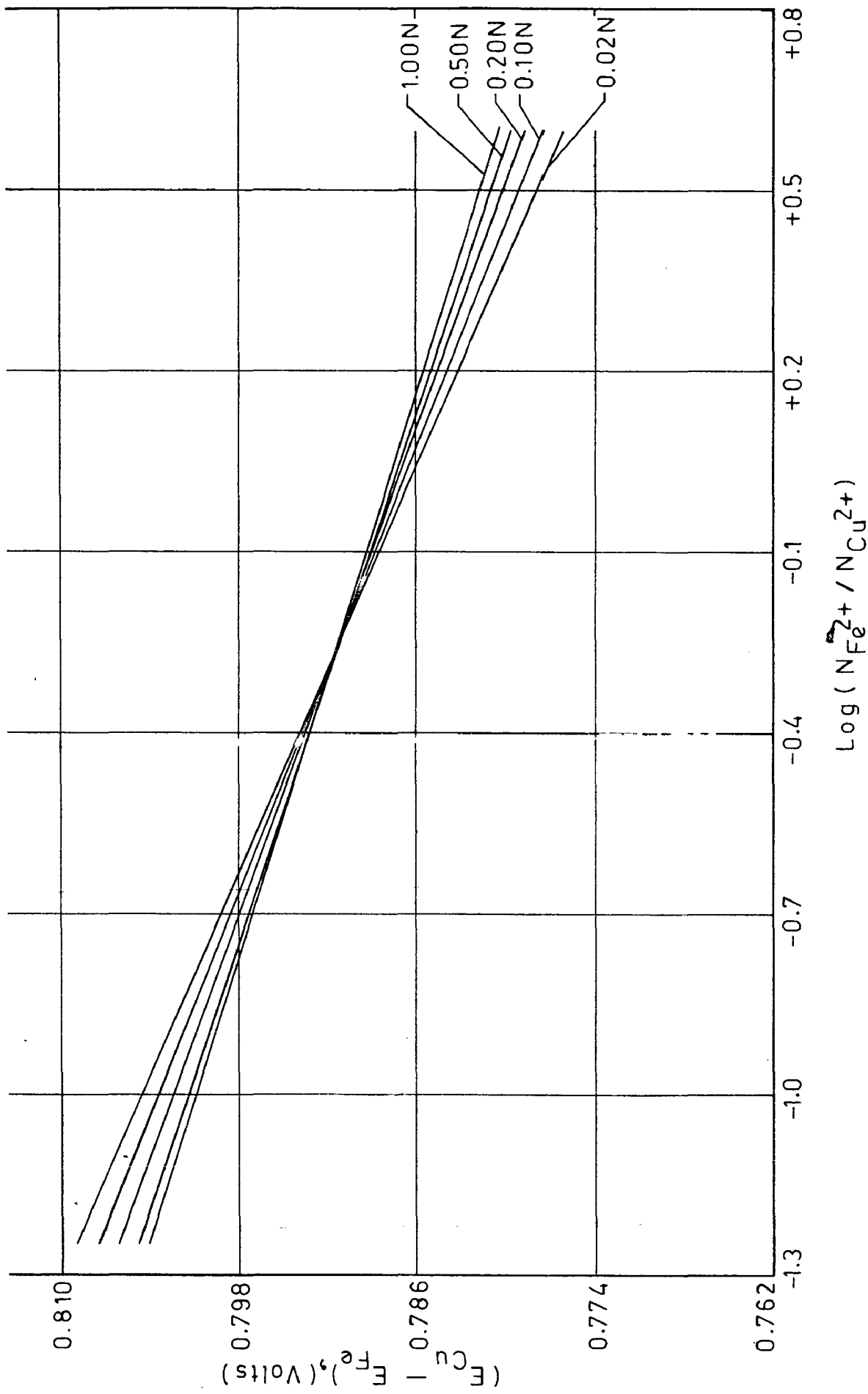


FIG.2.16 ($E_{Cu} - E_{Fe}$) VS. $\text{Log}(N_{Fe^{2+}} / N_{Cu^{2+}})$ AT VARIOUS CONSTANT TOTAL MOLALITY OF COPPER SULPHATE AND FERROUS SULPHATE MIXED ELECTROLYTE SOLUTION.

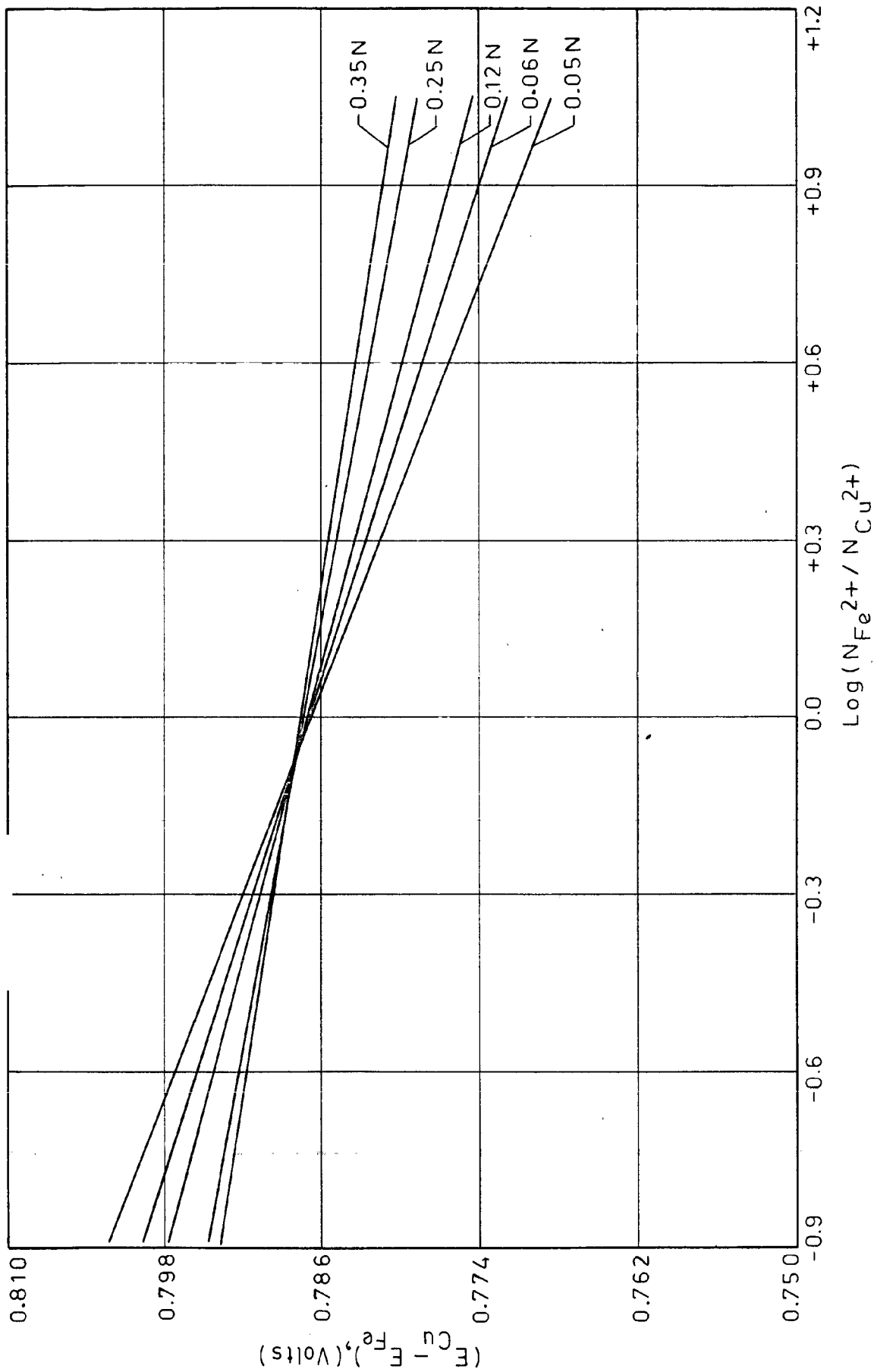


FIG.2.17 ($E_{Cu} - E_{Fe}$) VS. $\text{Log}(N_{Fe^{2+}} / N_{Cu^{2+}})$ AT VARIOUS CONSTANT TOTAL MOLALITY OF COPPER SULPHATE, SULPHURIC ACID AND FERROUS SULPHATE MIXED ELECTROLYTE SOLUTION.

CHAPTER - III

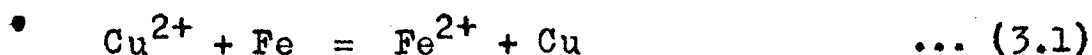
KINETICS OF CEMENTATION

3.1 Introduction

The thermodynamic condition for the feasibility of a cementation reaction gives no information regarding the rate of the reaction. Many such reactions that are thermodynamically feasible, do not proceed at useful rates under normal conditions, for instance, the precipitation of cobalt by zinc from zinc sulphate electrolytes⁷⁰. Almost all of the investigations in cementation field have been concerned with the study of reaction rates, and the elucidation of the factors controlling them. In this Chapter a theoretical as well as experimental study of the mechanism and kinetics of Copper cementation reaction is presented. First of all detailed theoretical analysis of this reaction would be presented which would be followed by description of experimental set-up and procedure and finally the results would be discussed in the light of the theoretical expressions put forward.

3.2 Theoretical

Copper cementation reaction which is represented by equation



involves a series of transport and electrode processes. These processes can be broadly classified into three main processes:

- i) Transport of Cu^{2+} ion from the bulk of aqueous phase to the solid metal surface.
- ii) Electrode process at the metal/aqueous phase interphase resulting in the precipitation of copper and dissolution of iron, and,
- iii) Transport of Fe^{2+} ion from the interface to the bulk of aqueous phase.

Each of the above processes can involve a number of reactions which take place in series. Apart from the main reactions, there may be others which also take place in the system simultaneously. In the following sections all the three processes would be discussed in detail with the view of deriving kinetic expressions for these processes.

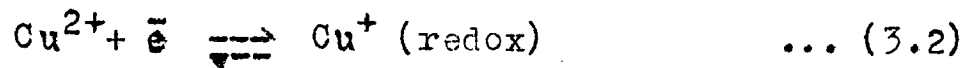
In order to qualitatively analyse the details of the cementation reactions into various steps, let us consider a copper ion or iron ion in the neighbourhood of the electrolyte/electrode phase boundary. The forces operating on such an ion are different from those operating on the ion present in the bulk of the electrolyte because of the anisotropic nature of the interface. As a result of this electroneutrality of the electrolyte

side of the boundary is broken down and it is electrified. The resultant field introduces an equal and opposite charge on the metallic conductor and thus a potential difference develops across the interface. The first row on the electrode is largely occupied by water dipoles and is called hydration sheath of electrode. The second row is largely occupied by solvated ions. The plane parallel to the electrode and joining the centres of these solvated ions is called Outer Helmholtz Plane (OHP). It is generally considered that the excess-charge density at the OHP is equal and opposite to that at the electrode. This situation gives rise to compact double layer. However, some of the solvated ions leave their second row seats and are dispersed into the solution due to thermal jostling from the particles of the solution. In this case the potential falls off into the solution, at first sharply and then asymptotically to a constant value (taken as zero) in the bulk of the solution. This gives rise to Diffuse Double Layer (DDL). Due to the transport of copper ions towards the electrode and that of iron ions towards the bulk of solution there would be a concentration gradient around the electrode, over and above the potential gradient. This gives rise to a boundary layer called Diffusion Boundary Layer (DBL). Quantitative analysis of the system requires the formulation of each of these steps into mathematical equations.

which will be the scope of the following sub-sections:

3.2.1 Electrode processes

The overall electrode process is composed of a series of electro-chemical reactions which may include some redox reaction. In case of copper cementation, the discharge of copper ion (Cu^{2+}) according to Bockris⁷¹, takes place over the following two reactions:

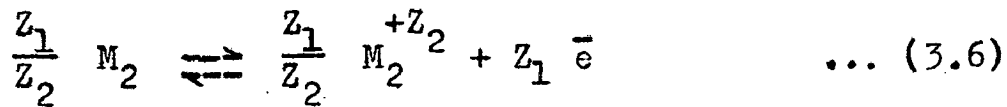
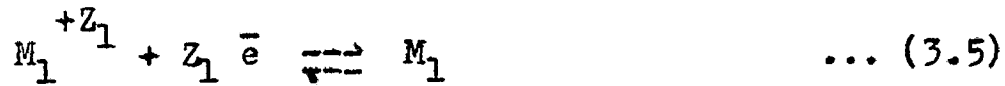


whereas the electrons for reduction of copper ions are provided by the oxidation of iron according to the following electrochemical reactions



The ferrous ion released in this process may get oxidised to Fe^{3+} ion by a further chemical reaction in the presence of an oxidising atmosphere. **Detailed analysis of electro-chemical half cells** have been made by Vetter⁷², and, Bockris and Reddy⁷³ and reviewed by Wadsworth⁵⁸. A brief discussion on the theoretical aspects of this process is given below.

The overall electrode process in cementation can be divided into two half cell reactions namely,



For either of the half cells the reaction kinetics can be considered in terms of absolute reaction rate theory. According to this theory, an electrochemical reaction proceeds in one or more reactions in series. For each of the reaction there is an activated state. As the reactions involve charged particles so the difference of potential between the initial and the activated state also affects the reaction rate. The activation energy barrier for the net cathodic half cell of a cementation reaction is illustrated in Fig. 3.1. The diagram has been constructed such that the reduction of cation is thermodynamically favoured. In this case the potential is seen to enhance the reduction reaction of the half cell by lowering the activation energy in the cathodic direction, from $\Delta G_0^- \neq$ to $\Delta G^- \neq$ i.e. by $(1-\alpha) ZEF$ and raising the activation energy for the anodic direction from $\Delta G_0^+ \neq$ to $\Delta G^+ \neq$ i.e. by αZEF . Here $\Delta G_0^+ \neq$ and $\Delta G_0^- \neq$ stand for activation energies for anodic and cathodic directions, respectively, in the absence of a potential gradient, whereas $\Delta G^+ \neq$ and $\Delta G^- \neq$ refer to the same in the presence of a potential gradient, Z is charge transfer valency and α is transfer coefficient. Assuming

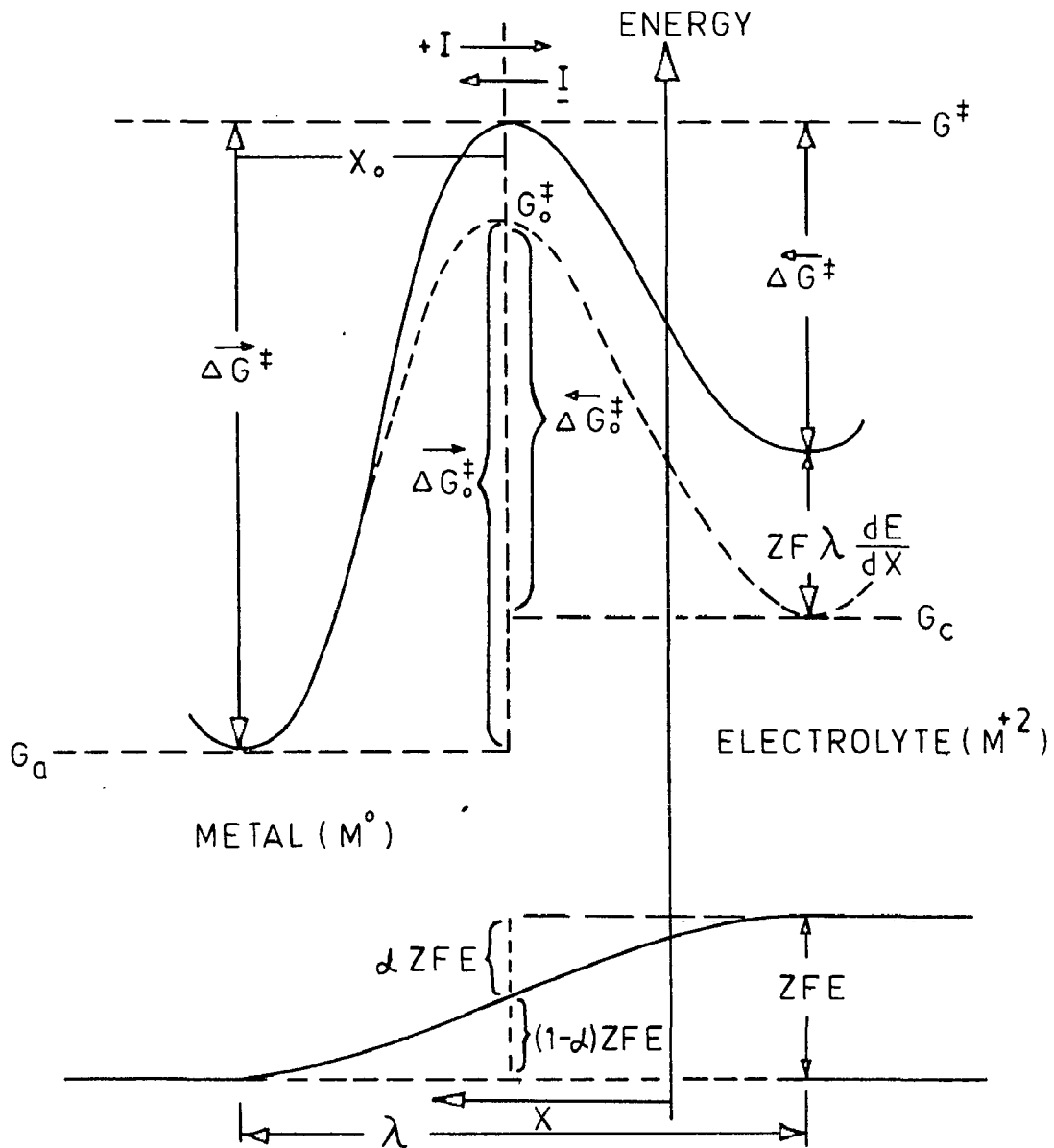


FIG.3.1 ACTIVATION ENERGY BARRIER FOR NET CATHODIC HALF CELL.

a constant potential gradient one can write:

$$\frac{dE}{dx} = \frac{E}{\lambda} \quad \dots (3.7)$$

where E is the potential associated with charge transfer reaction and λ is the distance between minima on either side of the activated state. Since the shape of the energy barrier is usually symmetrical, the decrease in activation energy in the cathodic direction due to the potential gradient can be considered to be equivalent to the increase in the activation energy in the anodic direction and $\alpha = 0.5$. The activation energy ΔG^\ddagger can be expressed in terms of the chemical contribution, ΔG_0^\ddagger , and the electrical contribution, $ZF\lambda \frac{dE}{dx} = -ZEF$ as follow:

$$\Delta G^\ddagger = (G_0^\ddagger - G_c) - ZF\lambda \frac{dE}{dx} + \alpha ZEF$$

$$\Delta G^\ddagger = \Delta G_0^\ddagger - ZEF + \alpha ZEF$$

$$\Delta G^\ddagger = \Delta G_0^\ddagger - (1 - \alpha) ZEF \quad \dots (3.8)$$

$$\Delta G^\ddagger = G_0^\ddagger + \alpha ZEF \quad \dots (3.9)$$

Assuming equilibrium with the activated complex for both the cathodic and anodic directions of the half cell, the equilibrium constants can be expressed as:

$$\begin{aligned} \overleftarrow{k} \neq &= \frac{\overleftarrow{C}^\ddagger}{C_c} = \exp\left(-\frac{\Delta \overleftarrow{G}^\ddagger}{RT}\right) \\ &= \exp\left(-\frac{\Delta \overleftarrow{G}_o^\ddagger}{RT}\right) \cdot \exp\left(-\frac{(1-\alpha)ZEF}{RT}\right) \dots (3.10) \end{aligned}$$

$$\begin{aligned} \overrightarrow{k} \neq &= \frac{\overrightarrow{C}^\ddagger}{C_a} = \exp\left(-\frac{\Delta \overrightarrow{G}^\ddagger}{RT}\right) \\ &= \exp\left(-\frac{\Delta \overrightarrow{G}_o^\ddagger}{RT}\right) \exp\left(-\frac{\alpha ZEF}{RT}\right) \dots (3.11) \end{aligned}$$

where $\overleftarrow{C}^\ddagger$ and $\overrightarrow{C}^\ddagger$ stand for the concentrations of the activated complex for the cathodic and anodic directions respectively, C_a is the effective concentration of metal sites capable of reacting in the anodic direction and C_c is the concentration of cation at the Outer Helmholtz Plane. From the theory of absolute reaction rate, the expressions for specific rate constants k' , in the absence of potential field, would be:

$$\overleftarrow{k}' = \frac{k T}{h} \exp\left(-\frac{\Delta \overleftarrow{G}_o^\ddagger}{RT}\right) \dots (3.12)$$

$$\overrightarrow{k}' = \frac{k T}{h} \exp\left(-\frac{\Delta \overrightarrow{G}_o^\ddagger}{RT}\right) \dots (3.13)$$

where k is Boltzman constant and h is Planck constant. Using these relations, the concentrations of the activated complex can be expressed as:

$$\overleftarrow{C}^\ddagger = C_c \frac{h}{kT} \overleftarrow{k}' \exp\left(-\frac{(1-\alpha)ZEF}{RT}\right) \dots (3.14)$$

$$\overrightarrow{C}^\ddagger = C_a \frac{h}{kT} \overrightarrow{k}' \exp\left(-\frac{\alpha ZEF}{RT}\right) \dots (3.15)$$

For unit area, the rate process for the half cell can be formulated in terms of the cathodic and anodic directions of the half cell reaction as follow:

$$I_- = ZF \lambda \overleftarrow{c}^* \frac{k_T}{h} \kappa \quad \dots (3.16)$$

$$I_+ = ZF \lambda \overrightarrow{c}^* \frac{k_T}{h} \kappa \quad \dots (3.17)$$

where I_- and I_+ are cathodic and anodic current densities respectively, κ is transmission coefficient. The net current density, I , for the half cell reaction, assuming $\kappa = 1$, can be written as:

$$I = (\overleftarrow{c}^* - \overrightarrow{c}^*) ZF \lambda \frac{k_T}{h} \quad \dots (3.18)$$

using equations (3.14) and (3.15) one gets

$$I = ZF \lambda \left[C_c \overleftarrow{k} \exp \left(\frac{(1-\alpha) ZEF}{RT} \right) - C_a \overrightarrow{k} \exp \left(- \frac{\alpha ZEF}{RT} \right) \right]$$

or

$$I = \overleftarrow{k} C_c \exp \left(\frac{(1-\alpha) ZEF}{RT} \right) - \overrightarrow{k} C_a \exp \left(- \frac{\alpha ZEF}{RT} \right) \quad \dots (3.19)$$

where $\overleftarrow{k} = \overleftarrow{k}^* ZF \lambda$ and $\overrightarrow{k} = \overrightarrow{k}^* ZF \lambda$. Defining half cell potential by E^0 , at which the electrode reaction is in equilibrium, one can write the above expression in the form:

$$I = I_0 \left[\exp \left(\frac{(1-\alpha) ZF \eta}{RT} \right) - \exp \left(- \frac{\alpha ZF \eta}{RT} \right) \right] \quad \dots (3.20)$$

where the equilibrium exchange current density

$$I_0 = I_- = I_+ \quad \text{and} \quad \text{the over potential } \eta = (E - E^0)$$

The above relation is called Butler⁷⁴-Volmer⁷⁵ equation and represents the basic law of charge-transfer reaction.

3.2.2 Transport from OHP to the Electrode Surface:

As the ions involved in cementation reactions are small in size, the possibility of existence of Inner Helmholtz Plane can be ignored. For ions in the outer Helmholtz plane with a corresponding potential ψ_0 , the effective potential difference between OHP and the electrode is $E - \psi_0 = \varphi$. The current due to the transport of the ions from OHP to the electrode will be given by Butler-Volmer relationship which, in the present case, takes the following form:

$$I = I_0 \exp\left(-\frac{(1-\alpha)ZF}{RT} \psi_0\right) \left[\exp\left(\frac{(1-\alpha)ZF}{RT} \eta\right) - \exp\left(-\frac{\alpha ZF}{RT} \eta\right)\right] \dots (3.21)$$

3.2.3 Transport Through Diffuse Double Layer:

In the diffuse double layer, the transport of ions takes place under simultaneous concentration and electrical potential gradient. If x' is the thickness of the diffuse double layer then the variation in potential from OHP in the direction of the bulk of the electrolyte is given, according to Gouy - Chapman theory⁷⁶, by the relationship⁷⁷:

$$|\psi_x| = \frac{2RT}{ZF} \ln \coth \frac{1}{2} (\delta x + a) \dots (3.22)$$

where,

$$a = - \ln \tanh \left| Z \frac{F}{4RT} \psi_0 \right| \quad \dots (3.23)$$

$2/\delta$ is the thickness of diffuse double layer and z is the absolute value of the electronic charge of the ion. In order to arrive at the transport equation through this layer let us divide the whole layer into a number of steps each containing an activation barrier and two minima around. If there are p such equidistant steps, then according to Eyring and Eyring⁷⁸ random Walk processes treatment, one can write for these steps the following expressions based on absolute reaction rate theory:

$$\begin{aligned} I_1 &= z'F \lambda C_0 k_0 \exp \left[- \frac{zF\lambda}{2RT} \left(\frac{d\psi}{dx} \right)_1 \right] \\ &\quad - z'F \lambda C_1 k_1' \exp \left[\frac{zF\lambda}{2RT} \left(\frac{d\psi}{dx} \right)_1 \right] \end{aligned} \quad \dots (3.24)$$

$$\begin{aligned} I_2 &= z'F \lambda C_1 k_1 \exp \left[- \frac{zF\lambda}{2RT} \left(\frac{d\psi}{dx} \right)_2 \right] \\ &\quad - z'F \lambda C_2 k_2' \exp \left[\frac{zF\lambda}{2RT} \left(\frac{d\psi}{dx} \right)_2 \right] \end{aligned} \quad \dots (3.25)$$

$$\begin{aligned} I_3 &= z'F \lambda C_2 k_2 \exp \left[- \frac{zF\lambda}{2RT} \left(\frac{d\psi}{dx} \right)_3 \right] \\ &\quad - z'F \lambda C_3 k_3' \exp \left[\frac{zF\lambda}{2RT} \left(\frac{d\psi}{dx} \right)_3 \right] \end{aligned} \quad \dots (3.26)$$

$$I_p = z'F \lambda C_{p-1} k_{p-1} \exp \left[-\frac{z'F\lambda}{2RT} \left(\frac{d\psi}{dx} \right)_p \right] - z'F \lambda C_p k'_p \exp \left[\frac{z'F\lambda}{2RT} \left(\frac{d\psi}{dx} \right)_p \right] \dots (3.27)$$

where z' is the number of electrons required for the total reduction process, λC_i is the number of ions in the i^{th} minimum per unit cross-sectional area while k_i and k'_i are the specific rate constants for an ion at the i^{th} minimum to jump forward and backward, respectively, in the absence of a potential, $(d\psi/dx)_i$ is the potential gradient for the i^{th} barrier. Under steady-state conditions one can write

$$I_1 = I_2 = I_3 \dots = I_p = I \dots (3.28)$$

If we assume that the diffusion coefficient D of the ion is independent of concentration, then

$$k_0 = k'_1 = k_1 = k'_2 = k_2 \dots k'_p = k \dots (3.29)$$

as the diffusion coefficient $D = \frac{2}{\lambda} k$.

Elimination of all intermediate concentrations $C_1, C_2, C_3 \dots C_{p-1}$ from the above set of equations leads to:

$$\frac{I}{Z'F\lambda k} = \frac{C_0 - C_D \exp \left[\frac{ZF\lambda}{RT} \sum_{i=1}^p \left(\frac{d\psi}{dx} \right)_i \right]}{\sum_{i=1}^p \exp \left[\frac{ZF\lambda}{RT} \sum_{j=1}^i \left(\frac{d\psi}{dx} \right)_j \right] \exp \left[-\frac{ZF\lambda}{2RT} \left(\frac{d\psi}{dx} \right)_i \right]} \dots (3.30)$$

where C_D stands for C_p , the concentration of reducible ion at the diffuse double layer. It is evident that for negative ψ_x values:

$$\lambda \sum_{i=1}^p \left(\frac{d\psi}{dx} \right)_i = \psi_0 \dots (3.31)$$

and

$$\lambda \sum_{j=1}^i \left(\frac{d\psi}{dx} \right)_j = (\psi_0 - \psi_{x,i}) \dots (3.32)$$

Replacement of summation in the exponential term from equation (3.30) with the help of equation (3.31) and (3.32) leads to the expression:

$$\frac{I}{Z'F\lambda k} = \frac{C_0 - C_D \exp \left(\frac{ZF}{RT} \psi_0 \right)}{\sum_{i=1}^p \exp \left[\frac{ZF}{RT} \left\{ \psi_{x,i} + \frac{\lambda}{2} \left(\frac{d\psi}{dx} \right)_i \right\} \right] \exp \left(\frac{ZF}{RT} \psi_0 \right)} \dots (3.33)$$

where,

$$\psi_{x,i} + \frac{\lambda}{2} \left(\frac{d\psi}{dx} \right)_i = \frac{\psi_{x,i-1} + \psi_{x,i}}{2} \dots (3.34)$$

when λ is small and i is large, then

$$\frac{\psi_{x,i-1} + \psi_{x,i}}{2} \approx \psi_{x,i} \quad \dots (3.35)$$

Using relation (3.22) one gets

$$\begin{aligned} \sum_{i=1}^p \exp \left[-\frac{ZF}{RT} \psi_{x,i} \right] &= \frac{1}{\lambda} \int_{x'}^0 \exp \left[-\frac{ZF}{RT} \psi_x \right] dx \\ &= \frac{1}{\lambda} \int_{x'}^0 [\text{Tanh}(\delta x + a)]^2 \frac{|z|}{dx} |Z| \\ &= \frac{2 \Omega}{\delta \lambda} \quad \dots (3.36) \end{aligned}$$

Thus, substituting equations (3.34), (3.35) and (3.36) into equation (3.33) one gets the following relation for transport of ion from D D L towards OHP:

$$\frac{I}{z'F} = \frac{\delta_D C_D}{2 \Omega} - \frac{\delta_D C_c}{2 \Omega} \exp \left[-\frac{ZF}{RT} \psi_0 \right] \quad \dots (3.37)$$

where, C_c stands for C_o , the concentration of cation at the outer Helmholtz plane. Thus we have arrived at the relation for transport of ions through DDL.

3.2.4 Transport Through Boundary Layer:

Due to the concentration gradient, there is also a thin film of stagnant boundary layer of the solution around each particle. The thickness of this layer is governed by the hydro-dynamics of the system. The

transport of an ion from the bulk of the solution phase to the particle surface involves transport of Chunks of solution to the boundary-film surface by the eddies in the solution. The rate of mass transfer can be calculated with the help of Fick's second law of diffusion which along with the boundary and initial conditions takes the following form:

$$\frac{\partial C}{\partial t} = D \frac{\partial^2 C}{\partial x^2} \quad \dots (3.38)$$

boundary conditions

$$C = C_b \text{ at } x = 0 \text{ for } t = 0 \quad \dots (3.39)$$

$$C = C_D \text{ at } x = 0 \text{ for } t > 0 \quad \dots (3.40)$$

$$C = C_b \text{ at } x = L \text{ for } t > 0 \quad \dots (3.41)$$

where C_b and C_D are the bulk and surface equilibrium concentrations of the ion, respectively and L is the thickness of the boundary layer. The solution of the equation (3.38) with these boundary conditions gives the following expression for the instantaneous rate of mass transfer (J) from solution to the interface:

$$\frac{I}{Z'F} = J = (C_b - C_D) \frac{D}{L} \left[1 + 2 \sum_{n=1}^{n=\infty} \exp \left(- \frac{n^2 \pi^2 D t}{L^2} \right) \right] \quad \dots (3.42)$$

The mean transfer rate can be obtained from the above expression, assuming that either all surface renewing chunks of fluid are exposed at the boundary layer surface for the same time t_e (Higbie Theory⁷⁹) or by assuming a random age distribution (Danckwerts model⁸⁰). In either case, one can write the equation (3.42) in the following form:

$$\frac{I}{z'F} = J = K_m (c_b - c_D) \quad \dots (3.43)$$

where K_m is mean mass transfer coefficient, which, for Higbie model, will be given by the expression

$$K_m = \frac{1}{t_e} \int_0^{t_e} \sqrt{\frac{D}{\pi t}} \left[1 + 2 \sum_{n=1}^{n=\infty} \exp\left(-\frac{n^2 L^2}{Dt}\right) \right] dt \quad \dots (3.44)$$

3.2.5 Generalised Rate Equation:

Metal deposition involves transport of an ion from the bulk of the solution by diffusion through the limiting boundary layer, followed by its transport to OHP through DDL under the combined influence of concentration and electrical potential gradient and finally its transport from OHP to the electrode. The rate of transport of the ion through these layers is given by the expressions (3.21), (3.37) and (3.43) respectively. Combination of these equations under steady state condition leads to the expression:

$$\frac{I_{Cu}}{z'F} = \frac{\lambda \overset{\leftarrow}{k}_{Cu} C_{b,Cu} \exp\left(\frac{(1-\alpha)ZF E_{Cu}}{RT}\right) \exp\left(\frac{ZF}{RT} \psi_0\right) - \lambda \vec{k}_{Cu} C_{a,Cu} \exp\left(-\frac{\alpha ZF E_{Cu}}{RT}\right) \exp\left(\frac{ZF}{RT} \psi_0\right)}{\exp\left(\frac{(1-\alpha)ZF}{RT} \psi_0\right) + \lambda \overset{\leftarrow}{k}_{Cu} \left(\frac{2\Omega}{\delta_{Cu} D_{Cu}} + \frac{1}{K_{m,Cu}}\right) \exp\left(\frac{ZF}{RT} \psi_0\right) \exp\left(\frac{(1-\alpha)ZF}{RT} E_{Cu}\right)} \dots (3.45)$$

$$\frac{I_{Fe}}{z'F} = \frac{\lambda \overset{\leftarrow}{k}_{Fe} C_{b,Fe} \exp\left(\frac{(1-\alpha)ZF E_{Fe}}{RT}\right) \exp\left(\frac{ZF}{RT} \psi_0\right) - \lambda \vec{k}_{Fe} C_{a,Fe} \exp\left(-\frac{\alpha ZF E_{Fe}}{RT}\right) \exp\left(\frac{ZF}{RT} \psi_0\right)}{\exp\left(\frac{(1-\alpha)ZF}{RT} \psi_0\right) + \lambda \overset{\leftarrow}{k}_{Fe} \left(\frac{2\Omega}{\delta_{Fe} D_{Fe}} + \frac{1}{K_{m,Fe}}\right) \exp\left(\frac{ZF}{RT} \psi_0\right) \exp\left(\frac{(1-\alpha)ZF}{RT} E_{Fe}\right)} \dots (3.46)$$

As $I_{Cu} = -I_{Fe}$ for a system at steady state, one can arrive at the following equation for the mixed potential E_m , in the system, which may be defined as the potential at which rate of copper deposition would be equal to the rate of iron dissolution:

$$\begin{aligned}
& A_c \left[\lambda \overleftarrow{k}_{Cu} C_{b,Cu} \exp\left(\frac{(1-\alpha)ZF}{RT} E_m\right) \cdot \exp\left(-\frac{ZF}{RT} \psi_o\right) \right. \\
& \left. - \lambda \overrightarrow{k}_{Cu} C_{a,Cu} \exp\left(-\frac{\alpha ZF}{RT} E_m\right) \cdot \exp\left(\frac{ZF}{RT} \psi_o\right) \right] \\
& \frac{+}{\left[\exp\left(\frac{(1-\alpha)ZF}{RT} \psi_o\right) + \lambda \overleftarrow{k}_{Cu} \left(\frac{2\Omega}{\delta_{Cu} D_{Cu}} + \frac{1}{K_{m,Cu}}\right) \cdot \exp\left(\frac{ZF}{RT} \psi_o\right) \cdot \right.} \\
& \left. \exp\left(\frac{(1-\alpha)ZF}{RT} E_m\right) \right] \\
& A_a \left[\lambda \overleftarrow{k}_{Fe} C_{b,Fe} \exp\left(\frac{(1-\alpha)ZF}{RT} E_m\right) \cdot \exp\left(\frac{ZF}{RT} \psi_o\right) \right. \\
& \left. - \lambda \overrightarrow{k}_{Fe} C_{a,Fe} \exp\left(-\frac{\alpha ZF}{RT} E_m\right) \cdot \exp\left(\frac{ZF}{RT} \psi_o\right) \right] \\
& \frac{+}{\exp\left(\frac{(1-\alpha)ZF}{RT} \psi_o\right) + \lambda \overleftarrow{k}_{Fe} \left(\frac{2\Omega}{\delta_{Fe} D_{Fe}} + \frac{1}{K_{m,Fe}}\right) \cdot \exp\left(\frac{ZF}{RT} \psi_o\right) \cdot \exp\left(\frac{(1-\alpha)ZF}{RT} E_m\right)} = 0 \quad \dots (3.47)
\end{aligned}$$

where A_c is cathodic area and A_a is anodic area. From a knowledge of the various parameters in the above expression, one can obtain mixed potential, E_m , as a function of the concentration of the various ions in the bulk of the solution. Using this value of mixed potential, one can calculate the rate of cementation from equation (3.45). Though the above equations (3.45) to (3.47) consider the effect of transport through various layers and electro-chemical reaction at the electrode on the overall kinetics of system, in general, one or the other step is the slowest one in the whole process and therefore controls the overall rate of

reaction. An indication towards the slowest step under given experimental conditions is provided from the thermodynamic data of the system as well as the results of kinetic experiments. The discussion regarding the slowest step under present experimental conditions will be given in section on results and discussions.

As far as the kinetic expression for a particular slow step is concerned, it can be derived from the overall rate equation (3.45) by neglecting the resistance due to all other steps. This indirectly means that all other steps are very fast as compared to this particular step and reach instantaneously the state of equilibrium. Though this is only a hypothetical state of the overall reaction, yet still in practice it holds good because the potential drops due to other steps are so small that these can be neglected. In section (3.4), it will be shown that the experimental data in the present case, also, can be explained by considering one of the steps in the overall reaction to be the slowest one.

3.3 Experimental

As the industrial cementation reactions are generally conducted with the use of iron particulates (sponge, powder, scrap) to recover copper from copper-bearing solutions, an investigation of the effect of solution/iron powder ratio and the size of iron powder on the kinetics of the process would be of great importance. The aim of the present work was, also, to produce composite powders by cementation. Hence for experiments, iron powders of different sizes were used. Since cementation reactions are heterogeneous in nature and their rate shall, among other factors, be governed by diffusion of the reactant ions to the precipitant metal surface, agitation is utilised to eliminate the system becoming controlled by bulk solution diffusion. Experiments have, therefore, been conducted at various rotational speeds in order to determine the optimum level of agitation. Similarly, hydrogen ion (pH) control in hydrometallurgical operation is an important task for a variety of reasons such as corrosion damage of cementation launders, excess dissolution of precipitant metal, hydroxide precipitation, excess acid consumption etc. Therefore, an investigation of the effect of pH of the solution on kinetics of cementation to establish commercial workable pH range for a minimum corrosion effect and acid consumption and for a maximum reaction rate has been

studied. Also the commercial success of a copper cementation process is strongly dependent on the copper ion concentration of the influent, pregnant leach liquor. Since this concentration may vary at any time depending on many factors in the leaching operation, a study of the copper recovery rates at different copper ion concentration levels by the cementation process are of great significance. Although commercial cementation processes are generally conducted at ambient temperature, an investigation of the effect of temperature on the reaction rate is essential because this gives additional evidence about the rate controlling mechanism of the reactions. Further, as the deposit morphology is of fundamental importance to the kinetics of reaction, in addition to the effects of above factors, a study of the effect of nature of the anions present, presence of addition agents and impurities, and the condition of the substrate metal on the kinetics of cementation is extremely important. Due to undesirable secondary reactions which may be caused by the dissolved gases such as redissolution of precipitated metal and formation of ferric ion due to dissolved oxygen and the possibility of reduction of cupric ion to cuprous and reduction of iron consumption in hydrogen atmosphere, it is important to study the effect of various atmospheres on kinetics of cementation. A study of back reaction kinetics is also required to

have a knowledge of redeposition of iron and redissolution of copper.

Though the effect of a number of these variables on kinetics of cementation have been studied by different investigators, they used mainly disc or cylindrical samples. Since the cementation system, which makes use of iron powders for cementation process, as in the present investigation, is entirely different from the ones studied and reported in literature, it has been essential to study the effects of all the variables. Thus, the complete experimental investigation on kinetics includes the study of following variables:

- i) Solution agitation
- ii) Hydrogen ion concentration (pH)
- iii) Initial concentration of copper ion
- iv) Temperature
- v) Powder size
- vi) Solution/iron powder ratio , and,
- vii) Atmosphere.

3.3.1 Experimental set-up:

The experimental assembly is shown in Fig. 3.2. The reaction solution was contained in a round bottom flask (capacity more than 2 litres) fitted with one B29, one B34 and one B55 standard taper joints of carning glass. The joint B55 was used to hold the stirring

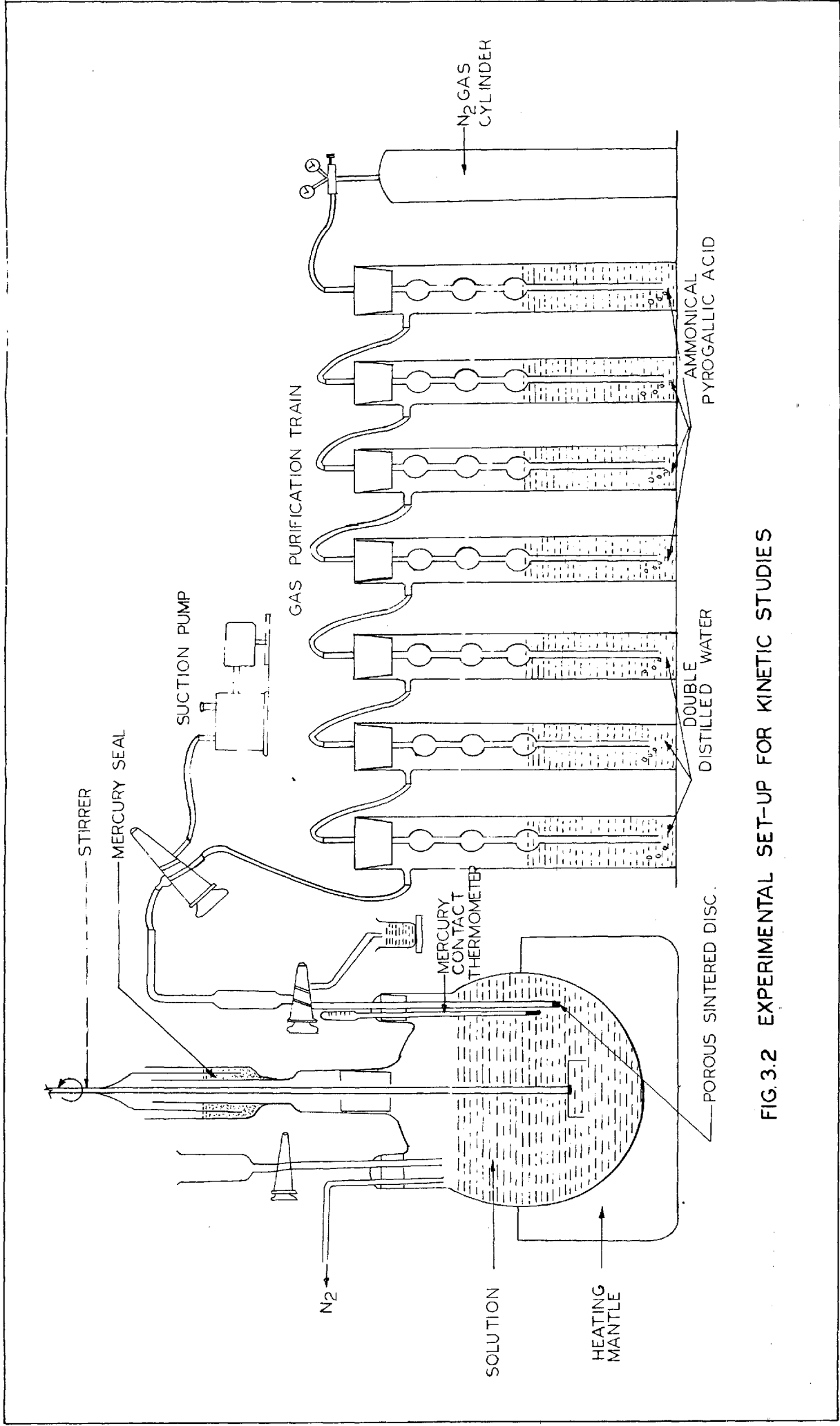


FIG. 3.2 EXPERIMENTAL SET-UP FOR KINETIC STUDIES

assembly and the joint B29 held a thermometer in an adapter and had arrangement to admit the iron powder to the flask. The joint B34 held the gas admission tube solution-sampler assembly. The solution was stirred with an inverted U-shaped perspex impeller attached to a Remi-model of multipurpose laboratory stirrer provided with a variable speed motor. The temperature was maintained at the desired level with an automatically controlled Glascol heating mantle, with a precision of $\pm 0.5^{\circ}\text{C}$. Purified nitrogen gas was used to deaerate the solution before kinetic study and to maintain a neutral atmosphere of nitrogen during experiment. The stirring assembly was fitted with mercury seal to prevent the entry of air into the reaction vessel.

3.3.2 Procedure:

Distilled water and Analytical Reagent grade B.D.H. make chemicals were used for all experiments. Stock solution of copper sulphate containing 10 gms of copper per litre was prepared which was diluted to various concentrations as required. S. Merck make electrolytic grade iron powder was used as precipitant. Oxygen was removed from the nitrogen used for various experiments by scrubbing the gas four times with an alkaline pyrogalllic acid solution and then with double distilled water.

The solution of copper sulphate in the reaction vessel was adjusted for initial copper concentration and pH and was then brought to temperature under a stream of purified nitrogen gas introduced through the pipette. To remove oxygen from the test solution nitrogen was bubbled through the solution eight hours before experiment and nitrogen flow was continued during the experiment. Solution was stirred at the desired speed and iron powder of desired size and amount added into the solution. Samples of the solution were taken at predetermined intervals through the side pipette, momentarily stopping the nitrogen flow. Experimental data were obtained by measuring the amount of copper and iron ions in solution at successive time intervals. The initial volume of the solution was 2000 ml, 10 ml aliquots being removed each time for chemical analysis. The corrections for the change in the volume of the solution resulting from the removal of aliquots for analysis has been applied as done by Power and Ritchie⁵². The impeller was immersed to the same depth during each run so that the stirring would be reproducible.

Copper in solution was determined by analysing 5 ml aliquot of the solution by the iodometric method and iron by analysing another 5 ml by a dichromate titration with diphenylamine as internal indicator.

3.4 - Results and Discussions

Results of the kinetic studies for different process variables are given in Tables 3.1 to 3.7. In order to find out the order of the cementation reaction, graphs were plotted between $\log \left[\frac{C_{Cu^{2+}}^t}{C_{Cu^{2+}}^0} \right]$ and time, using the above results. $C_{Cu^{2+}}^t$ stands for concentration of copper at time t and $C_{Cu^{2+}}^0$ for initial concentrations of copper ion in solution. These graphs are shown in Figs. 3.5, 3.7, 3.9, 3.12, 3.15, 3.17 and 3.19 for different process variables. It is seen that each graph has two linear parts, joined by a small non-linear curve. The initial linear part has a much steeper slope as compared to the final linear part of the curve which has only gentle slope. Calculations have shown that during this part, residual iron varies from a negligible amount to about 30% depending upon other process variables. Its linear nature indicates that the cementation is a first order reaction with respect to the concentration of copper ion in solution. This fact and the thermodynamic data of the reaction indicate that the overall reaction is controlled by the cathodic reduction of copper ions to copper. This implies that the anodic reaction is very fast and can be assumed to attain equilibrium instantaneously. From the results of an electro-chemical investigation of copper cementation by iron, Rickard and Fuerstenau³¹ noted that a ten-fold increase in current

TABLE-3.1: Results of Temperature Parameter Study
(Data for Fig. 3.5)

pH	2.8
[Cu ²⁺] _{initial}	0.5 gn/litre
RPM	2450
Iron powder	0.315 gn/litre
	-150 + 125 micron

S. No.	Time (min.)	T E M P E R T U R E (°C)			
		20°C Cu ²⁺ gn/l	35°C Cu ²⁺ gn/l	50°C Cu ²⁺ gn/l	65°C Cu ²⁺ gn/l
1.	3	0.4581	0.4539	0.4374	0.4275
2.	6	0.4236	0.4008	0.3881	0.3556
3.	9	0.3917	0.3572	0.3364	0.2971
4.	12	0.3622	0.3169	0.2944	0.2494
5.	15	0.3349	0.2890	0.2624	0.2448
6.	18	0.3054	0.2564	0.2254	0.2426
7.	21	0.2798	0.2254	0.2243	0.2426
8.	24	0.2648	0.2202	0.2233	0.2426
9.	27	0.2371	0.2182	0.2233	0.2415
10.	30	0.2202	0.2182	0.2233	
11.	33	0.2084	0.2172	0.2223	
12.	36	0.1963			
13.	39	0.1936			
14.	42	0.1857			
15.	45	0.1849			
16.	50	0.1832			
17.	60	0.1815			
18.	70	0.1815			

TABLE-3.2: Results of Stirring Parameter Study
(Data for Fig. 3.7)

Temperature	25°C
pH	2.8
[Cu ²⁺] _{initial}	0.5 gm/litre
Amount of iron powder	0.315 gm/litre
Size of powder	-150 + 125 micron

S.N No.	Time (min.)	Stirring Speed (rpm)			
		700 rpm Cu ²⁺ (gm/l)	1250 rpm Cu ²⁺ (gm/l)	1500 rpm Cu ²⁺ (gm/l)	2450 rpm Cu ²⁺ (gm/l)
1.	3	0.4753	0.4687	0.4644	0.4581
2.	6	0.4435	0.4354	0.4295	0.4236
3.	9	0.4178	0.4101	0.4026	0.3917
4.	12	0.3989	0.3810	0.3758	0.3622
5.	15	0.3723	0.3556	0.3459	0.3349
6.	18	0.3507	0.3349	0.3273	0.3054
7.	21	0.3288	0.3111	0.3026	0.2798
8.	24	0.3111	0.2903	0.2811	0.2648
9.	27	0.2944	0.2747	0.2588	0.2371
10.	30	0.2760	0.2505	0.2460	0.2202
11.	33	0.2685	0.2393	0.2264	0.2084
12.	36	0.2588	0.2327	0.2162	0.1963
13.	39	0.2517	0.2233	0.2142	0.1936
14.	42	0.2471	0.2212	0.2084	0.1857
15.	45	0.2448	0.2182	0.2036	0.1849
16.	50	0.2415	0.2123	0.2036	0.1832
17.	60	0.2404	0.2084	-	0.1815
18.	70	-	0.2074	-	0.1815

TABLE-3.3: Results of Initial Copper ion Concentration Study (Data for Fig. 3.9)

pH 2.8
 RPM 2450
 Temperature 25°C
 Iron powder 0.315 gm/litre
 -150 + 125 micron

S. No.	Time (min.)	Initial Concentration of Copper in Solution (gm/litre)			
		0.25 Cu ²⁺ (gm/l)	0.35 Cu ²⁺ (gm/l)	0.50 Cu ²⁺ (gm/l)	0.75 Cu ²⁺ (gm/l)
1.	3	0.2354	0.3236	0.4581	0.6903
2.	6	0.2217	0.2992	0.4236	0.6412
3.	9	0.2060	0.2792	0.3917	0.5930
4.	12	0.1913	0.2594	0.3622	0.5483
5.	15	0.1802	0.2410	0.3349	0.5094
6.	18	0.1690	0.2270	0.3054	0.4732
7.	21	0.1606	0.2080	0.2798	0.4416
8.	24	0.1478	0.1905	0.2648	0.4276
9.	27	0.1405	0.1786	0.2371	0.4065
10.	30	0.1288	0.1682	0.2202	0.4046
11.	33	0.1241	0.1527	0.2084	0.3972
12.	36	0.1153	0.1445	0.1963	0.3972
13.	39	0.1076	0.1264	0.1936	0.3954
14.	42	0.1027	0.1213	0.1857	0.3954
15.	45	0.0937	0.1148	0.1849	0.3954
16.	50	0.0847	0.1009	0.1832	0.3936
17.	60	0.0682	0.0961	0.1815	-
18.	70	-	-	0.1815	-

TABLE-3.4: Results of pH Parameter Study (Data for Fig. 3.12)

Temperature 25°C
 [Cu²⁺] initial 0.5 gm/litre
 Iron powder 0.315 gm/litre, -150 + 125 micron
 RPM 2450

S. No.	Time (min.)	Initial pH of Copper Sulphate Solution					
		pH = 1.5	pH = 1.8	pH = 2.8	pH = 4.9		
		Cu ²⁺ (gm/l)	Fe ²⁺ (gm/l)	Cu ²⁺ (gm/l)	Fe ²⁺ (gm/l)	Cu ²⁺ (gm/l)	Fe ²⁺ (gm/l)
1.	3	0.4774	0.0241	0.4666	0.0325	0.4581	0.0372
2.	6	0.4539	0.0480	0.4374	0.0614	0.4236	0.0675
3.	9	0.4295	0.0722	0.4139	0.0851	0.3917	0.0956
4.	12	0.4139	0.0882	0.3810	0.1148	0.3622	0.1215
5.	16	0.3899	0.1133	0.3605	0.1370	0.3349	0.1455
6.	18	0.3740	0.1288	0.3380	0.1585	0.3054	0.1715
7.	21	0.3556	0.1483	0.3154	0.1826	0.2798	0.1940
8.	24	0.3427	0.1618	0.2985	0.1987	0.2648	0.2072
9.	27	0.3198	0.1838	0.2785	0.2177	0.2371	0.2315
10.	30	0.3082	0.1957	0.2624	0.2339	0.2202	0.2464
11.	33	0.2930	0.2104	0.2426	0.2533	0.2084	0.2568
12.	36	0.2850	0.2183	0.2295	0.2649	0.1963	0.2674
13.	39	0.2798	-	0.2182	0.2758	0.1936	0.2698
14.	42	0.2785	0.2247	0.2093	0.2836	0.1857	0.2767
15.	45	0.2773	0.2258	0.2093	0.2844	0.1849	0.2774
16.	50	0.2773	0.2258	0.2084	0.2852	0.1832	0.2789
17.	60	-	-	-	-	0.1815	0.2804
18.	70	-	-	-	-	0.1815	0.2804

TABLE-3.5: Results of Particle Size Parameter Study
(Data for Fig. 3.15)

pH	2.8
Temperature	25°C
[Cu ²⁺] _{initial}	0.5 gm/litre
Iron powder	0.315 gm/litre
RPM	2450

S. No.	Time (min)	Size of Iron Powder			
		-150 μ +125 μ	-125 μ +106 μ	-106 μ + 90 μ	- 63 μ + 53 μ
		Cu ²⁺ gm/l	Cu ²⁺ gm/l	Cu ²⁺ gm/l	Cu ²⁺ gm/l
1.	3	0.4581	0.4560	0.4518	0.4354
2.	6	0.4236	0.4197	0.4026	0.3689
3.	9	0.3917	0.3810	0.3622	0.3125
4.	12	0.3622	0.3427	0.3303	0.2735
5.	15	0.3349	0.3198	0.2917	0.2254
6.	18	0.3054	0.2877	0.2564	0.1972
7.	21	0.2798	0.2624	0.2382	0.1832
8.	24	0.2648	0.2360	0.2103	0.1782
9.	27	0.2371	0.2243	0.1990	0.1757
10.	30	0.2202	0.2074	0.1866	0.1757
11.	33	0.2084	0.1954	0.1790	-
12.	36	0.1963	0.1909	0.1782	-
13.	39	0.1936	0.1832	-	-
14.	42	0.1857	0.1798	-	-
15.	45	0.1849	0.1798	-	-
16.	50	0.1832	-	-	-
17.	60	0.1815	-	-	-
18.	70	0.1815	-	-	-

TABLE-3.6 Results of Solution/Powder Ratio Study
(Data for Fig. 3.17)

PH	2.8
Temperature	25°C
[Cu ²⁺] _{initial}	0.5 gn/litre
RPM	2450
Iron powder	-150+125 micron

S. No.	Time (min.)	Solution/Powder Ratio			
		1.960	1.587	1.315	1.136
		Cu ²⁺ gn/l	Cu ²⁺ gn/l	Cu ²⁺ gn/l	Cu ²⁺ gn/l
1.	3	0.4644	0.4581	0.4560	0.4476
2.	6	0.4334	0.4236	0.4120	0.4045
3.	9	0.4082	0.3917	0.3740	0.3605
4.	12	0.3810	0.3622	0.3443	0.3288
5.	15	0.3507	0.3349	0.3040	0.2903
6.	18	0.3303	0.3054	0.2811	0.2672
7.	21	0.3068	0.2798	0.2552	0.2437
8.	24	0.2917	0.2648	0.2285	0.2162
9.	27	0.2685	0.2371	0.2132	0.1918
10.	30	0.2505	0.2202	0.1918	0.1757
11.	33	0.2382	0.2084	0.1733	0.1588
12.	36	0.2338	0.1963	0.1581	0.1422
13.	39	0.2295	0.1936	0.1435	0.1282
14.	42	0.2295	0.1857	0.1371	0.1156
15.	45	0.2285	0.1849	0.1328	0.1049
16.	50	0.2285	0.1832	0.1263	0.0898
17.	60	-	0.1815	-	-
18.	70	-	0.1815	-	-

TABLE-3.7: Results of Atmosphere Parameter Study (Data for Fig. 3.19)

pH 2.8
 Temperature 25°C
 [Cu²⁺] initial 0.5 gm/litre
 RPM 2450
 Iron powder 0.315 gm/litre
 -150 + 125 micron

S. No.	Time (min.)	Nitrogen		Hydrogen		A		E		R		I		E		R	
		Cu ²⁺ (gm/l)	Fe ²⁺ (gm/l)	Cu ²⁺ (gm/l)	Fe ²⁺ (gm/l)	Cu ²⁺ (gm/l)	Fe ²⁺ (gm/l)	Cu ²⁺ (gm/l)	Fe ²⁺ (gm/l)	Cu ²⁺ (gm/l)	Fe ²⁺ (gm/l)	Cu ²⁺ (gm/l)	Fe ²⁺ (gm/l)	Cu ²⁺ (gm/l)	Fe ²⁺ (gm/l)	Cu ²⁺ (gm/l)	Fe ²⁺ (gm/l)
1.	3	0.4581	0.0372	0.4581	0.0371	0.4666	0.0371	0.4666	0.0371	0.4666	0.0371	0.4666	0.0371	0.4666	0.0371	0.4666	0.0371
2.	6	0.4236	0.0675	0.4236	0.0675	0.4314	0.0675	0.4314	0.0675	0.4314	0.0675	0.4314	0.0675	0.4314	0.0675	0.4314	0.0675
3.	9	0.3917	0.0956	0.3881	0.0987	0.4045	0.0987	0.4045	0.0987	0.4045	0.0987	0.4045	0.0987	0.4045	0.0987	0.4045	0.0987
4.	12	0.3622	0.1215	0.3523	0.1302	0.3827	0.1302	0.3827	0.1302	0.3827	0.1302	0.3827	0.1302	0.3827	0.1302	0.3827	0.1302
5.	15	0.3349	0.1455	0.3318	0.1483	0.3556	0.1483	0.3556	0.1483	0.3556	0.1483	0.3556	0.1483	0.3556	0.1483	0.3556	0.1483
6.	18	0.3054	0.1715	0.2985	0.1775	0.3213	0.1775	0.3213	0.1775	0.3213	0.1775	0.3213	0.1775	0.3213	0.1775	0.3213	0.1775
7.	21	0.2798	0.1940	0.2773	0.1962	0.3054	0.1962	0.3054	0.1962	0.3054	0.1962	0.3054	0.1962	0.3054	0.1962	0.3054	0.1962
8.	24	0.2648	0.2072	0.2588	0.2125	0.2850	0.2125	0.2850	0.2125	0.2850	0.2125	0.2850	0.2125	0.2850	0.2125	0.2850	0.2125
9.	27	0.2371	0.2315	0.2317	0.2363	0.2624	0.2363	0.2624	0.2363	0.2624	0.2363	0.2624	0.2363	0.2624	0.2363	0.2624	0.2363
10.	30	0.2202	0.2464	0.2152	0.2508	0.2482	0.2508	0.2482	0.2508	0.2482	0.2508	0.2482	0.2508	0.2482	0.2508	0.2482	0.2508
11.	33	0.2084	0.2568	0.2008	0.2635	0.2415	0.2635	0.2415	0.2635	0.2415	0.2635	0.2415	0.2635	0.2415	0.2635	0.2415	0.2635
12.	36	0.1963	0.2674	-	-	0.2327	-	0.2327	-	0.2327	-	0.2327	-	0.2327	-	0.2327	-
13.	39	0.1936	0.2698	-	-	0.2233	-	0.2233	-	0.2233	-	0.2233	-	0.2233	-	0.2233	-
14.	42	0.1857	0.2767	-	-	0.2212	-	0.2212	-	0.2212	-	0.2212	-	0.2212	-	0.2212	-
15.	45	0.1849	0.2774	-	-	0.2182	-	0.2182	-	0.2182	-	0.2182	-	0.2182	-	0.2182	-
16.	50	0.1832	0.2789	-	-	0.2182	-	0.2182	-	0.2182	-	0.2182	-	0.2182	-	0.2182	-
17.	60	0.1815	0.2804	-	-	0.2172	-	0.2172	-	0.2172	-	0.2172	-	0.2172	-	0.2172	-
18.	70	0.1815	0.2804	-	-	-	-	-	-	-	-	-	-	-	-	-	-

density shifts the anodic potential of iron dissolution by only 0.03nV which is in confirmation with the above assumption that anodic process is near its equilibrium. With this observation, the overall rate equation reduces to the expression (3.48), in which E_{Cu} need not be equal to E_m :

$$\frac{I_{Cu}}{Z'F} = \frac{C_{b,Cu} [1 - \exp(\frac{\Delta G}{RT})]}{[\frac{2\Omega}{\delta_{Cu} D_{Cu}} + \frac{1}{K_{m,Cu}} + \frac{1}{\lambda \bar{K}_{Cu}} \exp(-\frac{(1-\alpha)ZF E_{Cu}}{RT}) \exp(-\frac{\alpha ZF \psi_0}{RT})]} \dots (3.48)$$

where $\Delta G = -ZF \Delta E$ and ΔE is the thermodynamic driving force for copper reduction and is given by the Nernst equation. Since the thermodynamic equilibrium constant for the cementation reaction is very large and is of the order of $10^{26.37}$ as given in Table 2.2, the equilibrium constant for the back reaction, which refers to the dissolution of copper, will be very small. As a result of this the exponential term of the numerator of the expression (3.48) which stands for the back reaction will approach zero. Thus

$$[1 - \exp(\frac{\Delta G}{RT})] \approx 1 \dots (3.49)$$

$$\frac{I_{Cu}}{Z'F} = \frac{C_{b,Cu}}{[\frac{2\Omega}{\delta_{Cu} D_{Cu}} + \frac{1}{K_{m,Cu}} + \frac{1}{\lambda \bar{K}_{Cu}} \exp(-\frac{(1-\alpha)ZF E_{Cu}}{RT}) \exp(-\frac{\alpha ZF \psi_0}{RT})]} \dots (3.50)$$

or,

$$\frac{I_{Cu}}{Z'F} = C_{b,Cu} k_c \quad \dots(3.51)$$

where,

$$k_c = \left[\frac{2 \Omega}{\delta_{Cu} D_{Cu}} + \frac{1}{K_{m,Cu}} + \frac{1}{\lambda \bar{k}_{Cu}} \exp \left(- \frac{(1-\alpha) ZFE_{Cu}}{RT} \right) \right. \\ \left. \exp \left(- \frac{\alpha ZF}{RT} \psi_0 \right) \right]^{-1} \quad \dots(3.52)$$

and k_c^{-1} stands for the sum of the resistances of the various processes in series. In the expression (3.52), the first term stands for the resistance to transport through diffuse double layer, the second term refers to resistance to transport through the diffusion boundary film and the third term stands for the resistance to surface reactions. In cementation process, any one of these or their combination may control the overall rate of the cementation. when,

$$\frac{1}{\lambda \bar{k}_{Cu}} \exp \left(- \frac{(1-\alpha) ZFE_{Cu}}{RT} \right) \exp \left(- \frac{\alpha ZF \psi_0}{RT} \right) \gg \frac{2 \Omega}{\delta_{Cu} D_{Cu}} \\ + \frac{1}{K_{m,Cu}} \quad \dots(3.53)$$

the surface reaction would be the rate controlling step in the overall process of cementation. As above relation (3.53) shows, under this condition the kinetics of cementation would be sensitive to changes in ϕ and ψ_0 , where $\phi = E - \psi_0$. In general for surface control

reactions, the activation energies are higher than those for diffusion controlled ones. As the diffusion controlled reactions involving an aqueous phase have activation energies from 2 to 6 Kcal, it is anticipated that for surface controlled reactions, the activation energy will be higher than 6 Kcal. When,

$$\frac{2 \Omega}{\delta_{\text{Cu}} D_{\text{Cu}}} \gg \frac{1}{\lambda^{\leftarrow} K_{\text{Cu}}} \exp\left(-\frac{(1-\alpha) Z F E_{\text{Cu}}}{RT}\right) \exp\left(-\frac{\alpha Z F \psi_0}{RT}\right) + \frac{1}{K_{\text{m}, \text{Cu}}} \dots (3.54)$$

the reaction is considered to be under the control of transport through diffuse double layer. The potential of the diffuse double layer, ψ_x , would control the concentration of the reducible cations within the diffuse double layer. A positive value of the potential, ψ_x , would decrease the cation concentration within the diffuse double layer below that expected by diffusion through the boundary layer alone, while a negative value of ψ_x would increase its concentration within the diffuse double layer and thus, it would control the rate of discharge reaction. Thus, when transport through diffuse double layer is the rate controlling step in the overall process of cementation, the rate constant would be strongly affected by the ionic strength. When,

$$\frac{1}{K_{\text{m}, \text{Cu}}} \gg \frac{2 \Omega}{\delta_{\text{Cu}} D_{\text{Cu}}} + \frac{1}{\lambda^{\leftarrow} K_{\text{Cu}}} \exp\left(-\frac{(1-\alpha) Z F E_{\text{Cu}}}{RT}\right) \exp\left(-\frac{\alpha Z F \psi_0}{RT}\right) \dots (3.55)$$

the resistance to transport the boundary film would be the slowest step and the reaction would be under diffusion control with regard to the transport of ion through the boundary layer. In this case the rate of cementation would be increased by increased turbulence in the aqueous phase.

In the present studies, the kinetics of cementation reaction have shown, as will be described in the following sections, that the overall rate of reaction has low activation energy (3.0216 Kcal/mole) and is strongly dependent on the hydrodynamic conditions of the bath. This leads, one to the conclusion, that the rate of cementation is controlled by the mass transport through the boundary film. To confirm this conclusion polarisation studies have been conducted using the experimental set-up shown in Fig. 3.3. The anodic and cathodic polarisation curves, so obtained, are shown in Fig. 3.4. It is seen that the anodic polarisation curve cuts the cathodic polarisation curves, drawn for the concentration range 0.5×10^{-4} mole/litre to 0.5 mole/litre of copper sulphate, in their limiting current region, thus certifying that the rate of cementation is controlled by diffusion through boundary layer. Under these conditions the overall rate equation takes the form:

$$\frac{A I_{Cu}}{Z'F} = C_{b,Cu} K_{m,Cu} A = -V \frac{dC}{dt} \quad \dots (3.56)$$

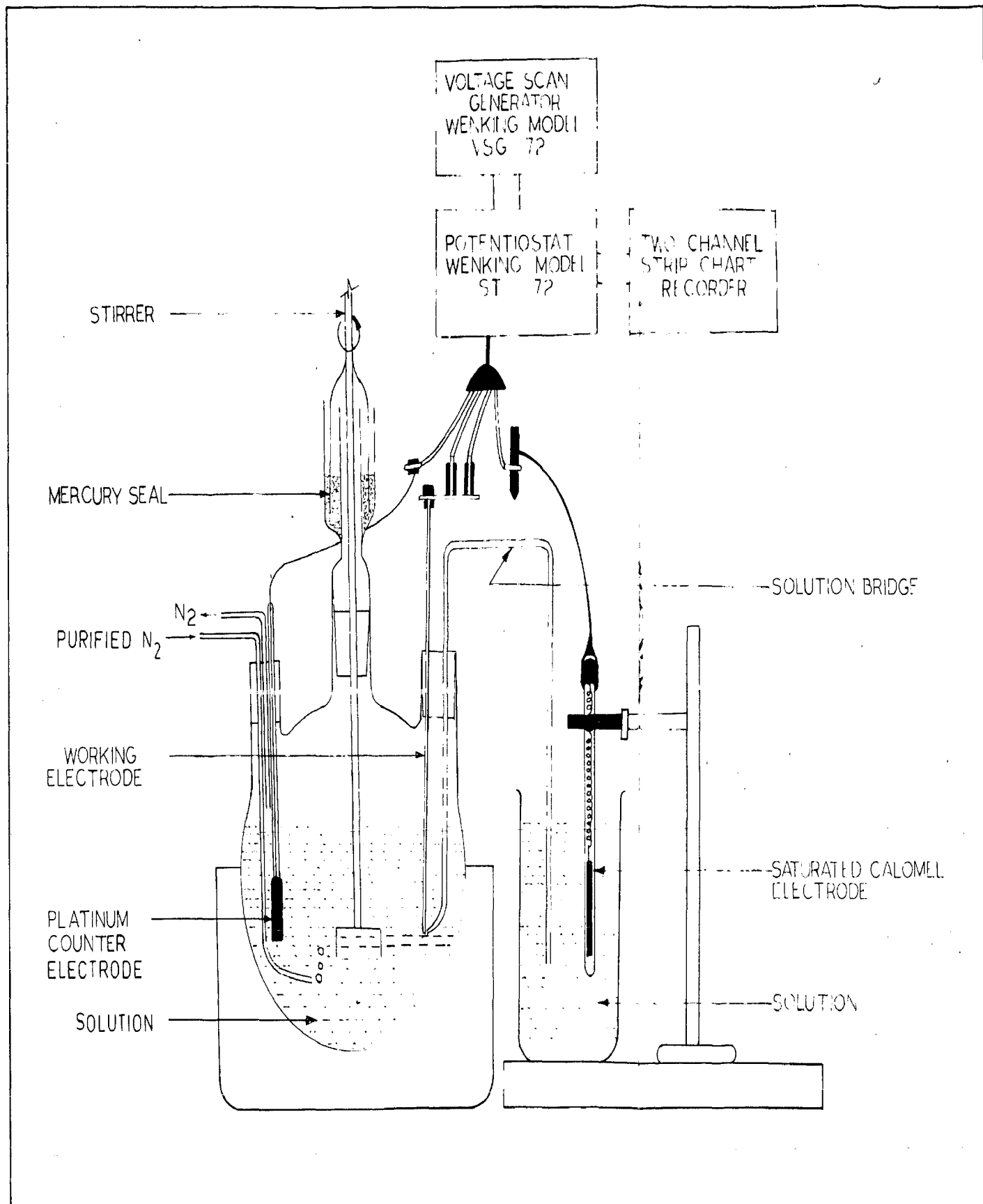


FIG. 3-3 EXPERIMENTAL SET-UP FOR POLARISATION STUDIES

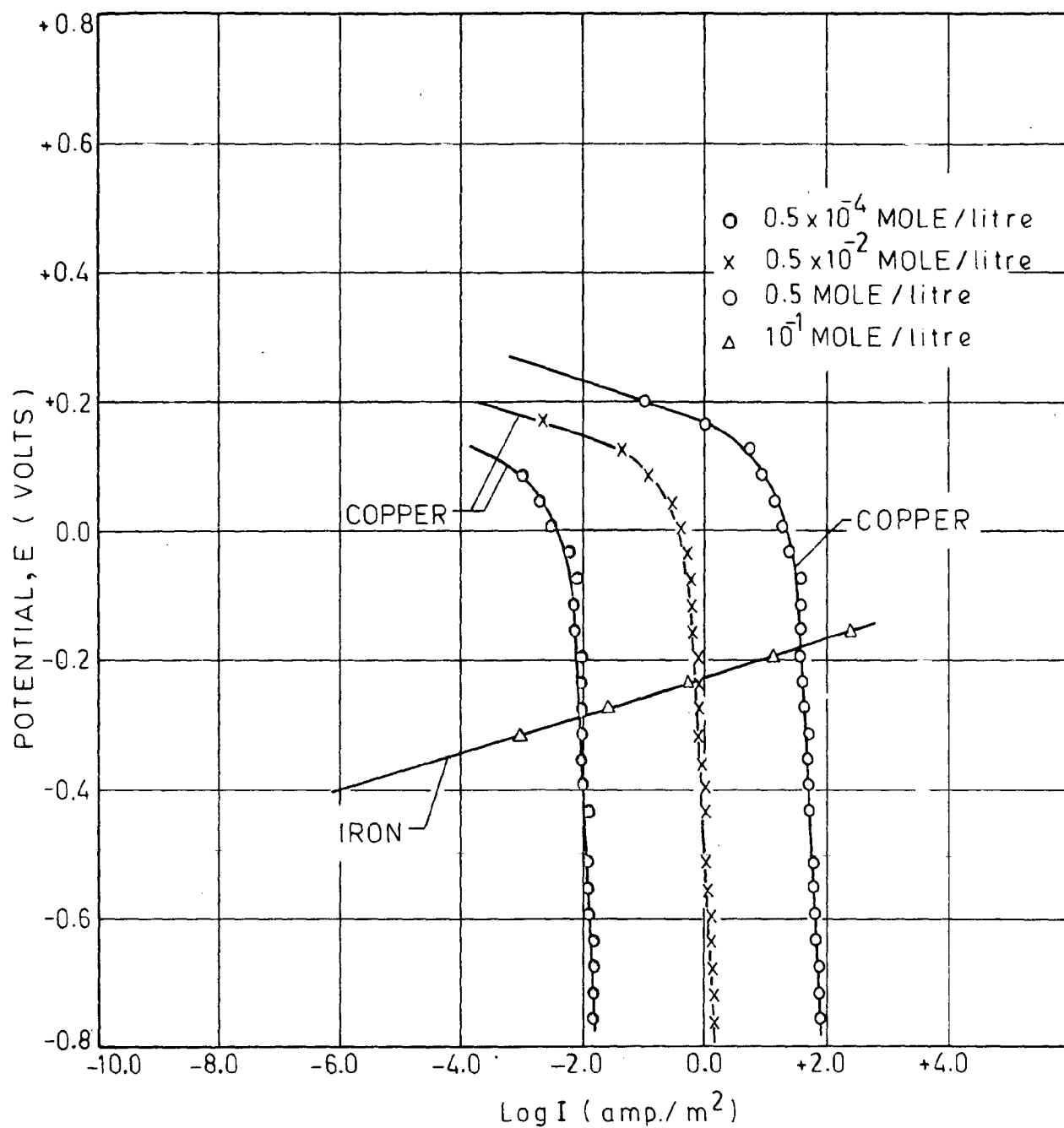


FIG.3.4 POLARISATION CURVES FOR COPPER AND IRON AT 25° C AND 1900 R.P.M.

where A is the surface area of the precipitant and V , the volume of the solution. $K_{m,Cu}$ in the above expression is related to diffusion coefficient of copper ion which, among other factors, is a function of activity coefficient of copper. The results of the thermodynamic investigations of the present work have shown that the effect of ferrous sulphate on the activity coefficient of copper sulphate is very small (Cf. section 2.3.5) and, therefore, one can assume that the activity coefficient of copper sulphate remains practically constant during a cementation run. Also the total ionic strength of the solution remains constant during a cementation run. Thus the diffusion coefficient and hence the mass transfer coefficient $K_{m,Cu}$ would be independent of concentration during a cementation run. The integration of the expression (3.56) would, therefore, give the following relation:

$$\log \left[\frac{c_{Cu^{2+}}^t}{c_{Cu^{2+}}^o} \right] = - \frac{A K_{m,Cu}}{2.303 V} \cdot t \quad \dots (3.57)$$

Using this relation the value of $K_{m,Cu}$ can be determined from the slope of the plot $\log \left[\frac{c_{Cu^{2+}}^t}{c_{Cu^{2+}}^o} \right]$ versus t , for known surface area A of the precipitant and volume V of the solution. For this, the surface area A of the precipitant was calculated, assuming spherical particles, from the theoretical relation:

$$A = \frac{6m}{\rho d} \quad \dots (3.53)$$

where m is the mass of the iron powder, ρ the material density of iron and d the particle diameter. For calculation of A from the above relation, mean particle diameter was used because the powder used for cementation was in a very close size range such as $-150 \mu + 125 \mu$, $-125 \mu + 106 \mu$, or $-106 \mu + 90 \mu$. The rate constant $K_{m,Cu}$ is determined under various experimental conditions as described in the following sections:

3.4.1 Effect of Temperature

Values of the rate constant, calculated for different temperatures from the slope of the plots of Fig. 3.5, have been used to draw the Arrhenius plot as shown in Fig. 3.6. The value of the activation energy has been calculated from the slope of the Arrhenius plot and found to be only 3.0216 Kcal/mole under the temperature range of investigation which varied from 20°C to 65°C. The first order of the cementation reaction and the very low value of the activation energy lead to the conclusion that the reaction is diffusion controlled. With regard to the effect of temperature on the rate controlling step, similar conclusions have been reported by many investigators for copper/iron system^{28,29,57} and other systems such as copper/zinc^{37,54}, copper/cadmium⁵⁴, silver/zinc²⁷, silver/iron⁵⁷, silver/copper²⁶ and cadmium/zinc³² etc.

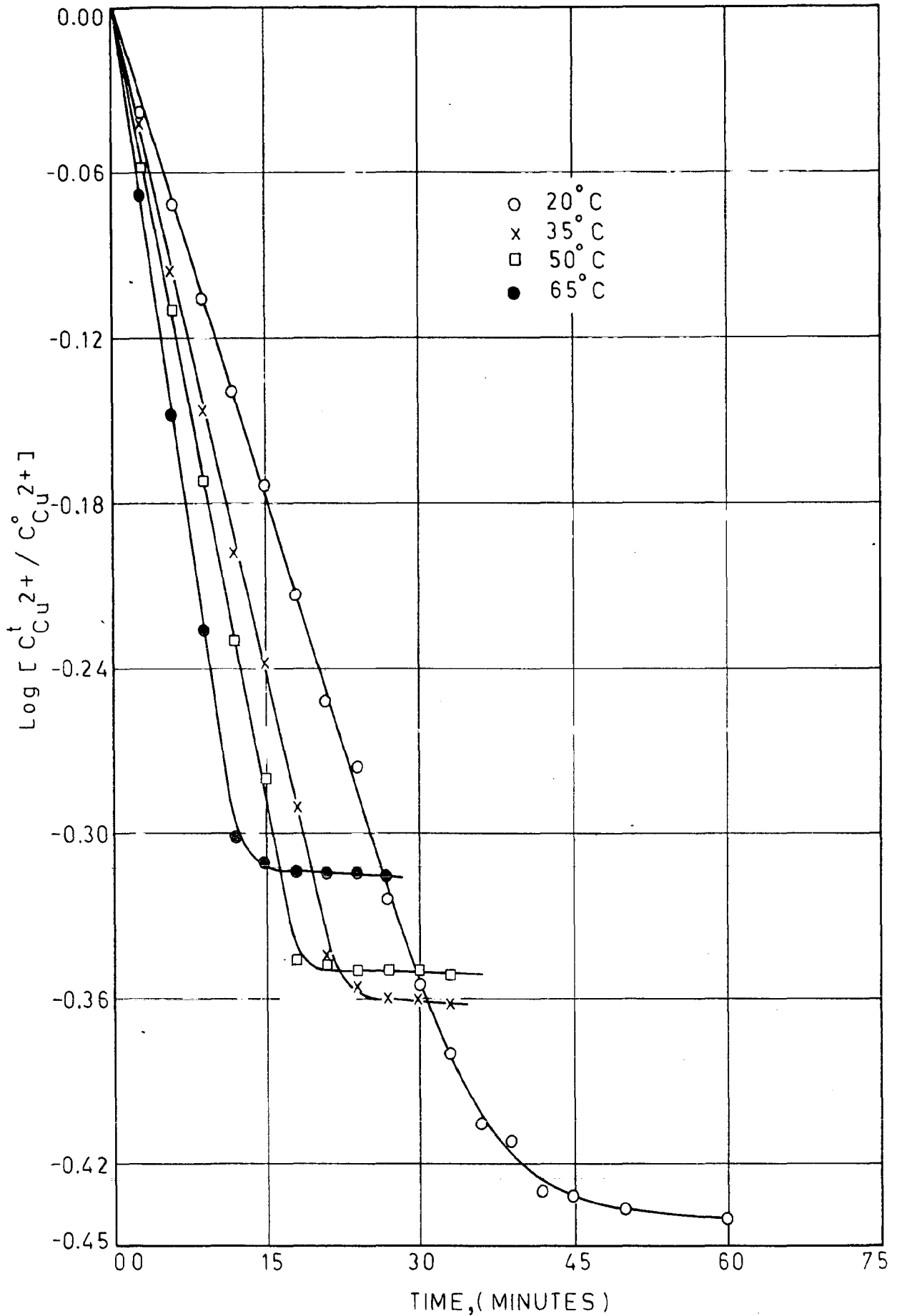


FIG.3.5 EFFECT OF TEMPERATURE ON RATE OF CEMENTATION.

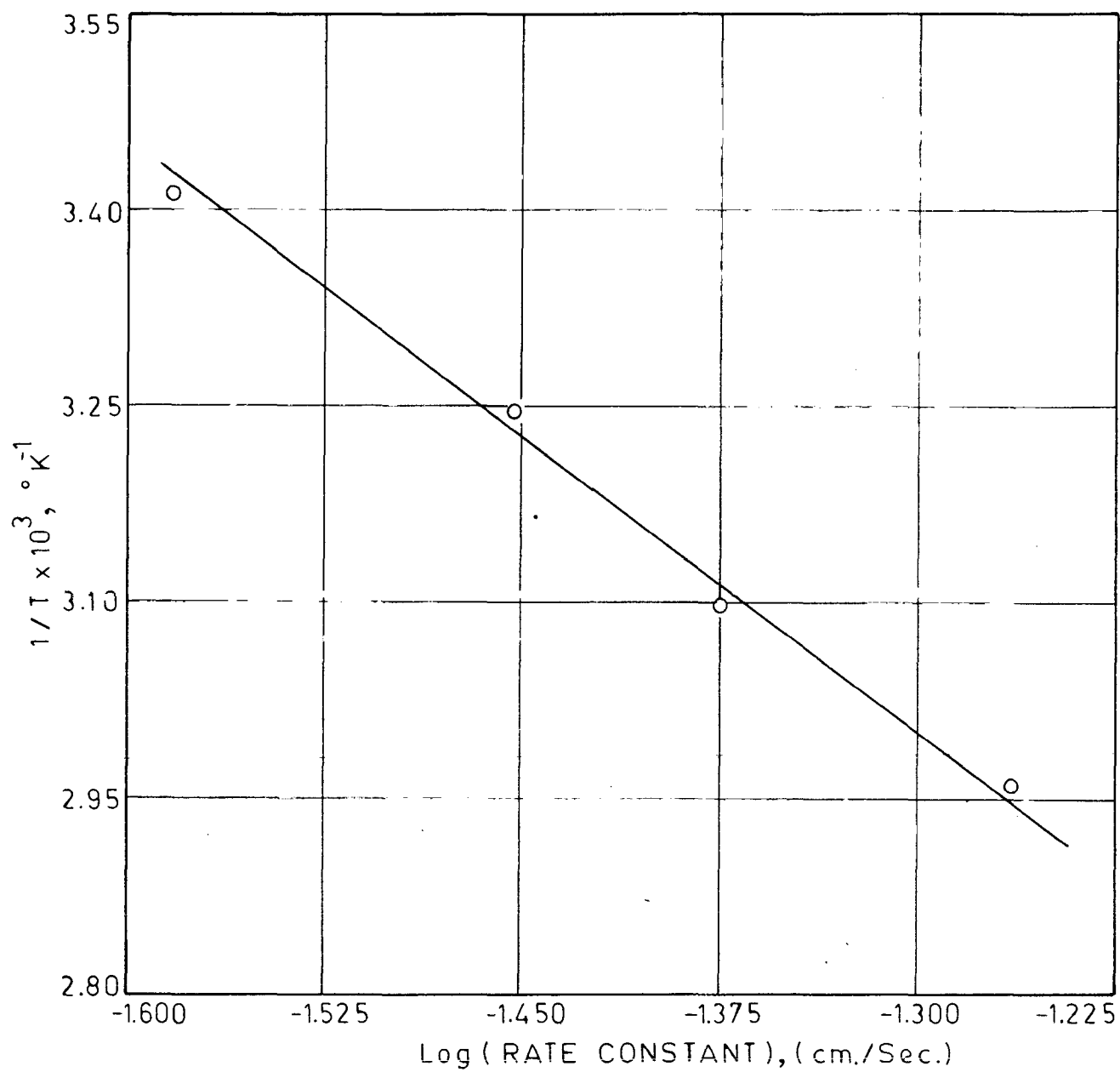


FIG.3.6 ARRHENIUS PLOT OF RATE CONSTANT OF COPPER CEMENTATION.

This activation energy compares well with the activation energy for diffusion of copper ion in aqueous phase which is reported to be 3.64 Kcal/mole⁵³. This further certifies that the overall reaction is mass transfer controlled.

3.4.2 Effect of solution agitation:

A qualitative information regarding the effect of solution-agitation on the rate of cementation can be obtained from the Fig. 3.7 which shows that the rate of cementation increases with increase in solution agitation. This indicates that the cementation is diffusion controlled process. For a quantitative evaluation of the effect of stirring on rate of cementation, dimensional analysis technique is used which shows that Sherwood number (Sh) would be a function of Reynolds number (Re) and Schmidt (Sc) number in this system. Mathematically one can write

$$\text{Sh} = f(\text{Re}, \text{Sc}) \quad \dots (3.59)$$

$$\text{where, Sh} = \frac{K_m \cdot \text{Cu} \cdot \bar{L}}{D}, \quad \text{Re} = \frac{\rho' v \bar{L}}{\mu} \quad \text{and} \quad \text{Sc} = \frac{\nu}{D} \quad \dots (3.60)$$

Here, D is the diffusion coefficient of copper ion in the solution, ρ' is density of the solution, μ is the viscosity of the solution, \bar{L} is the characteristic length and is a measure of the size of the system, v is the velocity of the fluid, and ν is the kinematic

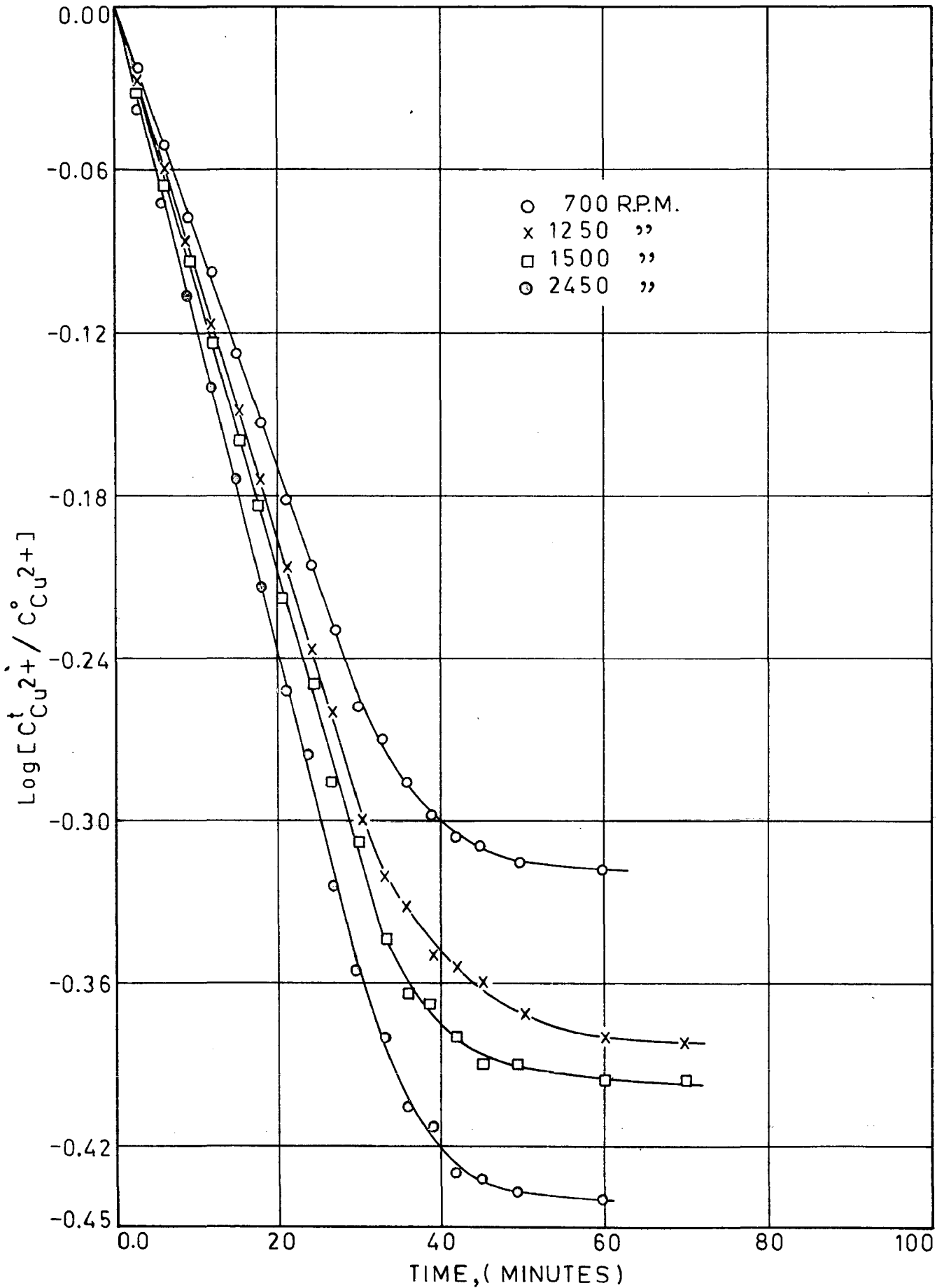


FIG.3.7 EFFECT OF STIRRING SPEED ON RATE OF CEMENTATION.

viscosity of the solution. Evolution of the Reynolds number requires a complete knowledge of the hydrodynamic conditions of the system which was not the scope of the present investigation. Reynolds number can, therefore, be expressed in terms of speed of stirring which in turn controls the fluid-dynamic condition in the bath. This procedure has been adopted by a number of other workers^{81, to 83}. As in our case L , D , μ , and ν are constant for a given solution, expression (3.59) can be rewritten as:

$$K_{n,Cu} = B (\text{rpm})^a \quad \dots (3.61)$$

where a and B are constants. In order to evaluate the constant a , K_{mCu} is obtained from the slope of the plots of the Fig. 3.7 at different rpm and then $\log K_{n,Cu}$ is plotted against $\log (\text{rpm})$ as shown in Fig. 3.8. The slope of this gives the value of $a = 0.2642$. This value of the slope is in agreement with the reported literature value for the dissolution of copper spheres of micron sizes in sulphuric acid in presence of potassium dichromate⁸³.

In order to explain the transport of material across the solution/solid particle phase boundary, a number of mechanisms such as two-film theory⁸⁴, penetration theory⁷⁹, surface renewal theory⁸⁰ and film-penetration theory⁸⁵ have been developed. In the

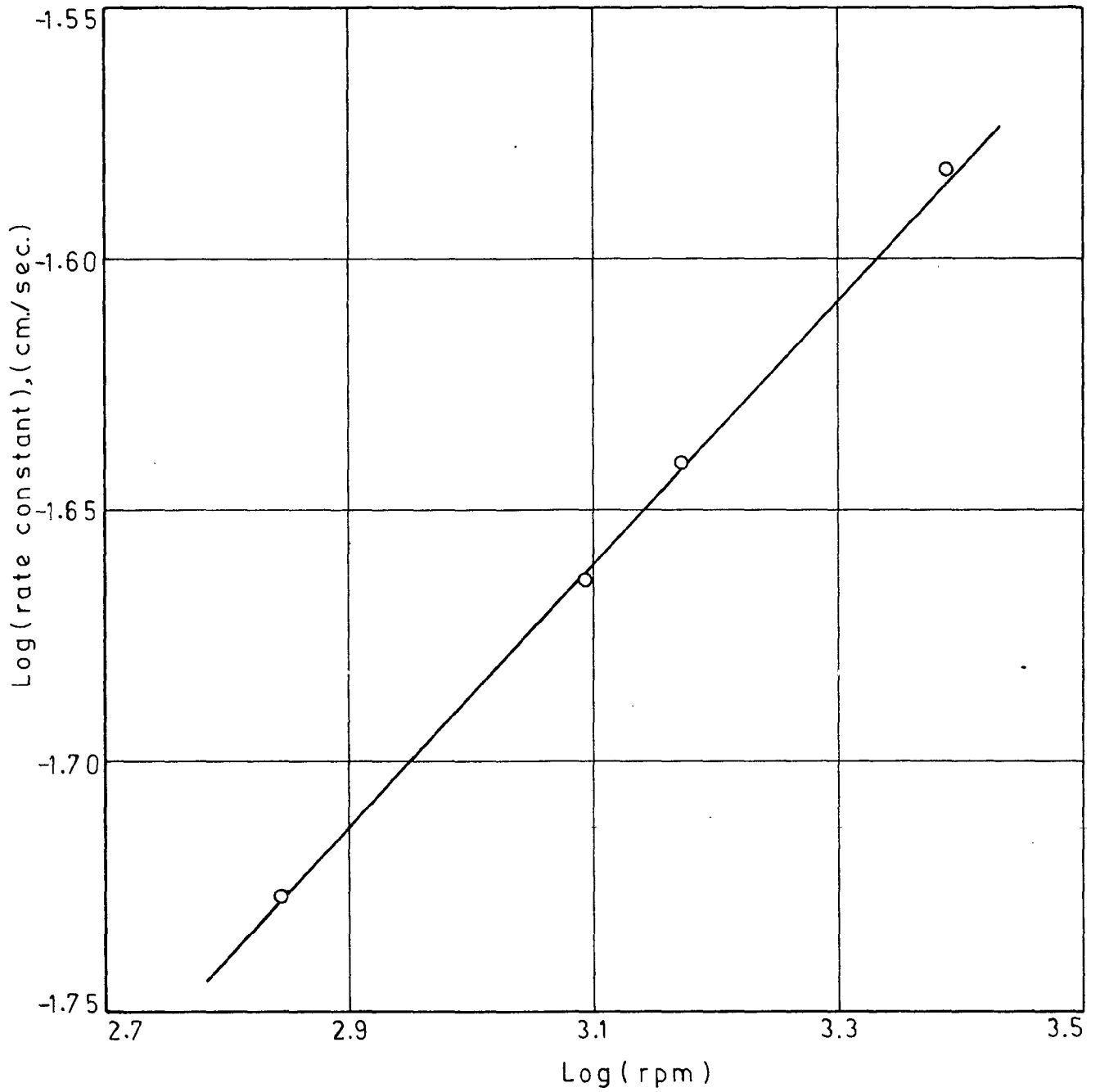


FIG.3.8 Log (rate constant) VS. Log (rpm) FOR COPPER CEMENTATION.

present system of stirred reactor, the material transport mechanism involves the transport of Chunks of fluid to the surface of the stagnant boundary film under the influence of eddies in the bulk of solution, followed by diffusion through the boundary film to the particle surface. As the rate of stirring increases, the thickness of the boundary film decreases until a limiting value is reached, and the rate of surface renewal increases. Thus, the rate of cementation increases with increase in stirring speed. However, increase in stirring speed beyond a certain limit would not result in any further increase in rate of cementation because at this stage solid particles are moving in the fluid at same speed and having the same velocity profile. In the present investigation such high stirring speeds were not used.

3.4.3 Effect of Initial Copper ion Concentration

First order plots of cementation rate data obtained for various initial copper ion concentrations are shown in Fig. 3.9. A plot of rate constant versus log of initial copper ion concentration, calculated from the slope of various plots of Fig. 3.9 is shown in Fig. 3.10. It is observed that initially the rate of cementation increases as the initial copper ion concentration increases upto about 0.5 gm copper/litre and thereafter the rate decreases with further increase in the initial concentration of copper ion in solution. The initial

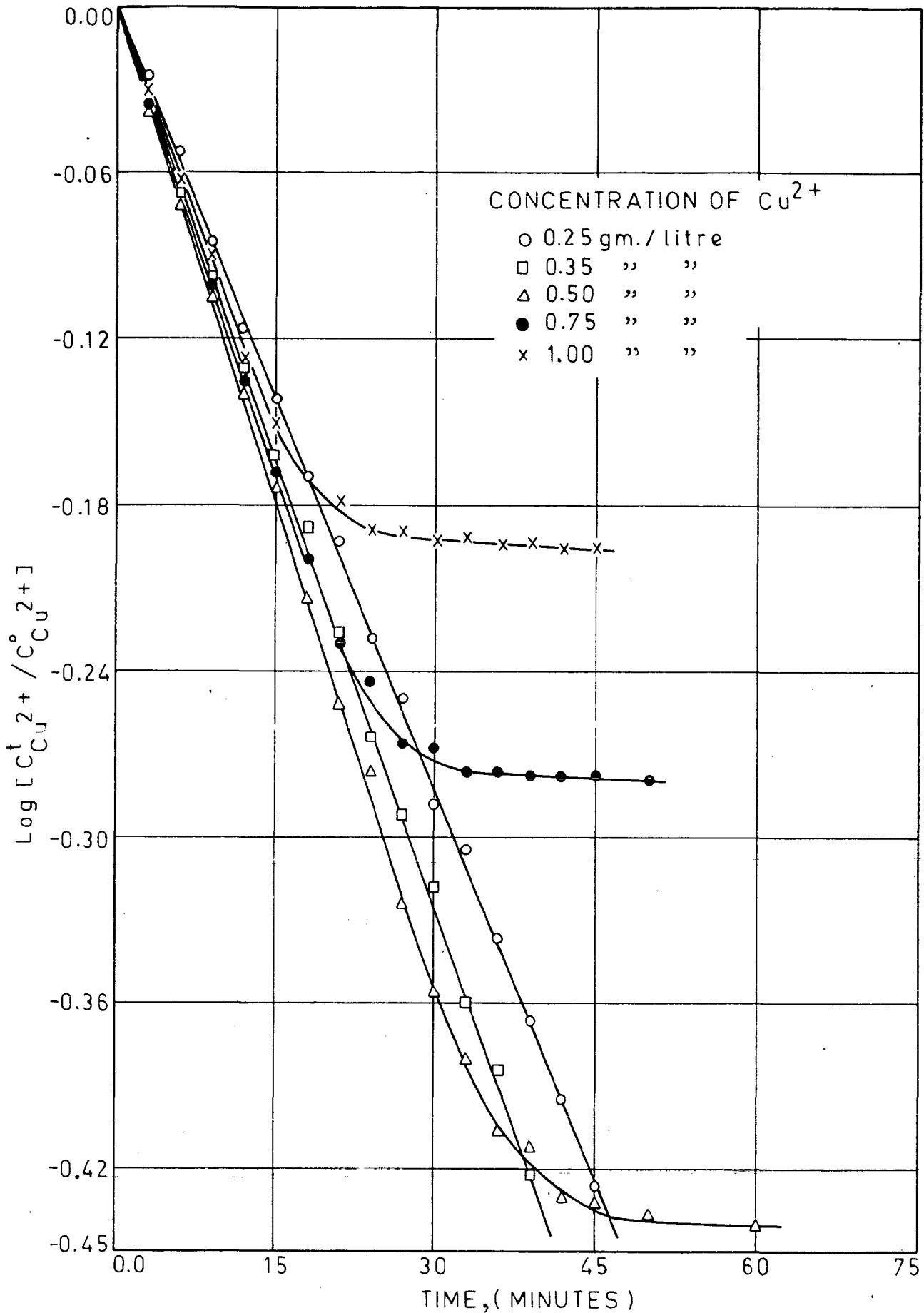


FIG.3.9 EFFECT OF INITIAL COPPER CONCENTRATION ON RATE OF CEMENTATION.

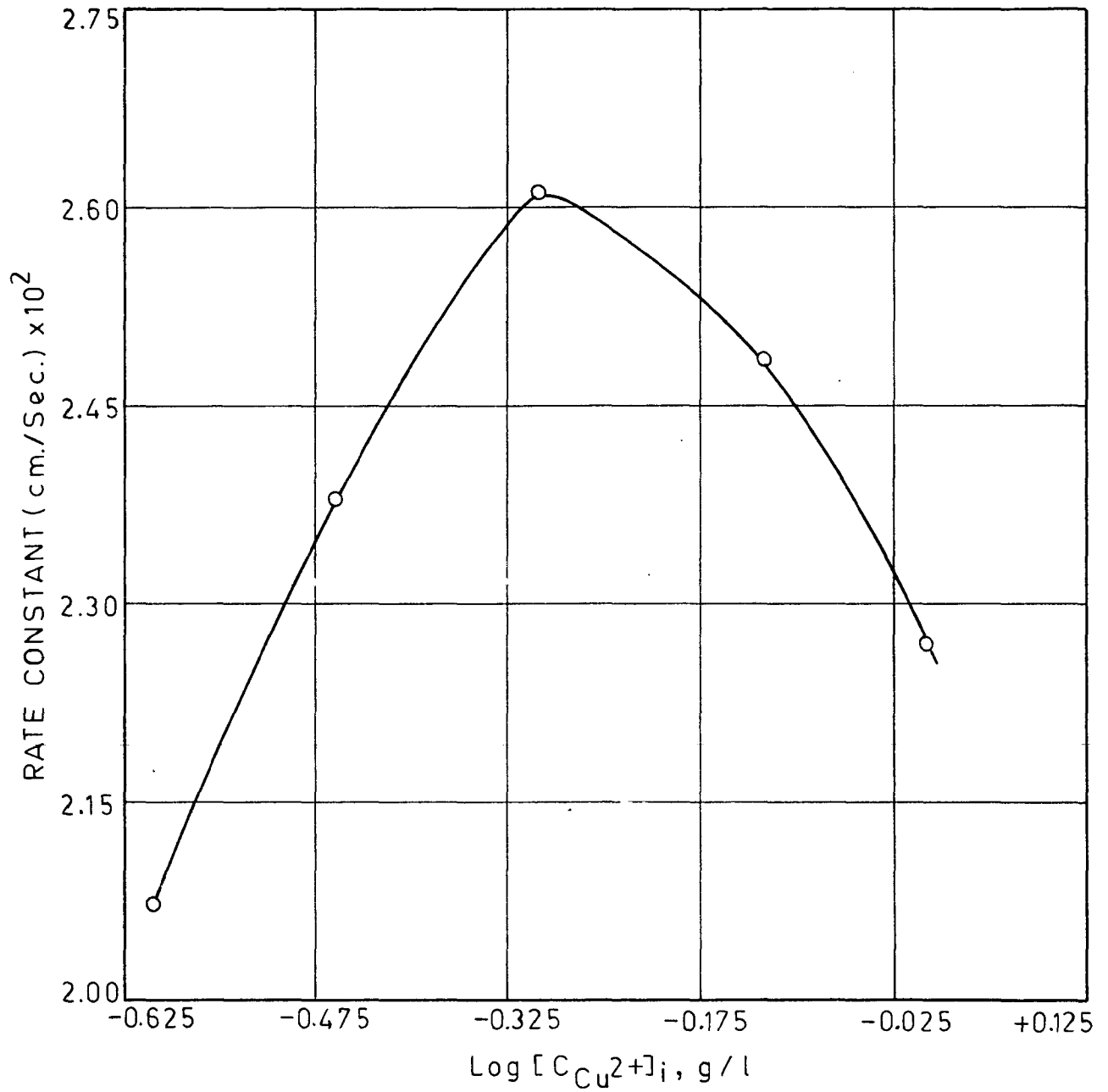


FIG.3.10 RATE CONSTANT VS. Log [C_{Cu²⁺]}_i.

increase in rate constant with increase in initial copper ion concentration in solution can be explained qualitatively in terms of the diffusion coefficient of copper. Addition of copper ion to water alters the structure of water by breaking up the short range order of water molecules owing to its size and charge and thus increases the diffusion coefficient by effectively decreasing the localised viscosity as a result of reduced intermolecular forces. As the concentration of ion increases, the diffusion coefficient reaches a maximum value, which corresponds to a minimum viscosity of the solution. Any further increase in concentration beyond this causes an almost complete removal of free water molecules and results in an increase in solution viscosity and decrease in diffusion coefficient. Variation of diffusion coefficient of copper sulphate solution at 25°C as a function of its concentration is shown in Fig. 3.11³⁶. The diffusion coefficient of copper ion is noticed to increase with increasing concentration of copper in dilute solution reaching a maximum value of about 0.95×10^{-5} cm²/sec at a concentration of 0.1 mole/litre. This explanation holds good only upto concentration value of about 0.5 g copper/litre. The decrease in rate constant with increase in initial copper concentration in the higher concentration range can be ascribed to the effect of activity coefficient on the rate constant. As activity

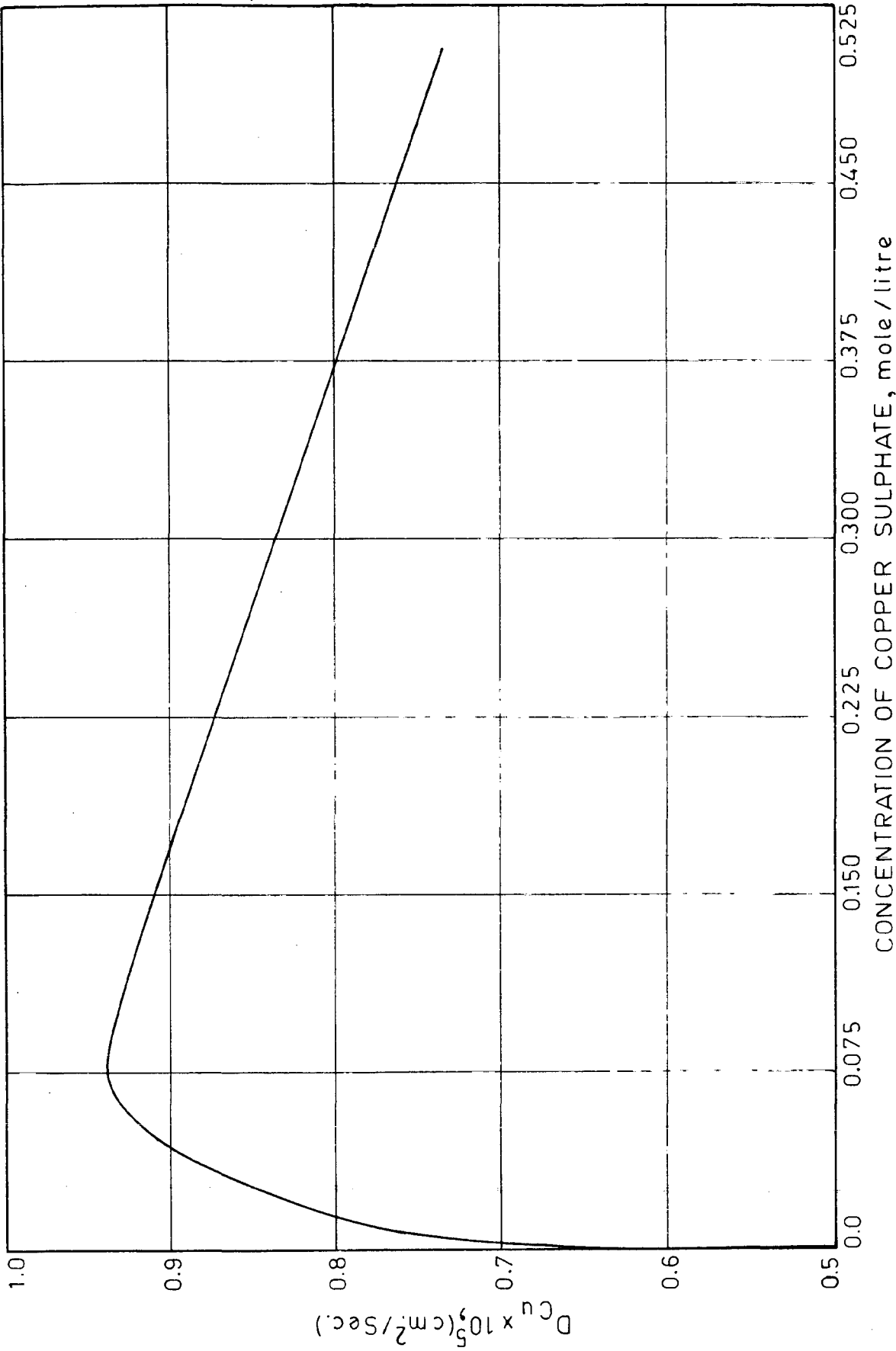
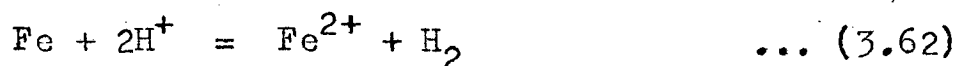


FIG.3.11 CATION DIFFUSION COEFFICIENT OF COPPER AS A FUNCTION OF CONCENTRATION AT 25°C⁽⁸⁶⁾

coefficient ~~decreases appreciably with increase in ionic strength,~~ rate constant goes on decreasing with increase in ionic strength.

3.4.4 Effect of Hydrogen ion Concentration (pH):

First order plot of rate data obtained for different initial pH values are shown in Fig. 3.12. It is observed that the rate constant decreases appreciably with decrease in pH from 2.8 to 1.5. A plot of specific rate constant versus pH is shown in Fig. 3.13. Conclusions from the thermodynamic investigations based on the inferences from Figs. 2.16 and 2.17 have indicated that the driving force for cementation is not affected by the presence of acid in the copper sulphate-ferrous sulphate mixed electrolytes. Therefore, the appreciable decrease in rate constant, as pH is decreased from 2.8 to 1.5, can be ascribed to the increased competition between copper ion and hydrogen ion for discharge sites on the metal surface at higher hydrogen ion concentration. Due to the following reaction between iron and hydrogen ion:



which can proceed to a higher extent at low pH, the surface area available for cementation reaction is decreased. The hydrogen so produced is likely to block the metal surface due to its slow desorption step⁸⁷.

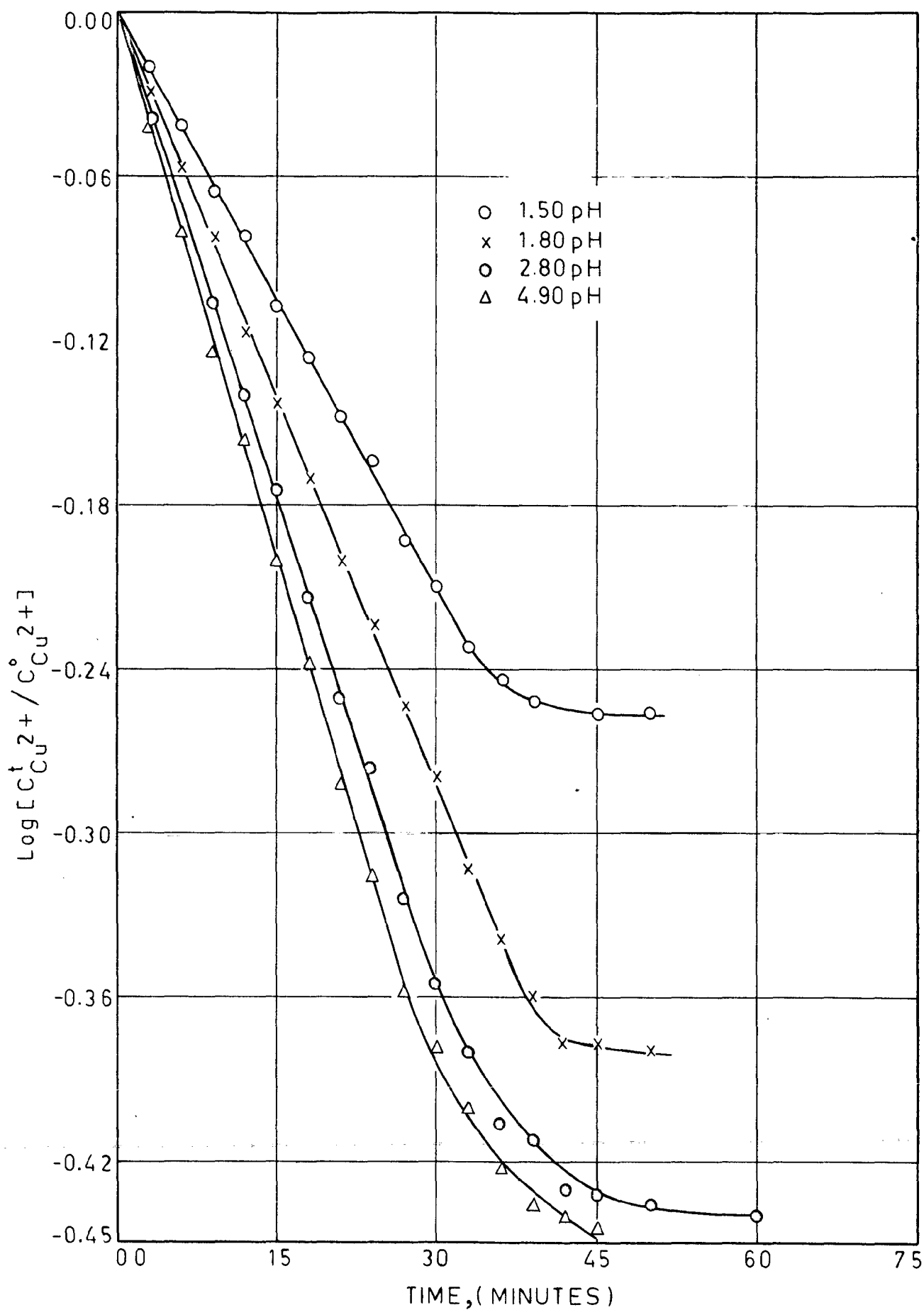


FIG.3.12 EFFECT OF pH ON RATE OF CEMENTATION.

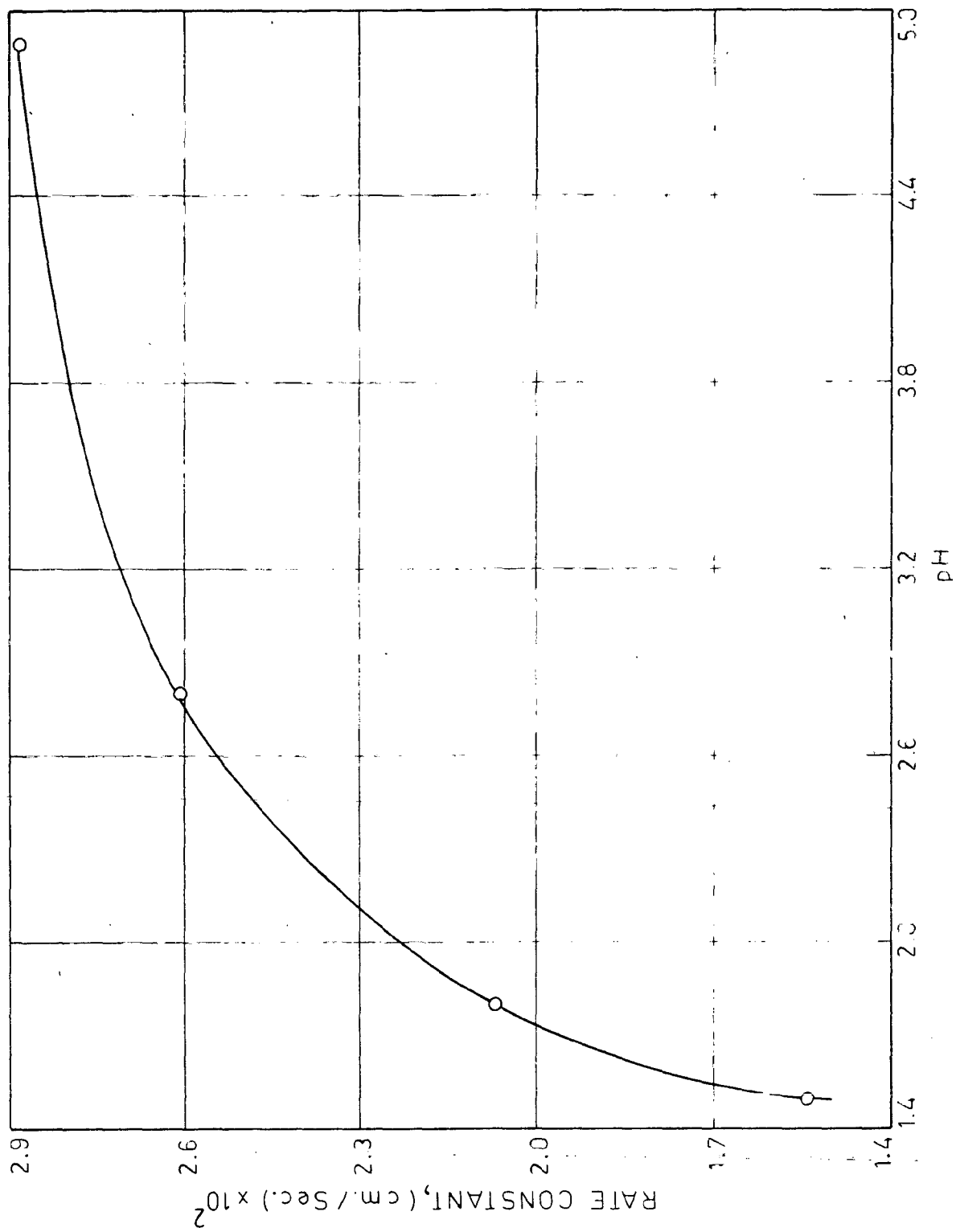


FIG.3.13 EFFECT OF pH ON RATE CONSTANT OF COPPER CEMENTATION.

To confirm this, the variation of excess iron in solution over the theoretically required amount is shown in Fig. 3.14 using pH as parameter. It is seen that the amount of excess iron consumed over the theoretical amount increases with decreasing pH at low pH. This certifies that there was a competition between copper ion and hydrogen ion for discharge sites on metal surface at very low pH.

3.4.5 Effect of Particle size and solution/powder ratio

First order plots of the cementation rate data obtained for different particle sizes of the iron powder are shown in Fig. 3.15. It is observed that the rate of cementation increases as the particle size of the iron powder decreases. For a quantitative evaluation of the effect of particle size on rate of cementation, expression (3.57) can be used. After substituting for A from relation (3.58) in this relation (3.57), the slope p of the first order plot comes out to be:

$$p = \frac{6 m K_{m,Cu}}{2.303 V d P} \quad \dots (3.63)$$

Taking log on both sides one gets the relation:

$$\log p = \log \frac{6 m K_{m,Cu}}{2.303 V P} - \log d \quad \dots (3.64)$$

The above relation shows that the variation of $\log p$

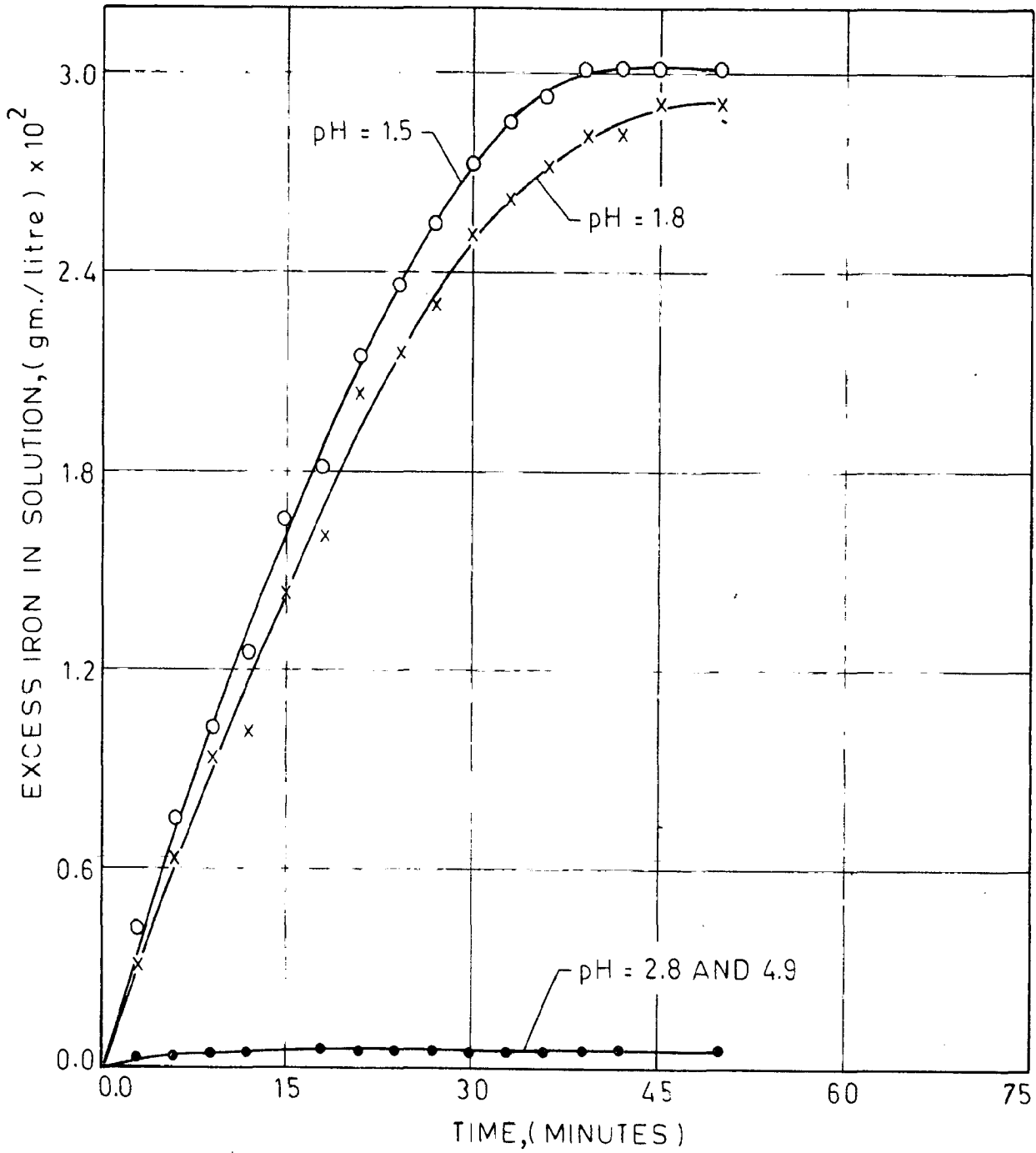


FIG.3.14 EFFECT OF pH ON EXCESS IRON CONSUMPTION.

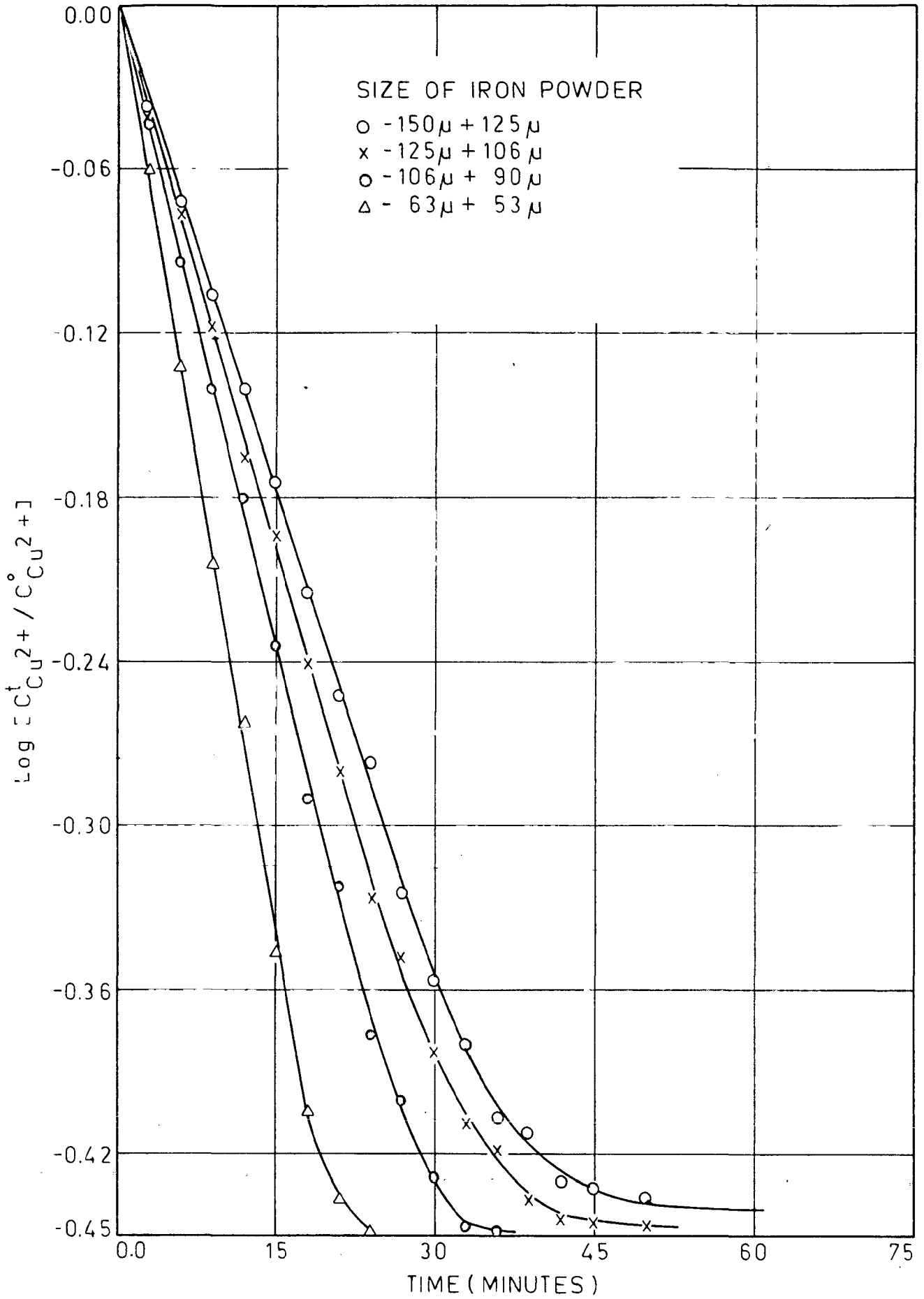


FIG.3.15 EFFECT OF SIZE OF IRON POWDER ON RATE OF CEMENTATION.

calculated from the slopes of the first order plot of Fig. 3.15, with $\log d$ is a straight line with a slope of 39° as shown in Fig. 3.16. The small deviation of this slope (39°) from 45° can be ascribed to the effects of surface and shape factors. This leads to the conclusion that the increase in the cementation rate with decrease in particle size is due to the increased surface area of the precipitant available for precipitation.

To study the effect of solution/powder ratio on the rate of cementation, the ratio was varied by changing the amount of iron powder added to the copper sulphate solution of fixed initial concentration. First order plot of the cementation rate data obtained for various initial solution/powder ratio are shown in Fig. 3.17. It is seen that as the solution/powder ratio decreases the rate of cementation increases. For a quantitative evaluation of the effect of solution/powder ratio on the rate of cementation, expression (3.63) can be used. In this d is constant and m is variable in the present case. Hence taking log on both sides of this expression (3.63) one gets

$$\log p = \log \frac{6 K_{m,Cu}}{2.303 V P d} + \log m \quad \dots (3.65)$$

This relation shows that variation of $\log p$ versus $\log m$ should be a straight line with 45° slope. This

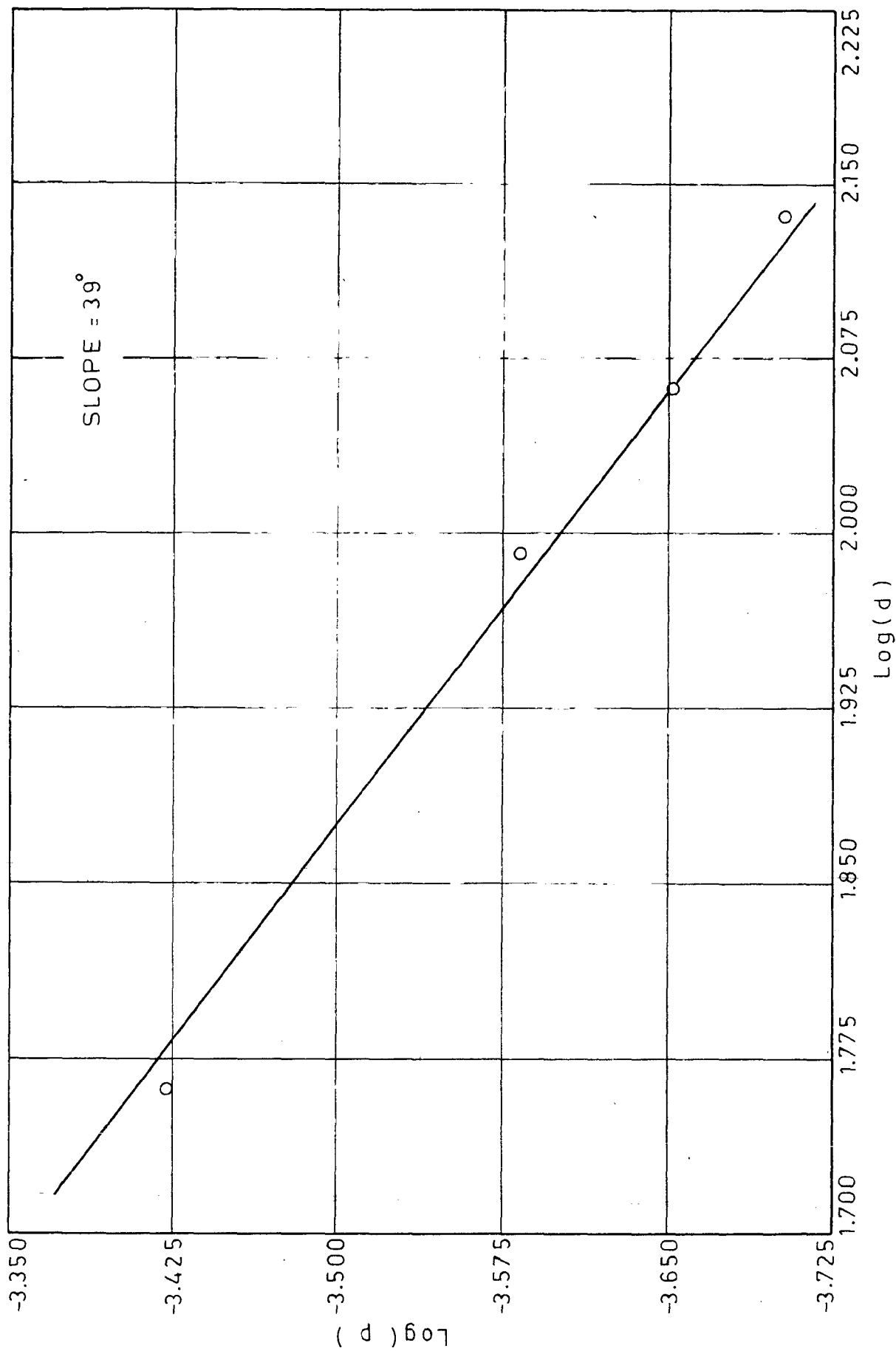


FIG.3.16 Log (p) VERSUS Log (d).

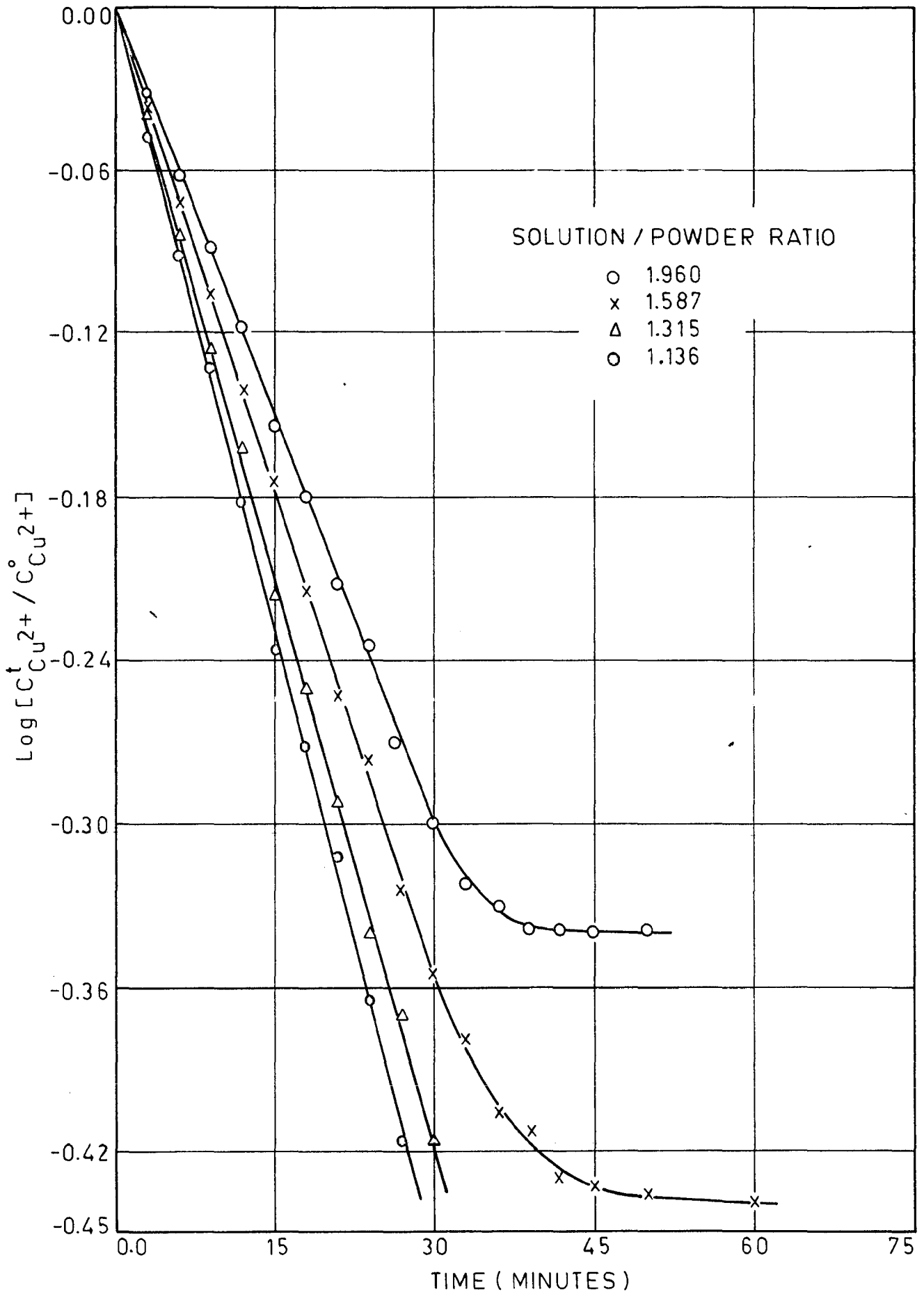


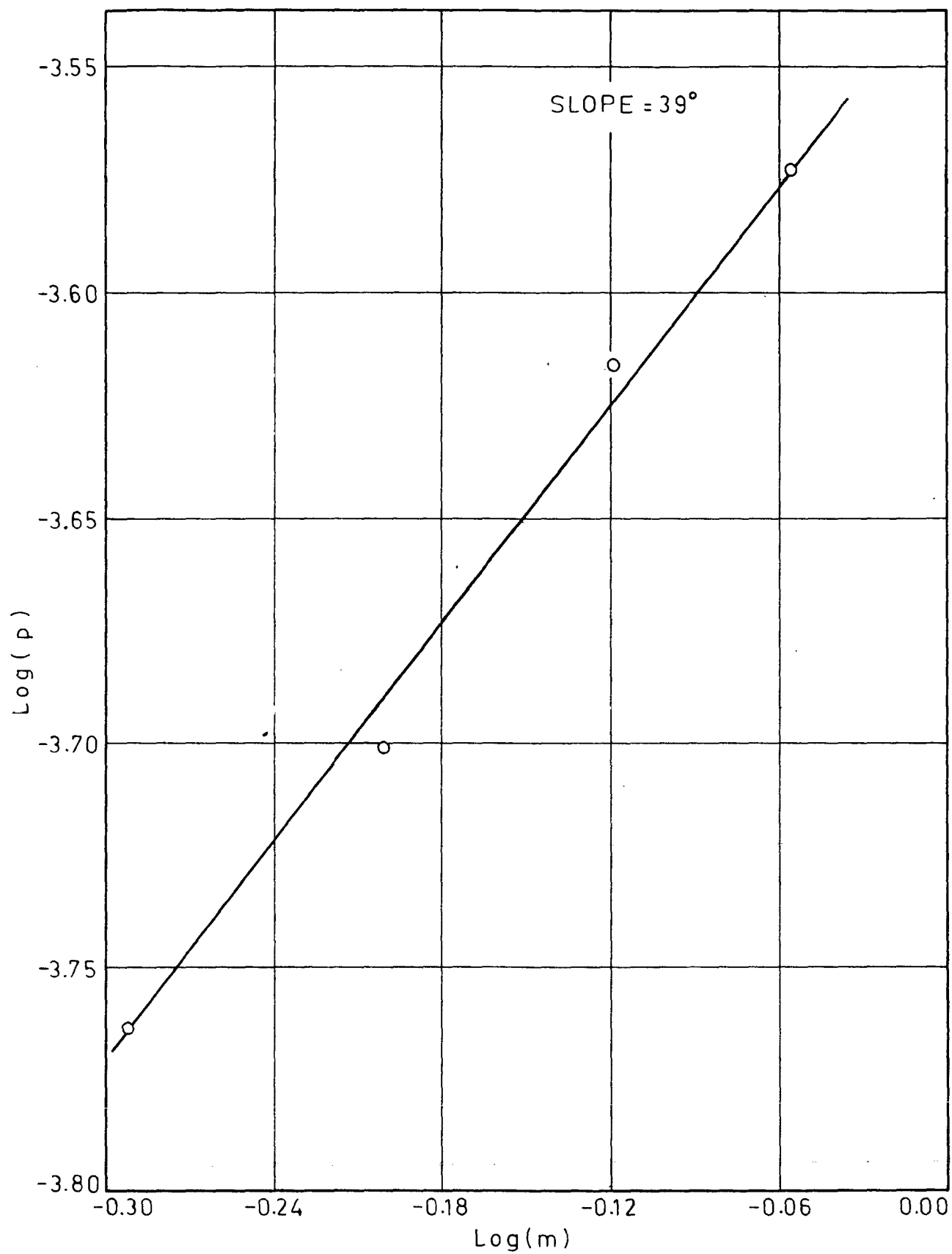
FIG.3.17 EFFECT OF SOLUTION / POWDER RATIO ON RATE OF CEMENTATION.

graph was plotted from the slopes of the first order plot of Fig. 3.17 and is shown in Fig. 3.18. The slope of this plot is 39° instead of 45° . This small difference can be ascribed to surface and shape factors effect which were not taken into consideration. Thus, increase in rate with decrease in solution/powder ratio is due to the increased surface area of the precipitant.

When solution/powder ratio is changed by changing the initial concentration of the solution for fixed amount of iron precipitant used, it has been observed earlier from Fig. 3.10 that the rate constant increases with increase in solution/powder ratio to an optimum value for the ratio 1.587 (corresponding to 0.5gm copper/l concentration) beyond which the rate constant decreases. This was attributed to the increase in diffusion coefficient in dilute solution range and considerable decrease in activity coefficient in concentrated solution range.

3.4.6 Effect of Atmosphere

First order plots of the rate data for cementation process carried out under nitrogen, hydrogen and air are shown in Fig. 3.19. It is seen that the use of hydrogen atmosphere in place of nitrogen has hardly any effect on rate of cementation. However, in air atmosphere there is a slight decrease in cementation rate. This decrease in rate in air atmosphere can be

FIG.3.18 $\text{Log}(p)$ VERSUS $\text{Log}(m)$.

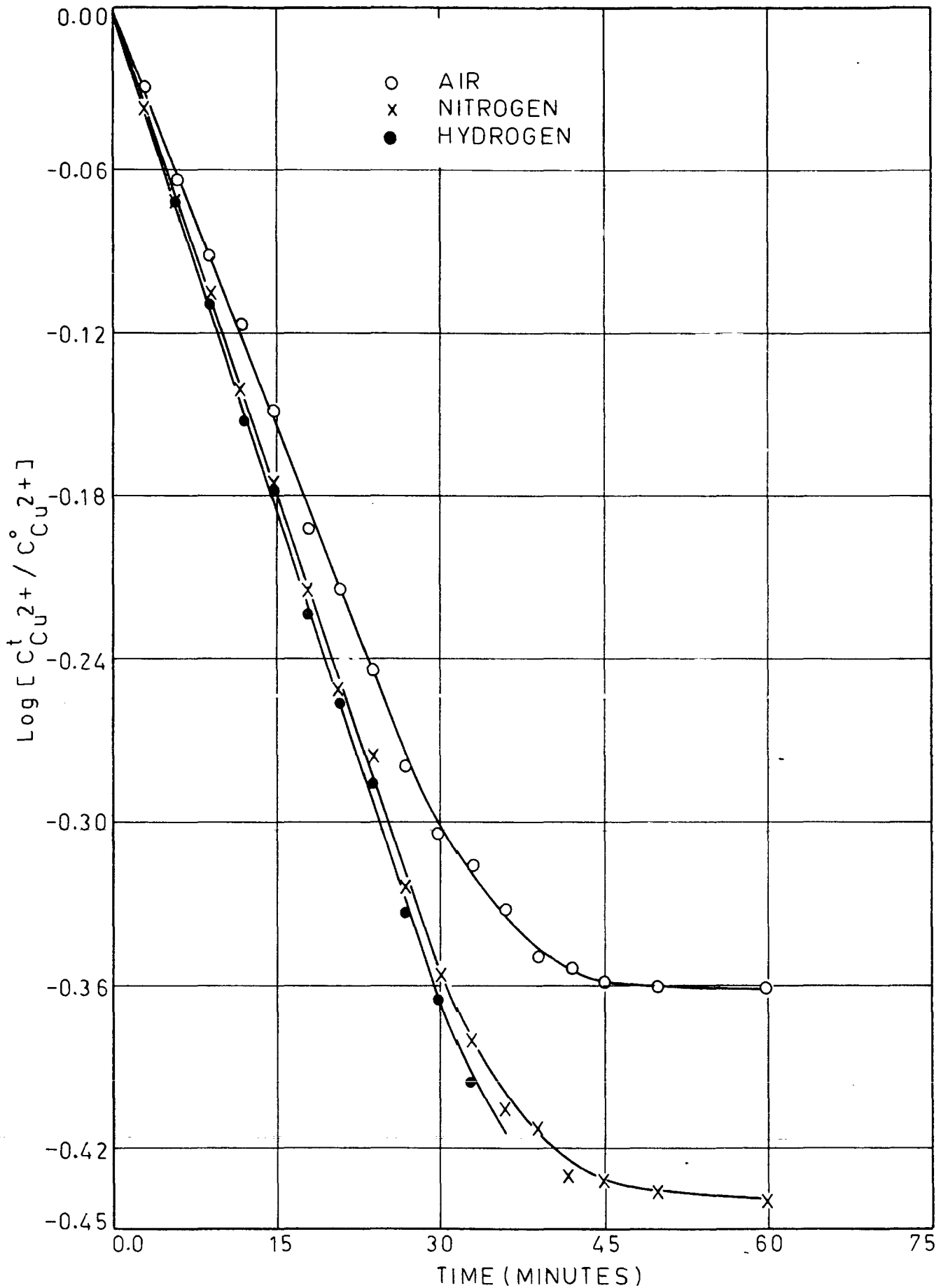
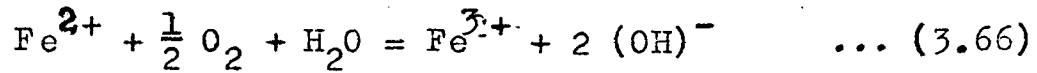
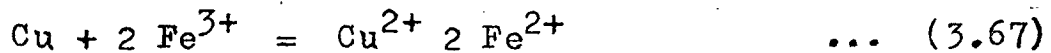


FIG. 3.19 EFFECT OF ATMOSPHERE ON RATE OF CEMENTATION.

ascribed to the formation of Fe^{3+} ion by the reaction:



followed by the oxidation of precipitated copper by the reaction



The observed increase in pH value of the solution from 2.5 to 3.8 towards the end of cementation run, carried out in air atmosphere, accompanied by precipitation of particles of ferric hydroxide confirms the formation of Fe^{3+} ion. Also there was an increase in the amount of iron consumed over the theoretical amount for this run as shown in Fig. 3.20 which confirms the occurrence of reaction (3.67) because Cu^{2+} so formed would require additional iron for cementation.

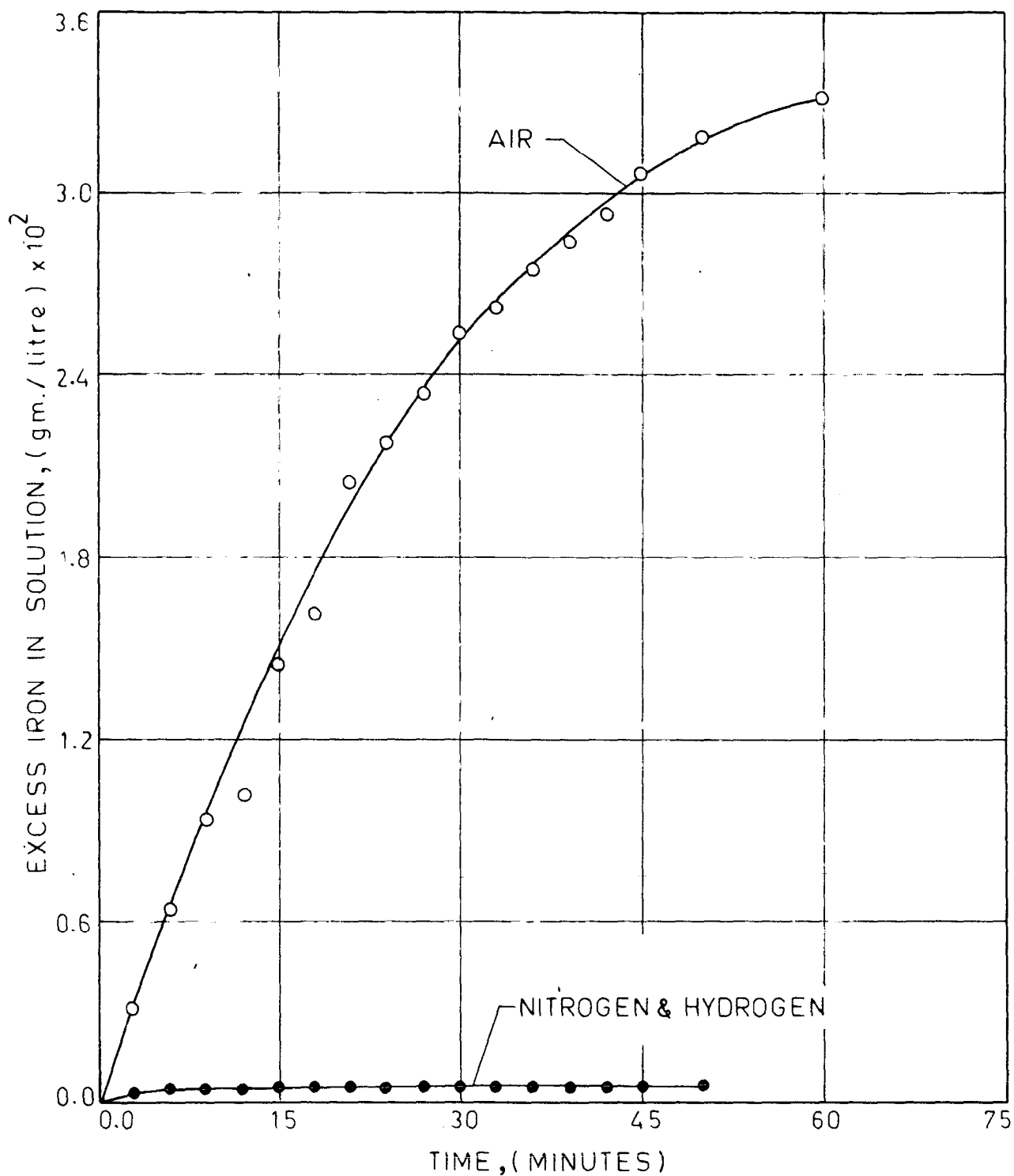


FIG.3.20 EFFECT OF ATMOSPHERE ON EXCESS IRON CONSUMPTION.

C H A P T E R - I V

CHARACTERISTICS OF CEMENT COPPER POWDERS

4.1 General

In order to find out the industrial utility of the cement copper powders, it would be necessary to evaluate the characteristics of these powders and the effect of process variables on their compaction and sintering properties. For this, cement copper powders were produced under different experimental conditions at room temperature, at pH = 2.8 under inert atmosphere and annealed under hydrogen atmosphere at 500°C. Following powder characteristics were studied using standard methods described in texts^{88,89}:

- i) Particle shape, size and size distribution
- ii) Apparent density
- iii) Flow rate , and,
- iv) Friction index

Effects of above characteristics on the following process variables were also studied:

- i) Green density and densification parameter
- ii) Compression ratio
- iii) Sintered density
- iv) Green porosity and sintered porosity
- v) Liquid-phase sintering
- vi) Microstructure of sintered products.

4.2 Powder Characteristics

4.2.1 Particle shape, size and size distribution:

A photomicrograph of the cement copper powder taken under Scanning electron micrograph is shown in Fig. 4.1. It is seen that the powders are of oval shape and are porous. Particle size distribution in a powder mass was studied by standard sieve analysis method. Effects of initial size of iron powder and initial concentration of copper sulphate solution on particle size distribution are given in Tables 4.1 and 4.2 and the results are plotted in Figs. 4.2 and 4.3 respectively. It is clear from Fig. 4.2 that the decrease in the size of the iron powder used for cementation results in a cement powder with a larger amount of finer size fraction and a wider range of particle size distribution. A combined reference to Table 4.2 and Fig. 4.3 leads to the conclusion that an increase in the initial concentration of copper sulphate in solution produces cement copper powder with a relatively close range of particle size. Thus using a coarser size of iron powder precipitant and a higher initial concentration of copper sulphate in solution, it would be possible to produce relatively coarse cement copper powder with close range of particle size distribution.



Magnification

80 X



Magnification

200 X

Fig. 4.1 Shape of Cement Copper Particles

TABLE-4.1: Effect of the Size of the Iron Powder Precipitant on Particle Size and Particle Size Distribution of the Cement Copper Powder Produced

Size of the Iron Precipitant (micron)	Direct Weight % , (Particle size in μ)											
	+ 300	-300	+212	+180	-180	+125	-125	+106	-106	-90	-75	-63
-150 + 125	9.5	0.27	16.2	26.4	41.4	4.5	Nil	Nil	Nil	Nil	0.87	0.5
-125 + 106	Nil	Nil	3.4	14.5	49.7	31.0	Nil	Nil	Nil	Nil	0.77	0.6
- 75 + 63	3.9	Nil	6.3	15.7	28.3	13.8	Nil	Nil	Nil	Nil	31.5	0.3

Cumulative Weight % , (Particle size in μ)												
-150 + 125	9.5	9.7	26.0	52.4	93.9	98.4	98.4	98.4	93.4	99.3	99.8	99.8
-125 + 106	Nil	Nil	3.4	17.8	67.6	98.6	98.6	98.6	98.6	99.3	99.9	99.9
- 75 + 63	3.9	3.9	10.2	24.0	54.2	68.1	68.1	68.1	68.1	99.6	99.9	99.9

TABLE-4.2: Effect of the Initial Copper Concentration in Solution on Particle Size and Particle Size Distribution of the Cement Copper Powder Produced

Initial copper concentration in solution (gr/l)	Direct Weight % (Particle Size in μ)									
	+ 300	- 300	-180	-150	-125	-106	-90	-75	-63	
3.177	Nil	Nil	0.17	25.1	61.2	7.8	0.6	0.4	0.8	2.6
6.354	9.5	0.27	16.2	26.4	41.4	4.5	Nil	Nil	0.8	0.5
8.895	Nil	Nil	2.8	2.8	33.1	11.5	Nil	Nil	Nil	0.3
Cumulative Weight % (Particle Size in μ)										
3.177	Nil	Nil	0.17	25.3	86.5	94.5	95.0	95.5	96.3	99.0
6.354	9.5	9.7	26.0	52.4	93.9	98.4	98.4	98.4	99.3	99.8
8.895	Nil	Nil	2.8	5.7	88.9	99.4	99.4	99.4	99.4	99.7

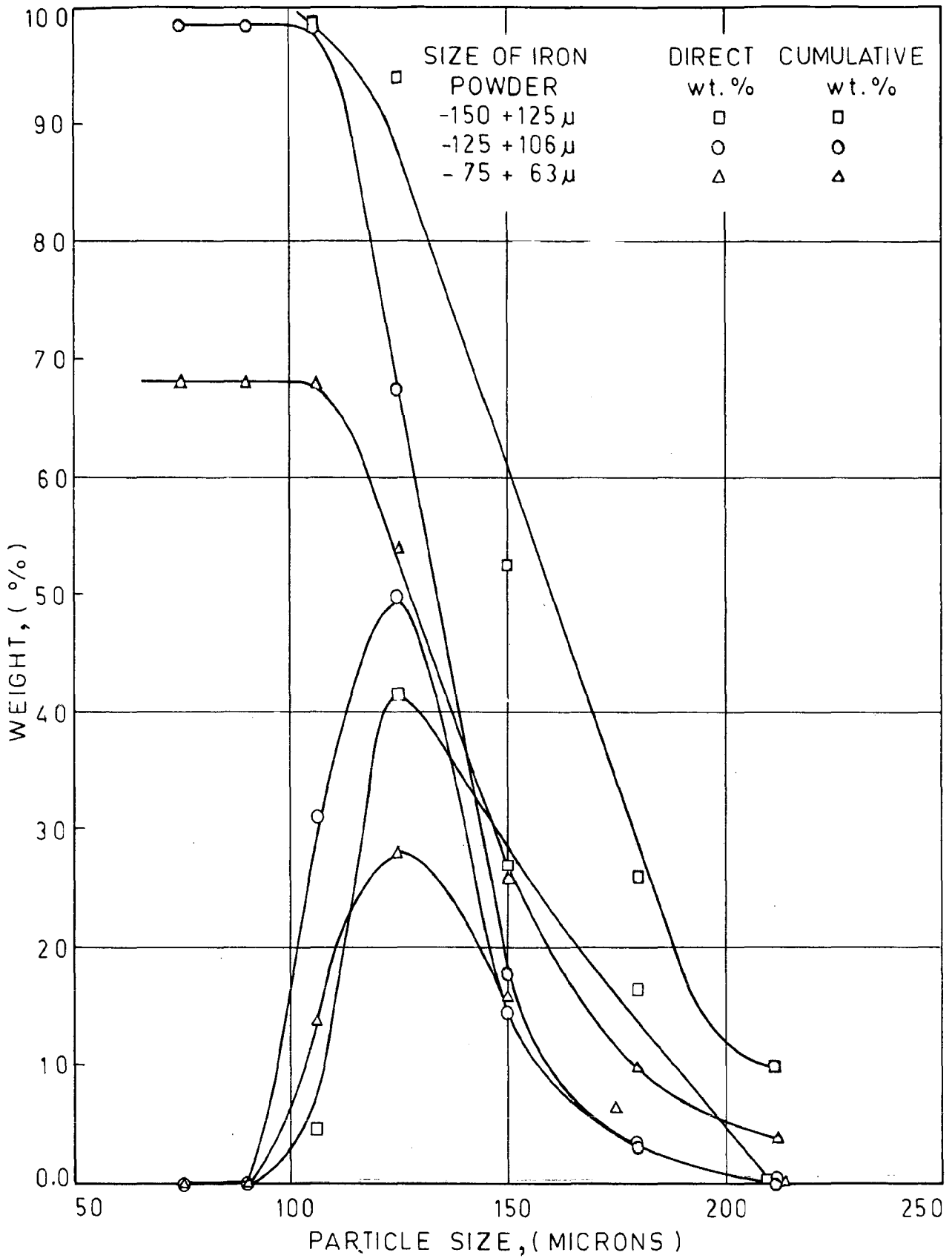


FIG.4.2 EFFECT OF IRON POWDER PARTICLE SIZE ON SIZE DISTRIBUTION OF CEMENT COPPER POWDERS PRODUCED.

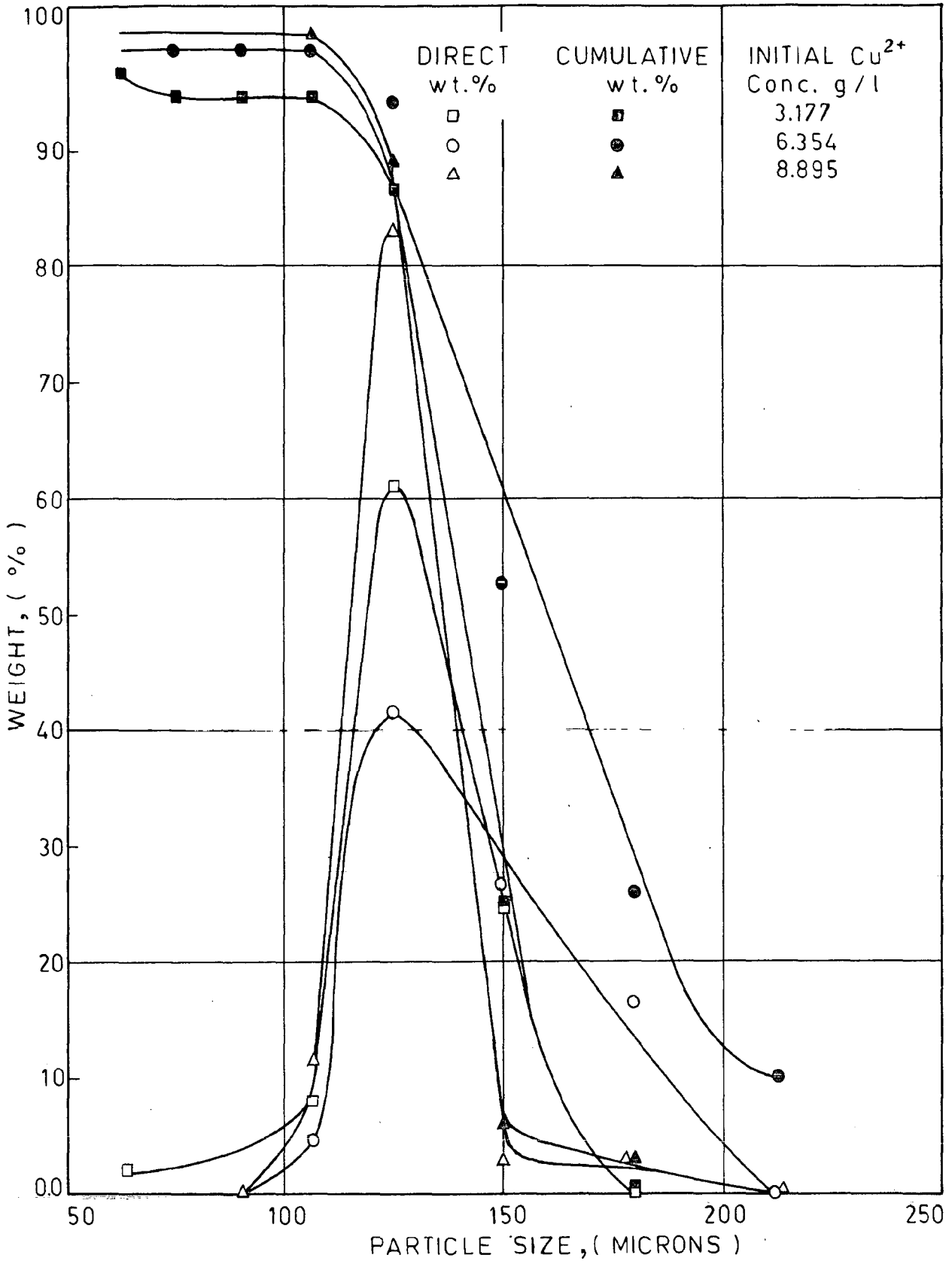


FIG.4.3 EFFECT OF INITIAL CONCENTRATIONS OF COPPER ON PARTICLE SIZE DISTRIBUTION OF CEMENT COPPER POWDER PRODUCED.

4.2.2 Apparent density

The calculated values of apparent densities of various cement powders are given in Tables 4.3 and 4.4. It is noted from Table 4.3 that as the size of the iron powder precipitant increases, the apparent density of the resultant cement powder increases to an optimum value beyond which any further increase in the size of iron powder decreases the apparent density of the powder product. This can be explained in terms of the effects of particle shape, size and size distribution in the cement powder and its friction index. As noted under section 4.2.1, a decrease in particle size of the initial iron powder produces cement powders with larger finer size fraction and wider particle size distribution. The lowest apparent density of the cement powder obtained from -75 + 63 micron size powder is due to its highest frictional surface area which reduces the ability of the particles to settle efficiently and causes bridging effect, thus producing a greater porosity in the loose powder mass. The lower apparent density of the cement powder obtained from -150 + 125 micron size iron powder as compared to that obtained from -125 + 106 micron size iron powder is due to the wider range of particle size distribution in it as compared to that in the latter powder which is clear from Fig. 4.2. With regard to the effect of initial concentration of copper sulphate

TABLE-4.3: Effect of the Particle Size of the Iron Powder Precipitant on Flow Rate, Apparent Density, Tap Density, and Friction Index.

Material	Flow Rate (gn/min)	Apparent Density, d_a (gn/cc)	Tap Density dt (gn/cc)	Friction Index	Apparent Density/ Material Density
Cement copper powder produced from -150 μ + 125 μ size iron powder	82.18	2.519	2.980	1.182	0.284
Cement copper powder produced from -125 μ + 106 μ size iron powder.	95.23	2.529	2.850	1.126	0.290
Cement copper powder produced from -75 μ + 63 μ size iron powder	74.62	2.294	2.782	1.212	0.267
Iron powder of -150 μ + 125 μ size	137.61	3.541	4.104	1.158	0.450
Iron powder of -125 μ + 106 μ size.	131.00	3.400	3.993	1.174	0.432
Iron powder of -75 μ + 63 μ size.	129.31	3.216	3.917	1.218	0.409

TABLE-4.4: Effect of the Initial Copper Concentration in Solution on Flow Rate, Apparent Density, Tap Density and Friction Index, and the Values of these Properties for the Iron Powder used as Precipitant

Material	Flow Rate (gm/min)	Apparent Density, d_a (gm/cc)	Tap Density, (gm/cc)	Friction Index	Apparent Density Material Density
Cement copper powder produced from 3.177g Cu/l solution.	115.38	3.101	3.535	1.140	0.377
Cement Copper powder produced from 6.354g Cu/l	82.18	2.519	2.980	1.182	0.284
Cement copper powder produced from 8.895g Cu/l solution	68.49	2.000	2.407	1.203	0.235
Iron powder of size -150 μ + 125 μ size.	137.61	3.541	4.104	1.158	0.450

solution on apparent density, a decrease in apparent density of the resultant cement powder is observed with increase in initial solution concentration. This variation can be explained in terms of friction index results, given in Table 4.4, which takes into account the nature of the particle surface in addition to the effect of particle size and particle size distribution. It is seen from Table 4.4 that the friction index of cement powder increases as the initial concentration of the solution increases and hence the apparent density decreases.

4.2.3 Flow rate

Flow rates of various cement powders produced and iron powders used as precipitant are given in Tables 4.3 and 4.4. As regards the effect of initial particle size of iron powder on flow rate of cement powder, it is seen that there is an optimum value of the iron powder size for which the flow rate of the resultant cement powder is maximum. To explain this following quantitative relationship is used⁸⁹:

$$\log t = \log \left(\frac{WS_w R}{AKC} \right) - \log \left(\frac{da}{d} \right) \quad \dots (4.1)$$

where, da is apparent density and d the material density of the powder, K and C are constants, A the cross-sectional area of the orifice of the flowmeter

funnel, W the total weight of the powder flowing, S_w specific surface area, R the surface roughness factor and t the total time for powder flow. From this relation, it is clear that t is inversely proportional to the da/d ratio. Calculated values of da/d ratio are given in Tables 4.3 and 4.4. The decrease in flow rate of the cement powders produced from solutions of higher initial copper concentrations can also be explained on similar lines.

4.2.4 Tap density and Friction index

Calculated values of tap density and friction index are given in Table 4.3 and 4.4 for various cement copper powders. A higher friction index value is an indication of the higher frictional forces between particles of the powder mass. Variation in the friction index are clearly due to the effects of particle size and size-distribution in the powder mass on the settling efficiency of the powder and its bridging tendency.

4.3 Process Variables

4.3.1 Compressibility and Green density

Details of the weight, diameter and height of the various green compacts are given in Table 4.5. Results of densification parameter and green density of different cement copper products and iron powder products are

TABLE-4.5: Weight, Diameter and Height of the Various Green Compacts
 diameter of die = 1.63 in

Material	Dimensions in (CGS unit)	Green Compact Produced at Different Loads				
		2.5T	4T	6T	8T	10T
Cement copper from -150+125 μ size iron	Wt.	7.960	7.960	7.961	7.960	7.961
	Dia.	1.630	1.630	1.630	1.630	1.630
	Ht.	0.642	0.582	0.535	0.503	0.483
-do- from -125+106 μ	Wt.	7.960	7.961	7.961	7.960	7.960
	Dia.	1.630	1.630	1.630	1.630	1.630
	Ht.	0.684	0.608	0.560	0.519	0.499
-do- from -75+63 μ	Wt.	7.960	7.960	7.961	7.961	7.960
	Dia.	1.630	1.630	1.630	1.630	1.630
	Ht.	0.725	0.647	0.579	0.541	0.513
Cement copper from 3.177s Cu/l	Wt.	7.960	7.961	7.960	7.960	7.960
	Dia.	1.630	1.630	1.630	1.630	1.630
	Ht.	0.703	0.637	0.579	0.547	0.536

...../Contd.

Material	Dimensions in (CGS unit)	Green Compact Produced at Different Loads				
		2.5T	4T	6T	8T	10T
Cement copper from 8.895g Cu/l	Wt.	7.961	7.961	7.960	7.961	7.961
	Dia.	1.630	1.630	1.630	1.630	1.630
	Ht.	0.698	0.628	0.572	0.541	0.530
Iron product from -150+125 μ size iron powder	Wt.	Nil	7.960	7.960	7.960	7.961
	Dia.	Nil	1.630	1.630	1.630	1.630
	Ht.	Nil	0.654	0.601	0.569	0.549
-do- from -125+106 μ size	Wt.	Nil	7.960	7.960	7.960	7.960
	Dia.	Nil	1.630	1.630	1.630	1.630
	Ht.	Nil	0.669	0.624	0.588	0.561
-do- from -75+63 μ size	Wt.	Nil	7.960	7.960	7.961	7.960
	Dia.	Nil	1.630	1.630	1.630	1.630
	Ht.	Nil	0.685	0.637	0.598	0.570

TABLE-4.6: Effect of the Iron Powder Precipitant on Green Density, Densification Parameter and Compression Ratio of the Cement Copper Powder Produced and the Iron Powder.
 diameter of die = 1.63 cm

	Green Density (g/cc)				Densification Parameter				Compression Ratio							
	2.5T	4T	6T	8T	10T	2.5T	4T	6T	8T	10T	2.5T	4T	6T	8T	10T	
Cement copper from -150 μ +125 μ size iron	5.93	6.54	7.12	7.53	7.89	7.89	0.54	0.63	0.72	0.79	0.84	2.35	2.59	2.82	3.00	3.13
-do- from -125 μ +106 μ	5.57	6.27	6.80	7.33	7.63	7.63	0.49	0.61	0.68	0.78	0.83	2.20	2.48	2.68	2.90	3.05
-do- from -75 μ + 63 μ	5.25	5.88	6.58	7.04	7.42	7.42	0.47	0.57	0.68	0.75	0.82	2.29	2.56	2.86	3.07	3.23
Iron powder of -150+125 μ	-	5.82	6.34	6.70	6.94	6.94	Nil	0.52	0.64	0.73	0.78	Nil	1.64	1.79	1.89	1.96
-do- of -125+106 μ	Nil	5.69	6.11	6.48	6.78	6.78	Nil	0.51	0.60	0.69	0.76	Nil	1.67	1.79	1.90	1.99
-do- of -75+63 μ	Nil	5.56	5.98	6.37	6.68	6.68	Nil	0.50	0.59	0.68	0.74	Nil	1.73	1.86	1.98	2.07

TABLE-4.7:

Effect of the Initial Concentration of Copper in Solution on Green Density, Densification Parameter and Compression Ratio of the Cement Copper Powder Produced, and the values of these Properties for the Iron Powder used as Precipitant

Diameter of die = 1.63 cm.

Material	Green Density (gm/cc)										Densification Parameter										Compression Ratio									
	2.5T	4T	6T	8T	10T	2.5T	4T	6T	8T	10T	10T	2.5T	4T	6T	8T	10T	10T	2.5T	4T	6T	8T	10T								
Cement copper powder produced from 3.177g Cu/l solution	5.42	5.98	6.50	6.96	7.11	0.45	0.56	0.63	0.75	0.73	1.74	1.93	2.12	2.24	2.29	2.35	2.59	2.82	3.00	3.13										
Cement copper powder produced from 6.354g Cu/l solution	5.93	6.54	7.12	7.58	7.89	0.54	0.63	0.72	0.79	0.84	2.73	3.03	3.32	3.52	3.59															
Cement copper powder produced from 3.395g Cu/l solution	5.46	6.06	6.65	7.04	7.19	0.53	0.62	0.71	0.77	0.79	2.73	3.03	3.32	3.52	3.59															
Iron powder of size -150 μ +125 μ	-	5.82	6.34	6.70	6.94	-	0.52	0.64	0.73	0.78	-	1.64	1.79	1.89	1.96															

given in Tables 4.6 and 4.7. These results are plotted in Figs. 4.4 to 4.7. Both these measures of compressibility show that as the size of the iron powder precipitant increases, the compressibility of the resultant cement powder increases. This variation can be explained in terms of chemical composition and plasticity of the powder mass. It is seen from Table 4.8 that the powder obtained from coarser size iron powder has higher copper content and, therefore, higher plasticity and compressibility. As far as the effect of initial copper concentration in solution is concerned, it is seen from Figs 4.6 and 4.7 that the compressibility of the cement powder increases with increase in initial copper ion concentration in solution to an optimum value beyond which any further increase in solution concentration results in a decrease in compressibility. This can again be explained in terms of the composition of the powder mass as given in Table 4.8.

A comparison of the compressibility of the cement copper powders with that of the iron powders indicates that a cement copper powder of even very low copper content has higher compressibility than iron powder due to the higher plasticity of copper than that of iron.

4.3.2 Compression ratio

Compression ratios of various cement copper powders

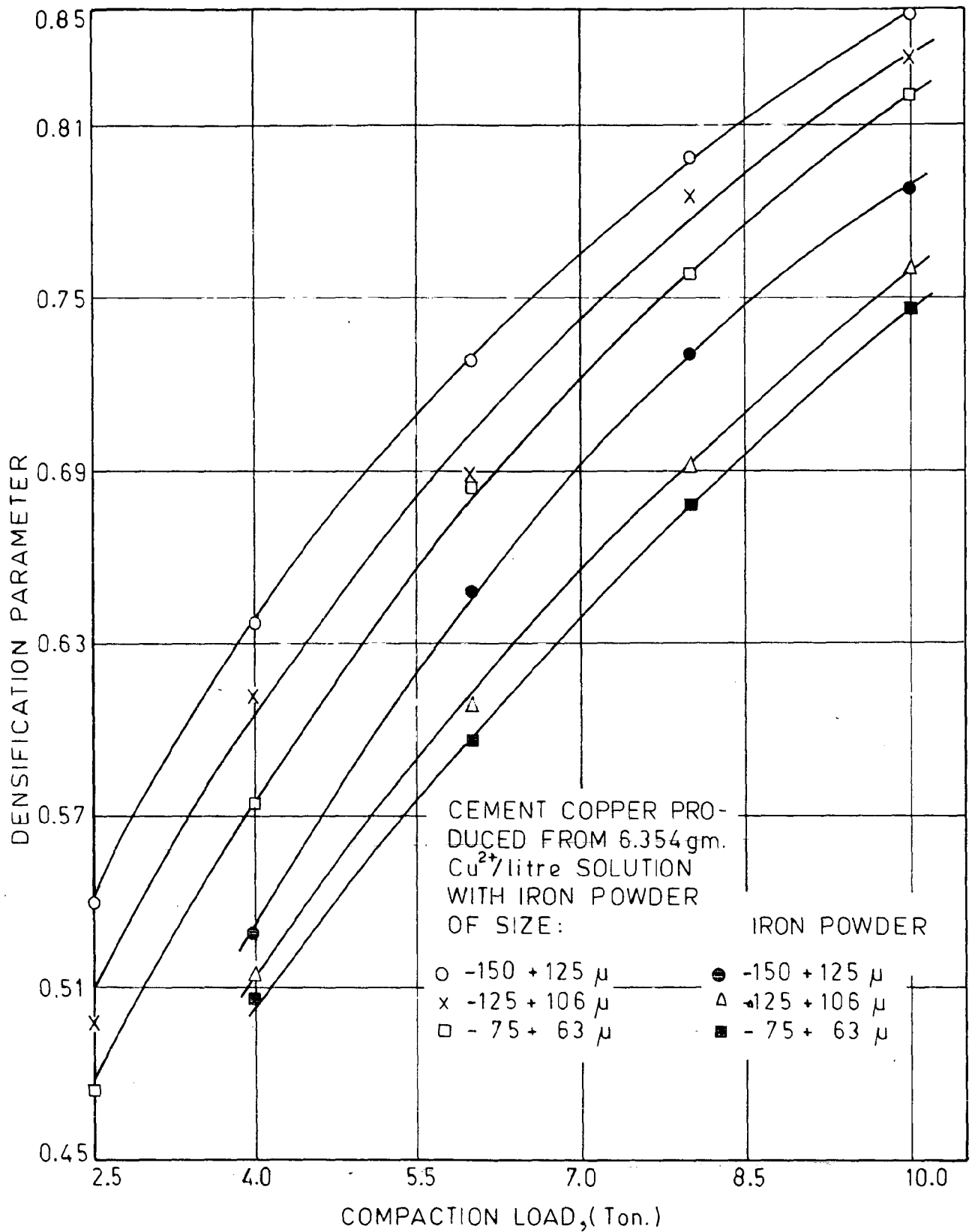


FIG.4.4 EFFECT OF IRON POWDER PARTICLE SIZE ON THE DENSIFICATION PARAMETER OF CEMENT COPPER AND IRON POWDERS.

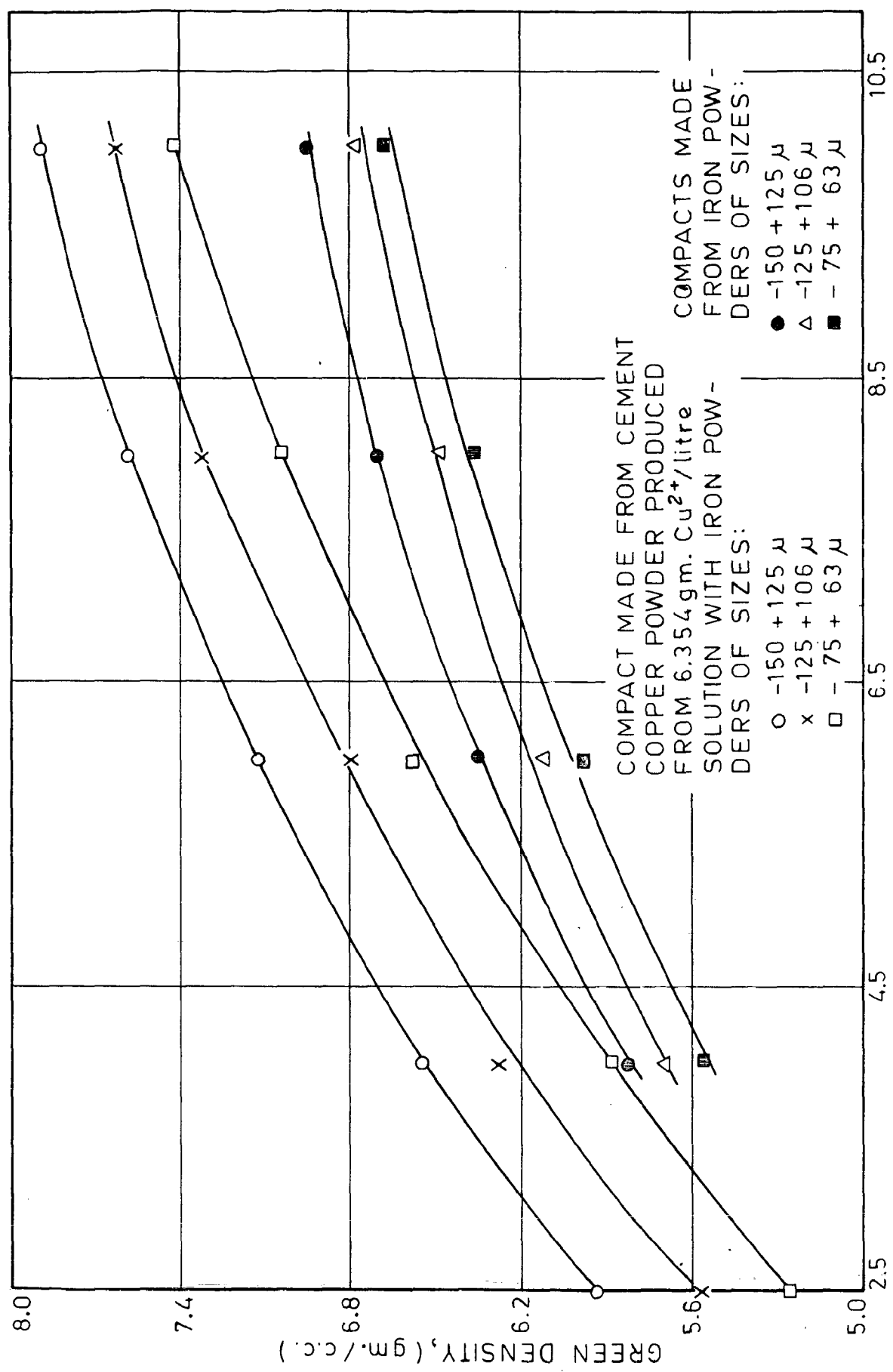


FIG.4.5 EFFECT OF IRON POWDER SIZE ON GREEN DENSITY OF CEMENT COPPER AND IRON PRODUCTS.

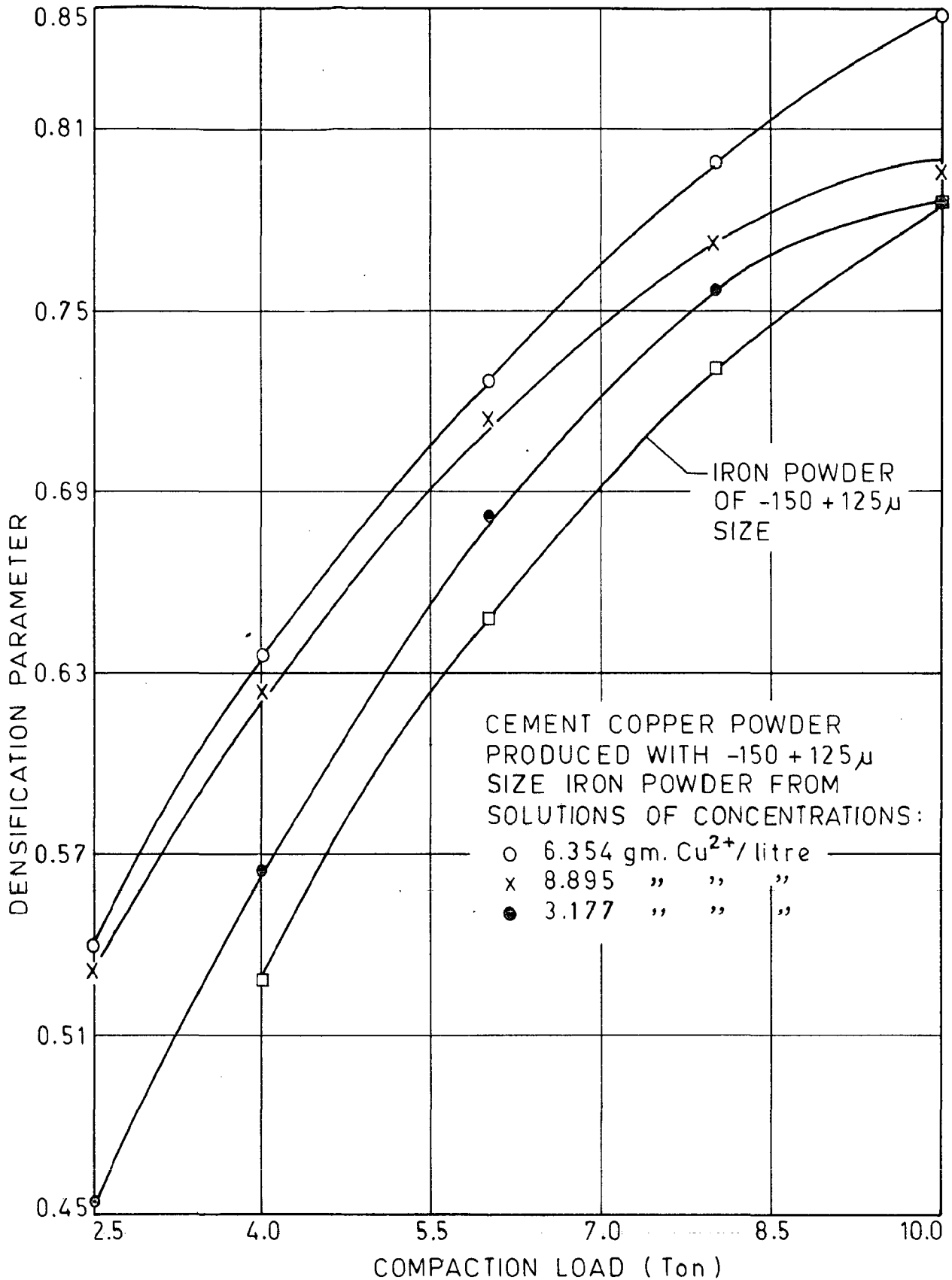


FIG.4.6 EFFECT OF SOLUTION CONCENTRATIONS ON DENSIFICATION PARAMETER OF CEMENT COPPER POWDERS.

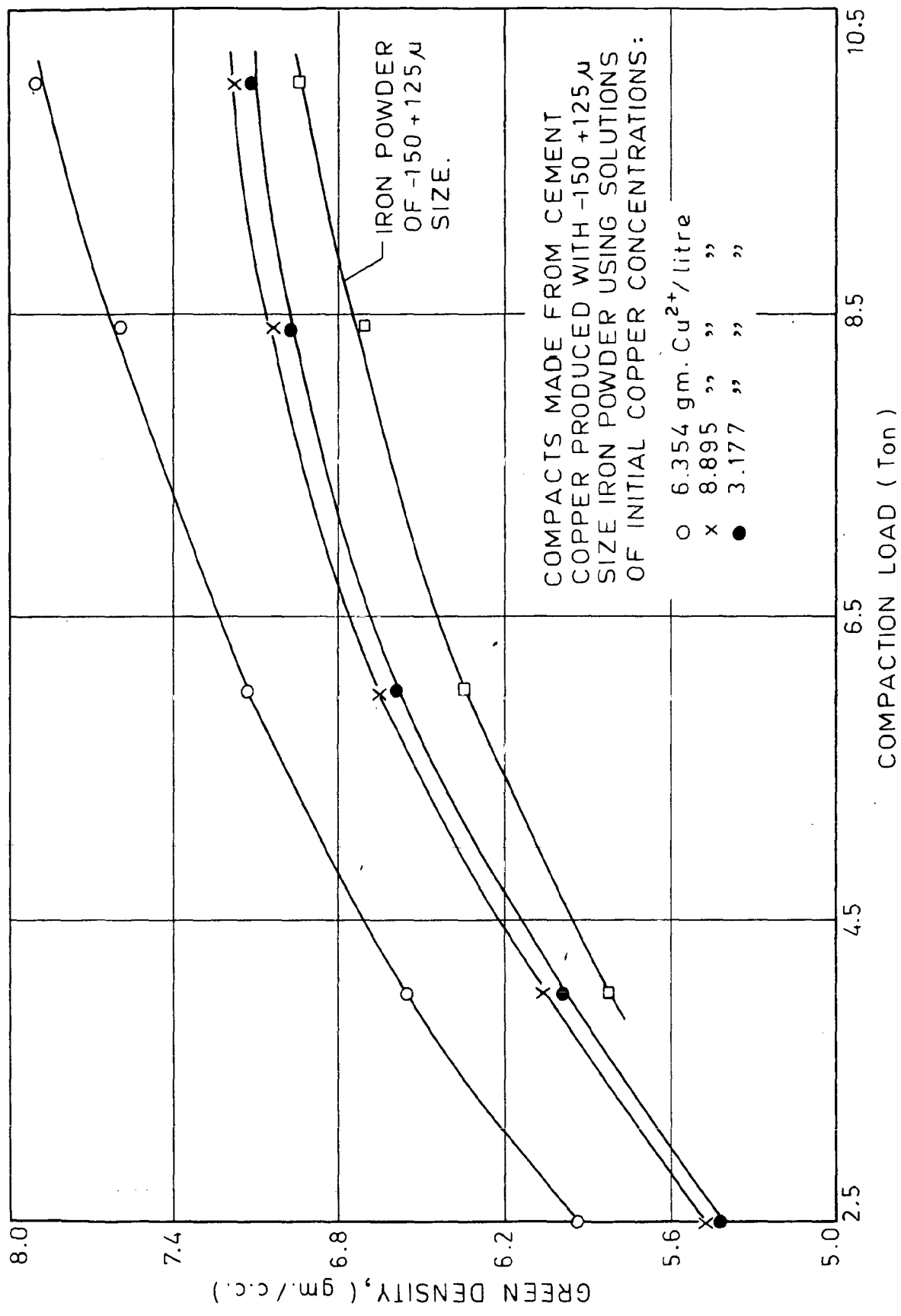


FIG.4.7 EFFECT OF INITIAL COPPER CONCENTRATIONS ON GREEN POROSITY OF CEMENT COPPER AND IRON PRODUCTS.

TABLE-4.8: Composition and Density of
Cement Copper Powders

Material	Composi- tion Cu, %	Density gn/CC
Cement copper powder obtained from -150 μ + 125 μ size iron powder	75.4	8.6534
Cement copper powder obtained from -125 μ + 106 μ size iron powder	73.4	8.6384
Cement copper powder obtained from -75 μ + 63 μ size iron powder	66.3	8.5564
Cement copper powder obtained from 3.177 gn Cu ²⁺ /litre solution	61.7	8.5097
Cement copper powder obtained from 3.895 gn Cu ²⁺ /litre solution	62.2	8.5098

are given in Tables 4.6 and 4.7. The results are plotted in Figs. 4.8 and 4.9. It is seen that there is an optimum size of the iron powder for which the compression ratio is lowest, as desired in industrial applications. Such variations can be explained in terms of the apparent density and compressibility results. The higher compression ratio for the powder produced from -75+63 micron size iron powder as compared to that obtained from -125 + 106 micron iron powder is due to the sufficient difference between the apparent density of the two. The higher compression ratio of the cement powder produced from -150 + 125 micron size iron powder as compared to that which is obtained from -125 + 106 micron size iron powder, is due to its higher compressibility, because the difference between their apparent densities is very small. With reference to the effect of the initial copper concentration in solution on compression ratio, it is seen from Fig. 4.9 that compression ratio increases as the initial copper concentration in solution increases. This variation can also be explained in terms of apparent densities and compressibilities of the concerned cement copper powders. The lowest compression ratio of the powder obtained from 3.177 gm Cu^{2+} /litre solution is due to its highest apparent density and lowest compressibility among the powders under discussion. Similarly, the powder obtained from 8.895 gm Cu^{2+} /litre solution has the

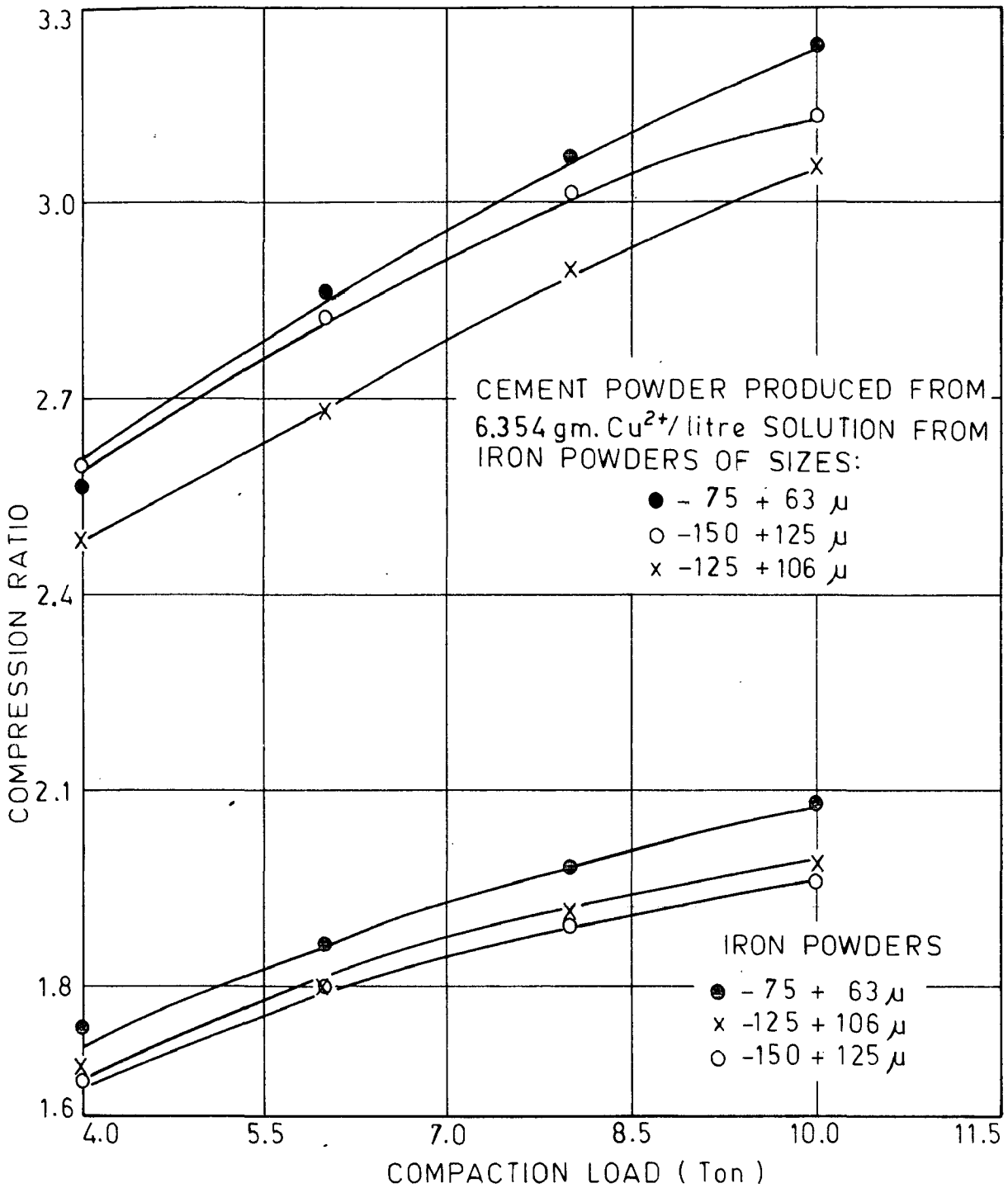


FIG.4.8 EFFECT OF IRON POWDER SIZE ON THE COMPRESSION RATIO OF CEMENT COPPER POWDERS AND IRON POWDERS.

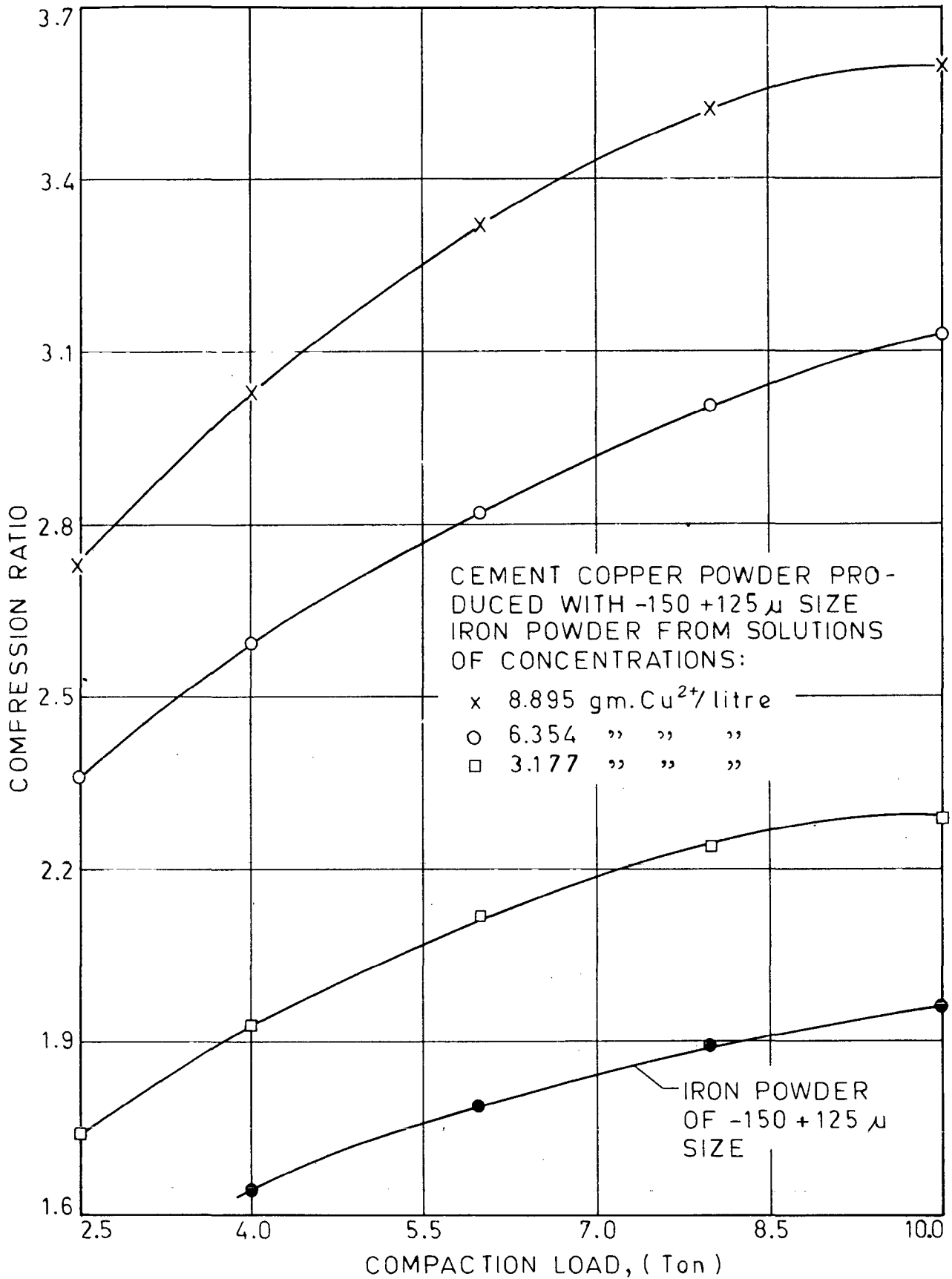


FIG.4.9 EFFECT OF SOLUTION CONCENTRATION ON COMPRESSION RATIO OF CEMENT COPPER POWDERS.

lowest apparent density and medium compressibility and, therefore, it has the highest compression ratio. The powder obtained from 6.354 gm Cu^{2+} /litre solution has the highest compressibility and has high apparent density and therefore the overall effect is a medium compression ratio of this powder.

4.3.3 Sintered density

Details of the weight, diameter and height of the various sintered products are given in Table 4.9. Values of the sintered density of the various cement copper products and iron products are given in Tables 4.10 and 4.11, and the results are plotted in Figs. 4.10 to 4.12. The curves show that the sintered density remains highest for the highest green density materials and that the higher green density materials exhibit very small change in density after sintering. Figs. 4.13 to 4.15 show the effect of sintering temperature. The observed increase in sintered density with increase in sintering temperature is due to the increased mobility of atoms, vacancies and other defects.

4.3.4 Green porosity and Sintered porosity

Values of green porosity and sintered porosity for different cement copper products are given in Tables 4.12 to 4.15. The results are plotted in

TABLE-4.9: Weight Diameter and Height of the Various Sintered Products

Material	Dia- men- sion CGS	Sintered Product 950°C												
		2.5T	4T	6T	8T	10T	2.5T	4T	6T	8T	10T			
A. Cement copper from -150+125µ iron	Wt.	7.952	7.952	7.953	7.953	7.953	7.952	7.952	7.953	7.953	7.953	7.953	7.953	7.954
	Dia.	1.615	1.620	1.630	1.630	1.630	1.600	1.610	1.615	1.620	1.620	1.620	1.620	1.630
	Ht.	0.625	0.573	0.525	0.495	0.479	0.625	0.553	0.534	0.501	0.479	0.501	0.501	0.479
B. -do- from -125+106µ	Wt.	7.952	7.952	7.953	7.953	7.954	7.952	7.952	7.953	7.953	7.953	7.953	7.953	7.954
	Dia.	1.620	1.625	1.630	1.630	1.630	1.605	1.610	1.620	1.620	1.620	1.620	1.620	1.630
	Ht.	0.665	0.599	0.550	0.512	0.495	0.662	0.609	0.555	0.518	0.495	0.518	0.518	0.495
C. -do- from -75+63µ	Wt.	7.952	7.952	7.953	7.953	7.954	7.952	7.952	7.953	7.953	7.953	7.953	7.953	7.954
	Dia.	1.625	1.630	1.630	1.630	1.630	1.615	1.620	1.620	1.620	1.620	1.620	1.620	1.630
	Ht.	0.703	0.633	0.572	0.534	0.509	0.693	0.635	0.576	0.541	0.508	0.541	0.541	0.508
D. Cement copper from 3.177g Cu/l	Wt.	7.952	7.952	7.953	7.953	7.954	7.952	7.952	7.953	7.953	7.953	7.953	7.953	7.954
	Dia.	1.630	1.630	1.630	1.630	1.630	1.630	1.630	1.630	1.630	1.630	1.630	1.630	1.630
	Ht.	0.654	0.603	0.559	0.540	0.520	0.650	0.600	0.553	0.533	0.519	0.533	0.533	0.519

-----/Contd.

Material	Dia- men- sion CGS	Sintered Produce											
		850°C					950°C						
		2.5T	4T	6T	8T	10T	2.5T	4T	6T	8T	10T		
E. Cement Copper from 8.895g Cu/l	Wt.	7.952	7.952	7.953	7.953	7.954	7.952	7.952	7.953	7.953	7.953	7.953	7.954
	Dia	1.615	1.620	1.620	1.630	1.630	1.610	1.615	1.615	1.615	1.620	1.620	1.630
	Ht.	0.642	0.595	0.550	0.519	0.506	0.641	0.594	0.552	0.525	0.525	0.525	0.506
F. Iron produce from -150+125μ	Wt.	Nil	7.958	7.958	7.950	7.950	Nil	7.958	7.958	7.958	7.950	7.950	7.950
	Dia	Nil	1.630	1.630	1.630	1.630	Nil	1.630	1.630	1.630	1.630	1.630	1.630
	Ht.	Nil	0.641	0.595	0.562	0.547	Nil	0.641	0.592	0.559	0.559	0.559	0.545
G. -do- from -125+106μ	Wt.	Nil	7.958	7.958	7.950	7.950	Nil	7.958	7.958	7.958	7.950	7.950	7.950
	Dia	Nil	1.630	1.630	1.630	1.630	Nil	1.630	1.630	1.630	1.630	1.630	1.630
	Ht.	Nil	0.660	0.611	0.580	0.558	Nil	0.660	0.608	0.577	0.577	0.577	0.557
H. -do- from -75+63μ	Wt.	Nil	7.958	7.958	7.950	7.950	Nil	7.958	7.958	7.958	7.950	7.950	7.950
	Dia	Nil	1.630	1.630	1.630	1.630	Nil	1.630	1.630	1.630	1.630	1.630	1.630
	Ht.	Nil	0.674	0.624	0.591	0.560	Nil	0.674	0.623	0.591	0.591	0.591	0.557

Material		Sintered Product 1050°C				
		2.5T	4T	6T	8T	10T
A.	Wt.	7.952	7.952	7.953	7.953	7.954
	dia	1.590	1.600	1.615	1.620	1.630
	Ht	0.609	0.565	0.523	0.495	0.476
B.	Wt.	7.952	7.952	7.953	7.953	7.954
	dia	1.590	1.600	1.615	1.620	1.630
	Ht	0.644	0.598	0.543	0.509	0.494
C.	Wt.	7.952	7.952	7.953	7.953	7.954
	dia	1.600	1.610	1.615	1.620	1.630
	Ht.	0.639	0.630	0.565	0.534	0.507
D.	Wt.	7.952	7.952	7.953	7.953	7.954
	dia	1.630	1.630	1.630	1.630	1.630
	Ht.	0.639	0.589	0.551	0.529	0.514
E.	Wt.	7.952	7.952	7.953	7.953	7.954
	dia	1.600	1.610	1.620	1.620	1.630
	Ht.	0.641	0.591	0.543	0.521	0.503
F.	Wt.	Nil	7.958	7.958	7.950	7.950
	dia	Nil	1.630	1.630	1.630	1.630
	Ht.	Nil	0.638	0.589	0.556	0.543
G.	Wt.	Nil	7.958	7.958	7.950	7.950
	dia	Nil	1.630	1.630	1.630	1.630
	Ht.	Nil	0.657	0.605	0.575	0.552
H.	Wt.	Nil	7.958	7.958	7.950	7.950
	dia	Nil	1.630	1.630	1.630	1.630
	Ht.	Nil	0.674	0.623	0.591	0.557

TABLE-4.10: Effect of the Size of the Iron Powder Precipitant on Sintered Density of the Cement Copper Product and Iron Product

Material	Sintered Density (g/cc), at different Temperatures, of Green Compacts															
	350°C						950°C						1050°C			
	2.5T	4T	6T	8T	10T	10T	2.5T	4T	6T	3T	10T	2.5T	4T	6T	8T	10T
Cement copper produced from -150μ+125μ size iron powder	6.20	6.72	7.26	7.70	7.95	7.95	6.32	6.76	7.27	7.70	7.95	6.57	6.99	7.42	7.80	8.01
	5.79	6.39	6.93	7.45	7.70	7.70	5.93	6.40	6.95	7.45	7.70	6.21	6.60	7.15	7.58	7.71
	5.44	6.01	6.66	7.13	7.48	7.48	5.55	6.07	6.67	7.13	7.49	5.73	6.26	6.87	7.22	7.51
Iron product from iron powder of size -150μ+125μ	-	5.93	6.39	6.76	6.96	6.96	-	5.93	6.43	6.80	6.98	-	5.96	6.46	6.84	7.01
	-	5.76	6.22	6.56	6.82	6.82	-	5.76	6.25	6.59	6.83	-	5.79	6.28	6.62	6.89
	-	5.64	6.09	6.44	6.79	6.79	-	5.64	6.10	6.44	6.82	-	5.64	6.10	6.44	6.83

TABLE-4.11: Effect of Initial Copper Concentration in Solution on Sintered Density of the Cement Copper Product, and Sintered Density of the Iron Product

Material	Sintered Density (gn/cc), at different Temperatures, of Green Compacts Produced at Various Loads														
	850°C					950°C					1050°C				
	2.5T	4T	6T	8T	10T	2.5T	4T	6T	8T	10T	2.5T	4T	6T	8T	10T
Cement copper produced from 3.177g Cu/l solution	5.82	6.31	6.82	7.14	7.33	5.86	6.34	6.83	7.14	7.35	5.96	6.46	6.91	7.20	7.42
Cement Copper produced from 6.354g Cu/l solution	6.20	6.72	7.26	7.70	7.95	6.52	6.76	7.27	7.70	7.96	7.57	6.99	7.42	7.80	8.01
Cement copper produced from 8.895g Cu/l solution	6.04	6.48	7.02	7.34	7.52	6.08	6.52	7.03	7.34	7.53	6.16	6.60	7.10	7.40	7.58
Iron product from iron powder of -150µ+125µ size	-	5.93	6.39	6.76	6.96	-	5.93	6.43	6.80	6.98	-	5.96	6.46	6.84	7.01

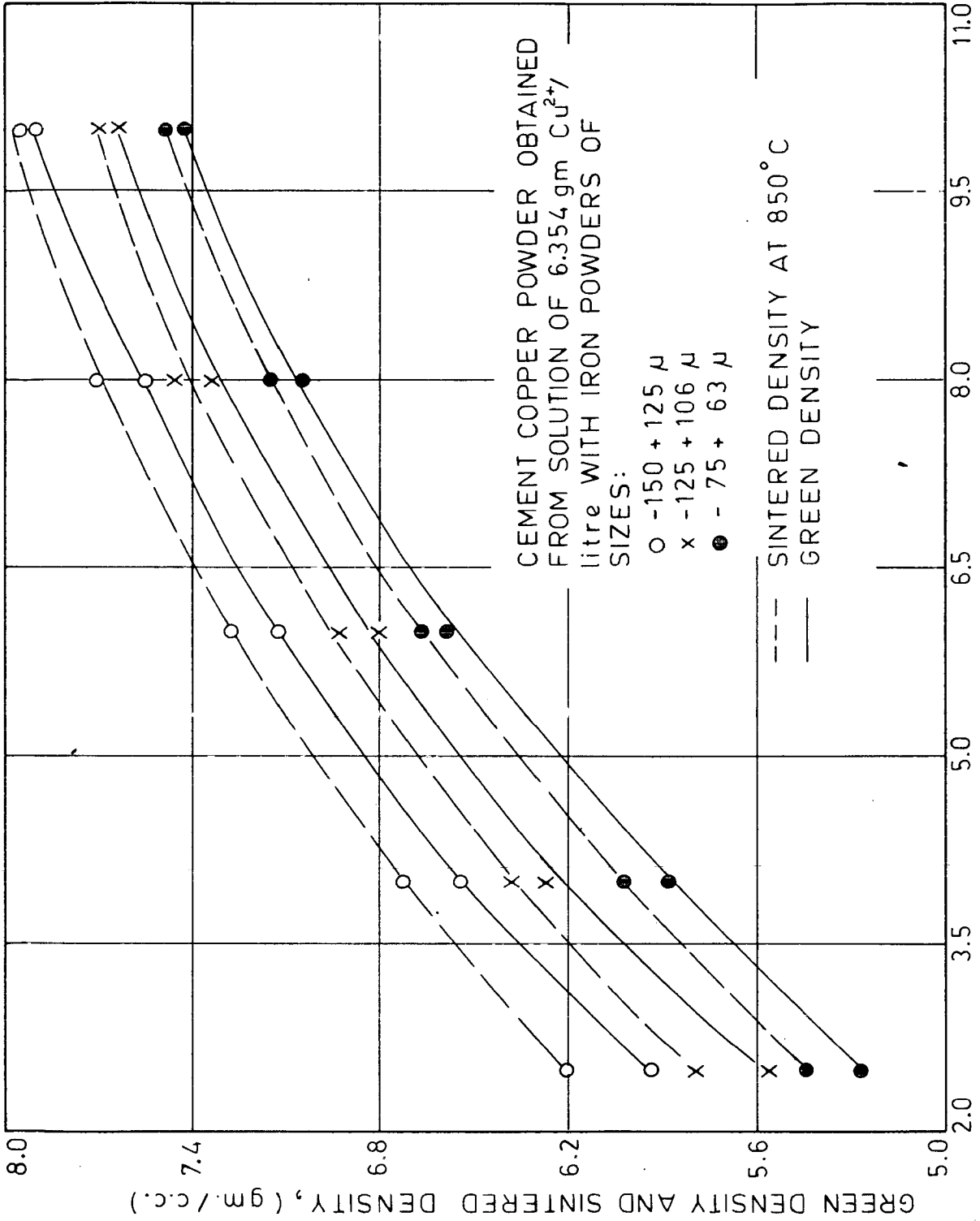


FIG.4.10 COMPARISON OF SINTERED DENSITY WITH GREEN DENSITY FOR CEMENT POWDER PRODUCTS.

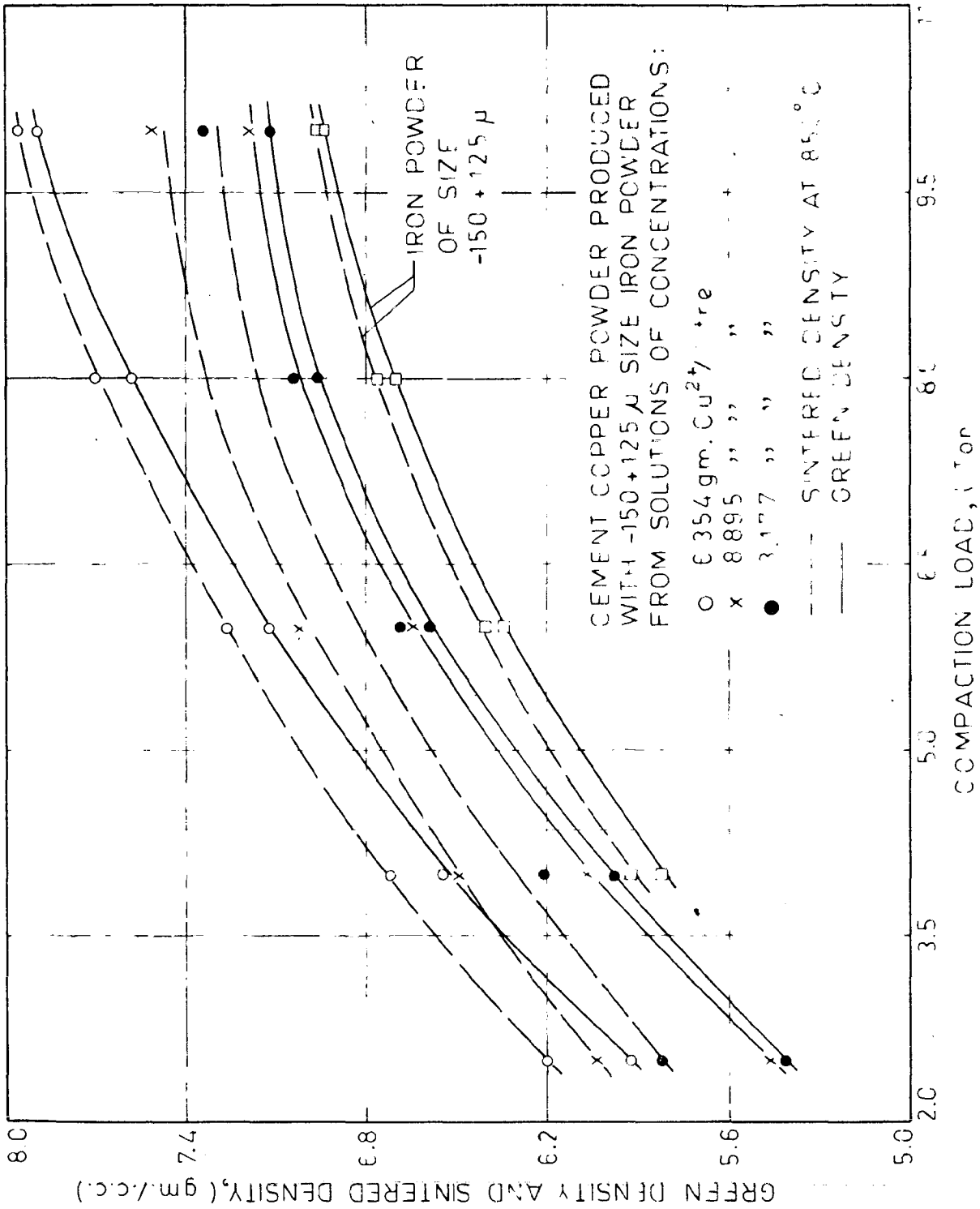


FIG.4.11 COMPARISON OF SINTERED DENSITY WITH GREEN DENSITY FOR CEMENT COPPER AS WELL AS IRON PRODUCTS.

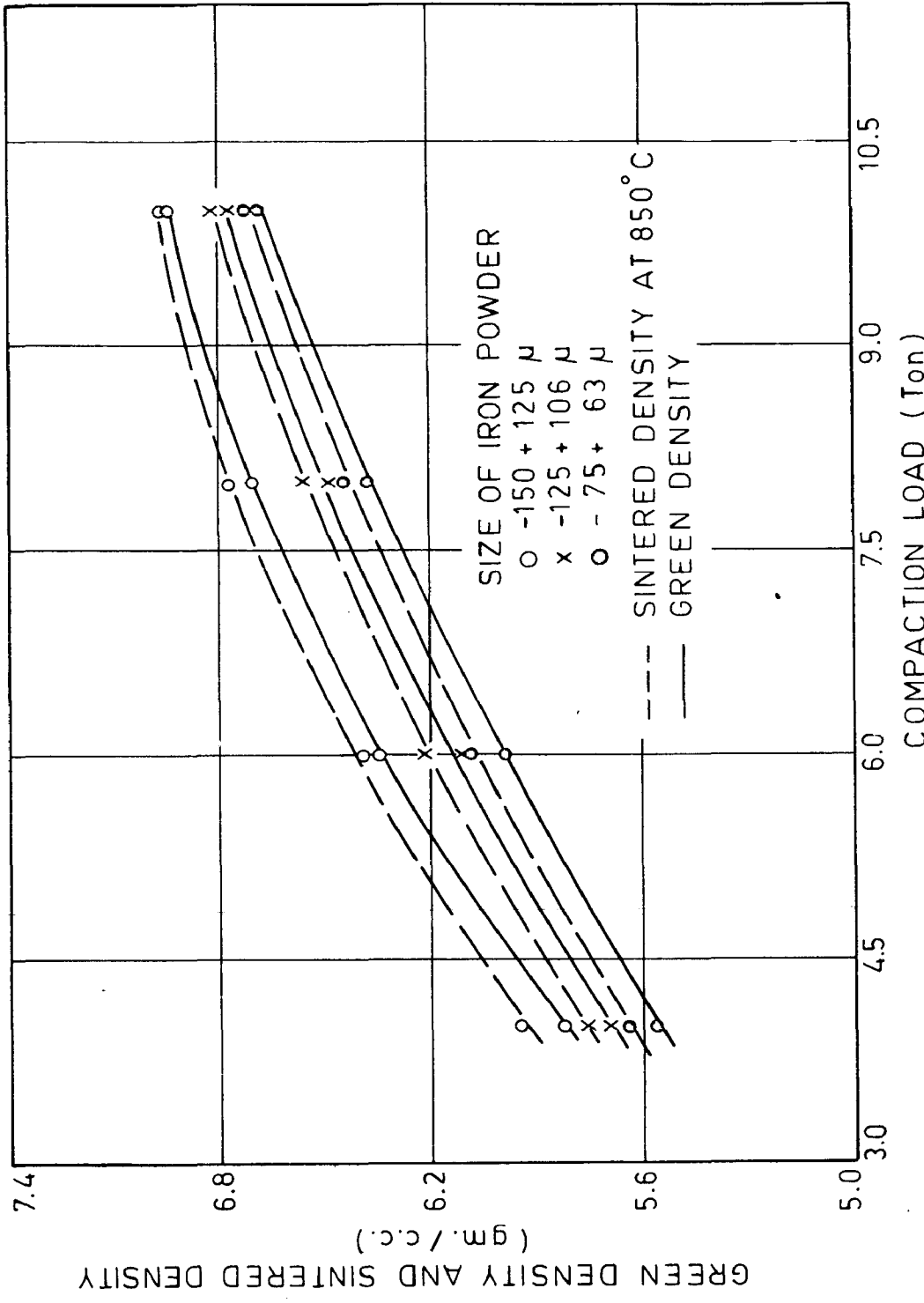


FIG.4.12 COMPARISON OF SINTERED DENSITY WITH GREEN DENSITY FOR IRON POWDER PRODUCTS.

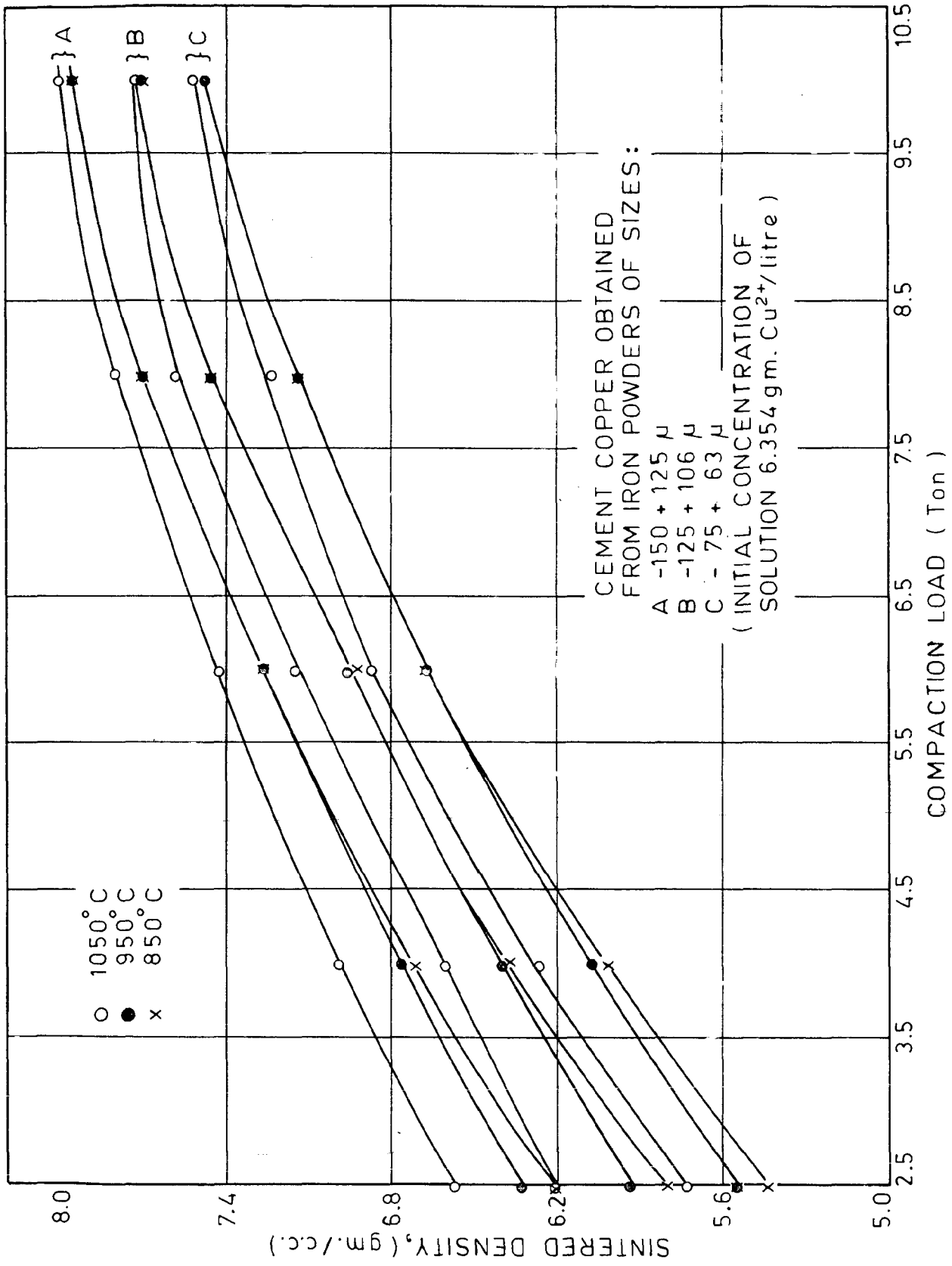


FIG.4.13 EFFECT OF TEMPERATURE ON SINTERED DENSITY OF CEMENT COPPER PRODUCTS.

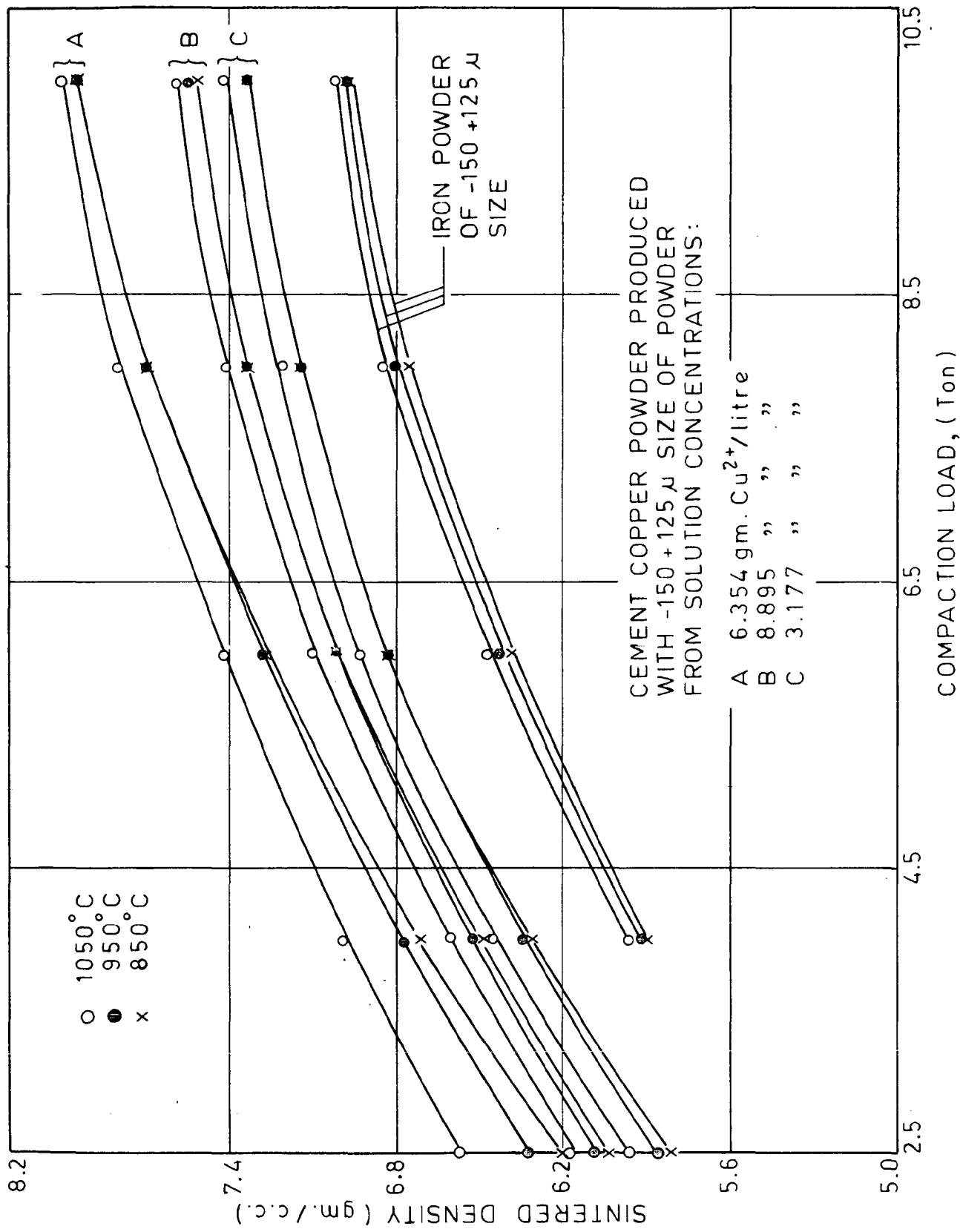


FIG.4.14 EFFECT OF TEMPERATURE ON SINTERED DENSITY OF CEMENT COPPER AND IRON PRODUCTS

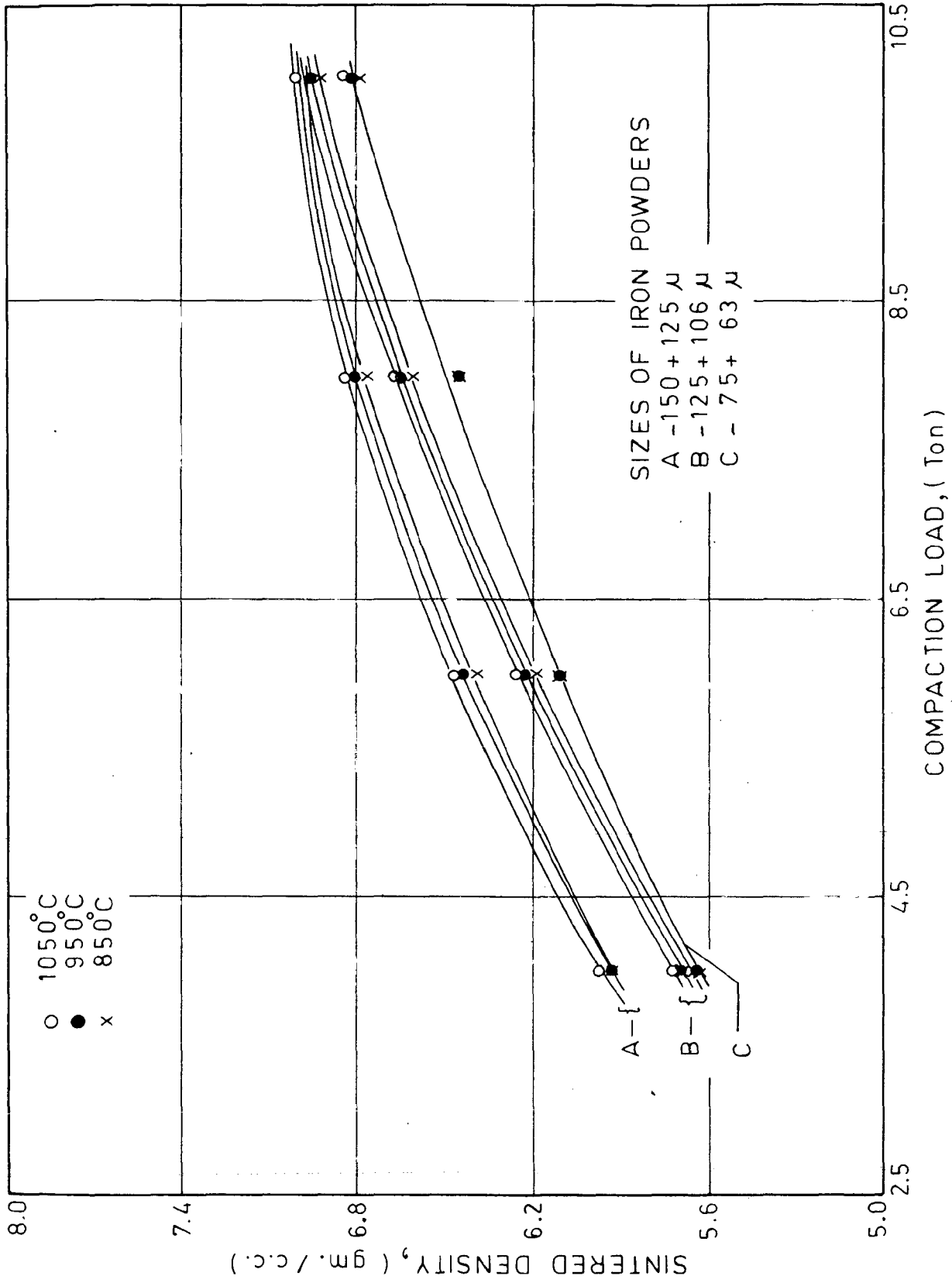


FIG.4.15 EFFECT OF TEMPERATURE ON SINTERED DENSITY OF IRON PRODUCTS.

TABLE-4.12: Effect of the Size of the Iron Powder Precipitant on Green Porosity of the Cement Copper Product and the Iron Product

Material	Green Porosity (%) in Green Compact Compacted at different Leads			
	2.5T	4T	6T	8T 10T
Cement copper product obtained from -150 μ +125 μ size iron powder	32.9	26.1	19.5	14.3 10.3
Cement copper product obtained from -125 μ +106 μ size iron powder	35.5	27.4	21.2	15.1 11.6
Cement copper product obtained from -75 μ +63 μ size iron powder	33.5	31.2	23.0	17.7 13.2
Iron product obtained from -150 μ + 125 μ size iron powder	-	25.9	19.3	14.7 11.6
Iron product obtained from -125 μ +106 μ size iron powder	-	26.7	20.8	16.5 13.2
Iron product obtained from -75 μ + 63 μ size iron powder	-	29.1	23.8	18.9 14.9

TABLE-4.13: Effect of the Size of the Iron Powder Precipitant on (Sintered Porosity) of the Cement Copper Product and the Iron Product

Material	Sintered Porosity (%) at different Temperatures, in Products Compacted at different Loads														
	350°C					950°C					1050°C				
	2.5T	4T	6T	8T	10T	2.5T	4T	6T	8T	10T	2.5T	4T	6T	8T	10T
Cement copper product obtained from -150μ +125μ size iron powder	29.9	24.0	13.0	13.0	10.1	20.6	23.6	19.8	12.9	10.1	25.3	21.0	16.1	11.8	9.1
do- from -125μ +106μ size iron powder	32.9	25.9	19.7	13.7	10.8	31.3	25.8	19.5	13.7	10.8	23.1	23.5	17.1	12.2	10.1
do- from -75μ +63μ size iron powder	36.3	29.7	22.1	16.6	12.5	35.0	29.0	22.0	16.6	12.3	32.9	26.8	19.6	15.5	12.1
Iron product obtained from -150μ +125μ size iron powder	-	24.4	13.7	13.3	11.4	Nil	24.4	18.2	13.4	11.1	Nil	24.1	17.3	12.9	10.8
do- from -125μ +106μ	Nil	26.7	20.4	16.1	13.0	Nil	26.3	20.0	15.7	12.3	Nil	27.5	22.2	17.5	13.6
do- from -75μ +63μ	Nil	28.2	22.4	18.0	13.5	Nil	28.2	22.3	18.0	13.1	Nil	28.2	22.3	18.0	13.1

TABLE-4.14: Effect of the Initial Copper Concentration in Solution on Green Porosity of the Cement Copper Product and of the Iron Product

Material	Green Porosity (%) in Green Compact Compacted at different Loads				
	2.5T	4T	6T	8T	10T
Cement Copper product obtained from 3.177g Cu/l solution	33.9	27.0	19.8	15.1	13.3
Cement Copper product obtained from 6.354 g Cu/l solution	32.9	26.1	19.5	14.3	10.8
Cement Copper product obtained from 8.395g Cu/l solution	35.3	28.7	21.7	17.2	15.4
Iron product obtained from iron powder of -150 μ + 125 μ size	-	25.9	19.3	14.7	11.6

TABLE-4.15: Effect of the Initial Copper Concentration in Solution on Sintered Porosity of the Cement Copper Product and of the Iron Product

Material	Sintered Porosity (%) at different Temperatures, in Products Compacted at different Loads														
	850°C				950°C				1050°C						
	2.5T	4T	6T	8T	10T	2.5T	4T	6T	8T	10T	2.5T	4T	6T	8T	10T
Cement Copper obtained from 3.177g Cu/l solution	29.0	23.1	16.9	13.0	10.7	28.6	22.7	16.8	12.9	10.4	27.4	21.2	15.7	12.2	9.6
-do- from 6.354g Cu/l	29.9	24.0	18.0	13.0	10.1	28.6	23.6	19.8	12.9	10.1	25.8	21.0	16.1	11.8	9.5
-do- from 8.895g Cu/l	28.9	23.8	17.5	13.7	11.5	28.5	23.3	17.3	13.6	11.5	27.6	22.4	16.5	12.9	10.9
Iron product from iron powder of -150μ +125μ	Nil	24.4	18.7	13.8	11.4	Nil	24.4	18.2	13.4	11.1	Nil	24.1	17.8	12.9	10.8

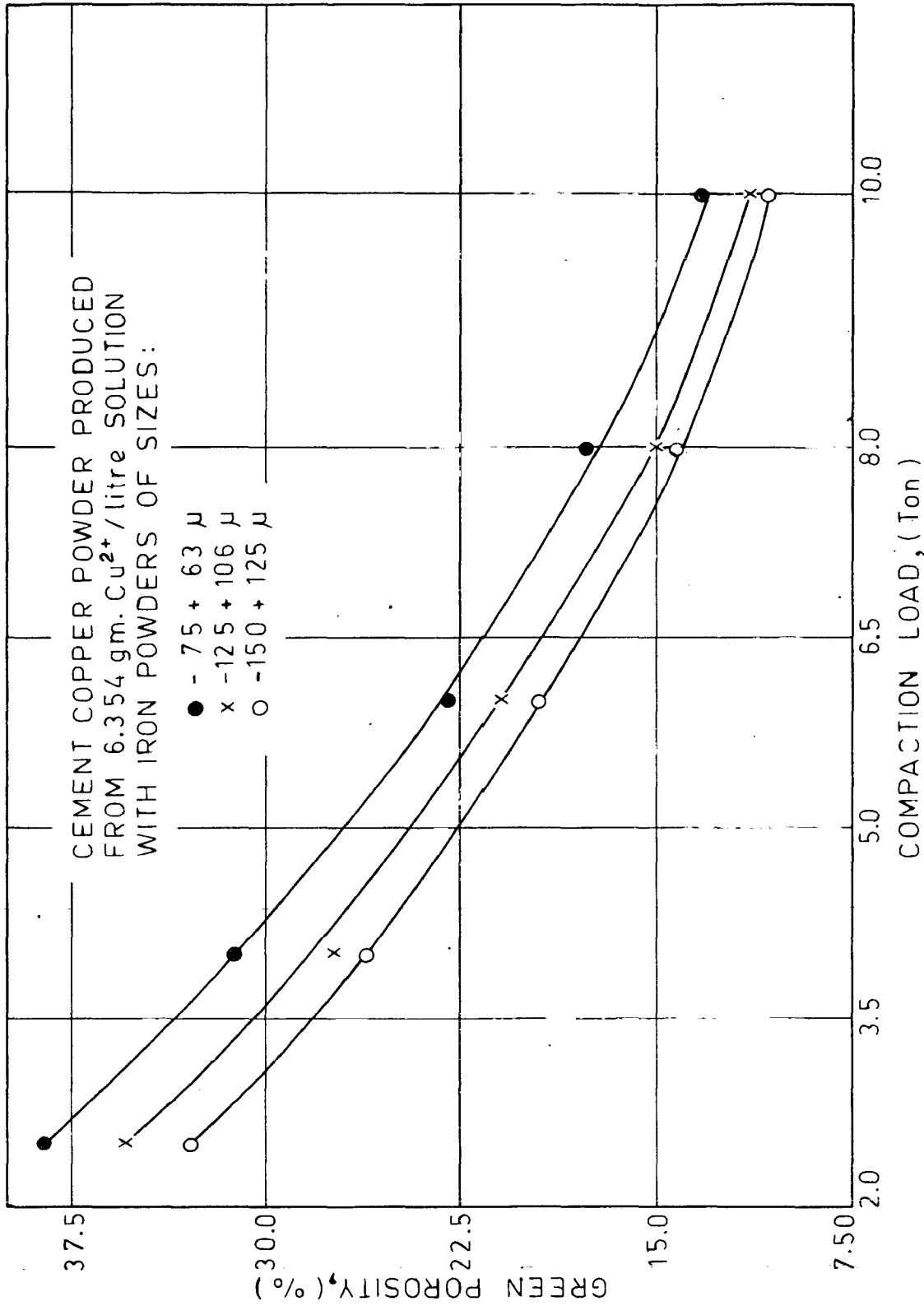


FIG.4.16 EFFECT OF IRON POWDER PARTICLE SIZE ON GREEN POROSITY OF CEMENT COPPER PRODUCTS.

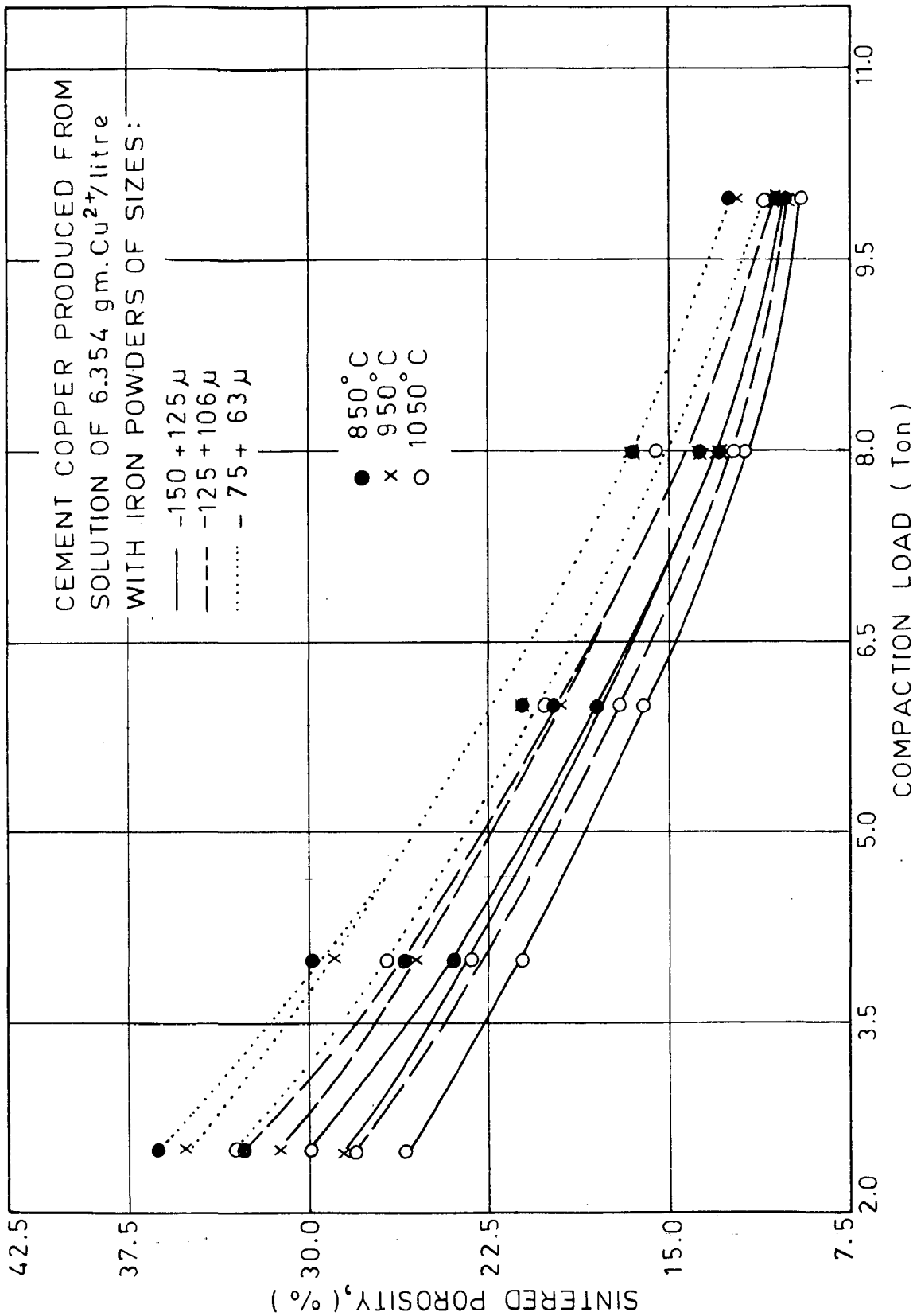


FIG.4.17 EFFECT OF IRON POWDER PARTICLE SIZE ON SINTERED POROSITY OF THE CEMENT COPPER PRODUCTS.

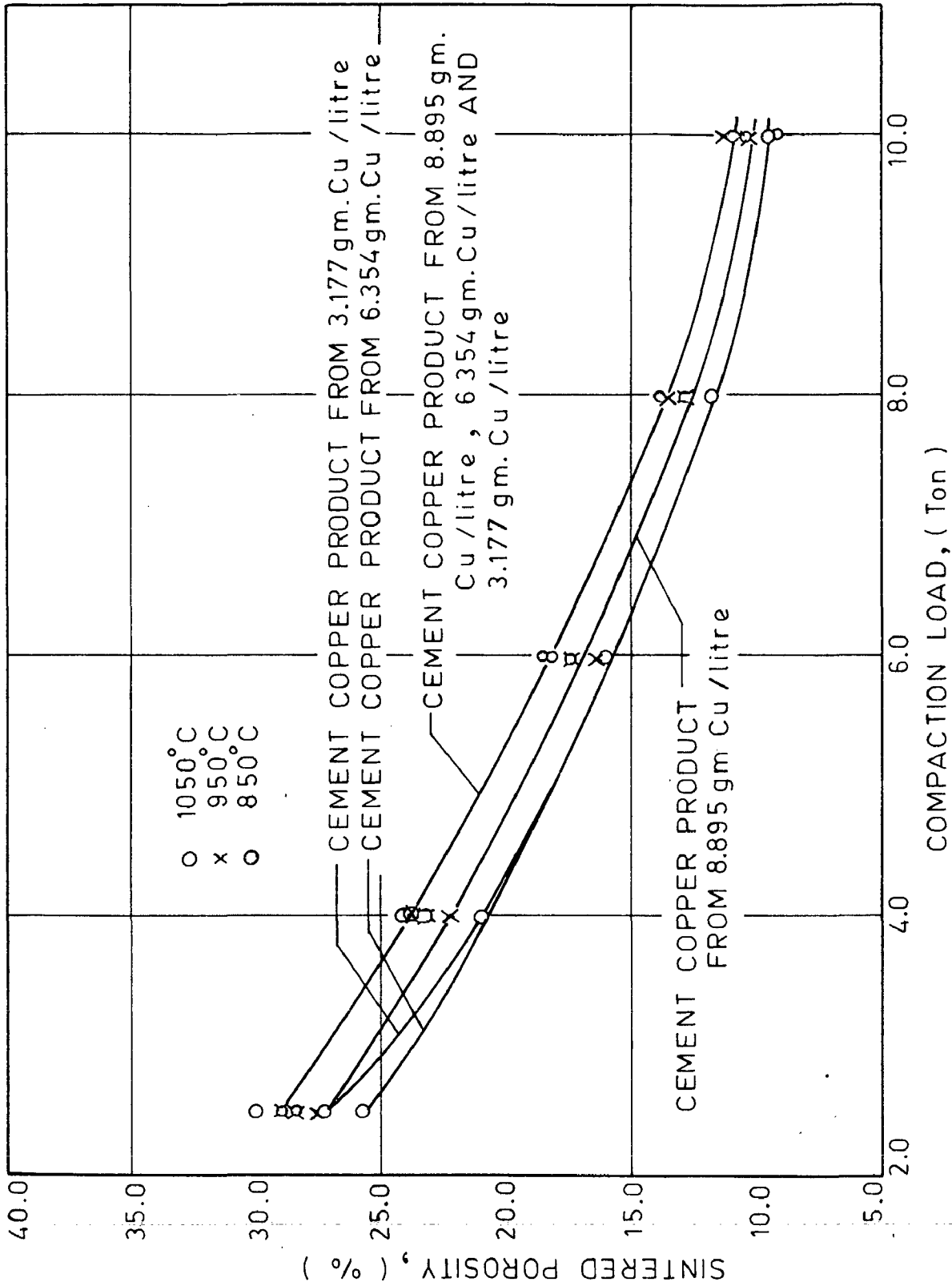
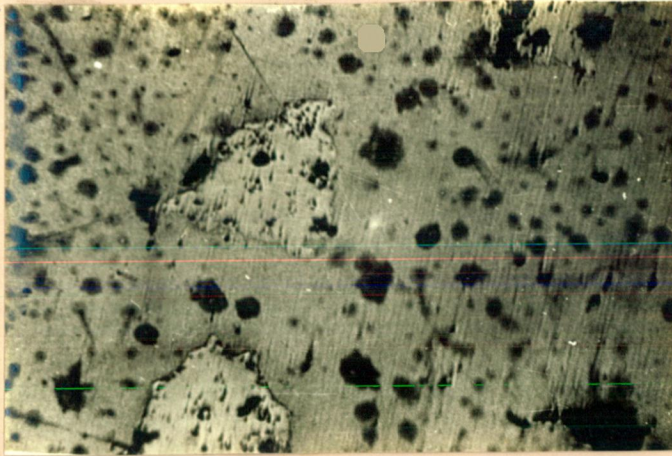


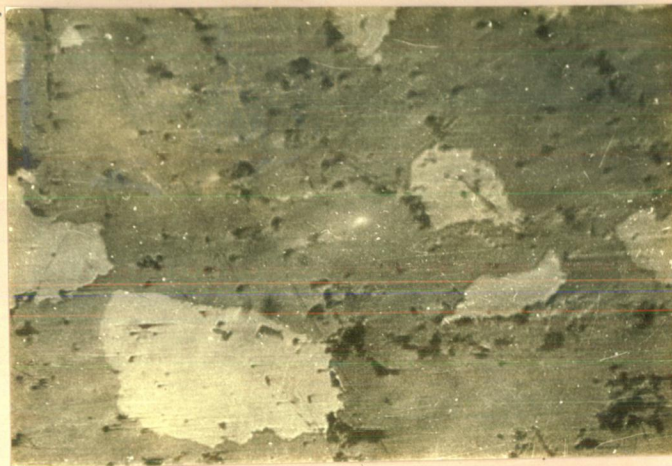
FIG.4.19 EFFECT OF SOLUTION CONCENTRATIONS ON SINTERED POROSITY OF CEMENT COPPER PRODUCTS.

Figs. 4.16 to 4.19. It is noted that, (i) sintered porosity is always less than green porosity for a given compaction load which indicates the occurrence of pore-shrinkage stage during sintering, (ii) for a given green density, increase in sintering temperature decreases the sintered porosity due to the increased mobility of atoms and vacancies at higher temperatures which enhances pore shrinkage, (iii) the cement copper product obtained from iron powder of coarser size has lower porosity which is due to its lower green porosity, (iv) the cement copper products obtained from solutions of different initial copper concentrations have almost the same sintered porosity in the sintering temperature range 350° to 950°C , but at 1050°C , the cement copper obtained from solution of higher concentration (8.895 gm Cu^{2+} /litre) has higher sintered porosity than that obtained from solutions of lower initial concentrations due to its higher initial green porosity, - removal of which requires long sintering time.

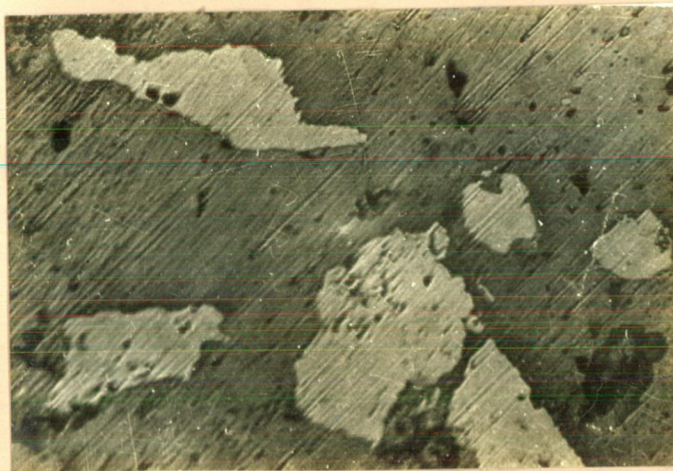
To support the above statements, photomicrographs of the various sintered cement copper products are given in Figs. 4.20 to 4.23 to show the effect of iron powder particle size, sintering temperature, compaction load and initial copper concentration in solution respectively, on porosity of the sintered products. It is observed from Fig. 4.20 that cement copper product



Size of Iron Powder
-75 + 63 microns

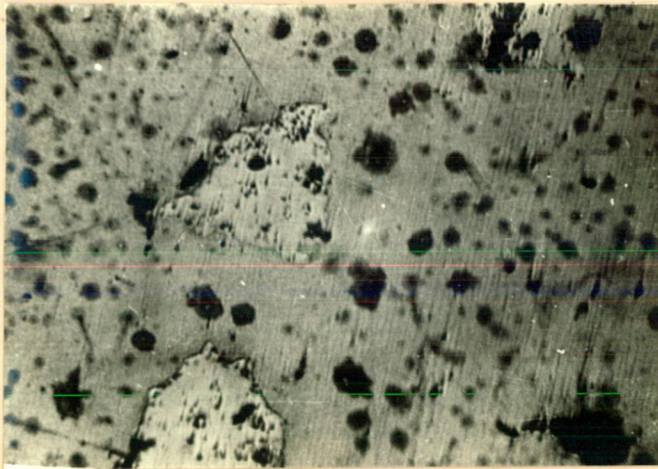


Size of Iron Powder
-125 + 106 microns

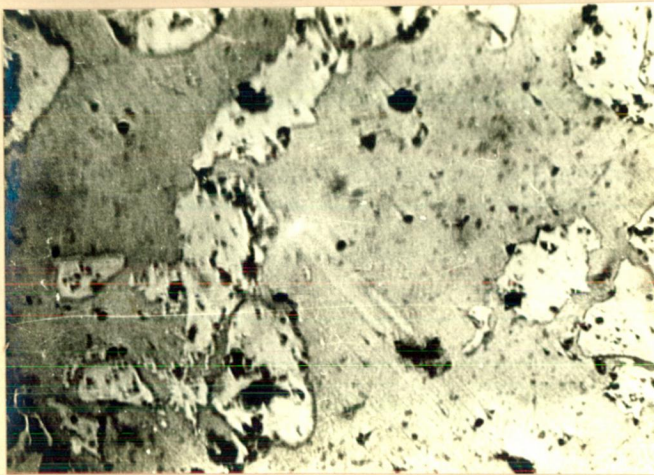


Size of Iron Powder
-150 + 125 microns

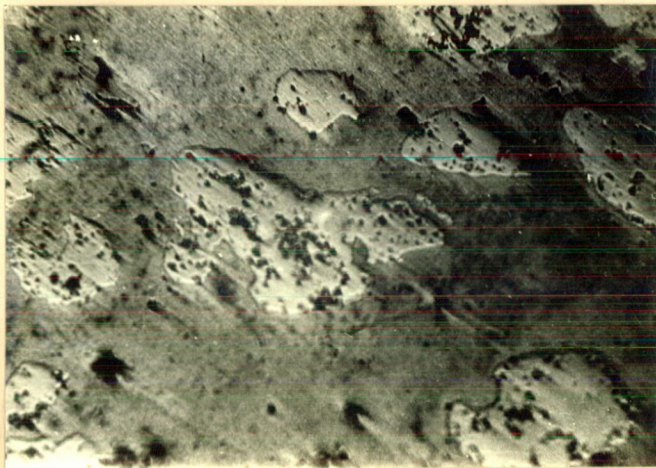
Fig. 4.20 Photomicrographs showing the effect of iron powder size on sintered porosity of Cement Copper parts produced by compaction at 2.5 ton load and sintered at 850°C (Initial Solution Concentration 6.354 gm Cu^{2+} / litre, Magnification 100 X)



850°C

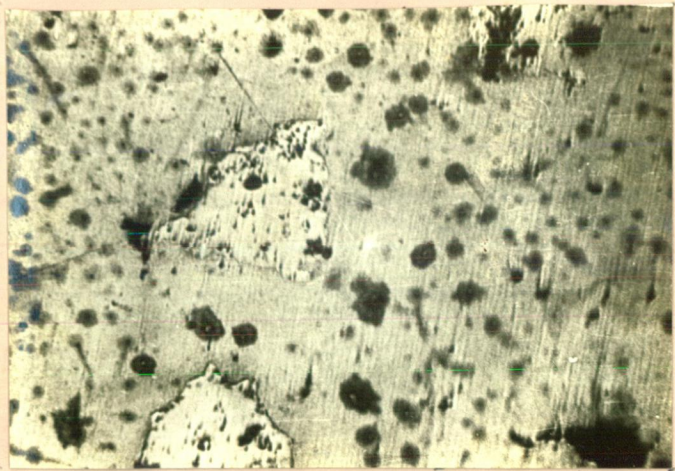


950°C

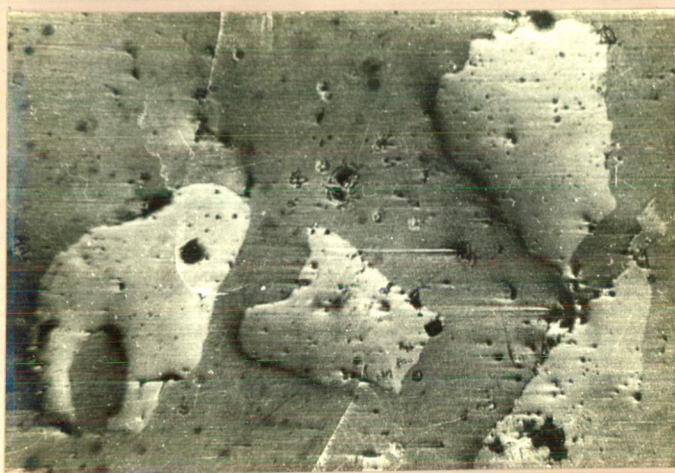


1050°C

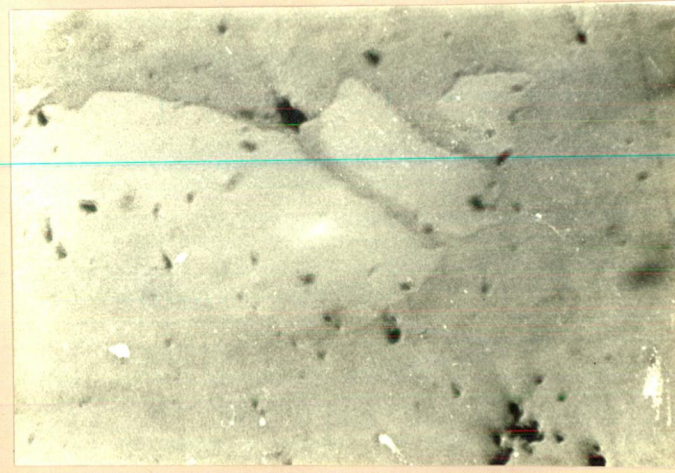
Fig. 4.21 Photomicrographs showing the effect of sintering temperature on sintered porosity of the Cement Copper parts produced by compaction at 2.5 Ton load (Iron powder size: -75 + 63 microns, Initial Solution Concentration: 6.354 gm Cu^{2+} / litre, Magnification: 100 X)



Compaction Load
2.5 Ton

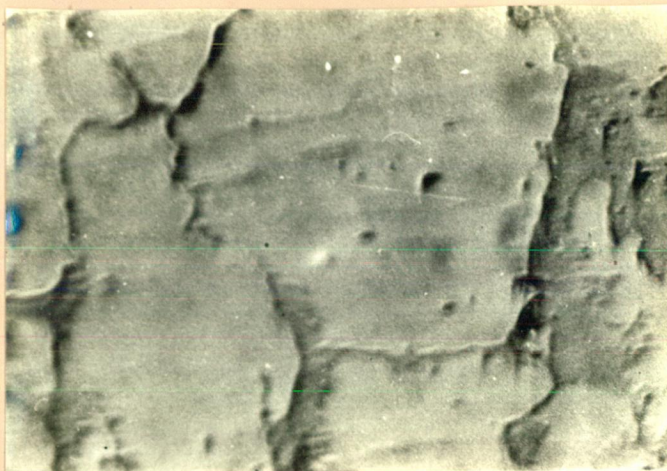


Compaction Load
6.0 Ton

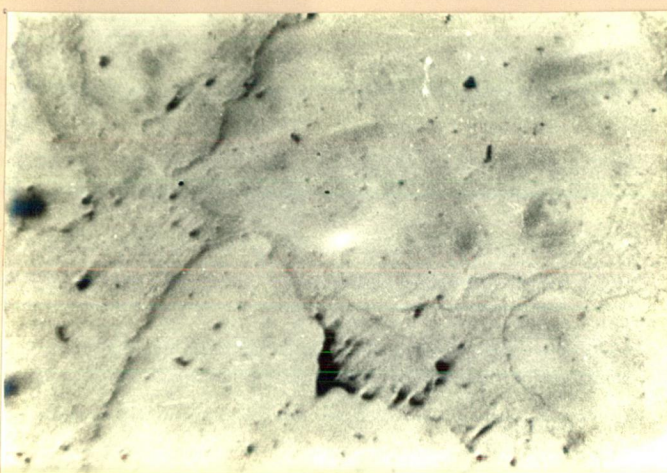


Compaction Load
10.0 Ton

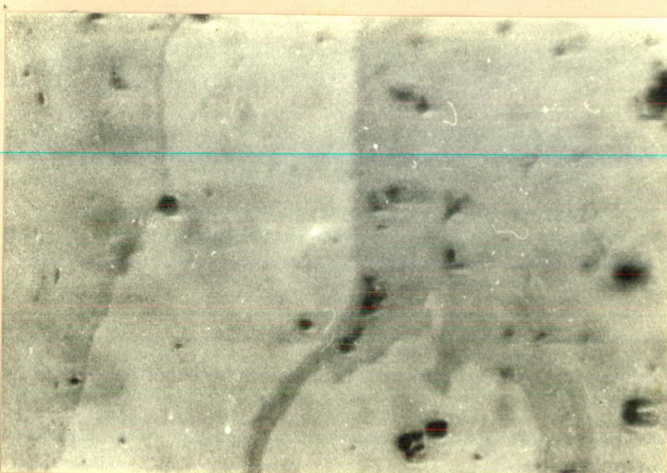
Fig. 4.22 Photomicrographs showing the effect of compaction load on sintered porosity of Cement Copper parts sintered at 850°C (Iron powder size: -75 + 63 microns, Initial Solution Concentration: 6.354 gm Cu²⁺/ litre, Magnification: 100 X)



3.177 gm Cu²⁺/ litre



6.354 gm Cu²⁺/ litre



8.895 gm Cu²⁺/ litre

Fig. 4.23 Photomicrographs showing the effect of Initial Solution Concentration of sintered porosity of Cement Copper products obtained by compaction at 10 Ton load and sintered at 850°C (Iron powder size: -150 + 125 microns, Magnification: 200 X)

obtained from iron powders of coarser size has lower porosity. Fig. 4.21 shows that an increase in sintering temperature decreases sintered porosity. From Fig. 4.22, a decrease in sintered porosity with increase in compaction load is quite clear. Fig. 4.23 testifies that cement copper products obtained from solutions of different initial copper concentrations, have almost the same sintered porosity at 850°C .

4.3.5 Liquid-phase Sintering

Apart from the above, Liquid-phase Sintering was also applied for sintering of cement copper powder compacts. Results of a few tests are given in Table 4.16. It is seen that the cement copper powder obtained from 8.895 gm Cu^{2+} /litre solution, when compacted just only at 2.5 ton load and then subjected to liquid phase sintering at 1150°C , only for five minutes, shows as high as about 21% increase in density and 13.6% decrease in porosity as compared to its green density and green porosity results respectively. However, the cement powder obtained from 3.177 gm Cu^{2+} /litre solution when compacted and subjected to liquid-phase sintering under similar experimental conditions, shows only about 4% increase in density and 2.7% decrease in porosity as compared to the results of green density and green porosity respectively. These results can be explained as follows: When sintering temperature is above the melting point of copper, the

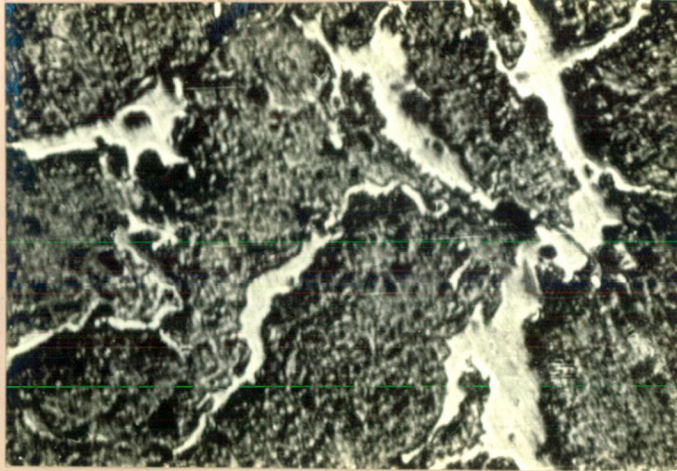
TABLE-4.16 : Results of Liquid Phase Sintering of Cement Copper Compacts
Produced at 2.5 T Load and Sintered at 1150°C.

Diameter of die = 1.63 Cm.

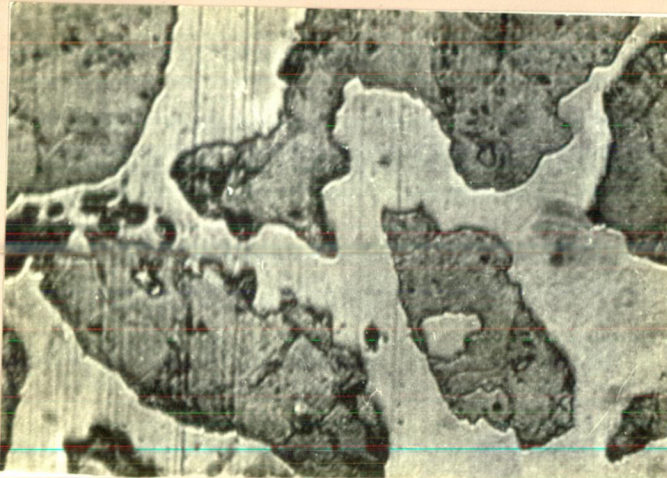
Properties	M A T E R I A L					
	Cement copper powder obtained from 8.895 gm Cu ²⁺ /litre solution using - 150 μ + 125 μ size iron powder			Cement copper obtained from 3.177 gm Cu ²⁺ /litre solution using - 150 μ + 125 μ size iron powder		
1. Green compact						
Weight (gm)	7.961					7.960
Diameter (cm)	1.630					1.630
Height (cm)	0.698					0.703
green density (gm/cc)	5.462					5.420
green porosity, %	35.8					33.9
2. Sintered product	6.010					9.610
Weight (gm)	1.550					1.620
Diameter (cm)	0.481					0.826
Height (cm)	6.619					5.642
sintered density (gm/cc)						
sintered porosity, %	22.2					31.2

molten copper dissolves quickly in the iron. In a simple iron-copper system, this formation of the solid-solution and the retention of the porosity created by the removal of the copper particles leads to an expansion of the compact. The expansion of the iron reaches a maximum with copper contents corresponding to the maximum solid solubility of copper in iron at the sintering temperature; this is about 8% at 1120°C - 1150°C. Increase in copper content beyond the solubility limit results in formation of a greater amount of liquid phase; this promotes the pore shrinkage mechanism associated with liquid-phase sintering and can offset the expansion due to the solutioning of the copper in the iron.

Photomicrographs of the products obtained from 3.177 gm Cu²⁺/litre solution and 8.395 gm Cu²⁺/litre solution are shown in Fig. 4.24. A very low porosity of the product obtained from high concentration solution and a relatively high porosity of the product obtained from low solution concentration certifies the results of liquid phase sintering.



3.177 gm Cu^{2+} / litre



8.895 gm Cu^{2+} / litre

Fig. 4.24 Photomicrographs showing the effect of Liquid-phase sintering on sintered porosity of Cement Copper parts produced from two different Initial Solution Concentrations, compacted at 2.5 Ton load and sintered at 1150°C (Iron powder size: -150 + 125 microns, Magnification: 200 X)

C H A P T E R - V

SUMMARY AND CONCLUSIONS

The present work leads to the following conclusions:

5.1 Thermodynamic Studies

The thermodynamic studies of aqueous copper sulphate and ferrous sulphate solutions by E.M.F. method have shown that,

- i) activity coeff. of copper sulphate decreases with increase in its concentration in pure copper sulphate solution. It has been found to obey the following expressions:

$$\log f = - \frac{2.4048 \sqrt{\mu}}{1+1.32 \sqrt{\mu}} - 0.004 \mu \text{ (Hückel relationship)}$$

and

$$\log f = - 2.0954 \sqrt{\mu} + 1.3872(\sqrt{\mu})^2 - 0.3389(\sqrt{\mu})^3$$

- ii) activity coefficients of copper sulphate and ferrous sulphate are increased by the addition of sulphuric acid and Harned's rule is observed to be followed in both the cases.
- iii) activity coefficient of ferrous sulphate decreases with increase in its own concentration in pure ferrous sulphate solution. It has been found to obey the following relationships:

$$\log f = - \frac{2.5114 \sqrt{\mu}}{1+ \sqrt{\mu}} + 0.1938 \mu \text{ (Guggenheim relationship)}$$

and

$$\log f = - 2.4170 \sqrt{\mu} + 1.9893 (\sqrt{\mu})^2 - 0.6425 (\sqrt{\mu})^3$$

This study has not been reported so far.

- iv) activity coefficient of copper sulphate is decreased by the substitution of ferrous sulphate for copper sulphate in its solution whereas, the activity coefficient of ferrous sulphate is increased by the substitution of copper sulphate for ferrous sulphate in its solution. Harned's rule is observed to be obeyed in both the cases.
- v) the thermodynamic driving force for cementation reaction has been found to be independent of pH and dependent on concentrations of both copper sulphate and ferrous sulphate.

5.2 Kinetic Studies

Studies of kinetics of cementation of copper on iron using powders have shown that,

- i) the cementation is a first order reaction with respect to concentration of copper ion in solution and, the overall rate of cementation is controlled by the mass transport in the aqueous solution.
- ii) the rate of cementation increases with increase in temperature. The activation energy for the

reaction has been found to be 3.0216 KCal/mole.

- iii) the rate of cementation increases with increase in stirring speed. It has been found to obey the following mathematical relationship:

$$K_{m,Cu} = B (\text{rpm})^{0.2642}$$

- iv) the rate of cementation increases with increase in initial copper ion concentration in solution upto a concentration of 0.5 gm Cu^{2+} /litre and thereafter it decreases with further increase in concentration.
- v) the rate of cementation decreases and amount of excess iron consumption over the theoretical amount increases with decrease in pH.
- vi) the rate of cementation increases with decrease in the size of the iron powder and is in good agreement with the following relationship:

$$\log p = \log \frac{6 m K_{m,Cu}}{2.303 V P} - \log d$$

- vii) the rate of cementation increases with decrease in solution/powder ratio, when the ratio is changed by changing the amount of iron powder. It also is in good agreement with the following relationship:

$$\log p = \log \frac{6 K_{m,Cu}}{2.303 V P d} + \log m$$

viii) use of hydrogen atmosphere in place of nitrogen has hardly any effect on rate of cementation. However, in atmospheric air there is a slight decrease in cementation rate and the excess iron consumption over the theoretical amount is increased.

5.3 Characteristics of Cement Copper Powder

Studies of the characteristics of cement copper powder and the effect of process variables on the properties of the cement powder products have shown that cement powders of low copper content are superior to plain iron powders with regards the green density, densification parameter and sintered density and can, thus, form a better substitute for plain iron powders. Powders having high copper content can be used either for the production of those powder metallurgical components which are normally produced with the help of pure copper powders or can be used for extraction of copper through melting.

The extraction of copper by cementation reaction with the help of powders will, thus, prove to be more useful and economical as the resulting product can be directly used for the production of finished powder metallurgical products.

SCOPE FOR FUTURE WORK

- 1) Cementation of metals from alkaline, acidic or complex salt solutions can be studied on similar lines for either (i) purification of their leach liquors, or (ii) their recovery from purified leach liquors. Typical cases for study could include cementation by aluminium or zinc of precious metals (gold and silver) from their cyanide solutions, or of copper, nickel or cobalt from complex amine solutions.

- 2) Industrial applicability of the cement metal, alloy or composite powders can also be studied for the production of specific powder metallurgical products such as bushes and bearings.

REFERENCES

1. Mellor, J.W., A Comprehensive Treatise on Inorganic and Theoretical Chemistry, Vol. 3, Logmans, Green and Co. Ltd., London, 1928.
2. Lamborn, R.H., The Metallurgy of Copper, 6th Ed., Lockwood and Co., London, 1875.
3. Read, T.T., Recent Copper Smelting, Mining and Scientific Press, San Francisco, 1914.
4. Ping, L.C., The Chemical Arts of Old China, J.Chem., Ed., Easton, Pennsylvania, 1943.
5. Partington, J.R., A History of Chemistry, Vol., 2, MacMillan and Co., London, 1961.
6. Piggot, A.S., The Chemistry and Metallurgy of Copper, Lindsay and Blakiston, Philadelphia, 1858.
7. Greenwalt, W., The Hydrometallurgy of Copper, McGraw-Hill Book Co., New York, 1912.
8. Hoffman, H.O. and Hayward, C.R., The Metallurgy of Copper, 2nd Ed., McGraw-Hill Book Co., New York, 1924.
9. Partington, J.R., A History of Chemistry, Vol. 3, MacMillan and Co., London, 1962.
10. Gladstone, J.H. and Tribe, A., J.Chem. Soc., 24, 1871, p 1123.

11. Jacky, H.W., *J.Metals*, Vol. 19, No.4, 1967, pp 22-32.
12. Frick, F.F., *Mining Congr. J.*, Vol. 37, No. 8, 1951, pp 42-44.
13. Huttel, J.B., *Eng. Mining J.*, Vol. 154, No.6, 1953, pp 90-93.
14. Butts, A., *Copper, the Metal, Its Alloys and Compounds*, Reinhold Publishing Co., New York, 1954.
15. Weed, R.C., *Eng. Mining J.*, Vol. 155, No.4, 1954, pp 88-91.
16. Ramsey, R.H., *Eng. Mining J.*, Vol. 155, No.8, 1954, pp 74-92.
17. Weed, R.C., *Trans. Met. Soc. A.I.M.E.*, Vol. 205, 1956, pp 721-23.
18. Argall, Jr., G.O., *Mining World*, Vol. 24, No. 12, 1962, pp 14-18.
19. Plecash, J. *Can. Mining Met. Bull.*, Vol. 56, 1963, pp 635-41.
20. Jacobi, J.S., in *Unit Processes in Hydrometallurgy*, Ed. by Wadsworth M.E. and Davis, F.T., Gordon and Breach Science Publishers, New York, 1964.
21. Wartman, F.S. and Robertson, A.H., *U.S.Bur. Mines, Rept. Invest. No.3746*, 1944, pp 1-16.
22. Bartlett, E.P., *U.S. Bur. Mines, Bull. No.519*, 1954, pp 1-143.


23. Smith, M.C., U.S. Bur. Mines, Inform, Circ. No. 7848, pp 1-37.
24. Hamdorf, C.J., Proc. Aust. Inst. Min. Met., No. 199, 1969, p 19.
25. Von Hahn, E.A. and Ingraham, T.R., Trans. Met. Soc. A.I.M.E., Vol. 236, 1966, pp 1098-1103.
26. Von Hahn, E.A. and Ingraham, T.R., Trans. Met. Soc. A.I.M.E., Vol. 239, 1967, pp 1895-1900.
27. Von Hahn, E.A. and Ingraham, T.R., Can. Met. Quart., Vol. 7, No.1, 1968, pp 15-26.
28. Nadkarni, R.M., Jelden, C.E., Bowles, K.C., Flanders, H.E., and Wadsworth, M.E., Trans. Met. Soc. A.I.M.E., Vol. 239, 1967, pp 581-585.
29. Nadkarni, R.M. and Wadsworth, M.E., Trans. Met. Soc. A.I.M.E., Vol. 239, 1967, pp 1066-1074.
30. Miller, R.L. and Wadsworth, M.E., Paper Presented at A.I.M.E. Annual Meeting, Paper A68-21, 1968.
31. Rickard, R.S. and Fuerstenau, M.C., Trans. Met. Soc. A.I.M.E., Vol. 242, 1968, pp 1487-1493.
32. Ingraham, T.R. and Kerby, R., Trans. Met. Soc., A.I.M.E., Vol. 245, 1969, pp 17-21.
33. MacKinnon, D.J. and Ingraham, T.R., Can. Met. Quart., Vol. 9, No.3, 1970, pp 443-448.

34. MacKinnon, D.J. and Ingraham, T.R., Can. Met. Quart., Vol. 10, No. 3, 1971, pp 197-201.
35. MacKinnon, D.J. and Ingraham, T.R., Can. Deptt. Energ. Min. Resources, Report R 241, 1971, pp 1-17.
36. MacKinnon, D.J., Ingraham, T.R., and Kerby, R., Can. Met. Quart., Vol. 10, No.3, 1971, pp 165-169.
37. Strickland, P.H. and Lawson, F., Proc. Aust. Inst. Min. Met., No. 236, 1970, pp 25-34.
38. Strickland, P.H. and Lawson, F., Proc. Aust. Inst. Min. Met., No.246, 1973, pp 1-6.
39. Strickland, P.H. and Lawson, F., Proc. Aust. Inst. Min. Met., No.237, 1971, pp 71-79.
40. Biswas, A.K. and Reid, J.G., Proc. Aust. Inst. Min. Met., No. 242, 1972, pp 37-45.
41. Biswas, A.K., and Reid, J.D., Trans. Inst. Min. Met., Vol. 82, 1973, pp C127-C131.
42. Reid, J.D. and Biswas, A.K., Trans. Inst. Min. Met. Vol. 82, 1973, pp C 221-C 224.
43. Reid, J.D. and Biswas, A.K., Proc. Aust. Inst. Min. Met., No. 249, 1974, pp 33-38.
44. Miller, J.D. and Beckstead, L.W., Met. Trans. Vol. 4, 1973, pp 1967-1973.
45. Fisher, W.W. and Groves, R.D., U.S. Bur. Mines, Rept. Invest. No. 7761, 1973, pp 1-9.

46. Fisher, W.W. and Groves, R.D., U.S.Bur. Mines, Rept. Invest. No.8098, 1976, pp 1-22.
47. Lee, E.C., Lawson, F., and Han, K.N., Trans. Inst. Min. Met., Vol. 84, 1975, pp C 87-C92.
48. Lee, E.C., Lawson, F., and Han, K.N., Trans. Inst. Min. Met., Vol. 84, 1975, pp C 149-C 154.
49. Sareyed-Dim, N.A. and Lawson, F., Trans. S.M.E., Vol. 260, 1976, pp 274-281.
50. Sareyed-Dim, N.A. and Lawson, F., Trans. Inst. Min. Met., Vol. 85, 1976, pp C 1-C 6.
51. Palmer, B.R., Gutierrez, G.M., and Fuerstenau, M.C., Met. Trans. B., Vol. 6B, 1975, pp 557-563.
52. Power, G.P. and Ritchie, I.M., Electrochimica Acta, Vol. 22, 1977, pp 365-371.
53. Lee, E.C., Lawson, F., and Han, K.N., Hydrometallurgy, 3, 1978, pp 7-21.
54. King, C.V. and Burger, M.M., J. Electrochem. Soc., Vol. 65, 1934, pp 403-411.
55. Schlitt, W.J. and Richards, K.J., in Solution Mining Symposium, Ed. by Aplan, F.F., McKinney, W.A., and Pernichele, A.D., A.I.M.E., Texas, 1974, pp 401-421.
56. Spedden, H.R., Malouf, E.E., and Prater, J.D., J.Metals, Vol. 18, No.10, 1966, pp 1137-1141.

57. Episkoposyan, M.L. and Kakovskii, I.R., *Tsvetn. Metal* 38-109, 1965, pp 15-19.
58. Wadsworth, M.E., *Trans. Met. Soc. A.I.M.E.*, Vol.245, 1969, pp 1381-1394.
59. Latimer, W.M., *Oxidation Potentials*, 2nd Ed., Prentice-Hall, Inc., New Jersey, 1952.
60. MacInnes, D.A., *The Principles of Electrochemistry*, Dover Publications, Inc., New York, 1961.
61. Weast, R.C., *Handbook of Chemistry and Physics*, C.R.C. Press, Cleveland, 1974, D120-D125.
62. Lewis, G.N. and Randall, M., *Thermodynamics*, McGraw-Hill Book Company, Inc., New York, 1923.
63. Lange, E., Monheim, J., and Robinson, A.L., *J. Am. Chem. Soc.*, Vol. 55, 1933, p 4733.
64. Robinson, R.A. and Jones, R.S., *J. Am. Chem. Soc.*, Vol. 58, 1936, p 961.
65. Robinson, R.A. and Stokes, R.H., *Electrolyte Solutions*, 2nd Ed., Butterworths and Co. Ltd., London, 1968.
66. Guntelberg, E., *Z. Phys. Chem.*, Vol. 123, 1926, p 199.
67. Butler, J. *Phys. Chem.*, Vol. 33, 1929, p 1015.
68. Guggenheim, E.A., *Phil. Mag.*, Vol. 19, 1935, p 588.

69. Harned, H.S. and Owen, B.B., The Physical Chemistry of Electrolytic Solutions, 3rd Ed., Reinhold Publishing Corp., New York, 1963.
70. Mathewson, C.H., Zinc, Reinhold Publishing Corp., New York, 1959.
71. Bockris, J.O'M., in Trans. Symposium on Electrode Processes, Yeager, E., Ed., John Wiley and Sons Inc., New York, 1961.
72. Vetter, K., Electrochemical Kinetics, Academic Press, New York, 1967.
73. Bockris, J. O'M and Reddy, A.K.N., Modern Electrochemistry, Vol. 1 and 2, Plenum Press, New York, 1970.
74. Butler, J.A.V., Trans. Faraday Soc., Vol. 19, 1924, pp 729-733.
75. Erdey-Gruz, T. and Volmer, M., J.Phys. Chem., Vol 150, 1930, pp 203-213.
76. Butler, J.A.V., in Electrical Phenomena at Interfaces, Butler, J.A.V., Ed., MacMillan Co., New York, 1951.
77. Gierst, L., in Trans. Symposium on Electrode Processes, Yeager, E., Ed., John Wiley and Sons, Inc., New York, 1961.
78. Eyring, H. and Eyring, E.M., Modern Chemical Kinetics, Reinhold Publishing Corp., New York, 1963.

79. Higbie, R., Trans. Am. Inst. Chem. Eng., Vol. 31, 1935, p 365.
80. Danckwerts, P.V., Ind. Eng. Chem., Vol. 43, 1951, p 1460.
81. Hansford, G.S. and Litt, M., Chemical Engineering Science, Vol. 23, 1968, pp 849-864.
82. Lal P., Nigam, K.K., Upadhyay, S.N., and Misra, P., III National Heat and Mass Transfer Conference, I.I.T., Bombay, Dec. 1975.
83. Nagata, S., Mixing, John Wiley and Sons, New York, 1975.
84. Whitman, W.G.,  Chem. and Met. Eng., Vol. 29, 1923, p 147.
85. Toor, H.L. and Marchello, J.M., J. Am. Inst. Chem. Eng., Vol. 4, 1958, p 97.
86. Chapman, T.W., Ph.D. Thesis, Berkeley University, California, 1967, UCRL 17768.
87. Uhlig, H.H., Corrosion and Corrosion Control, John Wiley and Sons Inc., New York, 1963, p 46.
88. Sands, R.L. and Shakespeare, C.R., Powder Metallurgy, George Newnes Ltd., London, 1966.
89. Hirschhorn, J.S., Introduction to Powder Metallurgy, American Powder Metallurgy Institute, Princeton, 1969.